FAR-INFRARED LASER SPECTROSCOPY OF NEUTRAL AND NEGATIVELY CHARGED SHALLOW DONORS IN GAAS AND INP

C.J. Armistead

A Thesis Submitted for the Degree of PhD
at the
University of St Andrews

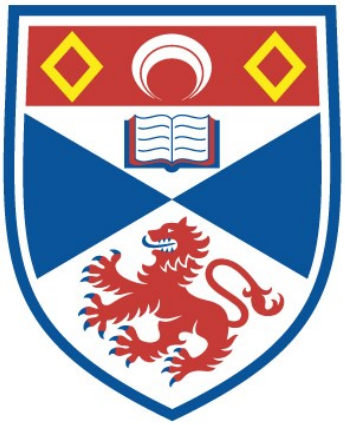

1986

Far-Infrared Laser Spectroscopy of Neutral and Negatively Charged Shallow Donors in GaAs and InP.

C.J.Armistead

St. Leonards College

St.Andrews University

September 1986

Abstract.

An optically pumped far-infrared laser and superconducting magnet have been used to perform high resolution studies of the energy levels of neutral and negatively charged shallow donors in high purity n-GaAs and n-InP in magnetic fields where the dimensionless magnetic field γ is approximately one (where $\gamma=\hbar\omega_c/(2R^*)$, $\hbar\omega_c$ is the cyclotron energy and R^* is the Coulomb binding energy).

The central cell structure caused by the presence of different shallow donor species has been studied on the $1s\text{-}2p_{\pm1,0}$ transitions of neutral shallow donors in undoped GaAs samples grown by molecular beam epitaxy, liquid phase epitaxy and vapour phase epitaxy (VPE). VPE material showed two new shallow donor species with negative central cell shifts. The $1s\text{-}2p_{-1}$ transition at magnetic fields where $\gamma>1$ shows exceptionally well resolved central cell structure. Detailed structure at magnetic fields below the $1s\text{-}2p_{+1}$ transition is due to transitions from the 1s to higher excited states.

Samples of undoped high purity InP grown by the VPE, metal organic chemical vapour deposition and bulk growth techniques have been studied. VPE samples always show a strong component related to sulphur though some also show a strong silicon related component, and some show up to 7 components. A bulk sample showed two strong components shallower than silicon which may have negative central cell shifts.

Transitions between the excited states of neutral shallow donors in GaAs have been studied. Recent theoretical work by Makado (1982) describes the transition energies very well. Clearly resolved central cell structure is observed on inter-excited state transitions involving the 2s state.

The first unambiguous observation of negatively charged shallow donors (D^- states) in GaAs is reported. Simultaneous observations of

transitions involving D^- states, the cyclotron resonance and inter-excited state transitions of neutral donors over a wide magnetic field range, $0.03<\gamma<3.5$, highlight the differences between the transitions and the relative effects of optical excitation, temperature, magnetic field and electric field bias.

Makado P.C.: PhD. Thesis, University of St. Andrews (1982).

Contents.

Declaration.

I hereby certify that this thesis has been composed by myself, that it is a record of my own work, and that it has not been accepted in partial or complete fulfilment of any other degree or professional qualification.

14th September 1986

C.J.Armistead

I was admitted to the Faculty of Science of the University of St. Andrews under Ordinance General No 12 on 1st October 1980 and as a candidate for the degree of Ph.D. in November 1981.

14th September 1986

C.J.Armistead

I hereby certify that the candidate has fulfilled the conditions of the Resolution and the Regulations appropriate to the degree of Ph.D.

In submitting this thesis to the University of St. Andrews I understand that I am giving permission for it to be made available for use in accordance with the regulations of the University Library for the time being in force, subject to any copyright vested in the work not being affected thereby. I also understand that the title and abstract will be published, and that a copy of the work may be made and supplied to any bona fide library or research worker.

Acknowledgements.

I would like to thank my supervisor Professor R.A.Stradling for his considerable support and encouragement while I have been working on the material for this thesis. I would also like to thank all my colleagues in the Physics Department at St.Andrews for their continual encouragement and many useful discussions, in particular Steve Najda, Tony Thorley, David Cowan, Pa Makado, Murray Davidson, David Marks, Carol Trager, Zbignew Wasilewski, Clivia Sotomayor-Torres and Peter Knowles, who have all been members of Tony Stradling's group. The assistance of the technical support services in the Physics Department, and particularly Bob Mitchell, is also gratefully acknowledged.

Outside St. Andrews my thanks must go to the following for the supply of samples: Peter Colter at the USAF Wright Patterson AFB, Greg Stillman at the University of Illinois, Elisabeth Bauser at the Max Planck Institute in Stuttgart, Peter Blood at Phillips Research in Redhill and Paul Dean and Maurice Skolnick at the Royal Signals and Radar Establishment in Malvern.

At the Max Planck Institute Hochfeld Magnetlabor my thanks go to Dr. J.C.Maan for his assistance while carrying out the series of high magnetic field experiments on D^- states and to Professor G.Landwehr for allowing me to use their facilities and for financial support.

The bulk of the work was carried out with the aid of an SERC grant.

Finally my thanks go to all my colleagues at STL for their encouragement while writing the thesis and to Sue Elven for assistance with the word-processing system.

Chapter 1.

Introduction.

The field of semiconductor physics is arguably the aspect of physics which has had the greatest impact on current technology in recent years. For example, the continuing development of silicon and germanium semiconductor devices from simple diodes and the transistor made by Bardeen, Brattain and Shockley, through small and medium scale integrated circuits, to LSI and VLSI devices could not have been sustained without a parallel improvement in the understanding of the fundamental physics involved.

Much current interest in the semiconductor industry centres around III-V devices. Discrete GaAs devices are now being manufactured in significant quantities while both analogue and digital GaAs integrated circuits are on the horizon. Indium phosphide is used on a smaller scale for specialist microwave devices and optoelectronic components. Devices based around ternary and quaternary III-V compounds are also in production, these generally being for LEDs and semiconductor lasers and detectors which find applications in optical fibre communications, where the advantage of the ternary/quaternary compounds are that the bandgap can be adjusted by changing the composition in order to match the wavelength where the lowest attenuation in the optical fibre occurs.

The development of all these devices involves the growth, processing and characterization of semiconductors to high levels of precision. In this context 'processing' can involve the various methods of fabricating small structures, or methods for making electrical contact to devices, or techniques for diffusion, proton bombardment and so forth.

The control and characterization of the impurity concentration and hence the electrical characteristics of the semiconductor, either during crystal growth or after growth using techniques such as

ion-implantation, diffusion, or neutron transmutation doping, is of utmost importance to the behaviour of these devices. Shallow impurities, where the binding energy is small compared to the bandgap energy, are perhaps the most important of the various impurity types as they have the greatest influence on the electrical conductivity of semiconductors.

The ability to identify the impurities present in semiconductors is of considerable importance and numerous techniques have been developed to do this. In GaAs and InP the problem of shallow donor identification is particularly difficult as the differences in binding energy of the different donor species are particularly small when compared to the situation in Si and Ge for example. At impurity concentrations down to $\sim 10^{15}$ cm^{-3} mass spectroscopic techniques such as SIMS (Secondary Ion Mass Spectrometry) may reveal the different impurity species, though this is a 'destructive' testing technique.

At impurity concentrations below this level 'optical' spectroscopy must be used. Far-infrared magnetospectroscopy, as used in this thesis, is one of the few techniques in this category which can resolve the small ground state energy differences due to different impurity species (known as chemical shifts). In fact, for reasons explained later, donor identification using this technique becomes more reliable as the purity increases and the number of impurities is reduced! Most previous spectroscopic studies of shallow donor spectra have used Far-infrared Fourier Transform Spectrometers since there have been no tunable sources of Far-infrared radiation. One of the aims of this thesis is to show the substantial improvements in resolution and sensitivity which can be achieved using Far-infrared laser based systems. The improvements are such that it is possible to

resolve the chemical shifts on impurity transitions which do not involve the ground state and are up to an order of magnitude smaller than the ground state splitting.

A further technique capable of resolving the small chemical shifts of donors is to study the near band gap photoluminescence spectrum. A number of transitions with energies just below that of the band gap are due to the recombination of excitons bound at neutral and ionised donors and chemical shifts and splittings can be observed on some of these. However the resolution is not as good as that which can be achieved by studying the impurity transitions directly using an FIR laser system.

In addition to work such as this which might have some immediate technological application it is clear that there are a great many areas of the subject of impurities in semiconductors which are fascinating in their own right.

The behaviour of the energy levels of isolated shallow donors in a magnetic field is of particular interest and much theoretical work has been carried out on this subject. The region of magnetic field accessible in our experiments is the most difficult to describe as the magnetic energy is comparable to the coulomb binding energy (ie $\gamma = \hbar\omega_c/2R^* \sim 1$) and neither the wavefunctions valid in the low field regime where $\gamma \ll 1$, nor those valid at high fields where $\gamma \gg 1$, are a good approximation to the situation. Recent theoretical studies by Makado are shown to accurately describe the energies of transitions of shallow donors in all the work described in this thesis and as a result a number of transitions between excited states which have been observed for the first time have been identified.

Identification of the various inter-excited state transitions of neutral hydrogenic donors is of particular importance with regard to

the work presented on negatively charged shallow donor states. A negatively charged shallow donor or D^- state is formed when an extra electron becomes bound at a neutral donor. The binding energy of the extra electron is very small, being only 5.5% of the binding energy of an electron at a neutral donor, and is similar to the binding energy of an electron in the n=4 excited state of a neutral donor. Prior to this work D^- states had only been tentatively identified in Si and Ge, and one could not rule out the alternative explanation that the spectral features observed were due to inter-excited state transitions of neutral donors which are observed under similar experimental conditions. As our spectra show inter-excited state transitions, the cyclotron resonance and transitions involving D^- states simultaneously no such confusion can occur. The binding energy of the D^- ground state can be followed from very low fields where $\gamma \sim 0.05$ to very high fields where $\gamma \sim 3.5$, and theoretical work by Larsen is shown to be in good agreement up to $\gamma \sim 1$.

Studies such as these on the behaviour of shallow hydrogenic donors are of interest not only to semiconductor physicists, but also to astro-physicists. Although the magnetic fields used in the experiments, up to 24 Tesla, are near to the maximum continuous fields that can be generated in a laboratory, they are many orders of magnitude below the magnetic fields which may exist in various parts of the universe. In the vicinity of neutron stars and pulsars it is thought that fields up to 10^9 Tesla (equivalent to $\gamma \sim 4000$ for real atoms) may exist. Thus the behaviour of neutral hydrogen atoms (which are a major constituent of stellar atmospheres) in such fields is of interest and can be related to the behaviour of the analogous system of hydrogenic donors in semiconductors.

A similar situation exists for the D^- state which is the

analogue of the free H^- ion. Much of the early work on H^- ions was carried out by astrophysicists interested in knowing how their presence would affect stellar spectra, as it is thought that significant numbers of H^- ions may form in the cooler outer layers of stars.

Until now very little information has existed on how H^- ions would behave in a magnetic field - especially at fields where $\gamma \sim 1$ as the equivalent field of 230,000 Tesla cannot be generated in a laboratory. Thus our work on the analogous D^- state in GaAs represents the first time that the theoretical work on the ground state energy can be compared with experiment.

Although results on D^- states in GaAs cannot be achieved at fields much in excess of those used in this thesis, the work could be extended to significantly higher values of γ by working with a semiconductor with smaller effective mass giving smaller binding energies for the shallow impurities. Indium antimonide is a good example, where the magnetic fields used in this thesis would give values of γ up to ~ 20.

Chapter 2.

Background Theory of Shallow Impurities in III-V Semiconductors.

The semiconductors studied for this thesis were high purity n-GaAs and n-InP. GaAs and InP were first made in the 1930's, though this early material was of poor quality, and studies of their semiconducting properties only became possible in the 1950's when methods of growing higher purity material became available. Since then many of their properties have been studied in great detail. Whole books are devoted to reviews of research on III-Vs in general and GaAs in particular (eg Physics of III-V Compounds Vols 1, 2, 3, 4, Eds. Willardson and Beer 1968) and so it is not thought necessary to give anything more than the barest description of the materials here. An up to date review of GaAs intrinsic properties has been published recently ('Semiconducting and other major properties of gallium arsenide', Blakemore 1982) while a collation of results on most semiconductors including GaAs and InP and covering impurity related features is also available (Landolt-Börnstein 1982).

Gallium arsenide and indium phosphide are similar materials from the point of view of shallow impurities. Both have the same type of crystal structure - the cubic zincblende lattice with face centred cubic symmetry as shown in Figure 2.1 - together with the same form of Brillouin Zone, a truncated octohedron as shown in Figure 2.2. For GaAs the nearest neighbour distance is that between the gallium and arsenic sites and is 2.45 Å, while the Ga-Ga and As-As distance is 4.00 Å. The corresponding figures for InP are In-P: 2.54 Å and In-In or P-P: 4.15 Å.

Figure 2.3 shows schematically the band structure of GaAs in the region close to the energy gap. InP has minor differences which are detailed in the figure caption. Most significantly, both materials have a direct energy gap at the Γ point, with the gap for GaAs being the larger.

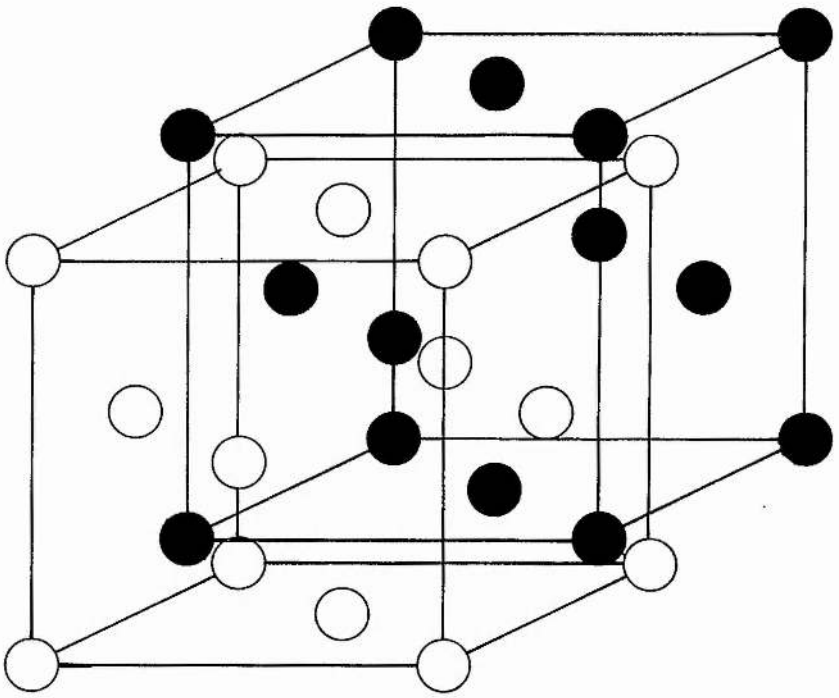

Figure 2.1: The crystal structure for GaAs and InP is formed from two intersecting face centred cubic lattices, where one lattice is offset from the other by (¼, ¼, ¼).

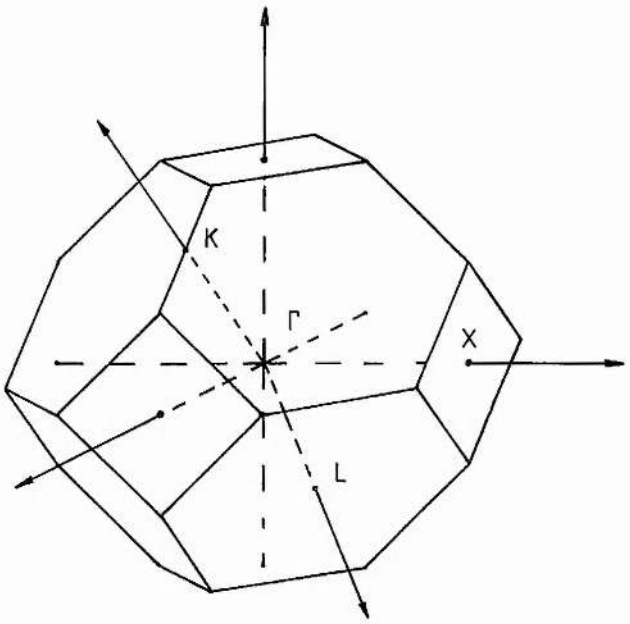

Figure 2.2: The Brillouin Zone for GaAs and InP is a truncated octahedron. The important lines and points of symmetry are marked.

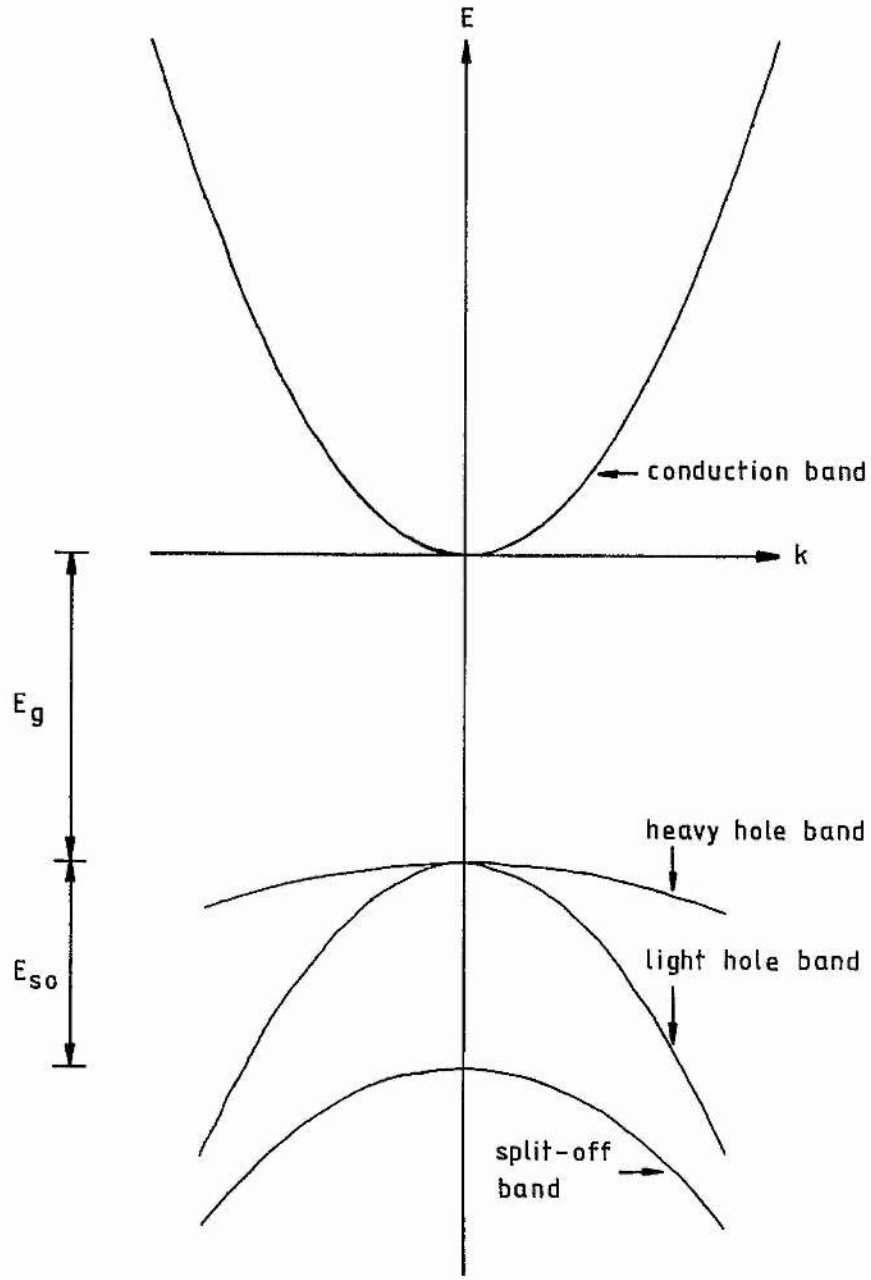

Figure 2.3: The band structure for GaAs and InP close to the Γ point. The various parameters for GaAs and InP are as follows (from Landolt Börnstein Tables):

	GaAs		InP	
E_G (eV)	1.518		1.423	all at T=4.2K
E_{so} (eV)	0.341		0.108	all at T=4.2K
m_e^*	0.0665		0.0803	all at T=4.2K
m^*_{hh}	0.48	T=50K	0.60	T=110K
m^*_{lh}	0.087	T=50K	0.12	T=4.2K
m^*_{so}	0.17	T=50K	0.12	T=110K

As all our interest involves electromagnetic radiation with a small wavevector compared to that at the zone edges we need only consider the region of the band diagram close to the Γ point. In this region the energy bands are nearly parabolic with differing curvatures accounted for by the effective mass. Thus at the Γ point the conduction band effective mass at a temperature of 4.2K has been found to be 0.0665 m_0 for GaAs while for InP it is $0.080m_0$.

Effect of a Magnetic Field on Band Structure.

When an electron moves in the presence of a static magnetic field it follows a helical path with the axis of the helix along the magnetic field direction. The motion parallel to the magnetic field is unaffected whereas in the plane perpendicular to the field the motion is orbital with an angular frequency known as the cyclotron frequency ω_c given by $\omega_c=eB/m$. Here e is the electronic charge, B is the magnetic field intensity and m is the mass of the electron. If the electron is subject to an electromagnetic field of frequency ω it will absorb energy from the field when $\omega=\omega_c$. This situation is known as cyclotron resonance.

A more rigorous classical analysis, as covered in most elementary textbooks on semiconductors, shows that if electrons of effective mass m^* are subject to collisions with a time between collisions τ (the collision time) then for cyclotron resonance to be observed the condition $\omega_c\tau>1$ must be satified. This is effectively stating that the electron must be able to complete almost half an orbit between collisions. To observe a sharp cyclotron resonance absorption one must have $\omega_c\tau\gg1$. To satisfy this condition experiments must be carried out at low temperatures (to minimise τ) and in high magnetic fields and at high frequencies. Such an analysis also shows

that

$$\omega_c\tau = \frac{\omega_c}{\Delta\omega_{1/2}}$$

or

$$\omega_c\tau = \frac{B_c}{\Delta B_{1/2}}$$

where $\Delta\omega_{1/2}$ and $\Delta B_{1/2}$ are half widths at half height for the cyclotron resonance peak observed at ω_c or B_c when the experiment is performed at constant field or constant frequency respectively. $\omega_c\tau$ calculated in this way is often used as a figure to characterize the sharpness of the cyclotron resonance peak.

From a quantum mechanical point of view the application of a magnetic field along the z-axis B_z, causes the electron energies in the x-y plane to be quantized in units of the cyclotron energy $\hbar\omega_c$ with a zero-point energy of $\frac{1}{2}\hbar\omega_c$. Motion parallel to the field is unaffected. A complete analysis, including the effects of the electron spin orientation gives

$$E(\underline{k}) = (N + \tfrac{1}{2})\hbar\omega_c + \frac{\hbar^2 k_z^2}{2m^*} \pm \tfrac{1}{2}\mu_B|g_e^*|B_z$$

where μ_B is the Bohr magneton and g_e^* is the effective g-factor for the conduction electrons. (The argument applies equally well for holes in the valence band). The levels N = 0, 1, 2 ... are known as Landau levels and the system of levels is often referred to as the Landau ladder. Cyclotron transitions correspond to changes in the Landau index N of $\Delta N = \pm 1$ where +1 corresponds to cyclotron resonance absorption and −1 corresponds to cyclotron emission.

To be able to observe cyclotron resonance the Landau level separation $\hbar\omega_c$ must be greater than the broadening of the Landau levels due to scattering with collision time τ which is $\hbar/\tau$. Thus the condition $\omega_c\tau > 1$ must be satisfied, which is the same as that obtained classically.

Cyclotron Resonance Linewidths.

Factors influencing the cyclotron resonance linewidth can be split into two categories: homogeneous and inhomogeneous broadening. In the first instance the broadening is symmetric on either side of the resonance while in the second instance it is not.

Treating homogeneous broadening first, this may be made up of two components: the natural linewidth determined by the radiative decay time of the carriers from a Landau level, and the collision linewidth which is related to the momentum relaxation time. Normally the collision linewidth will dominate the natural linewidth. Providing the scattering times are energy independent it can be shown that the lineshape is Lorentzian. However the two scattering mechanisms which dominate the collision time, namely phonon scattering and ionized impurity scattering, are both energy dependent and averages must be taken over the electron energy distribution. Clearly the problem becomes particularly difficult once account is taken of the various types of phonon scattering and neutral impurity scattering, as well as mechanisms causing inhomogeneous broadening, such as non-parabolicity. As the problem is not particularly important in relation to the work in this thesis it will not be discussed further. However the problem has been discussed recently by Cowan (1985).

Impurities in Semiconductors.

The simplest model of a shallow impurity in a semiconductor is one where an electron (or hole) is bound in the coulomb field of a positive (or negative) point charge, and is thus analogous to a hydrogen atom where an electron is bound in the coulomb field of a proton. However if the electron orbit is sufficiently large it will behave as though it has an effective mass m* and the point charge will

be screened by the valence electrons in the lattice, accounted for by using the static dielectric constant ε_s in the expression for the coulomb potential. These two factors influence the energy of an electron in the coulomb field of an impurity such that only discrete values of energy are allowed:

$$E_n = \frac{-R^*}{n^2} \qquad \text{where } R^* = \frac{m^* R}{m_0 \varepsilon_s^2}$$

and n, the principal quantum number, takes positive integral values. R is the free space Rydberg constant (13.6 eV). The effective Bohr radius of the nth state is given by

$$a_n^* = \frac{m_0}{m^*} \frac{\varepsilon_s}{} \; a_0 \; n^2$$

where a_0 is the free space Bohr radius (0.53Å). Thus for typical values of effective mass of $m^* = 0.1\ m_0$ and static dielectric constant of $\varepsilon_s = 10$ the binding energy is 0.001 R or ~13 meV and the effective Bohr radius for the ground state is $100a_0$ or ~53Å. Transitions may take place between levels with different n quantum number with series limits in the mid-, and far- infrared and millimetre wave spectral regions, and are analogous to the Lyman, Balmer series etc in atomic hydrogen, whose series limits lie in the ultraviolet and visible regions of the spectrum.

A model of this kind can be used for simple substitutional donors such as group V impurities in Si and Ge, or, in a III-V compound, for group IV and group VI donors on the group III and V sites respectively. Thus group IV impurities in III-V compounds can be either donors or acceptors depending on the whether the impurity is on the group III or group V site respectively - for example in GaAs Si_{Ga} is a donor but Si_{As} is an acceptor.

This hydrogenic model for shallow impurities was put on a more rigorous footing by the work of Luttinger and Kohn (1955) and is known

as 'Effective Mass Theory' (EMT). Their approach was as follows (after Kohn 1957).

Let the Hamiltonian of the unperturbed lattice be H_0 with eigenfunctions $\Psi_{n\underline{k}}$ such that

$$H_0\Psi_{n\underline{k}} = E_{n\underline{k}}\Psi_{n\underline{k}} \qquad \text{where } H_0 = \frac{-\hbar^2}{2m_0}\nabla^2 + V(\underline{r})$$

Then it is well known that if $V(\underline{r})$ is the periodic potential of a lattice the eigenfunctions are Bloch functions which can be written

$$\Psi_{n\underline{k}}(\underline{r}) = u_{n\underline{k}}(\underline{r})\ \exp(i\underline{k}.\underline{r})$$

where n denotes the energy band and $u_{n\underline{k}}(\underline{r})$ has the same periodicity as $V(\underline{r})$.

Suppose a perturbation is introduced by placing a positive point charge on one of the lattice sites. The perturbed Hamiltonian H is given by $H = H_0 + U(\underline{r})$ where

$$U(r) = \frac{-1}{4\pi\varepsilon_0\varepsilon_s}\ \frac{e^2}{r}$$

The eigenfunctions of the perturbed system can be written

$$H\Psi = E\Psi$$

and can be expanded as a linear sum of the Bloch functions of the unperturbed lattice (since the Bloch functions form a complete and orthogonal set). Thus

$$\Psi = \sum_{n\underline{k}} A_{n\underline{k}}\ \Psi_{n\underline{k}}(\underline{r})$$

If this linear expansion is substituted in the expression for the perturbed eigenvalue problem then it can be shown that

$$(E_{n\underline{k}} - E)\ A_{n\underline{k}} + \sum_{n'\underline{k}'} \left\langle \Psi_{n\underline{k}} \mid U \mid \Psi_{n'\underline{k}'} \right\rangle\ A_{n'\underline{k}'} = 0$$

In order to evaluate the matrix elements of the potential U one must make use of the periodicity of the Bloch functions and the Fourier Transform of $U(\underline{r})$, ie $U(\underline{k})$. Then

$$\left\langle \Psi_{n\underline{k}} \mid U \mid \Psi_{n'\underline{k}'} \right\rangle = \sum_{\nu} C^{\nu}_{n\underline{k};n'\underline{k}'}\ \frac{-e^2}{|\ \underline{K}_\nu + \underline{k}' - \underline{k}\ |^2\ \varepsilon_0\varepsilon_s}$$

where $\underline{K}_\upsilon$ are the reciprocal lattice vectors.

Now consider the limiting case as the impurity potential goes to zero. The wavefunction will move closer to that of a Bloch wave at the conduction band minimum.

We thus anticipate solutions where $A_{n\underline{k}}$ is significant when only one band is involved and $\underline{k}$ is small compared to the reciprocal lattice vectors. Consequently all terms $\underline{K}_\upsilon \neq 0$ in the matrix element can be dropped. Then it can be shown that

$$\langle \Psi_{0\underline{k}} \mid U \mid \Psi_{0\underline{k}'} \rangle = \frac{-e^2}{|\underline{k}' - \underline{k}|^2 \, \varepsilon_o \varepsilon_s}$$

Inserting this in the perturbed eigenequation and retaining only $A_{0\underline{k}}$ terms yields

$$(E_{0\underline{k}} - E) A_{0\underline{k}} - \frac{e^2}{\varepsilon_o \varepsilon_s} \sum_{\underline{k}'} \frac{1}{|\underline{k}' - \underline{k}|^2} A_{0\underline{k}'} = 0$$

If we now write E_{0k} as $\hbar^2 k^2/(2m^*)$ when k is small and extend the summation to one over all k-space then

$$\left\{ \frac{\hbar^2 k^2}{2m^*} - E \right\} A(\underline{k}) + \int d\underline{k}' \, U(\underline{k}-\underline{k}') \, A(\underline{k}') = 0$$

where $U(\underline{q}) = -e^2 / (\varepsilon_o \varepsilon_s \, q^2)$ is the Fourier Transform of $U(\underline{r})$.

This equation is isomorphic to the Schrödinger equation for the hydrogen atom in momentum space. After a number of algebraic steps it can be transformed into the more usual Hamiltonian

$$\left\{ \frac{-\hbar^2}{2m^*} \nabla^2 + U(r) \right\} F(\underline{r}) = E \, F(\underline{r})$$

which, if U(r) is coulombic, has energy eigenvalues

$$E = -\frac{R^*}{n^2} \qquad \text{where } R^* = \frac{m^* R_o}{\varepsilon_s m_o}$$

$F(\underline{r})$ is the Fourier Transform of $A(\underline{k})$, ie $F(\underline{r}) = \int A(\underline{k}) \exp(i\underline{k}.\underline{r}) d\underline{k}$.

Note that the total impurity wavefunction is not simply F(r) since F(r) is simply a slowly varying hydrogenic envelope function

modulating the Bloch waves of the lattice. For the hydrogenic ground state

$$F(r) = (\pi a^{*3})^{-\frac{1}{2}} \exp(-r/a^{*})$$

Taking the Fourier Transform gives

$$A(\underline{k}) \propto (k^2 + a^{*-2})^{-2}$$

Thus $A(\underline{k})$ dies away rapidly when $|k|>1/a^{*}$. This value of k is clearly small when compared to the zone boundary wavevector and is consistent with the approximations made earlier.

Consequently one can say that the wavefunctions of hydrogenic bound states are constructed from a mixture of all band states with wavevector $k \lesssim 1/a^{*}$. Thus any particle or quasi-particle with a wavevector less than this value can interact strongly with hydrogenic bound states.

For example, acoustic phonons with the correct energy may be absorbed and excite electrons to higher bound states or into the conduction band. Another mechanism would be for electrons to relax towards the ground state through acoustic phonon emission but, as the larger energy changes involved in relaxing to the ground state would require phonons of larger wavevector possibly greater than $1/a^{*}$ (which do not interact so strongly with hydrogenic systems), this is a mechanism with low probability. Thus it is far more likely that an electron in an excited state will be excited by phonon absorption than that it would relax by phonon emission. Under certain conditions the probability that an electron will be ionized by repeated phonon absorption is nearly one while the probability that it will relax to the ground state by repeated phonon emission is nearly zero, and thus the electron will almost certainly be ionized into the conduction band.

As the probability for this 'photo-thermal ionization' mechanism will be different for different bound states it is possible for the

conduction electron concentration and hence the dc conductivity to change if a semiconductor is illuminated with light resonant with bound to bound transitions of shallow impurities (Stillman et al 1972). In very high purity material where the background conductivity is low the sensitivity of this technique for detecting bound-bound transitions of shallow impurities far exceeds that of absorption measurements. Using this technique a total of less than 10^5 neutral donors have been detected at the edge of the depletion layer in Si MOS devices and 10^6 acceptors in samples of ultra high purity germanium (Nicholas et al 1976 and Skolnick et al 1974 respectively). A more detailed examination of this and other factors which influence the photoconductivity is given in chapter 3.

Shallow Hydrogenic Donors in a Magnetic Field.

If a magnetic field $\underline{B}$ is introduced into the effective mass theory of shallow donors in a spherical band it can be shown that the Schrödinger equation for the hydrogenic envelope functions F(r) becomes

$$\left\{ \frac{1}{2m^*} (\underline{p} + e\underline{A})^2 \quad - \frac{e^2}{4\pi\varepsilon_0\varepsilon_s r} \right\} F'(r) = E' \, F'(r)$$

where the dash suffix indicates wavefunctions and energies perturbed by the magnetic field and $\underline{A}$ is the magnetic vector potential of the field.

In order to solve this one first takes the magnetic vector potential in the symmetric gauge, $\underline{A} = \frac{1}{2} \underline{r} \times \underline{B}$ and assumes that the magnetic field lies along the z-axis. Then

$$(H_0 + H_1) \, F'(r) = E' \, F'(r)$$

where H_0 is the unperturbed Hamiltonian and H_1 is a perturbation

$$H_1 = \frac{-i\hbar\omega_c}{2} \left\{ x \frac{\partial}{\partial y} + y \frac{\partial}{\partial x} \right\} + \frac{m^*\omega_c^2}{8} (x^2+y^2)$$

The first term is proportional to L_z, the z-component of

orbital angular momentum of quantum number m, while the second term is a quadratic Zeeman shift. The complete Hamiltonian can be written in dimensionless coordinates as

$$H = -\nabla^2 + \gamma L_z + \frac{\gamma^2\rho^2}{8} - \frac{2}{r}$$

where energies are measured in effective Rydbergs R^* and dimensions are in units of the effective Bohr radius a_B^*, and $\gamma = \hbar\omega_c/(2R^*)$ is a dimensionless magnetic field.

In atomic physics where, even in the maximum magnetic fields available in a laboratory, $\gamma \ll 1$, the quadratic term can be dropped and the problem treated as a perturbation of the hydrogenic levels 1s, 2s, 2p, 3s etc at zero magnetic field. In a magnetic field states with non-zero orbital angular momentum L are split into 2L+1 states since the component of orbital angular momentum along the field direction, L_z, is quantized in multiples of $\hbar$, ie $L_z = m\hbar$ where m is the magnetic quantum number and $|m| \leq L$. Thus p states split into three states $p_{\pm1,0}$ while d states with L=2 split into $d_{\pm2,\pm1,0}$, and so on.

However in semiconductors the situation is quite different as values of γ from 1 to 100 may easily be achieved.

In the extreme case of an infinite magnetic field the coulomb term can be dropped and the Hamiltonian becomes separable in cylindrical coordinates with the wavefunction being a product of a function in the x-y plane and a function along the z-axis, ie

$$\Psi = f(\rho,\Theta)\, g(z)$$

The energies obtained on solving this are the familiar Landau level energies

$$E_{Nmk} = (N + \tfrac{1}{2})\hbar\omega_c + \hbar^2k^2/2m^* \quad \text{where } N \geq m \text{ and } N \geq 0$$

which is the same as that given earlier when spin is neglected. Here N

is the Landau level index and m is the magnetic quantum number as in the low field case noted above. Though m does not appear explicitly in the expression it is still a good quantum number and is valid throughout the magnetic field range.

If the coulomb term 2/r is now treated as a perturbation the wavefunctions and energy levels for $\gamma \gg 1$ can be obtained. The states obtained from this calculation form a ladder of levels below each Landau level, and are characterized by the set of quantum numbers (N, m, υ) where N is the principle quantum number of the Landau level, m is the magnetic quantum number as before and υ is related to the number of nodes in the component of the wavefunction along the field direction (ie g(z)). Although most of the high field states denoted by (N, m, υ) correspond to low field states denoted by (n, 1, m) certain low field states do not exist at high fields and vice versa.

Yafet, Keyes and Adams (1956) performed the first variational calculations in the high field limit using this 'adiabatic approximation' and showed that

a. at these high fields the binding energy of shallow hydrogenic states is dramatically increased, so that at $\gamma=10$ the binding energy is some 3.5 times the zero field binding energy.

b. the effect of the magnetic field is to strongly compress the wavefunction in the plane perpendicular to the magnetic field, while in the direction along the magnetic field the wavefunction is compressed, but to a lesser extent, resulting in a cigar shaped distribution elongated along the field direction.

Since the work of Yafet, Keyes and Adams increasingly more complex calculations have been performed, accounting for such effects

as non-parabolicity resulting from the influence of bands other than the conduction band (eg Larsen 1968).

The two situations discussed so far involve the extremes where $\gamma \ll 1$ or $\gamma \gg 1$, and accurate models can be made in both of these cases without their being too complex. In contrast the situation where $\gamma \sim 1$ is difficult to describe accurately as the states cannot be described as perturbations of high or low field states.

Accurate calculations have been carried out using variational techniques but these generally involve sets of basis functions with many parameters. Aldrich and Greene (1979) performed such a calculation, which Makado (1982; Makado and McGill 1986) refined by using a larger basis set and performing the calculation at a larger number of values of γ in the range $0<\gamma<10$. This calculation gives the energy levels of all the states up to n=4 with sufficient accuracy to enable nearly all of the peaks observed in submillimetre photoconductive spectra of GaAs in a magnetic field to be identified as transitions between states of shallow hydrogenic donors. Figure 2.4 shows the energy levels of all the states calculated by Makado over the range $0<\gamma<10$, and clearly shows the transition from the low field situation, where the levels are perturbed zero field states, to the high field situation where the states form a ladder below each Landau level. In this case all the states have been assigned using the low field notations $1s, 2p_{\pm 1}$, 2s etc. The most recent work giving the low field quantum numbers and their equivalent high field quantum numbers is by Rösner et al (1984). Table 2.1 lists these equivalents for all negative m states appearing in Figure 2.4.

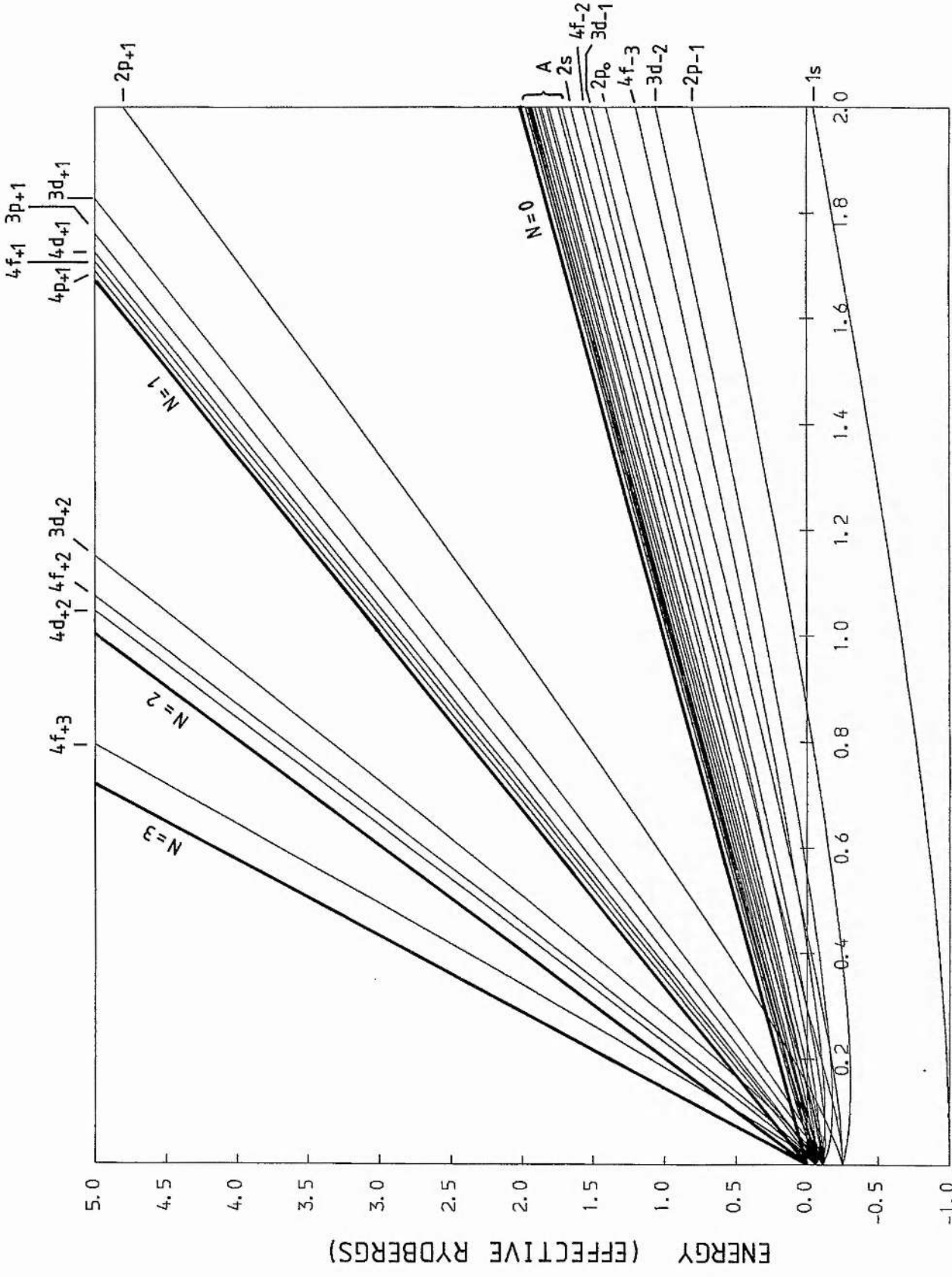

Figure 2.4: The behaviour of the energy levels of a shallow hydrogenic donor in a parabolic band in dimensionless units at intermediate magnetic fields (from the data of Makado 1982). The group of states marked 'A' are the $3p_{-1}$, $4d_{-2}$, $3p_0$, $4d_{-1}$, $3d_0$, $4f_{-1}$, $4f_0$, 3s, $4p_{-1}$, $4p_0$, $4d_0$ and 4s states in order of increasing energy. The Landau level energies are also shown.

Table 2.1.

This table lists the hydrogenic energy levels lying below the N=0 Landau level in Figure 2.4 in their correct energetic order at γ=2. The equivalent high field quantum numbers (N, m, υ) given by Rösner et al (1984) are also shown.

1s	000
$2p_{-1}$	$0\bar{1}0$
$3d_{-2}$	$0\bar{2}0$
$4f_{-3}$	$0\bar{3}0$
$2p_0$	001
$3d_{-1}$	$0\bar{1}1$
$4f_{-2}$	$0\bar{2}1$
2s	002
$3p_{-1}$	$0\bar{1}2$
$4d_{-2}$	$0\bar{2}2$
$3p_0$	003
$4d_{-1}$	$0\bar{1}3$
$3d_0$	004
$4f_{-1}$	$0\bar{1}4$
$4f_0$	005
3s	006
$4p_{-1}$	$0\bar{1}6$
$4p_0$	007
$4d_0$	008
4s	00 10

Chapter 3.

Experimental Techniques and Equipment.

Spectroscopic Studies of Shallow Impurities in Semiconductors.

If a semiconductor sample of sufficiently high purity (so that the impurities do not interact and can be regarded as isolated) is cooled to temperatures below ~10K then the conduction electrons freeze out onto the donor states. The absorption spectrum will then show peaks when the energy of the incident radiation is resonant with transitions between shallow impurity energy levels.

As the binding energy of shallow impurities is much less than the band gap energy the spectral region of interest extends from millimetre wavelengths to the mid-infrared. Within this region the availability of radiation sources is restricted and until recently no continuously tunable narrow band sources were available. The most convenient sources are blackbody radiation, FIR and IR lasers and millimetre wave sources such as GaAs and InP based Impatt and Gunn diodes.

As the spectral energy density of blackbody sources is very weak their use is generally restricted to Fourier Transform Spectrometers where no spectral filtering is necessary. Most of the early studies of the spectra of shallow impurities in semiconductors used these instruments.

In contrast, lasers and millimetre wave devices are narrow band sources running at substantial cw power levels up to 100mW. As these are fixed frequency devices a conventional spectrum showing absorption against energy cannot be obtained and a different technique is required to obtain a spectrum. The most common type of spectrum is obtained by measuring the absorption as the magnetic field is swept. As the magnetic field changes the transition energies change and whenever an impurity transition comes into resonance with the laser line a change in absorption is observed.

The use of lasers and microwave sources offer significant advantages over Fourier Transform techniques, namely that

i the much higher power and its concentration in a narrow bandwidth dramatically improve the signal-to-noise ratio and resolution compared to that obtained in a Fourier Transform Spectrometer where resolution is limited by the maximum path length difference that can be achieved.

ii the fourier transform that must be performed on the interferogram from the Fourier Spectrometer is computationally intensive and can introduce distortions to the peaks unless care is taken with the design of the computer program.

However it must be said that there are disadvantages to using FIR laser sources, principally that distortions of the lineshape can occur. This occurs if the populations of the impurity states change as the magnetic field is swept. Care must be taken when interpreting spectra obtained in this way, particularly if the line is spread over a substantial magnetic field. It is also possible to obtain a misleading impression of the relative linewidths of different transitions as the apparent linewidth, measured in Tesla, as the field is swept is inversely proportional to the rate at which the transition energy changes with magnetic field - thus if $\partial E/\partial B$ is large the apparent linewidth is small and vice versa. Thus the precise value of $\partial E/\partial B$ for each transition must be known in order to calculate the true linewidth in cm^{-1} or meV.

A further complication is introduced to FIR spectroscopy using lasers as in practice the detected signal is usually the photo-conductivity and not the absorption. This is discussed in more detail later in this chapter, but the problem arises that the photoconductive signal is proportional to the background resistivity, and can thus be

changed substantially as the magnetic field is swept. Consequently the amplitude of the photoconductive peaks can change with field.

Experimental Arrangement.

The Far-infrared laser spectrometer is shown schematically in Figure 3.1 and can be simply divided into three parts:

i The Far-infrared laser system (or millimetre wave sources).

ii The magnet and cryogenic systems.

iii The external electronics for detection.

A description of the FIR laser system is given towards the end of this chapter followed by a summary of the millimetre wave sources used. Once the laser system has been tuned to the desired wavelength the radiation is gathered into a brass lightpipe which directs the radiation to the top of the magnet.

The magnet used in the majority of the experiments was a high homogeneity superconducting magnet made by Oxford Instruments with a maximum field of 12.7 Tesla and a fast sweep capability (it can be swept to 80% of maximum field in 5 minutes).

A sample is mounted at the bottom of an 'insert' which can be removed and replaced in the magnet at will. These inserts principally consist of an outer case enclosing a thin walled stainless steel tube of ~1cm diameter acting as a light pipe, together with electrical connections to the two contacts on the sample. The top of the light pipe is sealed with a TPX window which is transparent to FIR and millimetre wave radiation, and prevents air being drawn into the insert and freezing. The sample is mounted at the end of a copper cone with an integrating hemisphere below it, as shown in Figure 3.1. With this arrangement the sample is studied in Faraday Geometry. When in

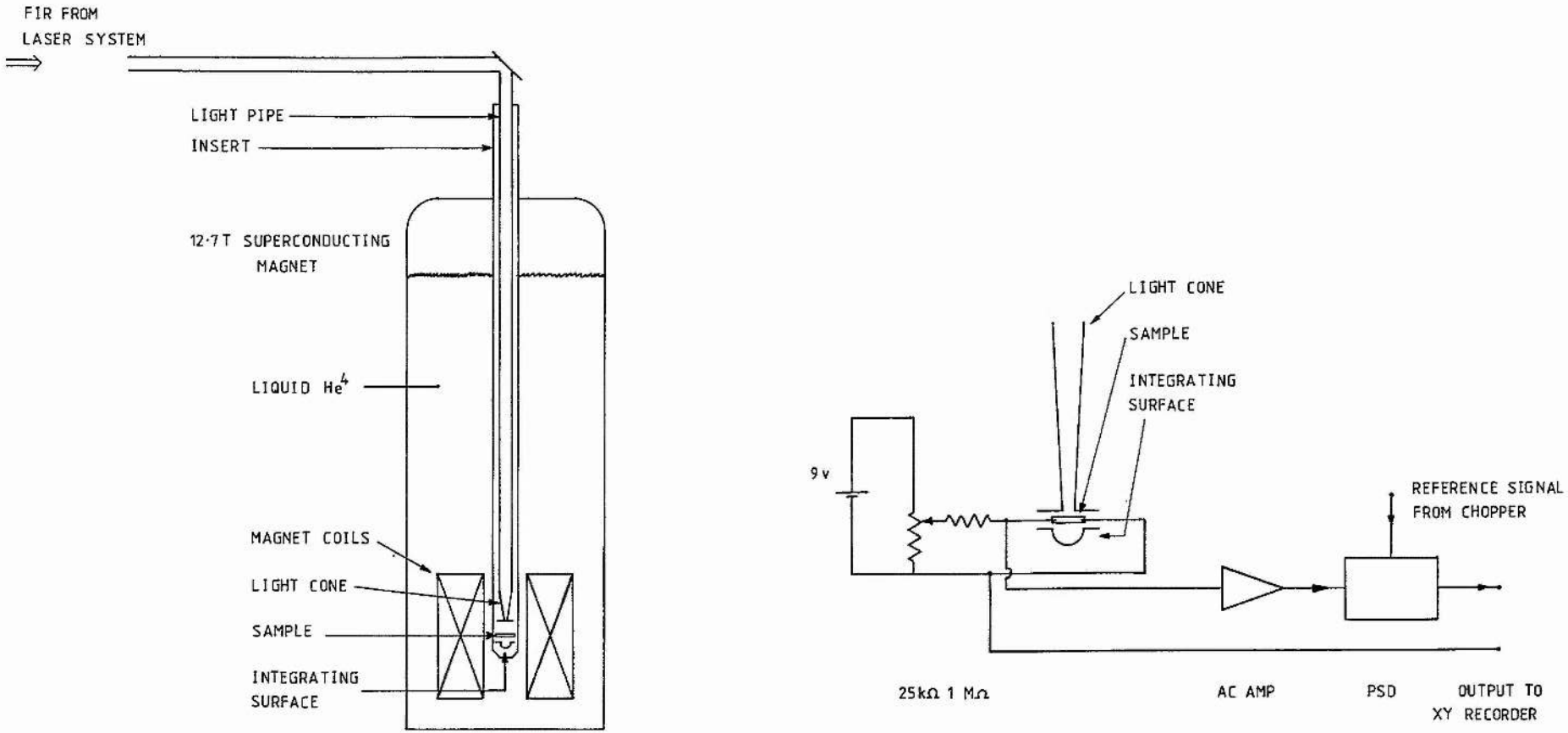

Figure 3.1: Schematic diagram of the experimental apparatus and the electronics used to measure the photoconductivity.

place in the magnet the sample is immersed in liquid helium at 4.2K.

A second insert was also available for experiments at temperatures other than 4.2K. The outer case of this 'double walled insert' has two walls with a vacuum space between them so that the sample and light pipe system are thermally isolated from the main liquid helium bath in which the magnet coils are immersed. The interior space can then be filled with liquid helium which can be pumped to reduce the sample temperature to ~1.8K. An Allen Bradley resistor mounted close to the sample monitors the temperature. Alternatively the sample could have a heater attached to enable it to be held at temperatures above 4.2K.

A second smaller magnet, with a maximum field of 6.7T, was occasionally used if time was not available on the shared 12.7T magnet. In practice this magnet would only operate up to a field of 4T, and would quench if swept beyond this. As a result its use was limited to studies of the $1s\text{-}2p_{+1}$ transition which occurs at 3.6T in both GaAs and InP when the laser line at 118.8μm was used. With this smaller magnet an insert was available so that Voigt geometry could be used. Experiments could be performed at temperatures down to 1.8K in the 6.7T magnet simply by pumping the whole of the helium space.

One problem with this smaller magnet was the lack of a good calibration technique, which made comparisons with results from the 12.7T magnet difficult. The 12.7T magnet was regularly used for NMR studies which provided an accurate calibration of the magnetic field. The magnetic field was monitored by measuring the current flowing through the coils with a series resistor. The voltage across the series resistor was converted into a magnetic field using the factor 0.0375 V T^{-1}, and was also used to drive the X-axis of the chart recorder. However if the magnetic field is being swept the actual

field lags behind that expected for a given current by an amount that depends on the sweep rate. Consequently a spectrum is always recorded twice, once with the field increasing and once with the field decreasing. The magnetic field for a given peak is then obtained by averaging the magnetic fields of the 'up' and 'down' peaks. Recording the spectrum twice has the added advantage that any changes in laser power can be detected by comparing the 'up' and 'down' sweeps. Care must be taken at the beginning and end of sweeps as the amount of lag changes and this can distort the spectrum in that region. In general care was taken to keep the transitions of interest away from the regions of distortion.

Optical Excitation.

Optical excitation using radiation with an energy close to the band gaps of GaAs and InP was provided by a quartz halogen bulb. This was positioned at the top of the insert and directed downwards into the light pipe through a small hole in the 45^{o} mirror. The actual intensity of the radiation reaching the sample is rather difficult to quantify. The bulb was rated at 150W and was driven with currents up to 10A, but only a small portion of the light is coupled through the hole in the mirror, and this would vary from experiment to experiment. In the thesis reference is made to 'medium' or 'strong' excitation or to the lamp current in amps. Medium corresponds to currents of 4 - 6 Amps and strong to 7 - 10 Amps, but in general the levels of excitation are very qualitative.

Detection Methods.

The most obvious method of detecting the presence of shallow impurities in a semiconductor is by measuring its FIR absorption

spectrum. In practice this would usually involve placing a detector in the optical path after the sample being studied.

Measurement of the absorption caused by the impurities in a sample has the inherent disadvantage that as the purity of samples increases the strength of the impurity absorption lines decreases. The GaAs and InP samples studied for this thesis are of very high purity and it would have been difficult to obtain impurity absorption spectra with good signal to noise ratios for this reason.

The technique used to obtain the spectra for this thesis was to measure the photoconductivity of the samples. Two electrical contacts are made to the ends of a sample by alloying small dots of indium onto the clean surface of the epitaxial layer at a temperature of between 300 and 400 ^{o}C in a reducing atmosphere obtained by bubbling a mixture of hydrogen and nitrogen through hydrochloric acid. Wires were then soldered to these alloyed contacts. The contacts were typically 5mm apart and a voltage of ~0.5V results in a field of ~1V cm^{-1}. Ideally a constant current supply is connected across the sample and the resulting voltage is a measure of the conductivity. In practice sample resistances at 4.2K were very high and it was not always possible to obtain a sufficiently low current (<1nA) from the constant current source that did not bias the sample beyond its impact ionization threshold.

The more usual experimental arrangement was to use a battery and potentiometer to provide a voltage across the sample and a 1MΩ series resistor as shown in Figure 3.1. The voltage across the sample was fed to an ac amplifier and phase-sensitive detector. The reference for the PSD is taken from a chopper in the FIR laser system and thus the PSD only responds to changes in the conductivity caused by the FIR radiation incident on the sample. The output from the PSD is recorded

on a chart recorder as a function of magnetic field (or, more strictly, the coil current).

Photoconductivity.

If experiments are conducted using constant current mode then the change in voltage across the sample can be written

$$\Delta V = -V \frac{\Delta\sigma}{\sigma}$$

and thus the photosignal is directly proportional to the external dc bias field V.

Since the conductivity can be written $\sigma=ne\mu$ (where n is the carrier concentration, e is the electronic charge and μ is the mobility) then the change in conductivity $\Delta\sigma$ is

$$\Delta\sigma = e(n\Delta\mu + \mu\Delta n)$$

Thus conductivity changes can occur as a result of changes in the carrier concentration or as a result of changes in the mobility of the carriers.

Various different mechanisms are responsible for the photoconductive signals measured in the experiments.

i Photothermal ionization - this was noted in Chapter 2 as the mechanism by which bound-bound shallow impurity transitions cause changes in the dc conductivity. Photon absorption induces a bound-bound transition to an excited state which is subsequently thermally ionized through low wavevector acoustic phonon absorption with a probability near 100%. Consequently there will be a change in carrier concentration and hence a change in conductivity. For photothermal ionization to occur temperatures must be sufficiently high for there to be a population of phonons, but not so high that the ground states of the impurities

may be thermally ionized. In GaAs and InP this temperature range is limited to between ~1K and ~20K. Other mechanisms may also ionize the intermediate excited state - background FIR, impact ionization, electric field ionization etc.

ii Photoionization - if the photon energy is greater than the impurity binding energy then impurities can be directly ionized by photon absorption and additional carriers excited into the band resulting in a change in the carrier concentration and thus a change in conductivity. This is a form of extrinsic photoconductivity. This mechanism is responsible for the D^- state spectra discussed in chapter 7, where $D^- + \hbar\omega \rightarrow D^0 + e^-$ and the electron is released to the conduction band. Intrinsic photoconductivity occurs when photons with energy greater than the band-gap are absorbed exciting electrons and holes into the conduction and valence bands.

iii Free carrier photoconductivity - this is the mechanism by which cyclotron resonance is observed in the photoconductivity. Two mechanisms can contribute:

a as carriers absorb energy their mobility changes and consequently the conductivity changes.

b as carriers are excited out of equilibrium more impurities are thermally ionized as the electron temperature rises, and consequently the carrier concentration increases leading to an increase in the conductivity.

Bluyssen et al (1978, 1980) have shown that in the temperature range 10 - 30K 'b' is the dominant mechanism. However in our experiments at 1.8 and 4.2K it is not clear which mechanism makes the dominant contribution to the cyclotron resonance induced conductivity.

iv Hopping photoconductivity - at sufficiently high impurity concentrations the impurities are close enough together for the excited state wavefunctions to overlap. Electrons excited from the ground states to the excited states by photon absorption can hop between adjacent states under the influence of an electric field and give rise to photoconductivity. Typically transitions occurring by this mechanism have slightly different transition energies to that seen with absorption (Carter et al 1977).

The photothermal ionization mechanism noted in i. is usually the dominant photoconductivity mechanism when studying high purity GaAs and InP at temperatures around 4K.

Principles of Optically Pumped Far Infrared Lasers.

The principles of optically pumped far-infrared lasers (OPFIRLs) are well known and are covered in extensive reviews (see eg Hodges 1977, 1978; De Temple and Danielewicz 1983). What follows is only a brief summary of the mechanisms involved.

In a far-infrared laser a vacuum tight container is filled with a gas at a pressure of the order of 100 mTorr. The gases used tend to be simple molecules such as methanol CH_3OH and the halomethanes CH_3F etc. The energy levels of these molecules are shown schematically in Figure 3.2 and consist of a ladder of vibrational states with each vibrational state being made up of a large number of rotational states. Typically the vibrational state separation is in the mid-infrared (~10μm) while the rotational state spacing is in the far-infrared (50-2000μm).

Radiation from an external source in the mid-infrared (usually a CO_2 laser at 10.6μm) is directed into the gas container and if the radiation is resonant with a vibrational transition it is absorbed. As the final state can be any of the rotational states in the excited vibrational state it is possible for a population inversion to be achieved within the ladder of rotational states. If a cavity is formed with mirrors then spontaneous emission from the rotational states can be amplified by stimulated emission leading to lasing.

The output power of such an optically pumped laser is limited by a number of factors. Initially the pumping power must be sufficiently great to overcome the various cavity losses. Once above this threshold the efficiency of conversion of pump power into output power is strongly influenced by the cavity losses and two relaxation times. The rotational relaxation time $\tau_{\Delta J}$ is usually orders of magnitude shorter than the vibrational relaxation time $\tau_{\Delta v}$ and both are

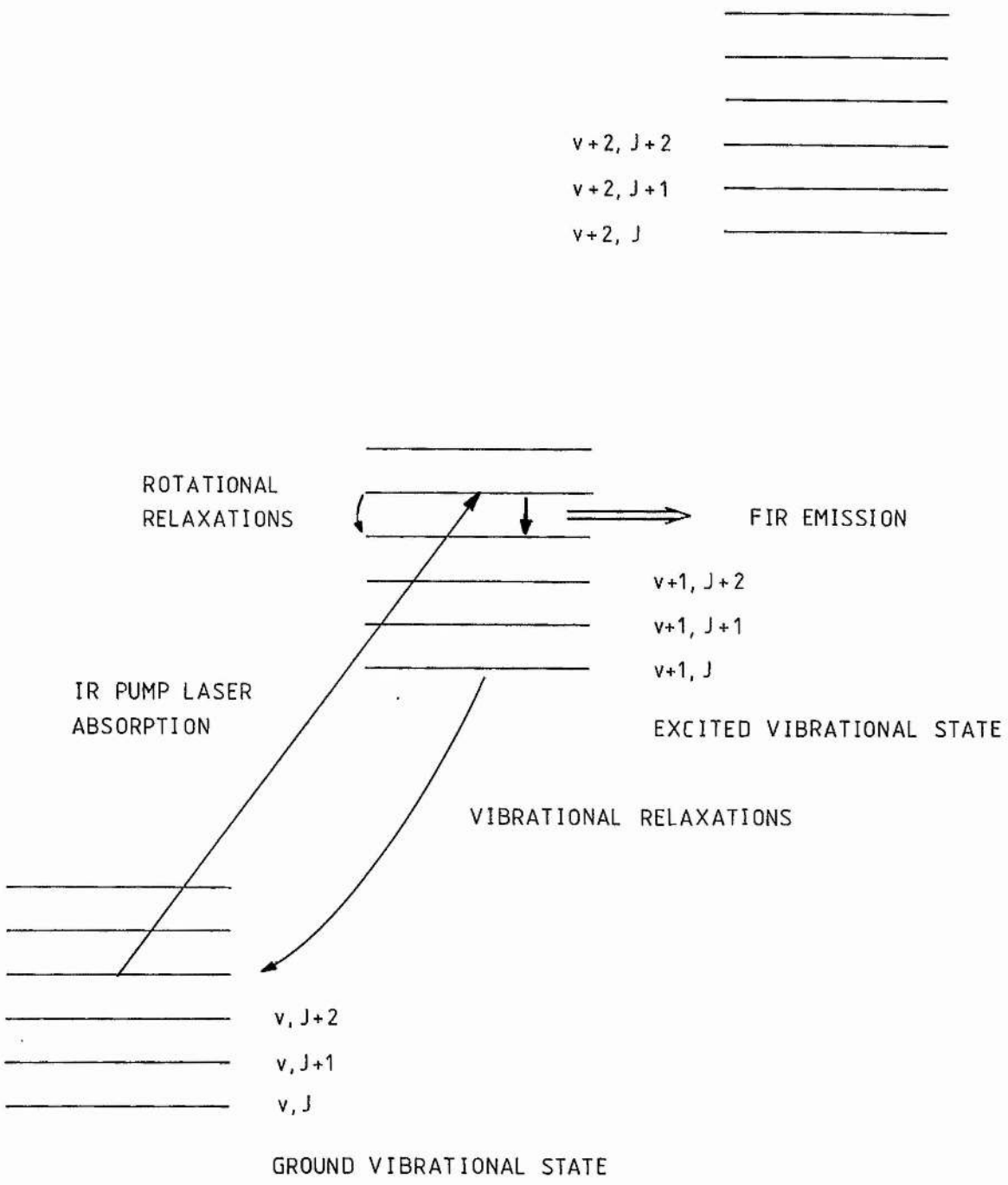

Figure 3.2: Schematic diagram of the energy levels in a simple molecular gas and transitions involved in FIR lasing.

inversely proportional to the gas pressure since relaxation is dominated by inter-molecular collisions and collisions with the walls of the laser cavity. As the rotational rates are fastest and act to thermalize the electron distribution in a vibrational state the FIR output power usually decreases rapidly as the gas pressure is increased above ~100 mTorr. However while it is a disadvantage to have a rapid rotational relaxation rate it is advantageous to have rapid vibrational relaxation rates, since the final state in a stimulated emission process should ideally be empty and long vibrational relaxation times can lead to a build up of electrons in the excited vibrational state and a 'vibrational bottleneck'.

The Optically Pumped Far-Infrared Laser System.

The optically pumped far-infrared laser used in the experiments was a commercial system made by Edinburgh Instruments and is shown schematically in Figure 3.3. The system was assembled on a large slate table for mechanical stability. A PL4 CO_2 laser capable of generating 50 W cw at the centre of each P and R branch was used as the pump laser. The beam from this was first passed through an optical chopper and directed by an arrangement of mirrors through a 1mm hole in one of the cavity mirrors so that it came to a focus ~50cm inside the cavity. The FIR laser cavity is formed with two plane mirrors separated by 1.5m with a 25mm diameter brass tube between them acting as a hollow waveguide resonator. As the gas pressure is low the CO_2 beam will usually make a number of passes of the cavity before being completely absorbed. The resonator material has a significant effect on its waveguiding properties and a brass tube favours operation in the long wavelength region of 100 - 1000μm when compared with a quartz resonator tube which would favour

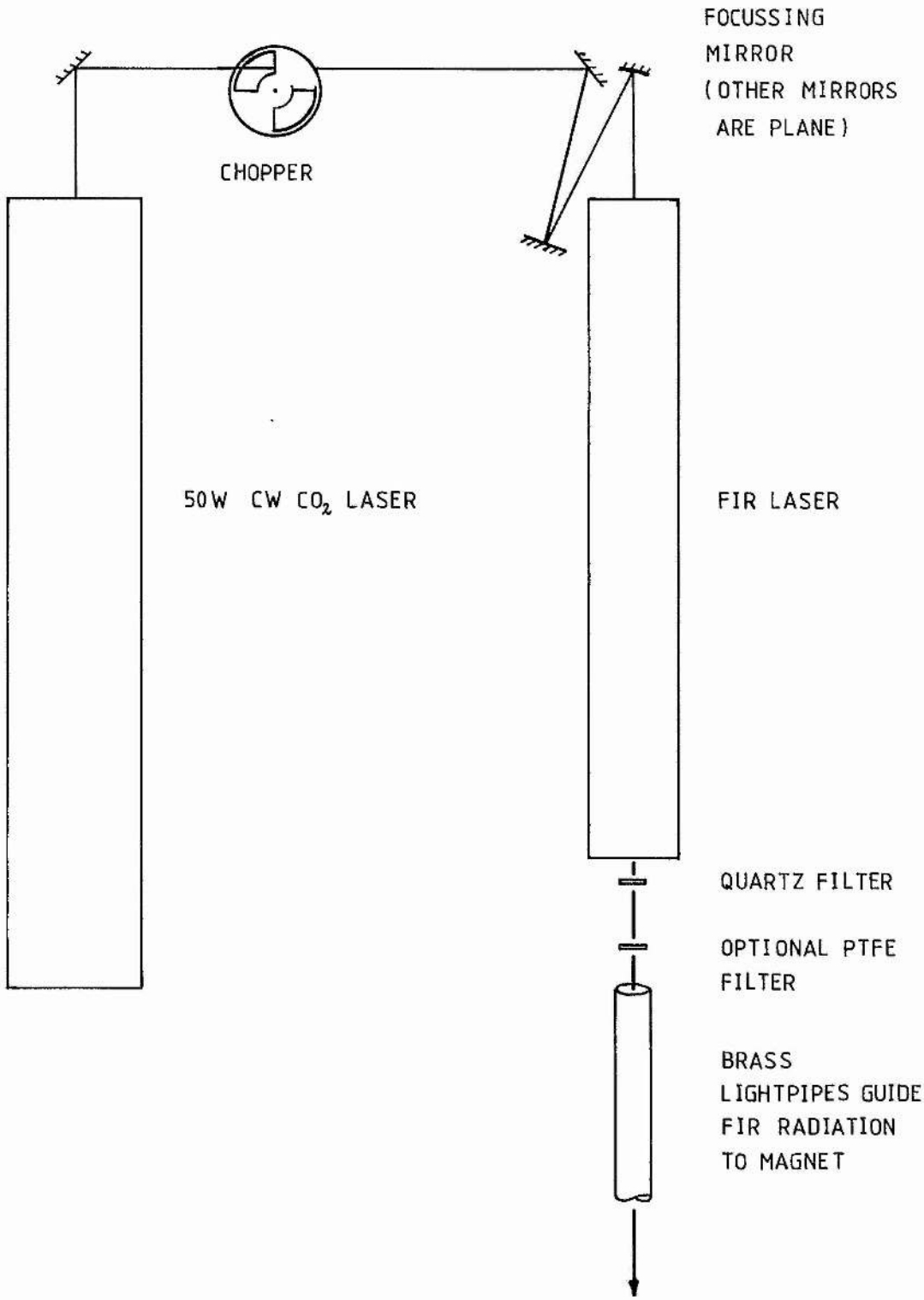

Figure 3.3: Schematic diagram of the Optically Pumped Far-infrared Laser System. The CO_2 laser and FIR laser were manufactured by Edinburgh Instruments Ltd.

short wavelength operation from 40 - 100 μm. As lasing operation with adequate power could be obtained between 70 μm and 1.2 mm with the brass tube there was no need to change it for these experiments.

Coupling of the FIR radiation out of the cavity is by means of a 5mm diameter silicon window mounted in the centre of the output mirror. This mirror is mounted on a bellows assembly so that it can be aligned parallel to the input mirror and translated along the cavity to select the various longitudinal modes. Any CO_2 radiation which passes through the output coupler is removed with a quartz filter. The FIR radiation is then gathered in a ~1cm diameter brass lightpipe system to guide it to the magnet.

Vacuum couplings are made to the laser cavity so that it can be evacuated with a diffusion pump and refilled with gas at an appropriate pressure.

As impurities in the gases appeared to severely degrade the lasing performance a laborious 'freeze-pump-thaw' purification technique was used for gases which were supplied as liquids. This involves first freezing the liquid in a test tube connected to the laser and pumping system and pumping the airspace above the solid. As the solid begins to thaw bubbles are seen coming off and the test tube is sealed off. Once it has completely thawed it is refrozen and the process repeated again. This would be repeated several times before the laser was filled with gas to a pressure of ~200 mTorr. Usually there was no need to optimize the gas pressure as sufficient FIR power to obtain good signal to noise ratios from the samples was often obtained immediately.

When FIR laser systems are designed considerable attention must be paid to the mechanical stability of both the CO_2 and the FIR cavities. The principle reason for this is that the CO_2 laser

frequency must be closely matched to the vibrational absorption frequency of the gas in the FIR laser, which may have a bandwidth of the order of 10 MHz. As the tuning range of a CO_2 laser is of the order of the longitudinal mode spacing which is ~150 MHz for a 2m long cavity it is clear that the CO_2 cavity length must be well stabilized so that changes in temperature or vibration do not cause its frequency to drift away from the vibrational absorption frequency. In many systems some form of active cavity length stabilization is used. The method used for our system involved modulating the cavity length at ~200Hz and observing the modulation of the electrical impedance of the cavity as a result of the optogalvanic effect. Unfortunately the electronics supplied by the manufacturer did not work at all well with our system (being originally intended for a different laser) and was rarely used. However after a one or two hour warm up period the FIR power was sufficiently stable for it to be left unattended during the twenty to thirty minute period necessary for a magnetic field sweep. Any fluctuations in FIR power could easily be seen by comparing the recordings taken when the field was sweeping up and down.

Lasing Wavelengths and Gases used with the FIR Laser System.

In spite of the close matching of pump laser frequency and vibrational absorption frequency of a gas that is required for FIR lasing to be possible, and the reliance placed on finding such chance coincidences, a remarkable number of lines have already been discovered. Some 1000 lines pumped with a CO_2 laser have been found and this number is increased further if gases are pumped with isotopic CO_2 lasers such as $^{13}CO_2$ or $C^{18}O_2$. A comprehensive list of optically pumped FIR lines is published and updated regularly by the

National Physical Laboratory.

Operation of the FIR laser system was limited to 7 gases but even so lasing was seen on at least 27 different wavelengths between 70.5μm and 1.223mm, as listed in Table 3.1. The table only lists the strongest lines where the wavelength could be assigned with certainty.

Notice that a gas being pumped by a given CO_2 line will often lase at a number of wavelengths. For example, 9P34 pumping methanol has been known to lase at 17 different wavelengths, but only λ=70.5μm and 699μm were identified in our system. If two lines are widely spaced in this way it is easy to select one or the other. A 4mm thick PTFE filter was found to block the 70.5μm wavelength but left the 699μm unattenuated. Alternatively, selection of the 70.5μm wavelength made use of the longitudinal periodicity of the cavity - as the cavity length is altered the 70.5μm signal peaks 10 times for every one peak of 699μm wavelength so it was easy to select a 70.5μm peak where there was no lasing at 699μm. However separating the lines using filters or cavity length tuning is not always practicable if the wavelengths are close together. For example, pumping formic acid near 9P22 produced a number of lines at λ~400μm. An external wire mesh mirror Fabry Perot filter might have separated the lines but as there were other lines near 400μm with 'clean' spectral characteristics there was no need to try this approach.

In general, as the shallow impurity spectra contained sharp lines, it was fairly obvious if lasing had ever occurred at a number of different wavelengths. The situation noted above with formic acid produced a spectrum with the same characteristic central cell split $2p_{-1}$-2s transition appearing in three places at different intensities.

Table 3.1.

The following gases were used in the FIR laser system:

CH_3OH (methanol)

CH_3OD (methanol-OD)

CD_3OD (methanol-d4)

CH_3Cl (methyl chloride)

CH_3I (methyl iodide)

CD_3I (deuterated methyl iodide)

HCOOH (formic acid)

Lasing operation has been seen with the Optically Pumped FIR laser system at the following wavelengths.

Wavelength(μm)	Gas	CO_2 Laser Pump Line
1223.658	CH_3OH	9.52P16
1005.348	CD_3I	10.74P34
944.0	CH_3Cl	9.32R12
869	CD_3OD	10.26R18
742.572	HCOOH	9.17R40
699.4226	CH_3OH	9.68P34
669.531	HCOOH	9.22R30
570.5687	CH_3OH	9.52P16
556.876	CD_3I	10.76P36
513.02	HCOOH	9.23R28
458.5229	HCOOH	9.18R38
447.14	CH_3I	10.57P18
444.3862	CD_3I	9.21R32
432.11	HCOOH	9.26R22
393.6311	HCOOH	9.28R18
392.0687	CH_3OH	9.69P36
349.3	CH_3Cl	10.26R18
305.72611	CH_3OD	9.34R08
302.2781	HCOOH	9.37R04
294.81098	CH_3OD	9.34R08
255	CD_3OD	10.15R36
251.1398	CH_3OH	10.14R38
170.57637	CH_3OH	9.69P36
163.03353	CH_3OH	10.14R38
118.83409	CH_3OH	9.69P36
96.52239	CH_3OH	9.33R10
70.51163	CH_3OH	9.68P34

FIR output powers vary widely from line to line. The strongest line was the λ=118.8μm line from methanol which would have an output power of the order of 100mW according to the Edinburgh Instruments specifications for the laser.

Gunn Diode and Impatt Sources.

Five millimetre wave sources were available consisting of

one Hughes Gunn diode at 80GHz

and four Plessey InP Impatt diodes at 88.2, 90.3, 95.0 and 110 GHz.

The Impatt diodes produced powers up to 8mW using drive currents up to 70 mA. The Gunn diode would produce over 10mW with a drive current of around 1.5 amps. All the devices were electrically tunable, in that the frequency increased with drive current, but in practice the tuning range is very narrow (the largest being 300MHz or ~0.3%) and was negligible from the experimental point of view.

The devices were very simple to use. Initially the radiation was directed through waveguide of the appropriate size, and through a mechanical chopper mounted on the top of the insert so that microwaves were directed through the TPX window on the top of the light pipe. With these long wavelength high power devices there can be a problem when using mechanical choppers as the chopper blades may heat up and emit significant amounts of black body radiation. This can be eliminated by placing a glass slide in the path.

This arrangement was later refined when the chopper was replaced by a Hughes PIN diode switch driven from a square wave oscillator at ~1kHz. The problem of chopper blades heating up then does not arise. In its open state the PIN switch had 3dB loss and when closed this increased to 16dB loss. No differences could be seen when spectra taken with the chopper or with the PIN switch were compared.

The arrangement on the top of the insert was such that light from a quartz halogen lamp for band gap excitation could be admitted to the light pipe in the same way as that used on the laser experiments.

Experiments Using Magnetic Fields Up To 23 Tesla.

In order to carry out a series of experiments using magnetic fields up to 23 Tesla arrangements were made to use the facilities at the Max-Planck Institut für Festkörperforschung Hochfeld-Magnetlabor in Grenoble. The assistance of Dr. J.C.Maan with the laser and magnet system during these experiments is gratefully acknowledged.

The experimental arrangement was very similar to that used in the experiments at St. Andrews.

The FIR laser system comprised an Apollo Instruments CO_2 laser pumping a 'home made' FIR laser cavity. The CO_2 laser could run in either pulsed or cw mode but was used exclusively in cw mode. The FIR cavity was basically the same as the commercial Edinburgh Instruments cavity described earlier, but differed in that a continuous flow of gas was used, with the pressure being controlled by a needle valve on the inlet. Only a few of the available laser lines were used:

Gas	λ (μm)	Pump Line
CH_3OH	469	10R38
CH_3I	447	10P18
HCOOH	432.6	9R20
CH_3OD	417	9P06
HCOOH	393.6	9R18
CH_3OD	229	9P06

The FIR radiation was directed through an evacuated brass light pipe system to the sample which was mounted in a cryostat containing liquid helium. The cryostat was mounted in the bore of a Polyhelix type electromagnet which could produce continuous fields of up to 23 Tesla. At this field the coil current would be nearly 30,000 amps and the system would consume approximately 10MW of power! The flow of

cooling water through the magnet was also astronomic: $400m^3$/min with a supply pressure of 27 bar.

The electronics used to record the photoconductive signal were similar to those used at St. Andrews and the method of biasing the sample was identical. The CO_2 beam passed through an optical chopper before it entered the FIR cavity and the signal from the chopper was used as the reference signal for the phase sensitive detector.

Background noise levels were very high and consequently the PSD was used on very narrow bandwidth setting. This has introduced some distortion and broadening of sharp impurity transitions, but as the experiments were principally to study the broad transitions from D^- states the problem was not significant.

The normal sample temperature was 4.2K but could be reduced to 1.8K by pumping on the helium. A GaAs LED mounted close to the sample was used to provide optical excitation. The excitation energy would be above that of the band gap of the sample due to the Burstein shift of the absorption edge in the heavily doped material of the LED.

Chapter 4.

Donor Identification in n-GaAs.

Central Cell Effects on the 1s-$2p_{\pm 1}$ Transitions.

The 'Effective Mass Theory' (EMT) described in Chapter 2 is able to account for the magnetic field behaviour of the energies of the shallow impurity states (particularly the excited states) in most semiconductors. It is most accurate for those semiconductors which have a small effective mass and a nearly parabolic conduction band at the gamma point (Γ) of the Brillouin Zone. Both GaAs and InP satisfy these conditions. In GaAs the difference in energy between the $2p_{-1}$ and $2p_0$ states of an isolated shallow donor in a magnetic field agrees with the theoretical predictions of effective mass theory to the extent that only one variable parameter, the effective Rydberg R^*, is required to fit the experimental data. For GaAs this was determined to be 46.10 ± 0.15 cm^{-1}, ie an error of <0.4% (Stillman, Larsen and Wolfe 1971).

However, although the energy difference between the excited states can be accurately fitted, the absolute energies of shallow impurity states can be perturbed from those of the hydrogenic EMT by a number of effects. Two of the largest contributions are due to the non-parabolicity of the conduction band and chemical shifts due to the presence of different impurity species.

Effects of Conduction Band Non-parabolicity.

Non-parabolicity is the term given to the phenomenon where the energy of a band deviates from the $E \propto k^2$ relation. This is usually expressed as a term in k^4 in the E(k) relation, or alternatively a variation in the effective mass m^* as k increases. Terms in k and k^3 may also be present. In narrow gap semiconductors the principle contribution to non-parabolicity is due to the interaction between the conduction band and the valence band system and becomes greater as the band gap decreases. This can be modelled on

a three level non-hydrogenic EMT, such as that used by Kane to describe the band structure of InSb (1957), but accurate models must take into account contributions from more distant bands (Larsen 1968). The non-parabolicity of the conduction band affects the energies of the shallow donor states since the donor wavefunctions are composed of a mixture of band states away from the Γ-point and states from other bands. According to Effective Mass Theory (see chapter 2) the donor wavefunction can be written

$$\Psi(\underline{r}) = \sum_{n\underline{k}} A_n(\underline{k})\ \Psi_{n\underline{k}}(\underline{r})$$

where if only one band is considered $A(\underline{k})$ is given by

$$A(\underline{k}) \propto [k^2 + a^{*-2}]^{-2}$$

and a^* is the effective Bohr radius of the donor state. Since $A(\underline{k})$ falls rapidly to zero for wavevectors where $k>1/a^*$ the quantity $1/a^*$ represents the extent of the wavefunction in k-space. Thus at zero magnetic field the 1s ground state, which is the most localized state in real space, has the greatest extent in k-space, and so will be most affected by the non-parabolicity of the conduction band. In high magnetic fields excited states associated with Landau levels where N>1 may also be significantly perturbed by non-parabolicity.

One important consequence of conduction band non-parabolicity is Δg-splitting (or spin splitting). In addition to changing the effective mass for excited Landau levels non-parabolicity affects the effective g-factor (g_e^*) of the electrons, and thus the effective g-factor for electrons in the N=1 Landau level is different to that for electrons in the N=0 Landau level. As the effective g-factor governs the energy difference between the two spin orientations for each Landau level (through the term $\pm \frac{1}{2}\mu_B|g_e^*|B$) the cyclotron resonance energy for transitions in the spin up ladder may be different to that for transitions in the spin down ladder, and

consequently the cyclotron resonance transition may be split.

Further, since shallow impurity states are composed of a mixture of band states they may also show a similar splitting. In practice splittings are only observed if the two states involved are associated with different Landau levels. Thus the $1s\text{-}2p_{+1}$ transition may show spin splitting but the $1s\text{-}2p_{0}$ and $1s\text{-}2p_{-1}$ transitions have spin splittings too small to be observed. The magnitude of the spin splitting on the cyclotron resonance and the shallow impurity transitions is not the same since the effective g-factor will be different for free and bound electrons. In practice in GaAs the spin splitting is greater on the cyclotron resonance than on the $1s\text{-}2p_{+1}$ transition, and both are proportional to the square of the magnetic field (Larsen 1978). Recently Zawadzki et al (1985) have shown that a simple three band $\underline{k}.\underline{p}$ theory is unable to describe the magnitude of the spin splittings in GaAs, but that a five band theory including contributions from two higher conduction bands provides satisfactory agreement with experimental results up to 22 Tesla.

Chemical Shifts of the Hydrogenic States.

Various factors contribute to a shift of the energies of neutral donor states which varies from one type of donor species to another. This is usually referred to as a 'chemical shift'. The dominant contribution to the chemical shift in semiconductors with a single conduction band minimum is usually due to 'central cell shifts'.

A central cell shift occurs if the wavefunction of a shallow impurity state has a non-zero amplitude at the impurity core. In this 'central cell region' the coulomb potential is not a good approximation to the impurity potential, and consequently the energy of a state will be perturbed from the EMT value. Since the nature of

the impurity potential in the central cell region depends on the core electron arrangement the perturbation will vary according to the chemical species of impurity which is present.

The magnitude of the energy shift due to the central cell effect can be shown to be proportional to the square of the wavefunction amplitude (the oscillator strength) at the impurity centre (Fetterman et al 1971), ie

$$\Delta E_{cc} \propto |\Psi(0)|^2$$

and hence the shift is strongest for the 1s ground state which has the greatest probability of being in the central cell region. Excited s states may also have significant shifts, though of lower magnitude than the 1s shift, but states such as the $2p_{\pm 1,0}$ states which have a node in the wavefunction at the origin will have negligible shifts (though chemical shifts of the 2p state in very high purity silicon have been detected (Ramdas and Rodriguez 1981)). In non-polar materials at zero magnetic field the ratio of the probabilities of an electron being at the origin for the 1s and 2s states is

$$\frac{|\Psi_{2s}|^2}{|\Psi_{1s}|^2} = \frac{1}{8}$$

and hence the ratio of central cell shifts on the 1s and 2s states is 8. However even in slightly polar materials the polaron interaction between the impurity and the lattice influences the oscillator strength $|\Psi(0)|^2$ and the ratio of the 1s and 2s central cell shifts may be reduced (Hönerlage and Schröder (1977) and Wasilewski and Stradling (to be published)).

Since a magnetic field compresses the impurity wavefunctions the electrons spend more time in the central cell region, resulting in increased central cell shifts. The variation of the oscillator strength, and hence the central cell shift, with magnetic field has

been calculated for the ground state by Cabib et al (1972) and is in good agreement with experiment. Cabib et al also calculated the variation of the central cell shift on the 2s state, and a comparison with experimental results can be found in Chapter 6.

The magnitude of the central cell shift is also influenced by the effective mass. In the simple theory of shallow impurities described in chapter 2 it was noted that the effective Bohr radius of a hydrogenic donor was inversely proportional to m^*. Consequently as the effective mass increases the wavefunction is less extended and so the electron will spend more time in the central cell region. Hence there will be larger central cell shifts.

Chemical shifts may also occur through other mechanisms. One is the effect of strain fields in the lattice. Strain may occur since a substitutional impurity will not be physically similar to the atom it is replacing, and the lattice spacing may change locally to accomodate it. If the impurity is an interstitial the strains will be even greater since the lattice must deform significantly to accomodate it. The strain field can produce an electric field through the piezo-electric effect, which in turn can perturb the energies of the impurity states (Fedders 1983). The effect of electric fields on shallow impurities is discussed in detail in the section on line broadening mechanisms. A further perturbation to EMT is that the dielectric constant usually depends on the wavevector $\underline{k}$, and so the use of the value for the static dielectric constant ε_0 in the expressions for the energies of the states is not a good approximation for highly localized states which are relatively extended in k-space (see eg Bassani, Iadionisi and Preziosi 1974; Pantelides 1978 for reviews of more complex effective mass theories).

Chemical shifts of the hydrogenic energy levels can be observed

directly by FIR spectroscopy of the impurity transitions. If a transition occurs between two states with different chemical shifts (eg the 1s and 2p states) then there will be a shift of the transition energy from that predicted by EMT. If a number of impurity species with different chemical shifts are present then the transition will be split into a number of components at different energies.

In addition to observing central cell shifts of the shallow impurity energy levels directly it is also possible to observe shifts by other techniques. Central cell structure has been observed by means of the magneto-impurity effect (Nicholas and Stradling 1978). This effect occurs when, as the magnetic field is swept, an integer multiple of the cyclotron energy $\hbar\omega_c$ becomes resonant with one of the hydrogenic shallow impurity transitions (eg $1s-2p_{-1}$), and resonant scattering of the carriers occurs which influences the sample resistivity.

Central cell structure has also been detected on certain lines in the near band gap photoluminescence spectrum due to the recombination of neutral donor bound excitons (Almassy et al 1981; Dean et al 1984). This technique is described in more detail in chapter 5.

In GaAs and InP the chemical shift away from the effective mass energy of the 1s ground state is $\sim 1\ cm^{-1}$. At zero magnetic field the linewidths of the narrowest impurity transitions are usually $>1cm^{-1}$ and thus it is only in the highest purity samples that splittings due to the central cell effect can be resolved.

A major contribution to the linewidth of the 1s-2p transition at zero magnetic field is due to the degeneracy of the three magnetic components $m=\pm1,0$. However when a magnetic field is applied the three components of the 2p state split and broadening due to the degeneracy vanishes. An additional advantage of applying a magnetic

field is that the impurity wavefunctions are compressed by the field which results in significant reductions in the linewidths of the impurity transitions and also results in an increase in the central cell shift of the 1s state since the electrons spend more time in the 'central cell regions'. The various mechanisms contributing to the linewidths are discussed in detail later. The overall effect of applying a magnetic field of a few Tesla is that the linewidths of transitions from the 1s to the Zeeman split $2p_{\pm1,0}$ states narrow dramatically and central cell splittings are more easily observed.

Studies of central cell structure due to the impurities present in high purity undoped (ie containing only residual impurities) and doped GaAs and InP have been carried out for a number of years now, generally using high magnetic fields up to ~10 Tesla and Fourier Transform Spectrometers (Stradling et al 1972; Stillman et al 1972 and 1976; Kirkman 1975, Cooke et al 1978; Low et al 1982a,b,c and references therein) though results taken with an FIR Laser Spectrometer have also been published (Fetterman et al 1971, 1972).

The experimental work described in this chapter concentrates first on the transition from the 1s to the $2p_{+1}$ state of neutral donors. This is in contrast to the earlier Fourier Transform studies which concentrated on the $1s-2p_{-1}$ transition, which has a smaller linewidth. Part of the extra contribution to the linewidth of the $1s-2p_{+1}$ transition is believed to be due to the $2p_{+1}$ state lying above the N=0 Landau level for magnetic fields >1.9 Tesla. Electrons can then be transferred from the bound state into the conduction band by electric field ionization or absorption of acoustic phonons, leading to a shorter lifetime for the $2p_{+1}$ state, and hence to additional broadening of the $1s-2p_{+1}$ transition when compared to the $1s-2p_{-1}$ transition. Both of these transitions are significantly

narrower than the $1s-2p_0$ transition for reasons which will be discussed later.

The reason for concentrating first on the central cell splitting of the $1s-2p_{+1}$ transition, as opposed to the $1s-2p_0$ or $1s-2p_{-1}$ transitions when using an FIR laser and swept magnetic field, is that it can be observed over a wide range of magnetic fields and laser energies, since the $2p_{+1}$ state is associated with the N=1 Landau level, while the 1s state is associated with the N=0 Landau level and thus the transition energy changes rapidly with magnetic field. In contrast the $2p_0$ and $2p_{-1}$ states are both associated with the N=0 Landau level and so the energy of transitions from the 1s state to these states changes much more slowly with field. At zero magnetic field the $1s-2p_{+1}$ transition has an energy very close to 0.75 R^*, equivalent to a wavelength of 290μm in GaAs while at a field of 7.6 Tesla the transition energy is coincident with the laser line at λ = 70.5μm (the shortest wavelength obtainable from the FIR laser system). Figure 4.1 illustrates this graphically by showing the theoretical energies of transitions from the 1s ground state to any of the n=2, 3 or 4 excited states of hydrogenic donors in a parabolic band (from the data of Makado 1982).

Even with the disadvantage of increased linewidth, studies of the $1s-2p_{+1}$ transition with an FIR laser and swept magnetic fields can still yield more information than those from Fourier Spectrometer studies of the $1s-2p_{-1}$ transition at fixed magnetic fields, due to the higher resolution and much greater signal to noise ratio of laser based systems.

However it would be desirable to be able to study the $1s-2p_{-1}$ transition with a FIR laser spectrometer, since in addition to the smaller linewidth of the transition, the low rate of change of

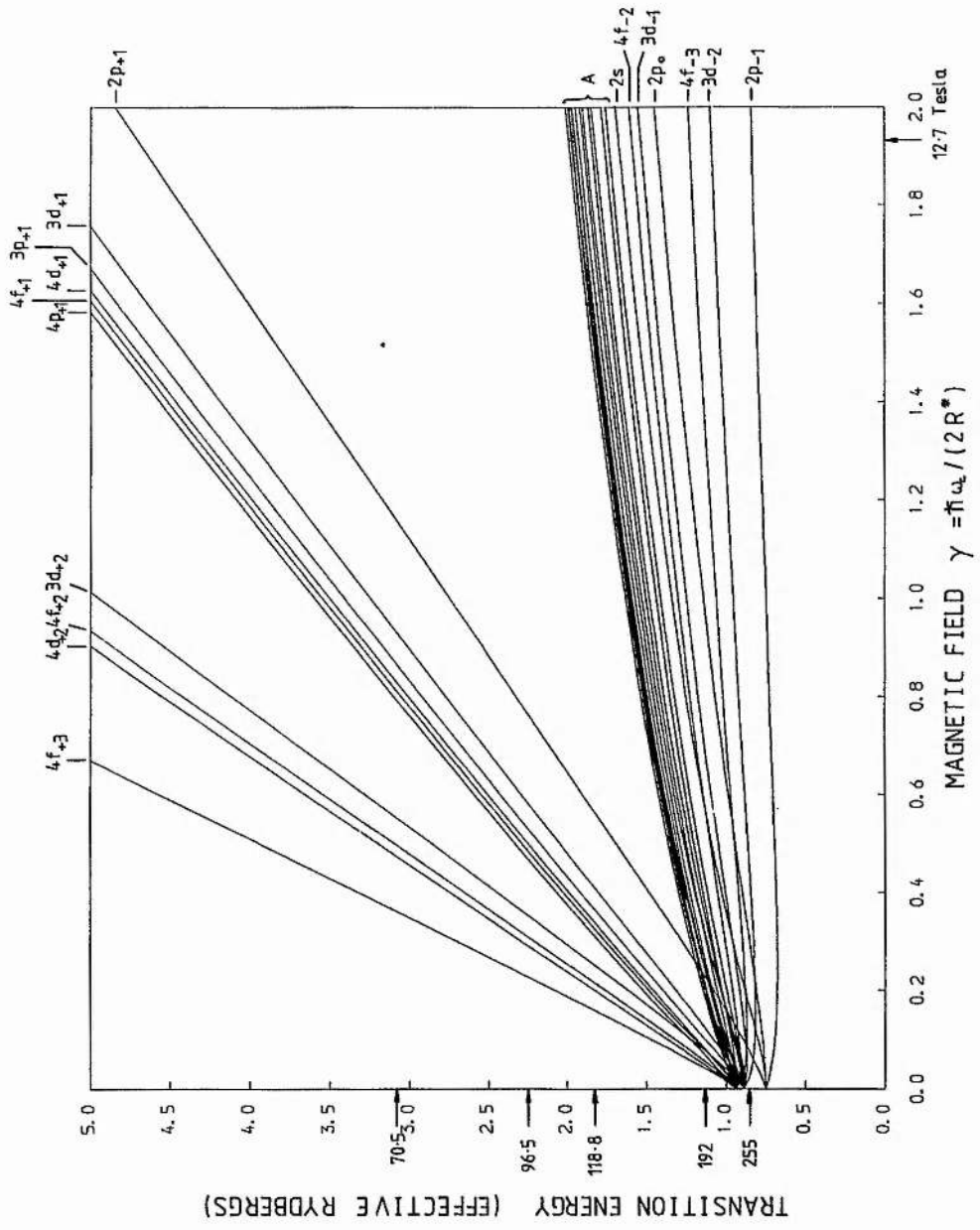

Figure 4.1: Energies of transitions from the 1s ground state of a hydrogenic donor in a parabolic band in the intermediate magnetic field region (from the data of Makado 1982). No account has been taken of selection rules and not all of these transitions would be allowed. The group of transitions labelled 'A' are from the 1s to the $3p_{-1}$, $4d_{-2}$, $3p_0$, $4d_{-1}$, $3d_0$, $4f_{-1}$, $4f_0$, 3s, $4p_{-1}$, $4p_0$, $4d_0$ and 4s states in order of increasing energy. The equivalent energies of some of the laser lines (in μm) and the 12.7T field limit for GaAs are shown.

transition energy with magnetic field ($\partial E/\partial B$) spreads the central cell structure out over a much greater magnetic field range than for the $1s-2p_{+1}$ transitions. Figure 4.2 illustrates the theoretical variation of $\partial E/\partial B$ with magnetic field for various transitions, calculated by numerically differentiating the transition energies plotted in Figure 4.1. If the transitions are spread out over a wide field range, then any inhomogeneities or errors in the field calibration of the magnet become less significant. However if the transition energy does not change rapidly with field then for a limited range of magnetic fields only a small range of laser wavelengths will be suitable. This is the case with the $1s-2p_{-1}$ transition: the available field range is from zero to 12.7 Tesla and for GaAs the wavelength of the transition must lie between λ=259 and 320μm. When the central cell effect is taken into account the wavelength region is shifted to shorter wavelengths by ~10μm. It was not until late in the author's program of research that suitable laser lines were found, initially at λ=302μm, and then at 255μm. Consequently spectra of the $1s-2p_{-1}$ transition were obtained only for the two highest purity samples. An extensive study of the central cell structure on the $1s-2p_{-1}$ transition following on from that described here has been published recently (Armistead et al 1984, Najda 1985).

However it should be noted that there are disadvantages involved in using FIR lasers compared to Fourier Transform spectrometers. Care must be taken in the interpretation of spectra obtained using lasers as parameters such as the electric field and magnetoresistance, which determine the amplitude of the photoconductive signals, can vary as the magnetic field is swept. In addition the population of the shallow impurity states varies throughout a laser recording, as the separation

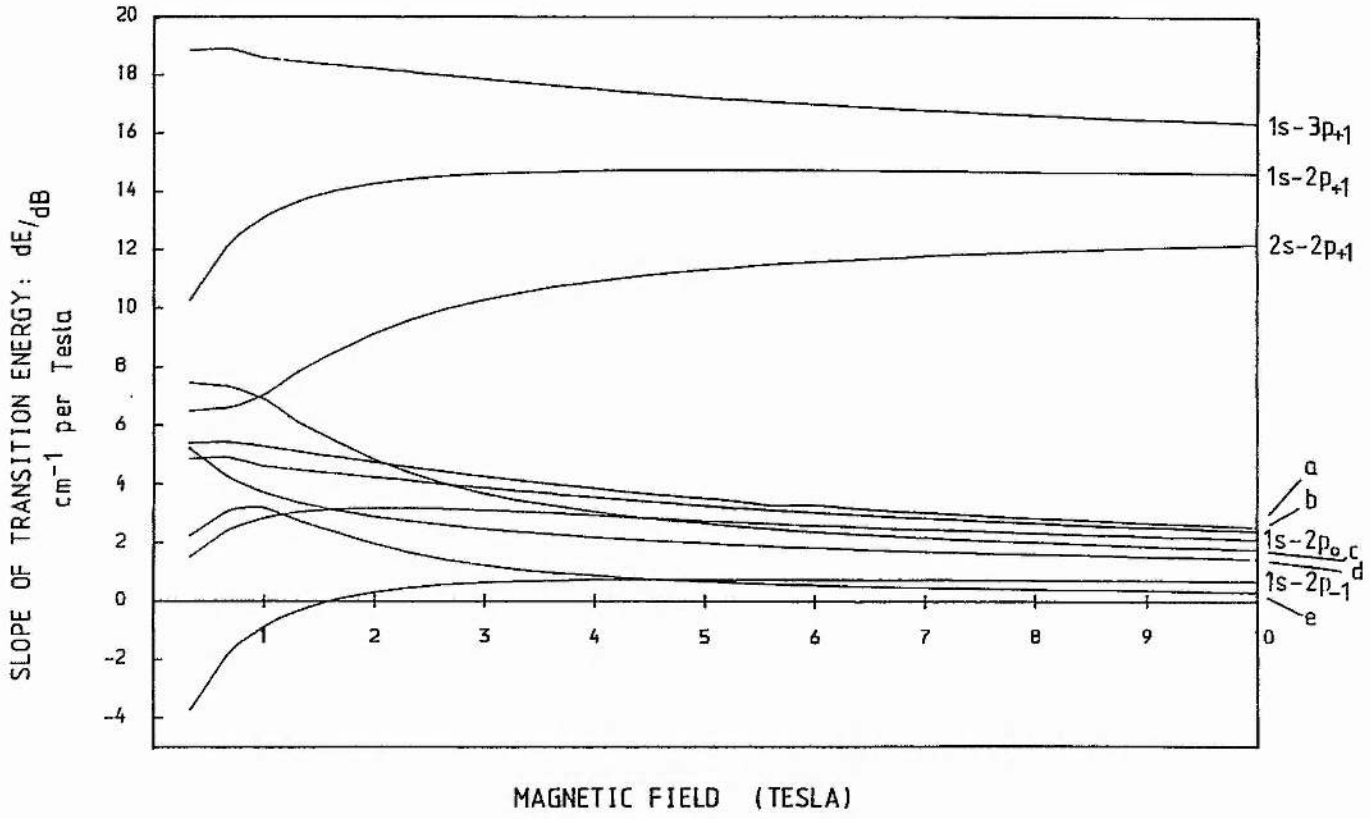

Figure 4.2: Rate of change of transition energy with magnetic field ($\partial E/\partial B$) for GaAs assuming a parabolic band with $R^*=46.1\ cm^{-1}$ and $m^*=0.0665\ m_0$ for various different transitions. The lines marked a, b, c, d and e are the $1s-3p_0$, $1s-3p_{-1}$, $2p_{-1}-2s$, $2p_{-1}-2p_0$ and $2p_0-2s$ transitions respectively. The figures were calculated by numerically differentiating the transition energies that were plotted in Figure 4.1.

of the energy levels varies with magnetic field. The population distribution may also may be modified by the presence of strong laser excitation, complicating the spectrum still further (Trager 1985). On the $1s-2p_{+1}$ transition where the central cell structure typically appears over a range of <0.3 Tesla these effects will not be significant. However this is not always the case, and for example at λ=229μm the central cell structure on the $1s-2p_{-1}$ transition falls between 14.5 and 20 Tesla and so great care must be taken when comparing the relative amplitudes of the central cell components. These problems do not occur in studies using Fourier Transform Spectrometers since the magnetic field is constant and the radiation is much weaker.

Linewidths of Transitions Between Shallow Donor Energy Levels.

Broadening of the transitions between shallow impurity energy levels can occur for a variety of reasons, eg the electron phonon interaction, lifetime effects, broadening due to interactions between near neighbour impurities etc. However in high purity material with impurity concentrations $<10^{15}$ cm^{-3} the dominant broadening mechanism is due to Stark shifts of the neutral donor energy levels as a result of the electric fields from ionized impurities (Larsen 1973). Ionized impurities will always be present as a result of the compensation process: in any semiconductor, whether intentionally doped or containing only residual impurities, there will be both donors and acceptors present. If the donor concentration is larger than the acceptor concentration then the material is of course n-type, the acceptors are the compensating impurities and the compensation ratio is given by $K = N_A / N_D$ (and vice versa for p-type material). At temperatures where the donor ionization energy is

considerably greater than the thermal energy the electrons 'freeze out' onto the donor sites. If acceptors are present then the electrons can relax further so that all N_A acceptor sites are negatively charged. There will then be N_A positively charged donor sites (D^+ states) and only $N_D - N_A$ neutral donors (D^0 states) in the crystal, ie

$$N_D{}^o = N_D - N_A = (1 - K)\, N_D$$

and $$N_{ions} = N_D{}^+ + N_A{}^- = 2\, N_A = 2\, K\, N_D$$

since $N_D{}^+ = N_A{}^-$, where N_{ions} is the population of charged centres and $N_D{}^o$ is the population of neutral donors.

To a first approximation the distribution of donors and acceptors is random, as is the distribution of ionized donor and acceptor sites. The ionized impurities can be regarded as point charges and create strong electric fields within the lattice which interact with the neutral donors and perturb the energy levels through the Stark effect. As the impurity distribution is random the distribution of the electric field values at the neutral impurity sites is also random. Consequently the Stark shift on the energy levels is random and the overall effect is a broadening of the energy levels.

For a dilute collection of donors and acceptors, with concentrations $\sim 10^{14}$ cm^{-3}, there are two different types of electric field broadening: one proportional to the difference in the quadrupole moments of the two states involved, and the other due to the quadratic Stark effect (Larsen 1973). The restriction to dilute concentrations arises since one must assume that the donors are non-interacting and that the electric field is constant over the spatial extent of the wavefunction. Then when the electrostatic potential $\phi(\underline{r})$ at the neutral donor site is expanded as a Taylor series

$$\phi(\underline{r}) = \phi(0) + \underline{r}.\nabla\phi + \left\{x^2\frac{\partial^2}{\partial x^2} + y^2\frac{\partial^2}{\partial y^2} + z^2\frac{\partial^2}{\partial z^2}\right\}\phi(0) + \ldots.$$

the higher order terms represented by .... can be ignored. The perturbation on an energy level ϵ_i due to this potential, to first order, can be written

$$\Delta\epsilon_i^{(1)} = e\left\langle\Psi_i|\phi(\underline{r})|\Psi_i\right\rangle$$

where Ψ_i is the wavefunction of the state i. For a simple hydrogenic impurity all the states have definite parity and so odd parity terms in the expansion of $\phi(\underline{r})$ will not contribute to $\Delta\epsilon_i$. Thus there will be no contribution from the linear Stark effect term $\underline{r}.\nabla\phi = -\underline{E}.\underline{r}$. The static potential term $\phi(0)$ can also be neglected since it shifts the whole energy level system up or down by the same amount and does not change the transition energies. This leaves only the last term in $\phi(\underline{r})$, which as a result of the cylindrical symmetry of $\phi(\underline{r})$ about the electric field direction, and the fact that the charges are discrete and none are at $\underline{r}$=0, can be rewritten as

$$\phi(\underline{r}) = -0.5\ (z^2 - 0.5\ \rho^2)\frac{\partial E_z(0)}{\partial z}$$

where $\rho^2 = x^2 + y^2$.

Thus the energy shift to first order is

$$\Delta\epsilon_i = -0.25\ Q_i\frac{\partial E_z(0)}{\partial z}$$

where $Q_i = e\left\langle\Psi_i|2z^2-\rho^2|\Psi_i\right\rangle$ is the quadrupole moment of the state. A difference in transition energy T_{i-j} can then occur if the quadrupole moments of the initial and final states are different:

$$T_{i-j} = \Delta\epsilon_j - \Delta\epsilon_i = -0.25\ (Q_j - Q_i)\frac{\partial E_z(0)}{\partial z}$$

When account is taken of the statistical distribution of the quantity $\partial E_z(0)/\partial z$ the lineshape is found to be Lorentzian and

centred on the unperturbed transition energy. This mechanism is known as quadrupole broadening or field gradient broadening. Figure 4.3 shows the quadrupole moments of a number of states of hydrogenic donors (after Larsen 1973). It can be seen that the 1s and $2p_0$ states have significantly different quadrupole moments and in practice the lineshape is found to be in good agreement with that calculated on the basis of quadrupole broadening.

However it is also found in practice that the linewidths and lineshapes of the $1s-2p_{\pm1}$ transitions are quite different from that of the $1s-2p_0$ transition, with the $1s-2p_{-1}$ in particular being considerably narrower and strongly asymmetric. Inspection of the quadrupole moments for the 1s and $2p_{\pm1}$ states in Figure 4.3 shows that for a range of fields on either side of $\gamma\sim0.8$ the moments are almost equal. Since the broadening depends on the difference between the moments of the two states it is expected that the linewidth due to this mechanism would be small and some other contribution may dominate.

Although the linear Stark term $-\underline{E}.\underline{r}$ in the expansion of the potential $\phi(\underline{r})$ was ignored in the first order approximation it will still cause strong distortion of the impurity wavefunction. Thus to include the effect of the linear Stark term second order perturbation theory is required since this takes into account the mixing of wavefunctions. The energy shift to second order is given by

$$\Delta\varepsilon_i^{(2)} = e^2 \sum_j \frac{\left| \left\langle \Psi_j | \phi(\underline{r}) | \Psi_i \right\rangle \right|^2}{E_j - E_i}$$

$$\simeq e^2 \sum_j \frac{\left| \left\langle \Psi_j | -\underline{E}.\underline{r} | \Psi_i \right\rangle \right|^2}{E_j - E_i}$$

The inclusion of the linear Stark term also has the effect that states of opposite parity may be mixed together: for example the 2s state will interact strongly with the $2p_{\pm1}$ states at low magnetic fields when the states are nearly degenerate, repelling them in

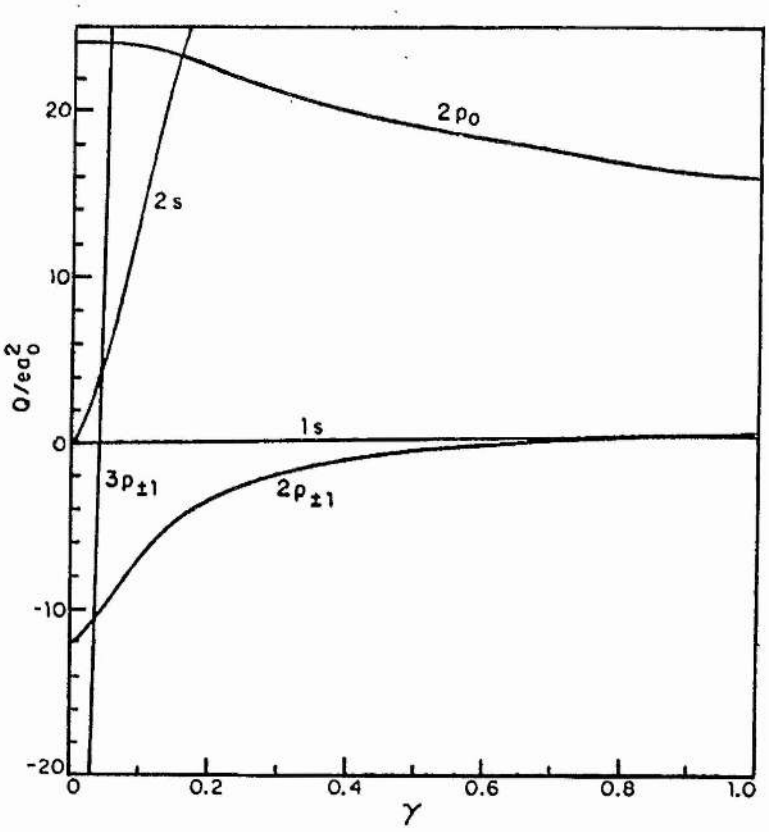

Figure 4.3: The quadrupole moments in units of ea_0^2 of various shallow impurity states in a dimensionless magnetic field (from Larsen 1973).

energy. This repulsion of the $2p_{\pm1}$ states at low magnetic fields is observed experimentally as an anomalously low effective mass if the effective mass is calculated from the Zeeman splitting of the $2p_{+1}$ and $2p_{-1}$ states ($E(2p+1) - E(2p-1) = \hbar\omega_c$): this is known as the 'mass anomaly' (Stillman et al 1971). In addition, since states of opposite parity (eg the 2s and $2p_{\pm1}$ states) are mixed together, transitions that are normally forbidden from parity considerations become weakly allowed. In this way the 1s-2s transition can be observed experimentally (eg. Figure 7.11). This perturbation, since it is quadratic in the electric field, is referred to as the quadratic Stark effect.

As is the case with quadrupole broadening the distributions of electric fields at the neutral donor sites determines the quadratic Stark lineshape, which for the $1s-2p_{-1}$ transition is strongly asymmetric with a long tail on the low energy side and a sharp edge on the high energy side. Furthermore the actual peak position is shifted to the low energy side of the unperturbed transition energy. Since the shift depends on the linewidth which in turn depends on the concentration of ionized impurities, it is both concentration and compensation dependent. However the shift is estimated to be only ~20% of the linewidth (Larsen 1973) and so it is only likely to be apparent in very high resolution spectra.

Effect of Intrinsic Illumination.

If radiation with energy greater than the band gap (referred to variously as optical pumping/excitation, intrinsic excitation or band gap radiation) is directed onto the crystal then electrons are excited from the valence band to the conduction band, leaving free holes in the valence band. These free electrons and holes may diffuse through

the crystal before recombination occurs. This might be through the formation of free or bound excitons, or through capture at ionized impurity sites followed by donor-acceptor pair recombination or alternatively non-radiative mechanisms such as Auger recombination.

Donor-acceptor pair recombination rates will vary depending on the nature of the energy gap and the impurity concentration. In direct gap semiconductors the process can be very fast, but in indirect gap semiconductors a phonon is required in the process, significantly reducing the probability of the interaction occurring. At high impurity concentrations the donor wavefunction is more likely to overlap with an acceptor wavefunction and so donor-acceptor recombination is more likely to occur.

Capture of carriers at charged impurity sites must occur before donor-acceptor pair recombination can take place. Thus a reduction in the number of ionized sites can occur and so the average electric fields within the crystal may fall, resulting in a reduction in the linewidths of the impurity transitions. However if donor-acceptor recombination is very fast, such as at high impurity concentrations in direct gap materials, no significant change in ionized impurity population may occur. Thus the benefits of band gap illumination become greater as the impurity concentration decreases, and unfortunately it is found experimentally that significant reductions in the linewidths of the shallow impurity transitions are only observed in the highest purity samples.

In addition to neutralizing a substantial portion of the ionized impurity population in compensated material, and thereby reducing the linewidths, optical pumping can substantially alter the intensity of the inter-excited state transitions. This results from the fact that the capture of photoexcited carriers by ionized impurities occurs by a

cascade process through the excited states rather than direct capture to the ground state. Thus in the presence of band gap excitation the excited state population may be significantly different from the equilibrium thermal populations in the absence of excitation. As the excited states have more extended wavefunctions than the ground state, and are thus more affected by the electrostatic fields in the lattice, the reduction in ionized impurity concentration with optical excitation can cause substantial reductions in the linewidths of the inter-excited state transitions. Inter-excited state transitions are studied in more detail in Chapter 6.

In addition to reducing the linewidths of the shallow impurity transitions and changing the intensities of the inter-excited state transitions, band gap radiation can also change the relative intensities of the central cell components. A number of explanations for this have been put forward and most assume that the spatial distribution of donors and/or acceptors is not random leading to either a particular donor species being excited preferentially, or alternatively the donor-acceptor pair recombination rate varying with impurity species.

The first effect would occur if a sample had an impurity species whose distribution was graded through the sample thickness. For example, there might be a high concentration of one impurity at the surface or the interface with the substrate. When band gap excitation is used the light is strongly absorbed and so only penetrates a small distance into the sample, approximately 1 or 2 μm. A reduction in linewidth may only occur for transitions originating near the surface of the layer, where the ratio of one impurity species to another might be different from the rest of the layer. As band gap radiation increases the carrier concentration the resistance of the surface

layer is lowered compared with the bulk material and the bulk material can be 'short circuited'. Thus the photoconductivity spectrum may only be representative of the surface layer. The extent of this surface layer depends on how far the photo-excited carriers can diffuse from the surface before trapping or recombination occurs. In photoluminescence experiments, where the excitation energy may be substantially above the band gap, it is known that the luminescence is only characteristic of the first few microns of the layer (Dean and Skolnick 1983).

The second effect that was noted was the possibility of the lifetime of the neutral donors being different for different impurity species. Although the illumination is continuous there is a steady state condition achieved in the samples which involves a continuous process of photo- excitation, capture at an ionized impurity and then donor-acceptor pair recombination. If a particular donor species is preferentially located near acceptors then the donor-acceptor pair recombination rate is likely to be greater than that for isolated donors, and the change in the neutral donor population on illumination with band gap radiation will not be as great as it would be for an isolated impurity.

In this discussion no mention has been made of the effect of below gap radiation. This is more difficult to treat since excitation can occur directly to free- and impurity bound- exciton states as well as to donor-acceptor pairs. A considerable amount of work on selective excitation of these states has been performed using photoluminescence techniques, though mostly on InP (Skolnick and Dean 1982; Dean and Skolnick 1983 and Dean, Skolnick and Taylor 1984; a brief explanation of this work is given in Chapter 5). In principle the selective excitation techniques used by Dean and co-workers ought

to yield reductions in the FIR transition linewidths. Unfortunately insurmountable problems with a near infrared dye laser system prevented any selective excitation experiments being performed.

Effect of Temperature on the Linewidths of Shallow Impurity Transitions.

The model of line broadening discussed so far, and due principally to Larsen, predicts lineshapes for the $1s-2p_0$ and $1s-2p_{\pm1}$ transitions which are in excellent qualitative agreement with those observed experimentally in very high purity samples ($N_D \sim 10^{14} cm^{-3}$). However quantitative values for the ionized impurity concentration deduced by fitting theoretical lineshapes to the experimental lineshapes were much lower than those deduced from measurements on the electrical transport properties.

A mechanism explaining this also contributes to the reduction in linewidth which occurs as the sample temperature is reduced below ~10K. Provided that broadening due to the electrostatic fields of ionized impurities is the dominant mechanism there should be no change in the linewidth as the temperature is reduced once freeze-out is complete, provided that the ionized impurity distribution is random. The decrease in linewidth observed experimentally has been attributed to an increase in the correlation between the sites of ionized donors and acceptors as the temperature is reduced (Golka et al 1977 and Fedders 1982). Consider two ionized donors D^+ close to an ionized acceptor A^- at absolute zero. If an electron is in the vicinity of this system it will be trapped onto the donor state furthest from the acceptor, since the electrostatic repulsion from the coulomb field of the acceptor is lower. Thus at low temperatures the preference is for ionized donors to be located close to ionized acceptors, constituting

a dipole system. The situation in which the neutral donor is closest to the acceptor has a higher energy and so will become thermally populated as the temperature increases, and so the average $D^+ - A^-$ separation will increase. As the temperature increases still further the distribution approaches that of a random distribution. Consequently, since the electrostatic field of an electric dipole decays more rapidly than that from a point charge, the average electric field at low temperatures, and hence the linewidth, will be smaller than that predicted by a purely random arrangement of ionized sites. Thus an attempt at fitting the lineshapes with a model based on a random impurity distribution would produce values for the ionized impurity concentration lower than that obtained from electrical measurements.

More recent calculations made on the 1s-2p lineshape at zero or low magnetic fields ($\gamma<0.05$) which take this correlation into account show that the linewidth is significantly reduced, and obtain a much better agreement with experiment (Kogan and Van Lien 1981). Unfortunately these calculations do not cover the intermediate magnetic field regime ($\gamma\sim1$) where Larsen performed his calculations, and where the results presented in this thesis were taken.

Complexes.

The model which has been discussed so far is based on the assumption that the impurity assembly is sufficiently dilute that the donors do not interact with each other and the electric fields are constant over the spatial extent of the donors. Thus in the concentration regime where $N_D + N_A > 10^{14}$ cm^{-3}, where these approximations are not valid, Larsen's theory begins to break down. Such concentrations are still well below the level at which impurity

banding begins to occur and where the metal - insulator transition takes place ($\sim 10^{16}$ cm^{-3}).

However even in the very dilute regime of $\sim 10^{14}$ cm^{-3} the random distribution of the impurities will place some of the neutral donors close enough together to create a significant interaction. This effect can be examined in terms of the molecular model of Bajaj et al (1975). This model is sometimes referred to as the charge transfer model (see eg Thomas et al 1981). In the molecular model the energy levels of the free space neutral hydrogen molecule H_2^0 or the hydrogen molecular ion H_2^+ are scaled, in a similar manner to that for neutral hydrogen when studying neutral donors, using the effective mass and dielectric constant for the semiconductor. It is found that the energy of some of the transitions is relatively independent of the inter-donor separation. When account is taken of the probability distribution for the impurity separations a moderately sharp line can be observed in spite of the random nature of the inter-nuclear separations. Lines attributable to transitions in the hydrogenic molecules D_2^0 and D_2^+ have been observed at energies of ~ 0.6 R^* in GaAs. Similar states have been observed in InP (Reeder et al 1986). However as the interaction between the molecules depends strongly on the overlap of the wavefunctions, the intensities and energies of any transitions will be strongly dependent on the magnitude and orientation of an applied magnetic field. The transitions observed by Bajaj et al and attributed to these molecular states decreased in amplitude rapidly as a magnetic field was applied and had vanished by 1 Tesla.

Peak Inversion or Notch Effects in Shallow Donor Spectra.

In spite of the numerous studies of the central cell structure of

undoped and doped GaAs which have been made since the early 1970's, there is still considerable uncertainty over the assignments of specific donor species to the individual central cell components. Even the dominant central cell component X_2, seen in almost all undoped samples irrespective of growth technique, has had its assignment changed from silicon to sulphur as recently as 1982 (Low et al 1982c).

There are numerous reasons which contribute to the uncertainties in assigning a particular impurity species to a central cell component. Firstly, although sharp central cell components are seen in very high purity undoped material, samples back doped with a particular impurity species invariably have a higher impurity concentration and significantly broader central cell components. The doping must be sufficiently strong so that the desired impurity species can be positively identified from other background contaminants (whose concentration may also be inadvertantly increased), but not so strong that the central cell components broaden so far that no structure can be resolved at all. Unfortunately the range of suitable concentrations is very small and few back doped samples show unambiguous central cell structure.

A further problem with back doped samples is that the application of band gap radiation does not have as great an effect on the linewidths as in high purity undoped samples, since the higher doping level leads to faster donor-acceptor recombination rates and thus relatively small changes in the ionized impurity concentration.

However in addition to these general problems of working with back doped samples there is a further effect which can lead to confusion over the origin of peaks in the central cell structure. This is the 'peak inversion' or 'notch effect', where a single central cell component is distorted so that it has two peaks separated by a minimum

at approximately the position where the maximum should have occurred. Although the effect has been seen in a number of samples studied by groups at Oxford and St. Andrews it has only recently been acknowledged in the literature (Low et al 1983b). The major problem associated with identifying its origin has been the apparently random way in which it affects samples. Some samples may be completely unaffected, whereas others may show 'notching' on only one of the central cell components, and some may be distorted beyond recognition.

Various mechanisms have been proposed to account for these effects, and usually involve some quirk of the photoconductivity mechanism. Bad contacts can give noisy spectra, and generate unwanted photovoltaic or bolometric signals. Alternatively, negative photoconductivity could create a notch, and has been shown to arise from the presence of compensating impurities, where the sign of the photosignal was found to depend on sample thickness (Kaplan et al 1968). As the apparent sample thickness could be influenced by the magnetic field or the application of band gap illumination it might be possible to observe size effect resonances in the extrinsic absorption at various combinations of laser wavelength, magnetic field and light intensity etc.

However these explanations were rather hypothetical. The problem of peak inversion has been put on a much more rigorous basis by the work of Stillman, Low and Lee (1985). Normally it is assumed that as the impurity concentration is very low the absorption of extrinsic radiation is very small, and consequently the behaviour of the material is not changed in the presence of FIR radiation. Stillman et al have shown that in fact this is not true: even in very high purity material the absorptance of a sample can be very high, almost unity, and consequently the dielectric response of a sample close to an

impurity transition is very frequency dependent. The effect can be so great that the complex dielectric constant can cross over from positive to negative values, at which point a sharp notch can appear in the absorption spectrum. Stillman et al modelled the dielectric response function and were able to calculate the absorption spectrum in the vicinity of an impurity transition, and generate notching effects with various degrees of severity.

Their model predicts structure on the central cell peaks which is in good agreement with that observed experimentally in certain samples. In particular their model predicts that notching becomes more severe as the sample thickness is increased, as the impurity concentration is increased, and as the imhomogeneous linewidth decreases. The latter effect can lead to an increase in the severity of notching if a magnetic field is applied or if band gap illumination is applied or if the sample temperature is reduced since all these effects can result in reductions in the inhomogeneous linewidth.

Stillman et al were able to demonstrate experimentally the increase in notching as the magnetic field or sample thickness is increased. One of the principle implications of this work is that studies of the central cell structure must be made on relatively thin samples, of the order of 10μm in order for meaningful results to be obtained. Much of the work described in the following sections of this chapter provides detailed confirmation of their work.

Experimental Results.

Five samples of very high purity epitaxial n-type GaAs have been studied. The electrical characteristics of these samples are given in Table 4.1. Mobilities and ionized impurity concentrations have generally been obtained from Hall analyses performed by the crystal growers. A detailed description of the Hall analysis for the sample RR98B has been published (Colter, Look and Reynolds 1983; Look and Colter 1983).

The samples can be divided into three groups according to the growth technique. These are

i Molecular Beam Epitaxy (MBE). MBV20 and MBV380 are fairly typical samples produced by MBE, with mobilities of the order of 50000 $cm^2V^{-1}s^{-1}$. Both samples were cloverleaf structures and were supplied with the electrical contacts already in place.

ii Liquid Phase Epitaxy (LPE). The one sample in this group, R137, is an exceptional example of the LPE growth technique since its central cell structure shows that there is only one major residual contaminant. However the electrical characteristics quoted are not as good as those of material produced routinely a number of years ago (which had 200,000 $cm^2V^{-1}s^{-1}$ mobilities at 77K).

iii Vapour Phase Epitaxy (VPE). Both RR98B and S1 are samples which represent the 'state of the art' for VPE growth. S1 has very high mobility and low impurity concentration, while RR98B has a very low compensation ratio (~0.05). Apparently the reduction in the residual acceptor concentration in RR98B was achieved by baking out the gallium source at high temperatures prior to the growth run. Prior to the use of the bake-out procedure photoluminescence studies showed that the dominant acceptor was

Table 4.1.

Electrical Characteristics of the GaAs Samples.

Sample	Growth Technique	Source	$N_D - N_A$ cm^{-3}	Mobility (77K) $10^3\ cm^2V^{-1}s^{-1}$
MBV20	MBE	Phillips	7×10^{14}	49
MBV380	MBE	Phillips	3×10^{14}	55
R137	LPE	Max-Planck	1×10^{13}	150
S1	VPE	Motorola	5×10^{13}	160
RR98B	VPE	Wright Patterson AFB	2×10^{14}	163

RR98B has a very low compensation ratio: ~0.05.

zinc but no zinc could be detected in runs using the bake out procedure. The impurity concentration profile for RR98B is shown in Figure 4.4. From this profile it is clear that RR98B has quite a thick layer of ~30μm.

The combination of very low compensation and high purity in RR98B was such that a second peak in the mobility versus temperature curve could be seen at a temperature of ~9K (shown in the inset to Figure 4.4 after Look and Colter 1983). This second mobility peak, which had not previously been observed in III-V materials, occurs as ionized impurity scattering is reduced as electrons freeze out onto the impurity sites.

All the material was undoped and contained only residual impurities and was grown on semi-insulating substrates. With the exception of the two MBE samples, electrical contacts to the samples were made by alloying indium dots to the epitaxial surface using the procedure described in Chapter 3. All the experiments were performed by measuring the photoconductivity as a function of magnetic field at temperatures of 4.2 or 1.8K.

In Figure 4.5 the spectrum of the $1s-2p_{+1}$ transition for each of the samples is shown. The recordings were taken with a laser wavelength of 118.8μm and at 4.2K and the samples were illuminated with intrinsic radiation from a quartz halogen lamp.

For the two MBE samples (MBV20 and MBV380) the $1s-2p_{+1}$ peak is rather broad and the central cell components are not well resolved. However it is clear that both samples contain two components. More unresolved components may also be present. The peak positions of MBV20 are at slightly higher magnetic field than those in MBV380 and both samples have an asymmetric lineshape with a longer tail on the high

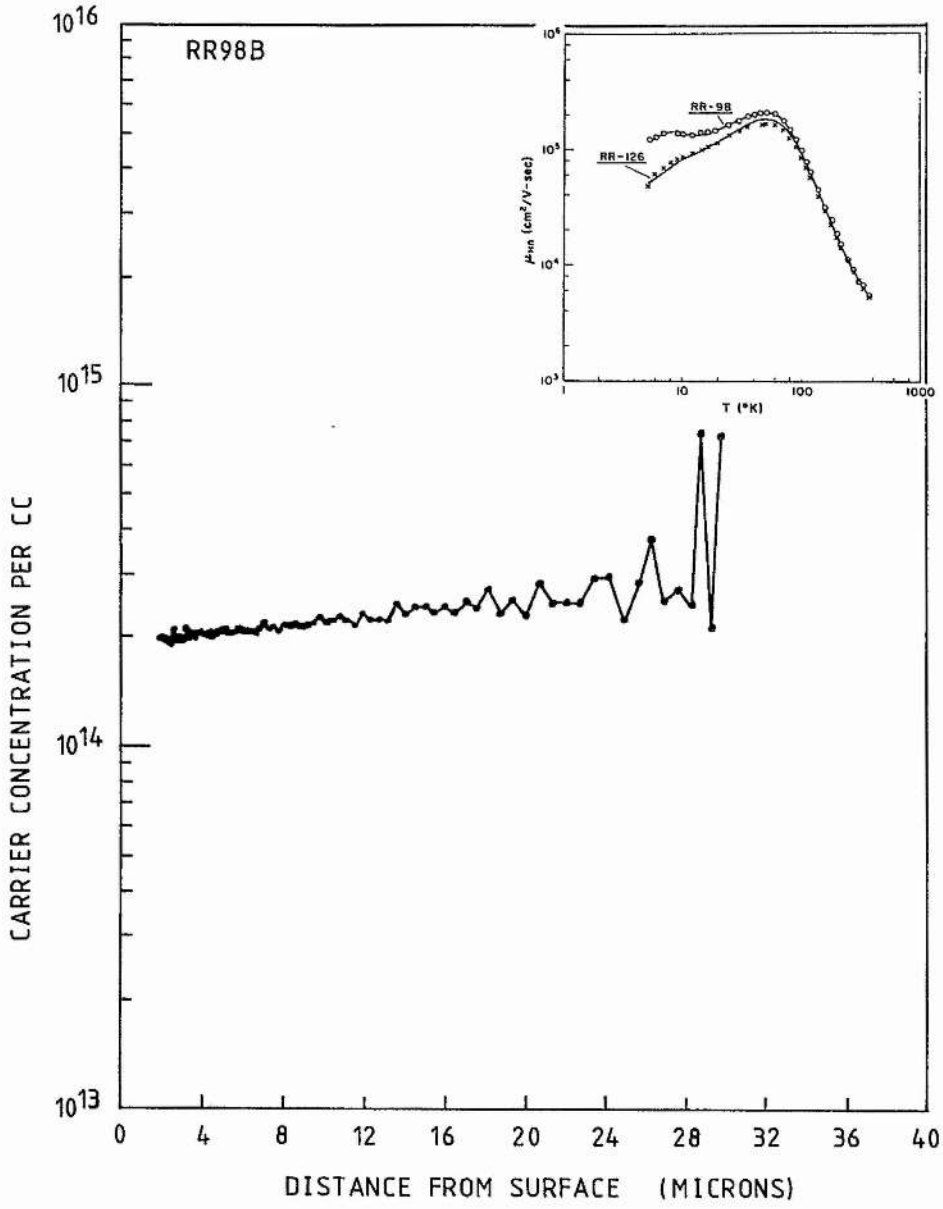

Figure 4.4: Carrier concentration against depth for sample RR98B (Colter, unpublished). The inset diagram shows the Hall mobility against temperature for RR98B. Note the second peak in the mobility at ~9K due to a decrease in the ionized impurity scattering as carriers freeze out and neutralize the donors (from Look and Colter, 1983).

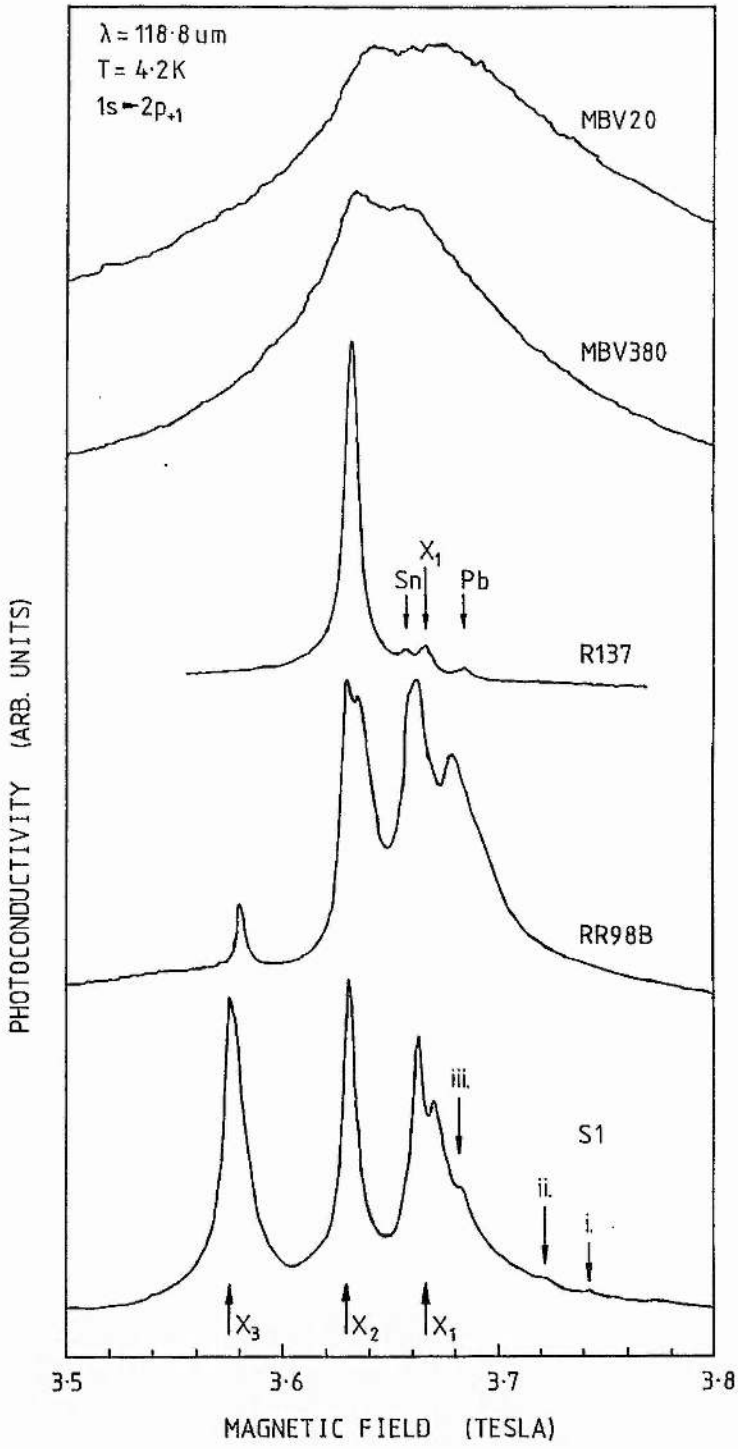

Figure 4.5: Spectra of the central cell structure of the $1s-2p_{+1}$ transition for the five n-GaAs samples using an FIR laser wavelength of 118.8μm. The sample temperature was 4.2K and the samples were illuminated with band gap excitation from a quartz halogen lamp. The currently accepted impurity identifications are: X_1 - Si, X_2 - S and X_3 - Ge.

magnetic field side. As the transition linewidth in MBV20 is significantly greater than that in MBV380 this shift in peak position and the asymmetry is probably a consequence of the quadratic Stark broadening mechanism discussed earlier. The low magnetic field component can be positively identified as the donor X_2 which is present in the other three samples, and which has been associated with sulphur donors. Originally X_2 was identified as silicon, but more recent work with back doped samples has resulted in the reassignment of X_2 to sulphur while X_1 has been identified as silicon (Low et al 1983a,b,c; Ozeki et al 1977). The identity of the high field donor is not clear, and it could be due to either of the components identified as Sn and X_1 (silicon) which are clearly resolved in the LPE sample R137. Other donors, eg selenium, may also appear in this region (Armistead et al 1984). Low et al (1982a) have made a detailed study of high purity MBE material (with 77K mobilities up to 110000 $cm^2V^{-1}s^{-1}$) and found that X_2 (S), Sn, X_1 (Si) and Pb were all present in undoped material. They also found that significant differences in the relative concentration of X_1 (Si) between samples could be correlated with differences in the temperature of the quartz cracking furnace, suggesting that the hot quartz furnace walls were a major source of silicon donors.

The middle trace of Figure 4.5 shows a spectrum of the LPE sample R137. Only one donor, X_2 (sulphur), is present in significant quantities, with three other donors being present below the 10% level of integrated intensity. However in most samples of undoped LPE GaAs only the three residual donors Pb, Sn, and S (X_2) are present in order of increasing central cell shift (Cooke et al 1978, Skromme et al 1982). The X_1 (Si) component present in R137 is usually absent in LPE material, but is always present in significant quantities in VPE

material (as seen in RR98B and S1). However a spectrum of an LPE sample from a different laboratory has shown almost identical structure to that of R137 (Skromme et al 1982). Silicon is expected to be a strong contaminant in VPE material, since considerable quantities are present in VPE reactors in the form of quartz fittings and during growth the slice is continually exposed to a gas stream which has flowed over these surfaces. However although there are also large amounts of quartz in LPE reactors the epitaxial surface is protected by the liquid melt during growth and is not exposed to a hot gas stream. In fact the early very high purity LPE material grown at STL (Harlow) was grown in a quartz boat, but showed no X_1 (Si) central cell component, and the central cell structure of material grown in quartz and graphite boats is very similar (Skromme et al 1982). However silicon contamination could still occur if the source materials were not sufficiently pure.

The 'full width at half height' linewidth (henceforth FWHH) of the X_2 peak in R137 is 0.008T, and the slope of the $1s\text{-}2p_{+1}$ transition at 3.63 Tesla (γ=0.55) is 14.7 cm^{-1}/T. Thus the linewidth in energy is 0.12 cm^{-1} (FWHH). Comparing the spectrum of R137 with the others in Figure 4.5 reveals that although the individual central cell components in the VPE sample S1 might have a marginally smaller linewidth, the presence of a number of central cell components results in an overall width much larger than that of R137 and thus R137 is the sample with the smallest overall linewidth. This makes R137 an almost ideal sample to use as a narrow band FIR detector, and it has been used in this way to observe FIR cyclotron emission from GaAs (see eg Gornik 1982).

The remaining two recordings in Figure 4.5 show the VPE grown samples RR98B and S1. As the structure in these two samples is

strongly dependent on the intensity of intrinsic illumination, the spectra of the two samples at various levels of illumination have been shown separately in Figure 4.6.

Without band gap illumination (traces i and iv) both samples show the three donors X_1, X_2 and X_3 characteristic of VPE material. X_3 is usually associated with germanium, X_2 with sulphur and X_1 with silicon. The peaks are almost symmetric and approximately equally narrow. A shoulder on the high field side of X_1 in RR98B indicates the possible presence of a fourth donor.

When band gap radiation is incident on the samples the linewidths are reduced and the spectrum in the region of donor X_1 splits so that two donors appear to be resolved. However the magnitude of the splitting in the two samples appears to be different. In S1 a further three donors labelled i, ii and iii appear. The deepest of these three donors which appear with optical pumping, donor iii, is likely to be the donor labelled as lead observed in R137 in Figure 4.5 and which has been previously reported at low levels in VPE material (eg Stillman et al 1976). The remaining two donors i and ii have not previously been reported in GaAs. However studies of the central cell structure of InP have shown up to 12 central cell components, some of which had very shallow shifts (Davidson et al 1980; Armistead et al 1982, 1984 and Chapter 5 of this thesis). Thus the appearance of similar components with shallow central cell shifts in GaAs is not particularly surprising.

The absolute central cell shifts of the donors can be estimated as follows. In the absence of illumination the peaks of the X_3, X_2 and X_1 central cell components of sample S1 are at 3.577, 3.632 and 3.667 Tesla respectively. The peaks of the three components iii, ii and i which appear with band gap illumination are at 3.683, 3.722 and

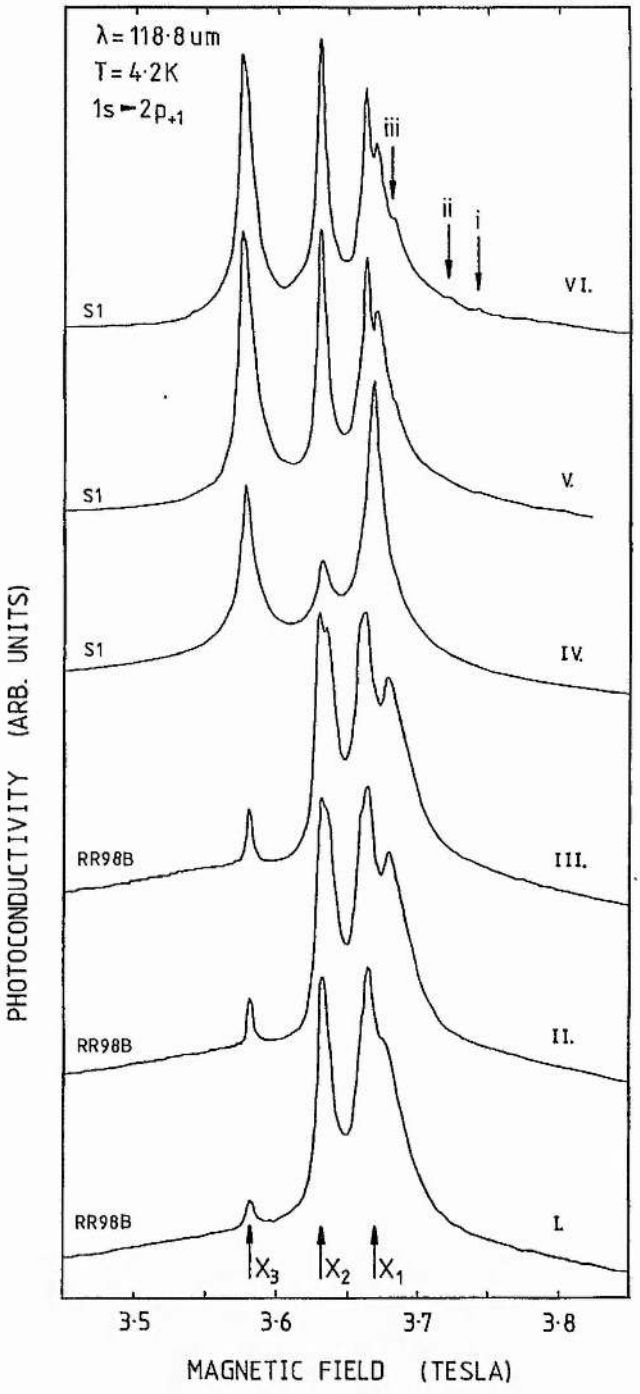

Figure 4.6: Spectra showing the $1s-2p_{+1}$ central cell structure for the two VPE samples at T=4.2K under various conditions of illumination with optical excitation. The laser wavelength was 118.8μm. The traces are: i: RR98B, no illumination; ii: RR98B, medium illumination; iii: RR98B, strong illumination; iv: S1, no illumination; v: S1, medium illumination; and vi: S1, strong illumination.

3.742 Tesla respectively. In Table 6.2 below the splitting of each donor from the X_3 donor is calculated in Tesla. This field splitting is converted to the energy splitting in cm^{-1} at the mean magnetic field of the transition assuming $\partial E/\partial B = 14.7\ cm^{-1}/T$. The theoretical work of Cabib et al (1972) giving the variation of the oscillator strength of the 1s state with magnetic field (see Figure 6.1) indicates that the central cell splitting at the mean magnetic field of 3.6 Tesla is 1.2 times greater than at zero magnetic field, so the mean field splitting is divided by 1.2. Cooke et al (1978) reported that the absolute central cell shift of the X_3 donor is $+1.6\ cm^{-1}$, and so the absolute central cell shift at zero magnetic field for each donor can be obtained.

Table 6.2

Donor	Magnetic Field	Splitting X_3 - Donor			Absolute central
		at mean field		at B=0	cell shift
	Tesla	Tesla	cm^{-1}	cm^{-1}	cm^{-1}
X_2	3.631	0.054	0.79	0.66	+0.94
X_1	3.667	0.090	1.32	1.10	+0.50
iii	3.683	0.104	1.53	1.27	+0.33
ii	3.722	0.145	2.13	1.78	-0.18
i	3.742	0.165	2.43	2.02	-0.42

Thus both donors ii and i have negative central cell shifts.

Although at first sight the application of intrinsic radiation appears to resolve two donors in the region of the X_1 peak, a closer inspection of the spectra of S1 reveals that the minimum between the two new peaks is coincident with the maximum of the peak when no illumination was present. It is thus possible that the double peak structure is spurious, and that only one donor is present in this

region. The structure on the X_1 peak in these samples is very similar to that seen by Stillman et al (1985) on the X_3 donor in a sample grown, like RR98B, at the Wright Patterson AFB and which they attributed to the peak inversion or notch effect discussed earlier. With their sample the epitaxial layer thickness was 46μm, more than the 32μm of RR98B, but they found that although the notched structure was reduced as the thickness was reduced, it did not disappear completely until only 16μm of the layer remained. In addition the increase in the notch in S1 and RR98B as the band gap illumination is increased, and hence as the transition linewidth decreases, is consistent with the model of notching developed by Stillman et al, since they showed both theoretically and experimentally that a reduction in the inhomogeneous broadening was linked to an increase in notching. The notching appears to be more severe on RR98B and the splitting of the X_2 donor may also be due to notching.

In order to help identify peaks on which notch effects are occurring it is useful to examine the structure on the $1s-2p_{+1}$ transition at different magnetic fields and also to study the structure on other transitions such as the $1s-2p_{-1}$ or $1s-2p_0$ were possible.

Figure 4.7 shows the $1s-2p_{+1}$ transition of both RR98B and S1 at T=4.2K and at ~8 Tesla using λ=70.5μm radiation. At this field the $1s-2p_{+1}$ transition shows significant 'Δg-' or 'spin-' splitting. This splitting is a result of the non-parabolicity of the conduction band, and is also present on the cyclotron resonance. The cyclotron resonance line of S1 is shown in Figure 4.8 at two wavelengths and has an $\omega\tau$ of the order of 1000 - the short line marked 'a' in Fig 4.8 shows the FWHH that a cyclotron resonance line

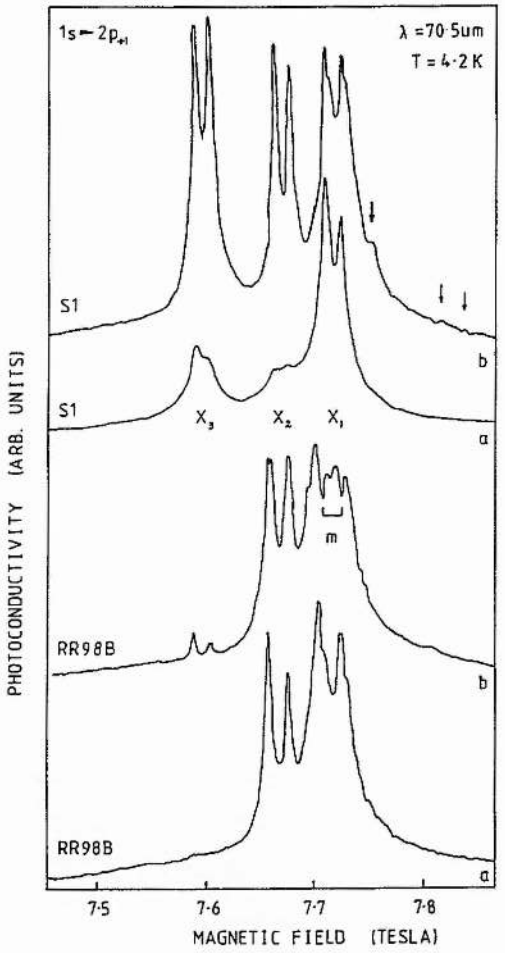

Figure 4.7: Spectra showing the central cell structure on the $1s-2p_{+1}$ transition for the VPE samples RR98B and S1 at T=4.2K with 70.5μm wavelength radiation. At these magnetic fields each central cell component appears twice due to the spin-splitting effect. The traces marked 'a' and 'b' are without and with optical excitation respectively.

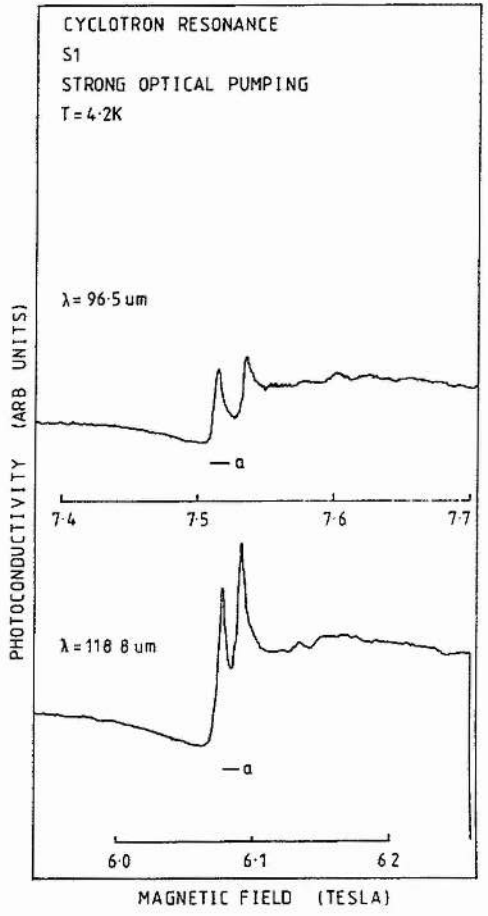

Figure 4.8: Spectra of S1 at T=4.2K showing the spin-split cyclotron resonance transition at two laser wavelengths, 118.8 and 96.5μm, and with optical excitation. The short line marked 'a' corresponds to the FWHH of a cyclotron resonance transition with an $\omega\tau$ of 1000, and is comparable with the width of the transition in S1.

with an $\omega\tau$ of 1000 would have, and it is clearly comparable to the experimental transition. This makes the cyclotron resonance of S1 one of the sharpest yet seen.

In Figure 4.7 S1 without intrinsic illumination clearly shows three spin split residual donors, X_3, X_2 and X_1. Optical pumping improves the resolution considerably, again resolving the three shallower donors (marked by arrows) which are i, ii and iii of Figure 4.6. However these do not appear to show their spin components, probably as a result of their low amplitude or possibly that they overlap with some of the other spin components. There is no indication of the strong notch effect present on the X_1 peak in spectra of S1 at 118.8μm, though the small shoulder on the high field side of both X_1 spin components may be a precursor to notching.

The situation is more complicated in RR98B. Without band gap illumination, trace (a), only the spin split components of X_1 and X_2 are present although the X_1 components show some structure on the high field side of each peak. With band gap illumination, trace (b), the two components of X_3 appear, but the components of X_1 and X_2 distort badly. X_2 is least affected, with the low field component developing two very closely spaced peaks at the same intensity as the high field component. In the region of X_1 the distortion is very severe, and two strong minima, marked 'm' develop at the positions of the peaks in trace a.

Figure 4.9 shows the $1s-2p_0$ transition of RR98B at T=4.2K using a laser wavelength of 192μm. The energy of the $1s-2p_0$ transition changes more slowly with magnetic field than the $1s-2p_{+1}$ transition since both the initial and final states lie below the N=0 Landau level. $\partial E/\partial B$ = 2.60 cm^{-1}/T at 5.9 Tesla for the $1s-2p_0$ compared to 14.7 cm^{-1}/T at 3.6 Tesla for the $1s-2p_{+1}$, and so the

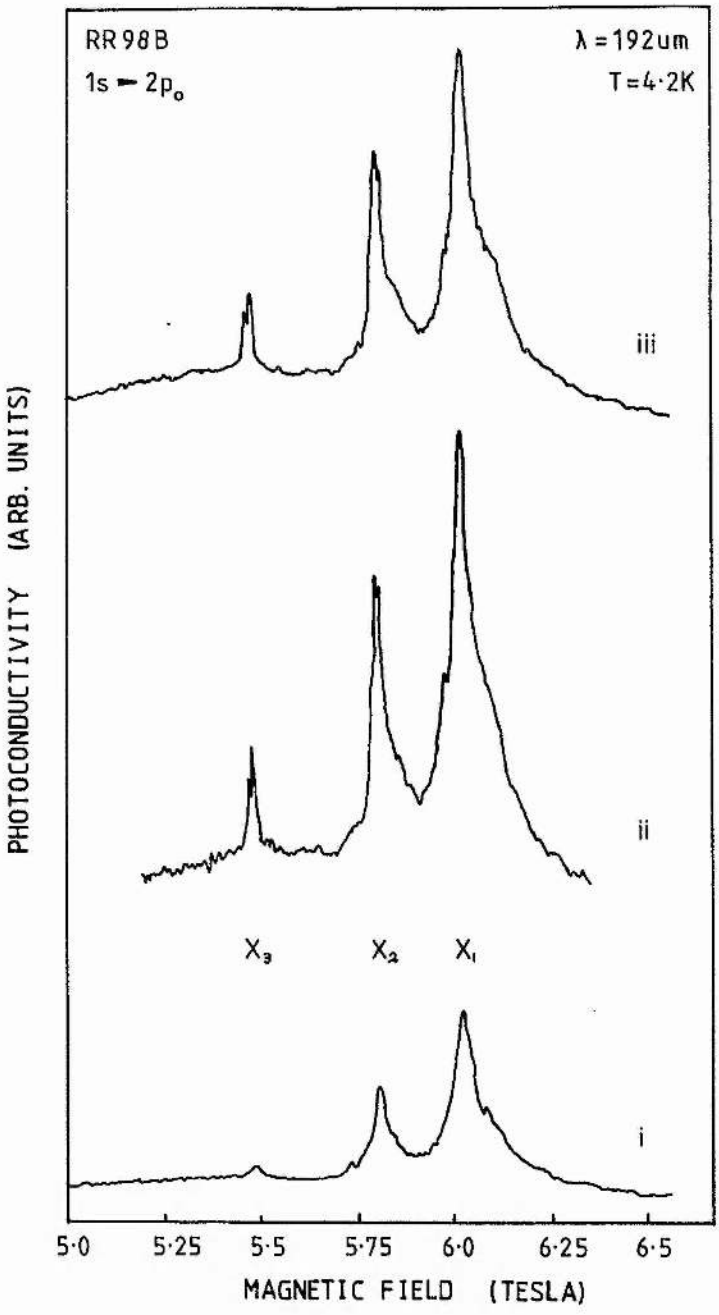

Figure 4.9: Spectra showing the central cell structure on the $1s-2p_0$ transition for the VPE sample RR98B at T=4.2K with 192μm wavelength radiation. The traces marked i, ii and iii are without and with 'medium' and 'strong' optical excitation respectively.

central cell structure is spread out over a greater magnetic field range: ~0.5 Tesla as opposed to 0.1 Tesla. This also results in the $1s-2p_0$ transition having a much smaller and unobservable spin splitting than the $1s-2p_{+1}$ transition. According to Larsen's theory of line broadening the dominant broadening mechanism on the $1s-2p_0$ transition is quadrupole broadening (which is negligible on the $1s-2p_{\pm1}$ transition at these fields). The $1s-2p_0$ transition should then be much broader than the $1s-2p_{\pm1}$ transition. Fourier Transform recordings of other samples, which show all three transitions under identical experimental conditions, show that this is true. However if Figures 4.5 and 4.9 are compared it is apparent that the $1s-2p_0$ transition in RR98B appears to be better resolved than the $1s-2p_{+1}$ transition by a substantial margin, and furthermore shows only one strong donor in the X_1 region. This is further evidence that peak inversion is present on the $1s-2p_{+1}$ recordings of RR98B, since if the peaks are truncated by inversion then this will give the impression of an increased linewidth. The small splitting apparent on the $1s-2p_0$ X_2 and X_3 peaks may also be the result of peak inversion. The absence of a more significant splitting such as that seen on X_1 in Figure 4.5 may be a result of the experiment being conducted in near Faraday Geometry, since the $1s-2p_0$ transition is forbidden in pure Faraday Geometry, and consequently the observed transition is of much lower amplitude than the corresponding $1s-2p_{+1}$ transitions.

In order to get more detailed information on the central cell structure studies were also made of the $1s-2p_{-1}$ transition of both RR98B and S1.

In Figure 4.1 if the curve showing the $1s-2p_{-1}$ energy is studied it is apparent that as the magnetic field is increased the

transition energy initially decreases over the field range $0<\gamma<0.2$ and then rises slowly. The curve is shown again in Figure 4.16 with an expanded y axis and scaled in cm^{-1} and Tesla for GaAs. The minimum transition energy of 31.3 cm^{-1} occurs at a magnetic field of ~1.6 Tesla. Thus for a small range of laser wavelengths two transitions will be seen for certain donors, one in the range 0 to 1.6 T, and the other above 1.6 T. Furthermore if the laser energy is not sufficient some of the donors may not be seen at all. This is the case with the 302.28μm laser line (Formic acid HCOOH), used in some of the experiments: the energy of the line is 33.1 cm^{-1}, which is less than the minimum energy needed to excite the deepest donor state X_3 to the $2p_{-1}$ level, and so the X_3 component is absent from the spectra.

Figure 4.10 shows the spectra of the $1s-2p_{-1}$ transition using a laser wavelength of 302.28μm for samples RR98B and S1 at T=4.2K both with and without band gap excitation. In the absence of excitation S1 (trace iii) shows the strongly asymmetric lineshape resulting from the quadratic Stark broadening mechanism. The two central cell components are X_2 (sulphur) and X_1 (silicon) with peaks at 2.952 ±0.005 and 3.663 ±0.005 Tesla respectively. Although the two components in S1 appear to have similar linewidths in magnetic field the high field peak X_1 is actually broader in energy terms since the factor to convert field to energy, $\partial E/\partial B$, changes significantly over the field range of the recording. $\partial E/\partial B$ was calculated by numerically differentiating the $1s-2p_{-1}$ transition energy obtained by Makado (1982) for donors in a parabolic band. At 3.0T (near the X_2 peak) $\partial E/\partial B$ is 0.63 cm^{-1}/T while at 3.6T ($\sim X_1$) it is 0.72 cm^{-1}/T. Then the FWHH for X_1 is 0.10 cm^{-1} while that for X_2 is 0.08 cm^{-1}. Two lines at the top of the figure indicate the equivalent sizes in Tesla of a 0.1 cm^{-1} energy interval.

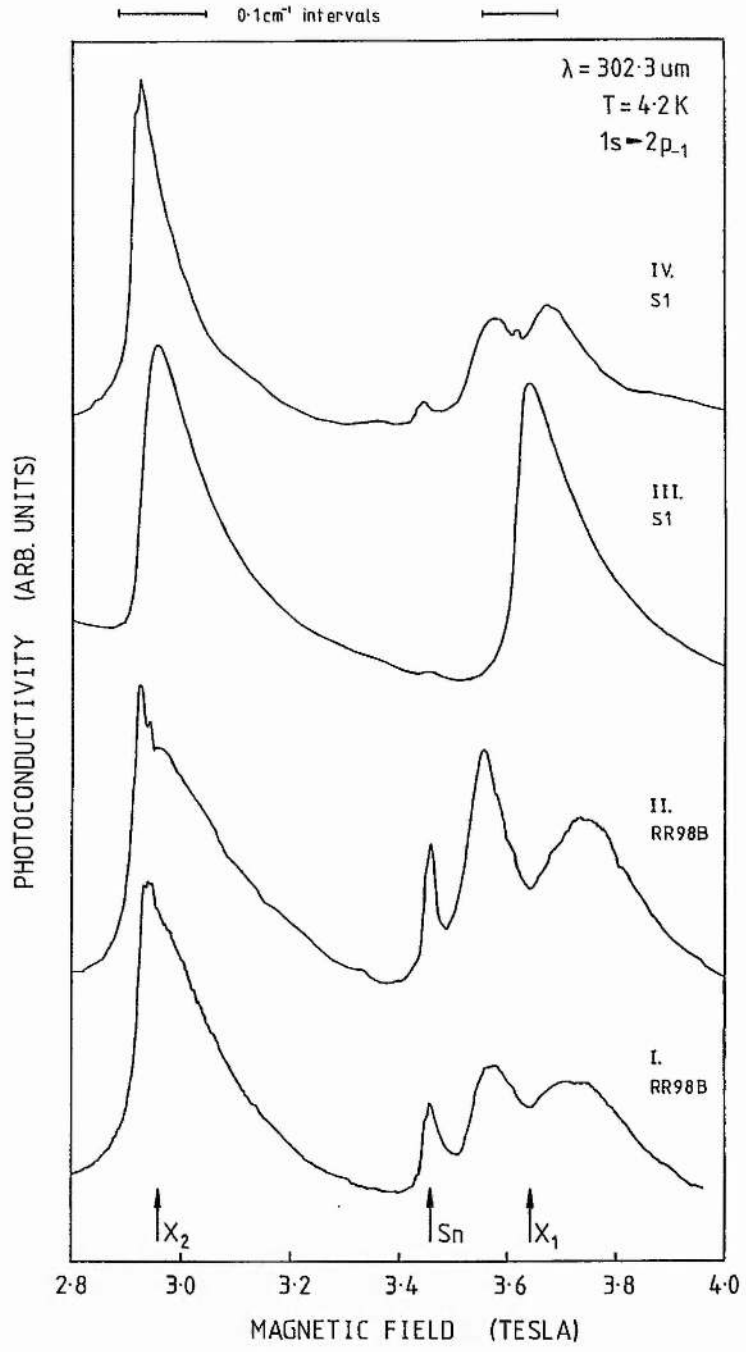

Figure 4.10: Spectra showing the 1s-$2p_{-1}$ transition for the two VPE samples at T=4.2K with 302.28μm wavelength radiation. With this laser wavelength the deep X_3 central cell component is absent from the spectra as the photon energy is too low to excite it. Recordings i and iii are without optical excitation, while ii and iv are with optical excitation.

In the traces of RR98B in Fig 4.10 it is apparent that even without intrinsic illumination the linewidths of the individual central cell components are significantly narrower than those observed on the $1s-2p_{+1}$ transition, to the extent that a fourth donor is unambiguously resolved at approximately the position of the tin donor in R137: ie just on the low field side of X_1 at a magnetic field of 3.447 T. A very low amplitude tin peak is also present in S1. It is possible that the tin peaks might have been detected on the $1s-2p_{+1}$ transition had there been less distortion due to the notch effect.

Clearly the notch effect in these $1s-2p_{-1}$ spectra is particularly severe. S1 without illumination (trace iii) is the only recording not affected. In S1 with band gap illumination the X_1 component develops two major peaks with a small glitch in the notch between them, while X_2 acquires a 'pointed' lineshape. The situation in RR98B is even worse - even without any band gap excitation the X_1 region shows structure similar to the distorted X_1 peak of sample S1 with a deep notch between two peaks which could easily be misinterpreted as two separate central cell components, while X_2 has a rather unusual lineshape. The application of band gap illumination results in even more structure developing on the X_2 peak in RR98B. The increase in the severity of the distortion with band gap illumination seen in these spectra is consistent with the model of Stillman et al which predicts an increase in notching as the inhomogeneous linewidth is reduced.

As a reduction in temperature can also lead to reductions in the shallow impurity linewidths due to the preferential formation of ionized donor-acceptor pairs (as discussed earlier in the chapter) then according to Stillman's model the magnitude of the notch effect should increase. This is clearly the case in Figure 4.11 which shows

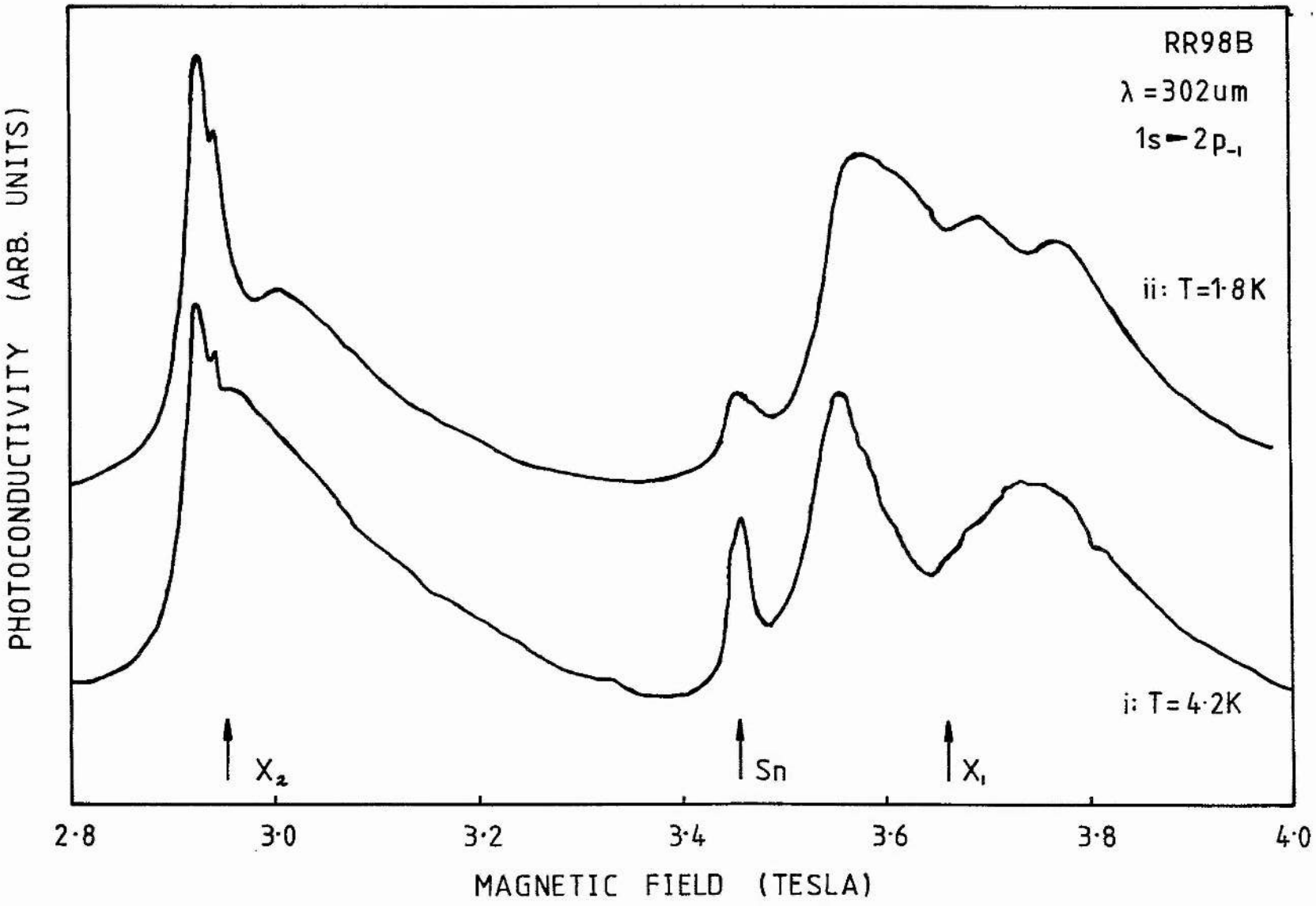

Figure 4.11: Spectra showing the 1s-2p$_{-1}$ central cell structure for RR98B at i: T=4.2K and ii: T=1.8K with 302.28μm wavelength and optical excitation.

spectra of RR98B at two different temperatures, 4.2 and 1.8K with intrinsic illumination. The recording at 4.2K is the same as that in Figure 4.10 (trace ii). At 1.8K a further peak appears in the X_1 region and the structure on the X_2 peak develops further. The similarity between the structure on the X_2 peak and the heavily notched lineshape predicted by the model of Stillman et al is remarkable. Both show a sharp peak with a broad 'wing' at lower energy (higher magnetic field in these spectra).

It should be noted that all the spectra shown in this chapter were obtained well before the work of Stillman et al was published and at first a different interpretation was placed on this structure. These alternative interpretations are still reasonable, but are unlikely to be the cause of the structure seen in these spectra. For example, when looking at the two sharp peaks of the X_2 donor one cannot rule out the possibility that they are due to two separate donors with nearly identical central cell shifts. Such a coincidence of central cell shifts would not previously have been observed in studies using a Fourier Transform Spectrometer due to its lower resolution. The appearance of a sharp peak and broad 'wing' as seen on X_2 could be attributed to layers with different impurity concentrations. For example a heavily doped layer would give the broad shifted wing while a lightly doped layer would give a sharp transition. Other alternative explanations are discussed later.

Spectra of the $1s-2p_{-1}$ transition have been obtained at higher magnetic fields using laser lines with wavelengths of 255 and 229μm. Using these shorter wavelengths all the central cell components are accessible, whereas at λ=302μm the X_3 component was at too high an energy to be observed. In practice with the 12.7T superconducting magnet and the λ=255μm line only the $1s-2p_{-1}$ central cell

components up to X_1 can be observed, while shallower components such as Pb are beyond the field limit. With λ=229μm radiation all the structure falls outside the range of the 12.7T magnet and so a completely different magnet is required.

Spectra taken with λ=255μm radiation are shown in Figure 4.12 both with and without intrinsic illumination. The very good signal to noise ratio achieved on these recordings is immediately apparent, as is the dramatic improvement in resolution due to the combination of increased central cell splitting and reduced linewidth at higher magnetic field. Figures 4.13 and 4.14 show the individual central cell components for each sample on an expanded magnetic field scale. Note that on the $1s-2p_{+1}$ transition of S1 three particularly shallow central cell components were observed (iii/Pb, ii and i in Figures 4.5 and 4.6), but as noted above these would lie above the 12.7 T field limit of the magnet.

Unfortunately all of these spectra show peak inversion effects with various degrees of severity. From Figure 4.12 it can be seen that S1 without band gap illumination is least affected while RR98B with illumination is worst. Figure 4.13 shows the structure in the vicinity of the X_1 and Sn donors. The tin donor is clearly resolved at 11.77T in RR98B but although it appeared to be present at low amplitude in S1 in the λ=302μm spectra (Figure 4.10) it is not present in these spectra. Severe distortion is occurring on the X_1 peak of RR98B both with and without illumination. S1 also appears to show distortion when illuminated with band gap excitation and a number of shoulders appear, together with a peak shift to higher magnetic field. Some interesting interpretations involving complexes which could be placed on these shoulders are discussed in more detail later.

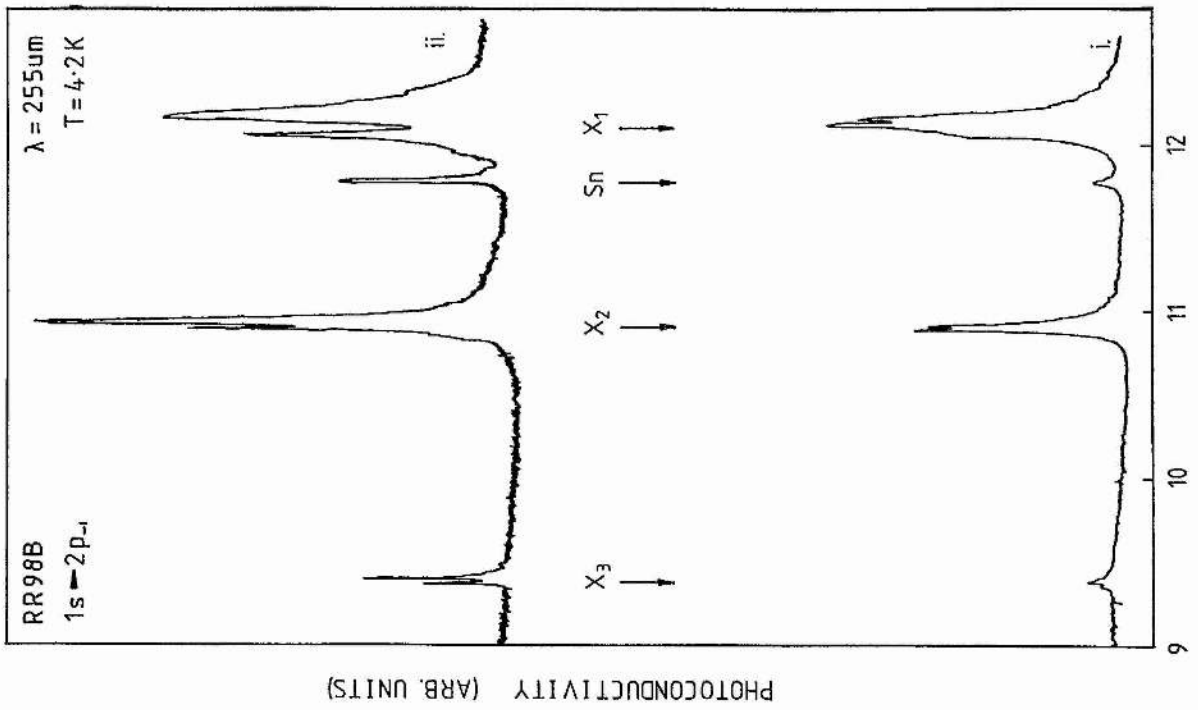

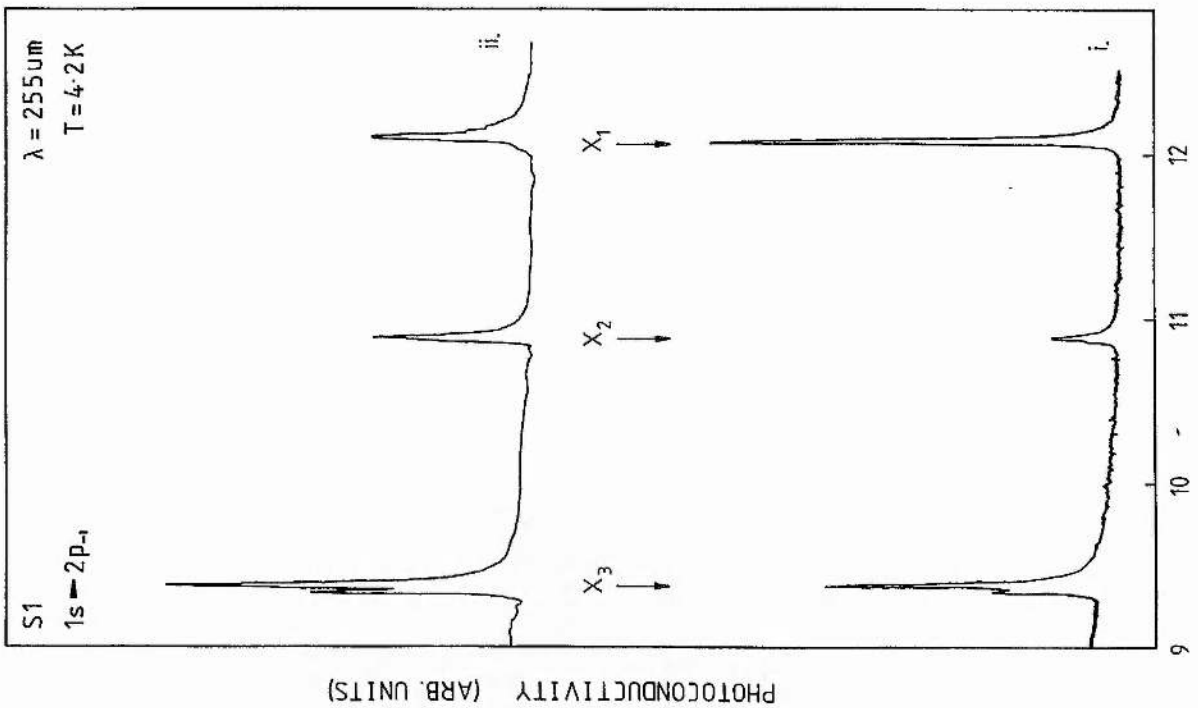

Figure 4.12: Spectra showing the central cell structure on the $1s-2p_{-1}$ transition at high magnetic field for the VPE samples S1 (left hand figure) and RR98B (right figure) at T=4.2K with 255μm wavelength radiation. Traces i and ii on each figure were taken without and with optical excitation respectively.

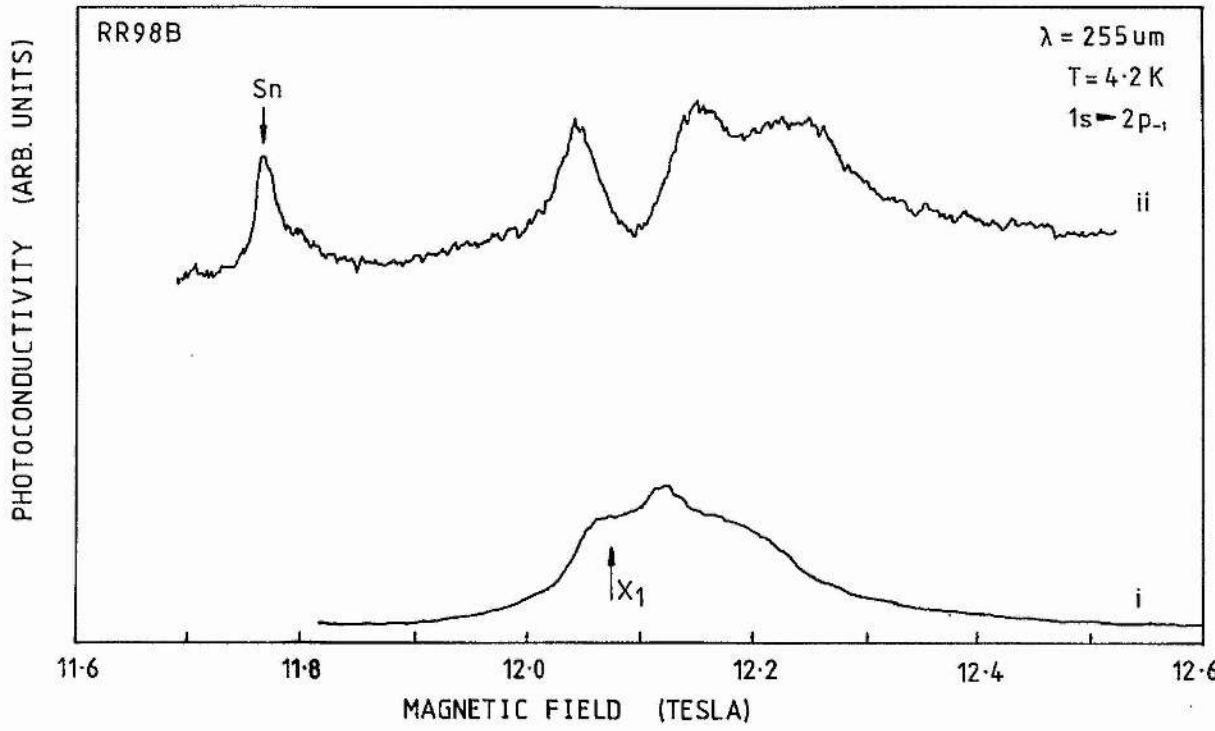

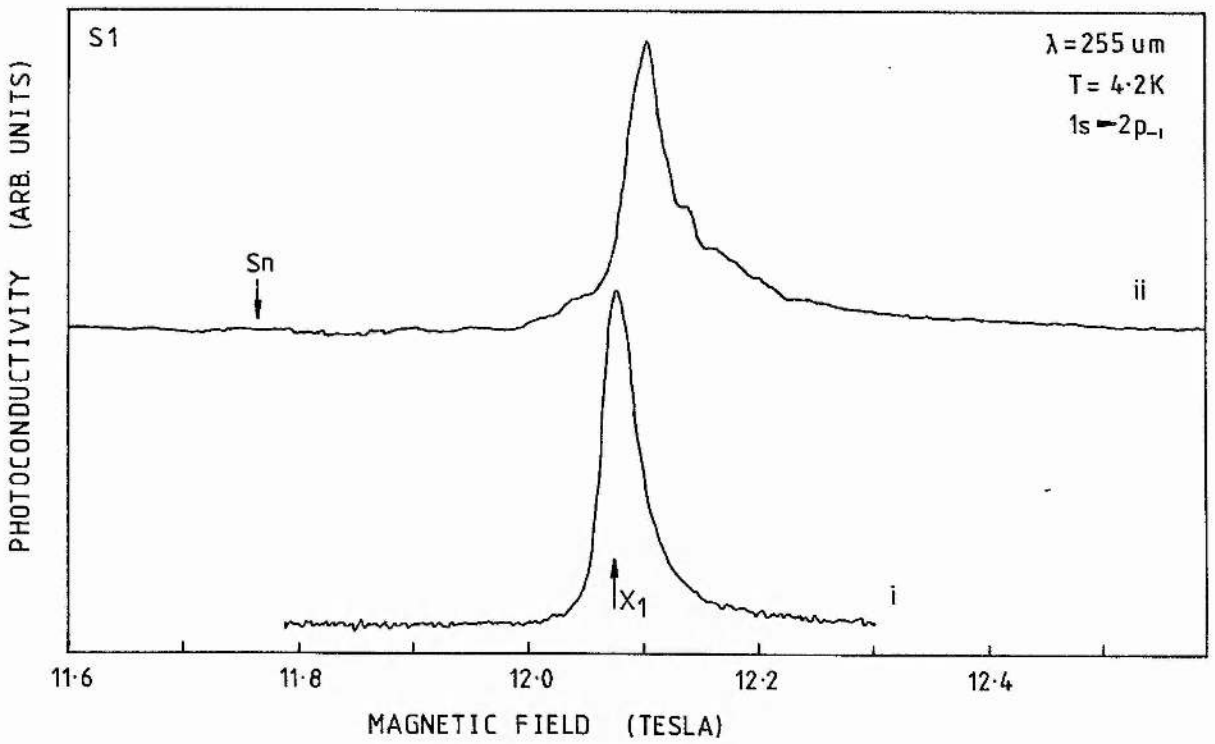

Figure 4.13: Spectra showing the X_1 and Sn $1s-2p_{-1}$ central cell components at high magnetic field for S1 and RR98B at T=4.2K with 255μm wavelength radiation. Recordings i and ii were taken without and with optical excitation respectively.

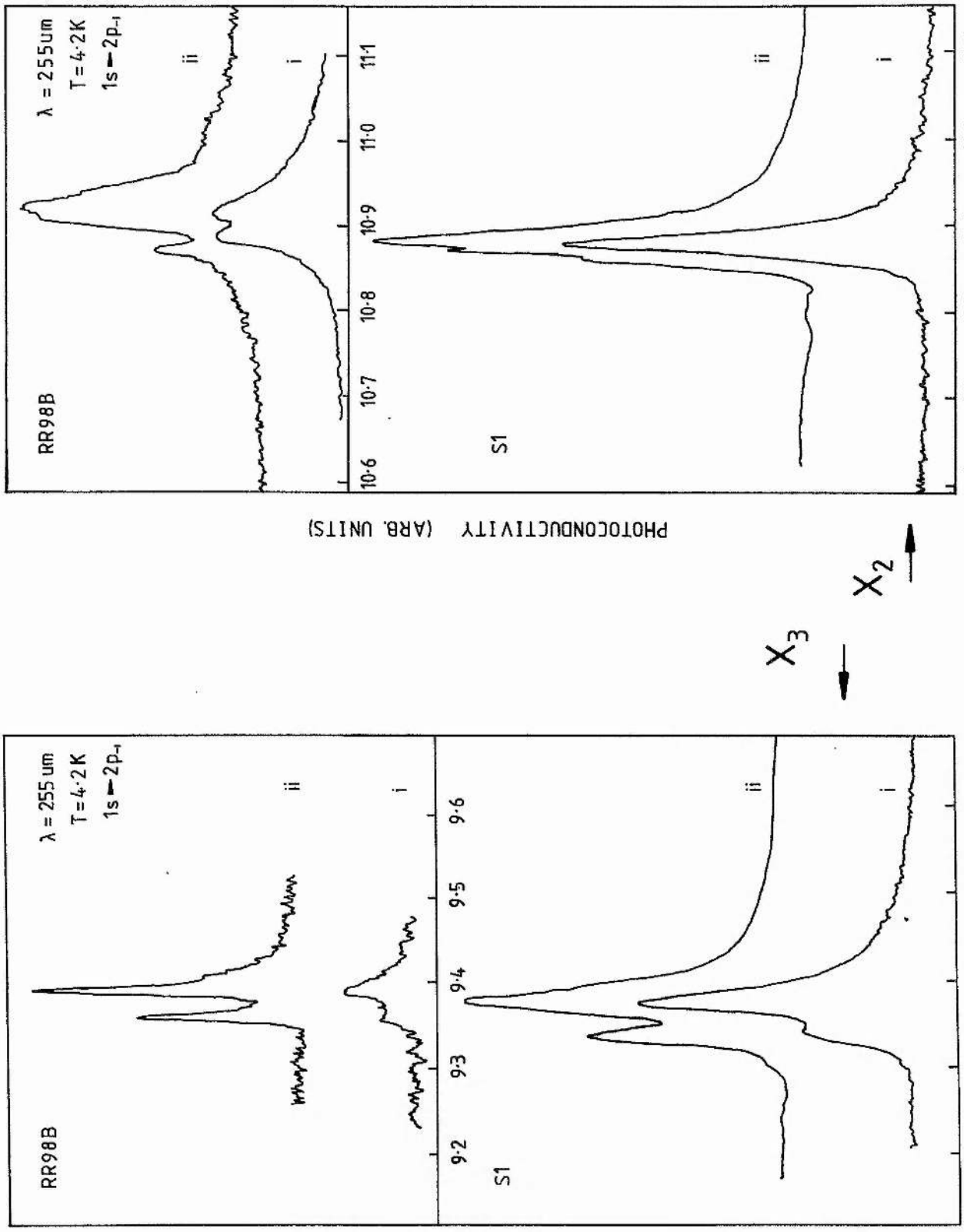

Figure 4.14: Spectra showing the X_3 (left figure) and X_2 (right figure) $1s\text{-}2p_{-1}$ central cell components at high magnetic fields for S1 and RR98B at T=4.2K with 255μm wavelength radiation. Recordings i and ii were taken without and with optical excitation respectively.

In the absence of band gap excitation the X_1 component of S1 shows a typical asymmetric lineshape with a peak at 12.075 ±0.002 Tesla and a width of 0.037 T (FWHH), which corresponds to the remarkably low linewidth of 0.023cm^{-1} (FWHH) ($\partial E/\partial B$ = 0.62 cm^{-1}/T). A similar calculation can be performed for the X_2 donor of S1 shown in Figure 4.14 (trace i: no illumination), which has a peak at 10.877 ±0.002 Tesla and a width of 0.030 T, equivalent to 0.020 cm^{-1} (FWHH) ($\partial E/\partial B$ = 0.65 cm^{-1}/T).

These figures should be compared with those obtained for S1 under similar conditions (4.2K and no illumination) at ~3T: 0.10 and 0.08 cm^{-1} (FWHH) for X_1 and X_2 respectively. Thus increasing the field to ~12 Tesla has reduced the linewidths by a factor of ~4.

It is also interesting to compare these linewidths with those of the 1s-2p_{+1} transition. In the absence of illumination the central cell components of S1 at 3.6 Tesla (λ=118.8μm) have FWHH linewidths of ~0.3 cm^{-1}, more than an order of magnitude greater than those on the 1s-2p_{-1} transition at ~12 Tesla.

To a certain extent this large reduction in linewidth is not expected, since the quadrupole moments of the 1s and 2p_{-1} states, which are equal as well as being near zero at ~3T, are expected to increase and diverge from each other at higher fields (see Figure 4.3, from Larsen 1973), resulting in an increase in the linewidth of the 1s-2p_{-1} transition at higher fields due to the reappearance of a significant quadrupole broadening element in addition to the quadratic Stark broadening. However Afsar, Button and McCoy (1980) observed similar increases in the central cell splittings and reductions in the linewidths in Fourier Transform Spectrometer studies of GaAs at fields up to 20 Tesla. It would thus appear that the quadrupole moments do not increase and split as much as expected at high magnetic fields.

A similar comparison of the linewidths at both high and low magnetic fields cannot be made for RR98B due to the severe distortion of the central cell components. In Figure 4.13 the Sn donor at 11.77T is very clearly resolved and appears unaffected by peak inversion, perhaps because of its low amplitude compared to X_1. Both the X_3 and X_2 components of RR98B in Figure 4.14 show a strong splitting which is enhanced on application of band gap illumination. A similar strong splitting is also seen on the X_3 component of S1. In both samples the magnitude of the splitting on X_3 shows very little dependence on the level of intrinsic illumination, though the relative intensities of the two peaks are strongly affected.

Figure 4.15 shows a recording of the $1s-2p_{-1}$ transition of RR98B over a field range of 14 to 20 T. This recording was made during a course of experiments at the Max-Planck Institute (Grenoble) using a 23 T Polyhelix electromagnet and a laser wavelength of 229μm. The sample temperature was T=4.2K and intrinsic illumination was provided by a GaAs LED positioned in the cryostat close to the sample. The radiation provided by the LED is above the band gap energy of the epitaxial material as a result of the Burstein shift. As there was a considerable amount of background noise when the magnet was running a very narrow band lock-in amplifier was used (Q~50). This has resulted in an overdamped recording and consequently narrow lines will have been distorted and broadened. However the principle features of RR98B seen in Figure 4.12 (under similar conditions but at 10 - 12 T and with λ=255μm) are reproduced at these very high magnetic fields.

Yet again strong distortion due to peak inversion is present and even the low amplitude tin and X_3 donors show splittings. However note how well resolved the individual central cell components have

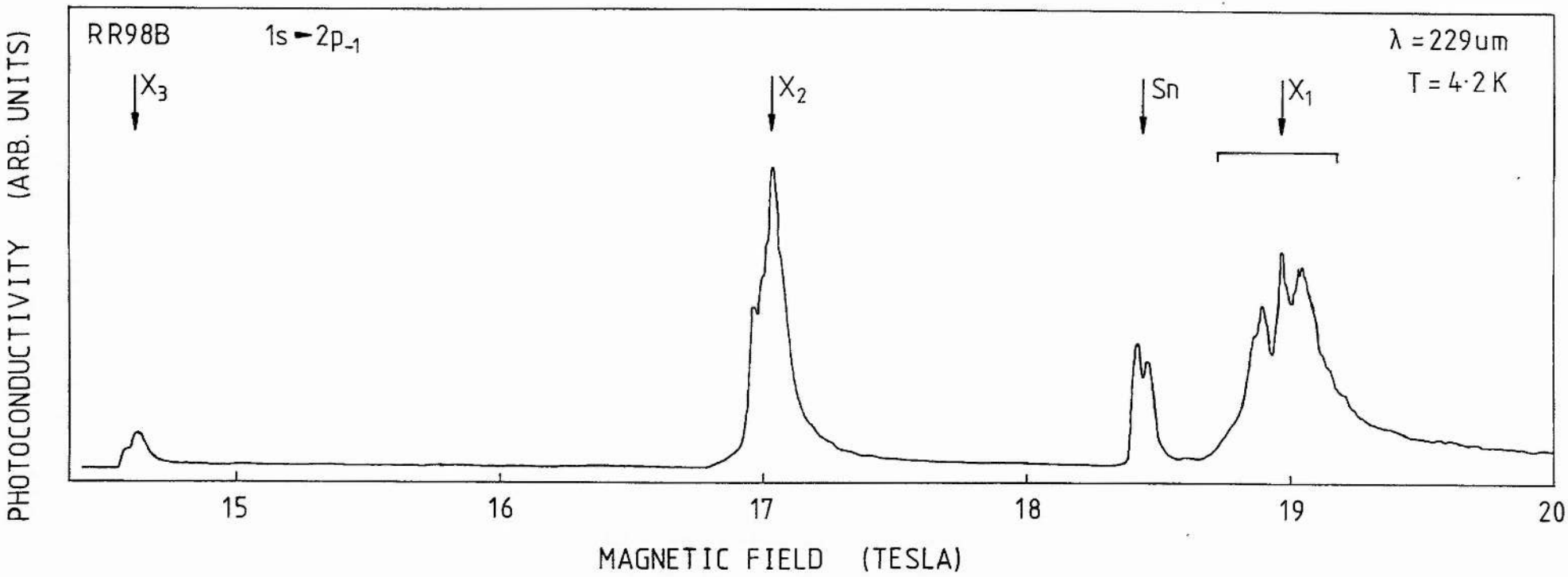

Figure 4.15: A spectrum showing the central cell structure on the $1s-2p_{-1}$ transition at very high magnetic field for RR98B at T=4.2K with 229μm wavelength radiation. The spectrum was taken at the Max-Planck Institute in Grenoble using a Bitter-Polyhelix type electromagnet. Above band gap excitation was provided by a GaAs LED positioned close to the sample.

become. The positions of the principle peaks observed in the recordings taken at wavelengths of 302.28, 255 and 229μm have been plotted in Figure 4.16 and compared to the theoretical calculation for a simple parabolic band.

In addition to the effects of peak inversion there are a number of mechanisms which could give rise to multiple components on the individual central cell lines. The possibility of a coincidence in the central cell shifts of two different impurities which can only be resolved at high fields has already been mentioned. This could explain a simple double peak structure, such as that observed on the X_3 component in both RR98B and S1.

Spin-splitting effects due to non-parabolicity could also be responsible for the observed splittings. Spin-splitting is strong on the $1s-2p_{+1}$ transition where the energy difference between the two states is large and one of the states is much further into the band than the other. However since the 1s and $2p_{-1}$ states both lie below the N=0 Landau level the effects should be significantly reduced. To first order the effective g-factor g_e^* can be assumed to be a linear function of the energy of a state above the band edge. Since the energy of a state including the spin term is given by the $\left\{\text{hydrogenic energy} \pm \frac{1}{2}\mu_B g_e^* B\right\}$ this would give rise to the experimentally observed B^2 dependence of the spin splitting (Larsen 1978).

An estimate of the value of the spin splitting on the $1s-2p_{-1}$ transition can be made as follows. At 7.6 Tesla $\gamma \sim 1.2$, and from the calculations of Makado (1982) the energies of the 1s, $2p_{-1}$ and $2p_{+1}$ states relative to the zero field band edge are -0.550, 0.219, and 2.619 R^* respectively. Thus the ratio of the $2p_{+1}$ and $2p_{-1}$ energies above the band edge is ~12, and so the ratio of the change

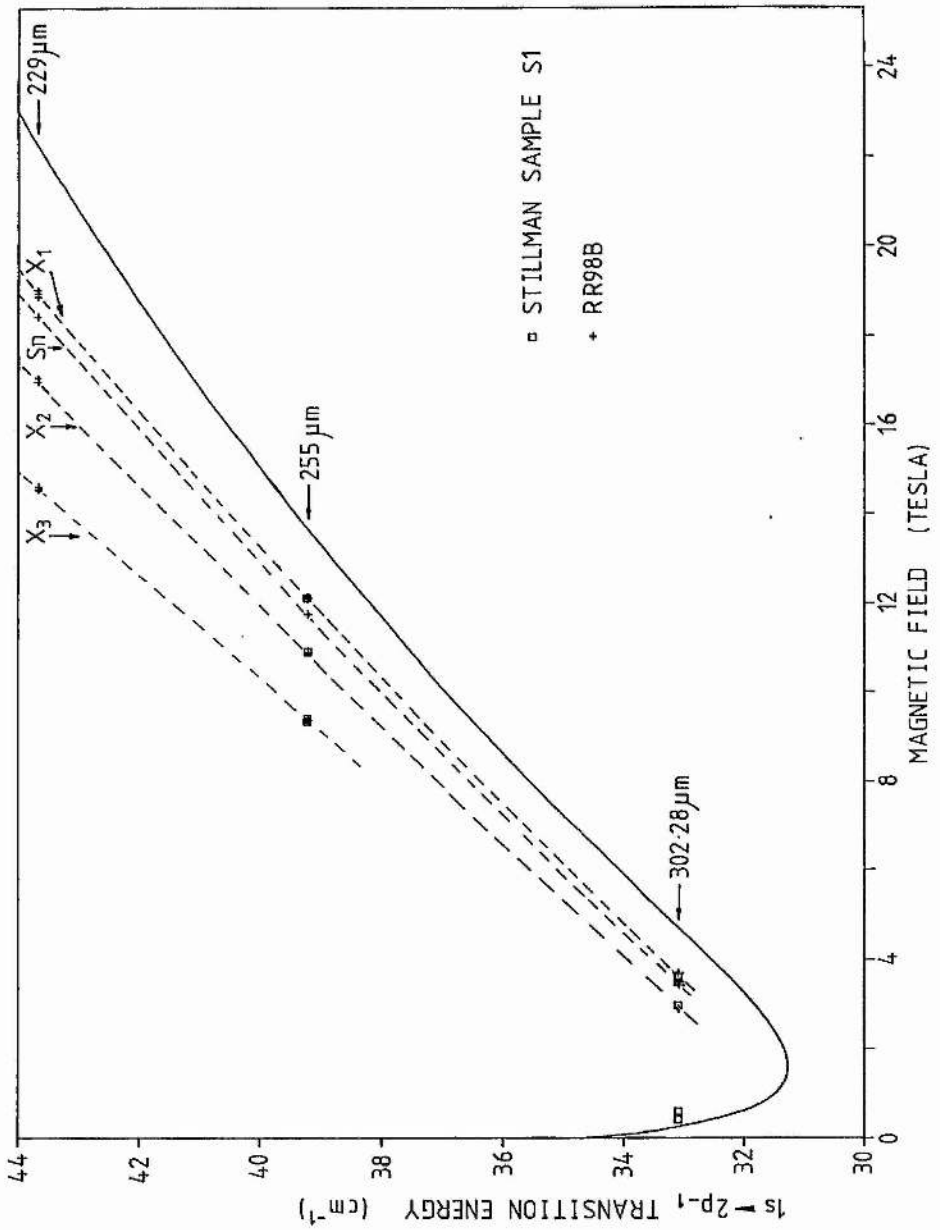

Figure 4.16: Graph showing the experimental energies and magnetic fields of the central cell components of the $1s-2p_{-1}$ transition for the three laser wavelengths used. The solid curve shows the theoretical $1s-2p_{-1}$ transition energy in a parabolic band (using the data of Makado 1982).

in effective g-value will be ~12. Thus the spin splitting on the $1s-2p_{-1}$ transition should be approximately 1/12 th of the splitting on the $1s-2p_{+1}$ transition. The $1s-2p_{+1}$ transition of RR98B and S1 at ~7.6 Tesla was shown in Figure 4.7 and the spin splitting was ~0.013 Tesla. Assuming $\partial E/\partial B$ ~14.7 cm^{-1}/T then this corresponds to a splitting of ~0.20 cm^{-1}. Thus the spin splitting on the $1s-2p_{-1}$ transition at the same field should be ~0.02 cm^{-1}. This is consistent with a comment made by Larsen (1978) that his theory predicted spin splittings on the $1s-2p_{-1}$ and $1s-2p_0$ transitions of the order 0.01 cm^{-1}.

The spectra of the $1s-2p_{-1}$ transition shown in Figures 4.13 - 4.15 covered the range 9 - 12 Tesla, and showed linewidths of 0.02 cm^{-1}. Thus spin splittings such as those just estimated ought to be observable. However though splittings are present on certain components, eg X_3, they cannot be due to spin splitting since spin splitting ought to be present on all central cell components. This is clearly not the case - the X_2 and X_1 components of S1 without optical illumination show no indication of splittings.

A further effect that could introduce splitting is due to the optical excitation itself. In the discussion on the Larsen theory of line broadening it was pointed out that the peak position of a transition would be shifted to lower energy as the linewidth increases, since the long tail of the transition is on the low energy side. When above band gap radiation is incident on the sample it is absorbed in the first few microns of the epitaxial layer as a result of the high absorption coefficient above the band gap. Neutralization of the ionized donors would then take place principally within this layer at the surface, leading to narrowed lines in that portion of the sample only. The region of neutralization would depend on how far the

photo-excited carriers could diffuse into the bulk from the surface layer. Furthermore the high concentrations of electrons and holes in the surface layer increases the conductivity and effectively short-circuits the remainder of the layer. The changes in the photoconductivity induced by photothermal ionization will thus be predominantly from the surface layers. However if signals did originate from the unexcited material these lines would not be narrowed and would result in a broader absorption with a peak position shifted from that of the narrow lines. The combination of a sharpened transition with the broad unperturbed transition could give rise to the structure observed on the X_2 donor of RR98B in the 302μm spectra (Figure 4.11). However it has already been noted that this structure bears a strong resemblance to that predicted by Stillman's model of peak inversion.

This effect is complicated further if the impurity distribution in the sample is not homogeneous. Any areas in which the impurity concentration is higher than in the surroundings will give transitions with an increased linewidth, as a result of the inevitable reduction in ionized-neutral impurity separation and the increase in donor-donor effects. A number of mechanisms for the incorporation of impurities into III-V compounds which result in a graded impurity concentration are already well documented (eg Kang and Greene 1968).

It is inevitable that the levels of contaminating impurities in growth reactors will vary and depend strongly on the past history of the reactor. Thus if tin was used as a dopant in one growth run the tin impurity concentration in a layer grown immediately afterwards might be strongly graded with depth.

A further mechanism which might split individual central cell components is due to the formation of complexes. Even if the impurity

distribution is homogeneous, the random nature of the distribution will create impurity pairs with separations ranging from a single lattice spacing to many Bohr radii. Transitions arising as a result of complexes involving two weakly interacting neutral donors (D_2^0) or alternatively a neutral and an ionized donor (D_2^+) have been observed in zero and low magnetic field experiments as broad, low intensity lines at energies below the $1s-2p_{-1}$ transition in GaAs (Bajaj et al 1975; Golka et al 1973, 1974, 1975). However the energies of these complexes are strongly dependent on the overlap of the wavefunctions on the two impurity sites. Consequently any variations in the spatial extent of the wavefunctions caused by changes in the strength or orientation of the magnetic field significantly affect both the energies and the strengths of the transitions. Experimental observations showed that the transition amplitude decreased rapidly in a magnetic field.

Unfortunately no calculations have been performed on this type of complex at high magnetic fields. However calculations have been performed on a complex where the charge, instead of being a single point charge +e, is spatially dispersed through some volume, with the proviso that the total integrated charge is still +e (Fedders 1983a). These calculations show that certain types of charge distribution may still have a set of hydrogenic shallow donor energy levels perturbed by only a small amount from the effective mass values. These perturbed states could then give rise to additional central cell components or to splittings of central cell components. Fedders obtained numerical values for the perturbation for GaAs using the formula

$$\Delta E(\gamma) = B(\gamma)\ Q(\Omega_i)$$

where γ is the dimensionless magnetic field $\hbar\omega_c/(2R^*)$, ΔE is the energy shift in units of R^*, $B(\gamma)$ is a function indicating

how the splitting varies with field. $Q(\Omega_i)$ is determined by the charge distribution of the complex. For a complex with two charges +2e and -e then

$$Q(\Omega_i) = a^2 \ (3 \cos^2\Theta - 1)$$

where 'a' is the distance between the two charges in units of the effective Bohr radius a_0^* and Θ is the angle between the axis of the complex and the magnetic field.

At 6.5 Tesla (ie γ=1) and with a = 5.65 Å (ie one lattice spacing) then the shift can move over 0.082 cm^{-1} depending on the angle between the axis of the complex and the magnetic field. Bearing in mind the linewidth of the $1s-2p_{-1}$ transition at 12T, which was 0.02 cm^{-1}, shifts of this magnitude would be clearly resolved.

One problem is that these equations suggest that the perturbation is proportional to the square of the spacing between the two charges. This is unusual since the perturbation due to a complex should decrease to zero as the separation increases. This unusual behaviour may result from the fact that the charge distribution used does not reduce to a single point charge at large separations.

To conclude this study of the central cell structure of the $1s-2p_{\pm1,0}$ transitions in GaAs it is apparent that there is great scope for continued studies, both theoretical and experimental, on the central cell structure of the $1s-2p_{\pm1,0}$ transitions. It has been shown that the technique of FIR laser spectroscopy of the $1s-2p_{-1}$ transition at high magnetic fields is capable of very high resolution and offers an excellent opportunity to study the various deviations from effective mass theory. However it is essential that the distortions and additional structure introduced by the mechanism leading to peak inversion are avoided. The work of Stillman, Low and Lee (1985) explaining and modelling peak inversion is particularly

important since it shows that peak inversion is strongly dependent on sample thickness, which is the only parameter which can be controlled. Thus in the future studies must investigate the effects of thinning the epitaxial layer down to ~10μm. Once this is done and peak inversion effects are avoided the very low linewidths of the $1s-2p_{-1}$ transition at high magnetic field can be exploited and the identities of the various background impurities can be settled once and for all.

Impurity Transitions Between Ground States and N=3 and N=4 Excited States.

In addition to the $1s-2p_{\pm1,0}$ transitions which appear in the spectra of high purity GaAs and InP substantial structure is present at other magnetic fields. The magnetic field region below the $1s-2p_{+1}$ transition is particularly rich since transitions from the 1s ground state to levels with principle quantum numbers n>2 can be observed. Figure 4.17 shows a complete spectrum of RR98B at T=1.8K in the magnetic field range from zero to 8.5 Tesla using a laser wavelength of λ=118.8μm. Figure 4.18 shows RR98B under the same conditions but with a laser wavelength of 70.5μm, together with sample S1 at 4.2K.

The theoretical positions of a number of the impurity transitions, calculated in the parabolic band approximation (Makado 1982), are shown in both figures. (An effective mass of $0.0665m_0$ and an effective Rydberg of 46.1 cm^{-1} were used in the calculation). The positions of the series limits for the sets of transitions associated with the N=1...4 Landau levels are also indicated (ie the positions of the 1s→N=1...4 transitions). Even at these intermediate fields where $\gamma\sim1$ the energy levels form well defined groups below the Landau levels, and the transitions appear in groups below the series limits. Note how the detailed structure at magnetic fields above the N=1 series limit is duplicated above the N=2, 3, 4... limits, albeit with progressively poorer resolution. On the group of transitions at magnetic fields above the N=1 series limit the central cell structure is clearly resolved. This is most apparent on the $1s-3p_{+1}$ transition at 70.5μm in Figure 4.18. Figure 4.19 shows the $1s-3p_{+1}$ transition in RR98B in more detail at both λ=118.8 and 70.5μm. In addition to the central cell structure the Δg-splitting is clearly resolved

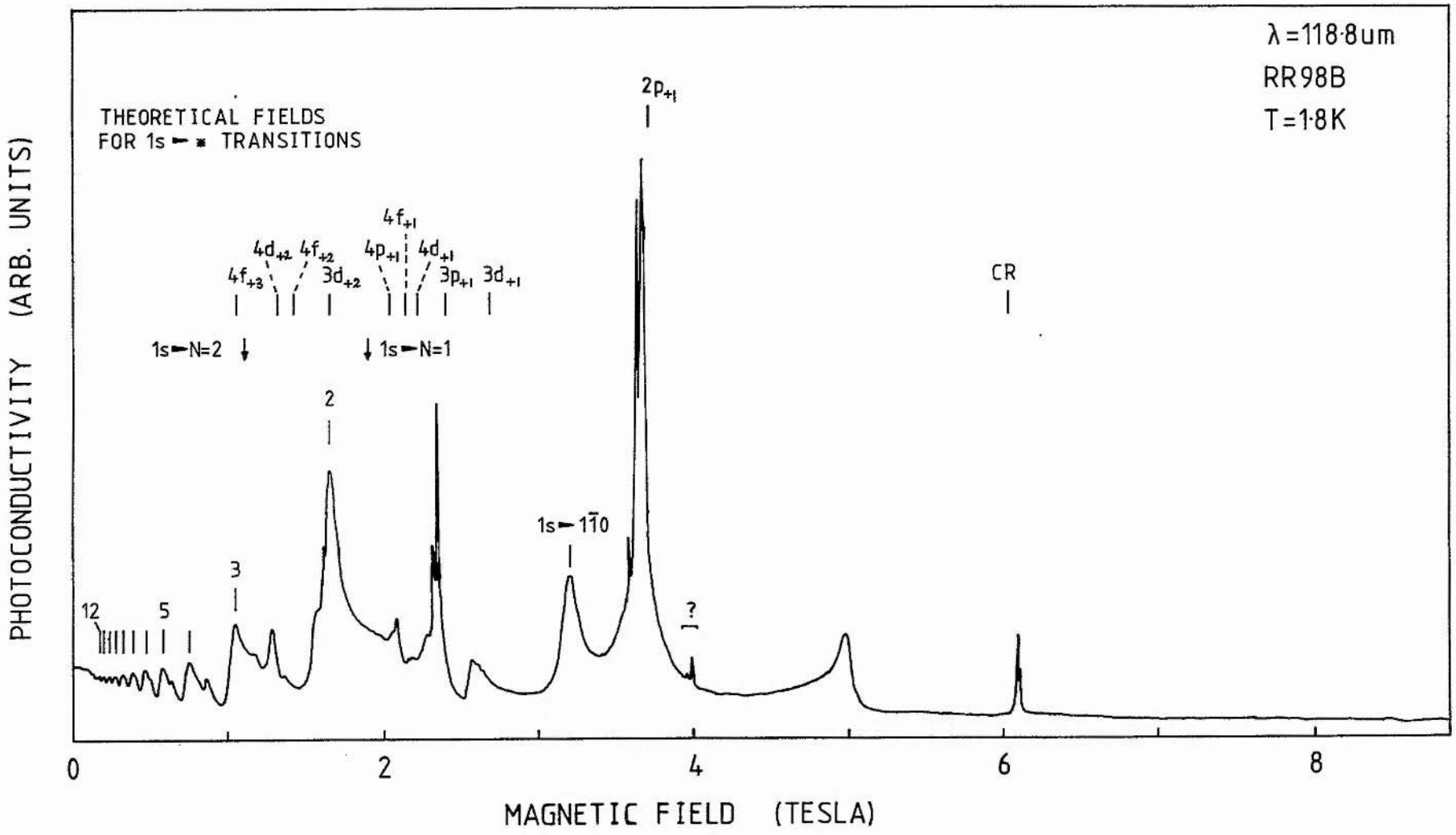

Figure 4.17: The spectrum between zero and 9 Tesla of RR98B at T=1.8K using λ= 118.8μm radiation and optical excitation. The origin of the two sharp peaks marked '?' and the unidentified transition at 5 Tesla are discussed in the text.

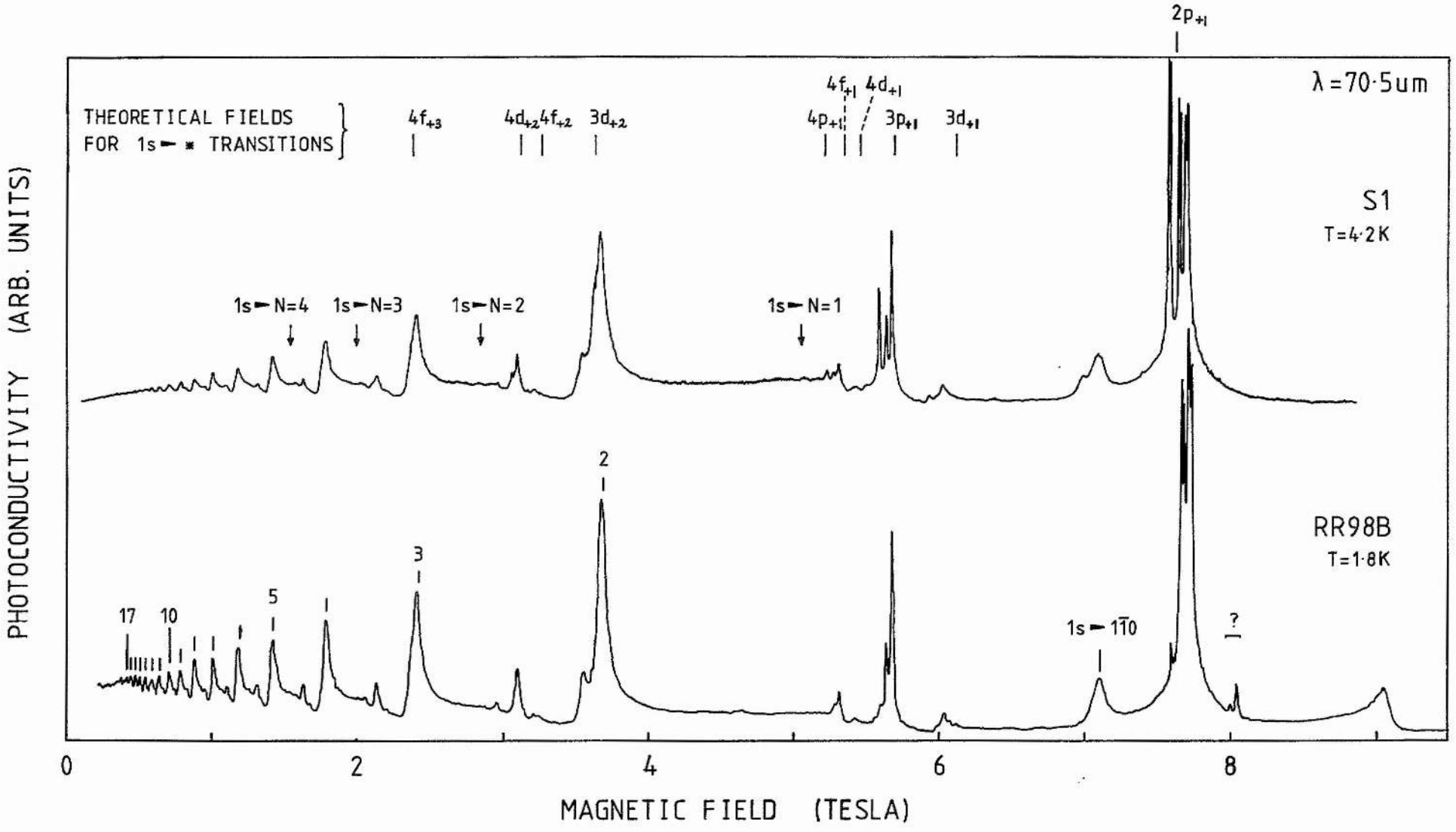

Figure 4.18: The spectrum between zero and 9 Tesla of RR98B at T=1.8K and S1 at T=4.2K using λ=70.5μm radiation and optical excitation.

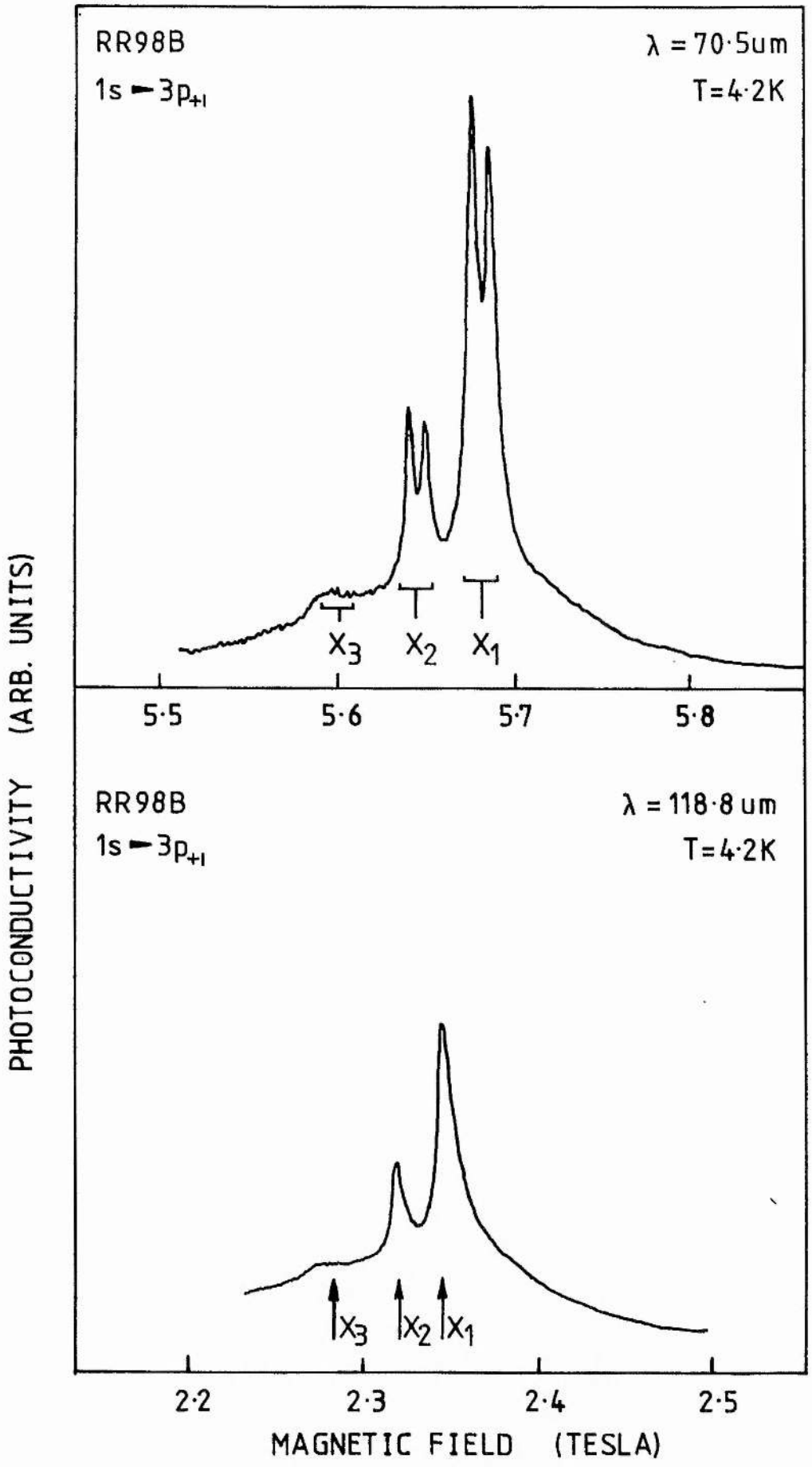

Figure 4.19: Spectra showing central cell structure on the 1s-3p$_{+1}$ transition of RR98B at T=4.2K with λ= 118.8 and 70.5μm radiation and optical excitation. At λ=70.5μm the spin splitting is clearly resolved.

on the 70.5μm recording. The central cell split components which can be seen on the high field side of the $1s-3p_{+1}$ transition in Figure 4.17 and 4.18 are in good agreement with the theoretical position of the $1s-3d_{+1}$ transition while the components on the low field side are in good agreement with the $1s-4f_{+1}$ transition. The central cell components of all three transitions, 1s to $4f_{+1}$, $3p_{+1}$ and $3d_{+1}$, all appear at slightly lower magnetic field than that predicted theoretically. The $1s-4d_{+1}$ transition is probably responsible for some of the low amplitude structure in between the $1s-3p_{+1}$ and $1s-4f_{+1}$ components.

In both the λ=118.8 and 70.5μm spectra (Figs 4.17 and 4.18) there are two broad peaks on either side of the $1s-2p_{+1}$ transition which cannot be assigned to any of the hydrogenic states. One of these has been identified by Narita and Miyao (1971) as the transition from the 1s state to a state labelled with quantum numbers valid in the high field regime $\gamma \gg 1$, the $1s \rightarrow 1\bar{1}0$ transition. Such states do not appear in theoretical calculations which use basis sets comprising zero field hydrogenic wavefunctions. The unidentified line observed at 5 and 9 Tesla in the 118.8 and 70.5μm spectra respectively probably involves transitions to another high field state. However to positively identify it would require a completely new set of calculations. The $1s \rightarrow 1\bar{1}0$ transition in S1 at 70.5μm (Fig 4.18) shows a low magnetic field shoulder which is not present in either of the RR98B spectra. As S1 shows the X_3 donor in significant quantities, which RR98B does not, the splitting can be attributed to central cell structure.

Narita and Miyao (1971) also calculated the energy of the $1s \rightarrow 210$ transition and found that it was in good agreement with the energy of the peak labelled $1s-3d_{+2}$ (or '2') in Figures 4.17 and

4.18 (also Simmonds 1974). However they incorrectly associated the 210 state with the $3p_{+1}$ low field state. $3p_{+1}$ is in fact the 112 state (Rosner et al 1984). In both figures the transition labelled '2' shows a low amplitude peak or shoulder on its low field side. This splitting cannot be due to central cell structure as it was also observed in spectra of R137 which has only one major central cell component, and the structure does not match the central cell structure of S1 and RR98B on the other transitions- ie the peak/shoulder is strong in RR98B which has only a weak X_3 component, but is weak in S1 which has a strong X_3 component. The splitting is probably due to the presence of both the $1s-3d_{+2}$ transition and the 1s-210 transition, though it might have been expected that the $3d_{+2}$ state evolved into the 210 state as the magnetic field increased. However more recent work associates the $3d_{+2}$ state with the (220) high field state (Forster et al 1984), so it is possible that the 210 state might exist independently of the $3d_{+2}$ state. The existence of both the $220/3d_{+2}$ and 210 states below the N=2 Landau level would be consistent with the existence of the $110/2p_{+1}$ and $1\bar{1}0$ states below the N=1 Landau level, where neither the $1\bar{1}0$ or 210 states appear in theoretical calculations using zero field wavefunctions as the starting point.

Although the $1s-3d_{+2}$ transition would be forbidden at zero magnetic field as the selection rule $\Delta l=\pm 1,0$ would hold, the effect of a magnetic field is to mix different states and the normal selection rules for hydrogenic states are no longer rigorous. This can be seen in the unambiguous appearance of the $1s-3d_{+1}$ transition. From this point of view the existence of the $1s-3d_{+2}$ transition involving $\Delta l=+2$ and $\Delta m=+2$ is not unusual.

It is interesting to note how many of these peaks can be resolved

at lower magnetic fields. The $1s-3d_{+2}$ peak was labelled '2' since its energy lies below the N=2 Landau level. Numbering the main peaks from here, the last to be resolved is 17, ie a transition to a state below the N=17 Landau level. It is interesting to make comparisons between the behaviour of these highly excited states in a magnetic field with the behaviour of highly excited Rydberg atoms in superstrong magnetic fields. Very similar oscillatory structure is predicted (Clark and Taylor 1980 and Connerade et al 1983).

A further interesting feature in the spectra of RR98B is the presence of two sharp peaks at fields just above the $1s-2p_{+1}$ transition (marked by a question mark in Figures 4.17 and 4.18). These peaks were absent in the spectra taken at 4.2K and are absent from the recording of S1 at 4.2K. However they are present at two wavelengths using two different pump lines and so the possibility of lasing at more than one wavelength giving rise to spurious peaks can be discarded immediately. There are a number of possible explanantions for these peaks:

i they are further central cell components of the $1s-2p_{+1}$ peak.

ii they are transitions from some form of complex.

iii they result from a different impurity transition.

The most likely explanation is that central cell shifts are responsible for the two components, although the other two explanations cannot be completely discounted. Note that the components are at magnetic fields well above those of the very shallow donors present in S1 and labelled iii (Pb), ii and i in Figures 4.5 and 4.6. If the peaks are due to central cell structure they ought to show spin splitting in 70.5μm spectra just like the other central cell components. No spin splitting can be discerned in the 70.5μm spectrum of RR98B, but the splitting would be on the limit of the

resolution of the trace and ideally a spectrum with an expanded magnetic field scale is required. If the peaks are due to central cell structure they would represent a considerable shift in the opposite direction to the normal central cell shifts in GaAs, ie a reduction of the 1s binding energy. The actual shift can be estimated in the following way. In the 118.8μm spectra the strongest of the two peaks appears at the highest field, 3.995 Tesla, while the X_3 donor is at 3.577 Tesla, a splitting of 0.418T. As $\partial E/\partial B$ = 14.7 cm^{-1}/T this corresponds to a splitting of 6.1 cm^{-1}. If central cell shifts are responsible then this splitting can be scaled to the zero magnetic field splitting. The calculations of Cabib et al (1972) for the variation of the central cell splitting in a magnetic field show that it is ~1.20 times greater at 3.6T than at zero field. Thus the splitting between X_3 and the high field peak is ~5.1 cm^{-1} at B=0. Now since the total central cell shift of X_3 at B=0 is +1.6 cm^{-1} (Cooke et al 1978), then the central cell shift for the largest '?' peak is -3.5 cm^{-1}, ie twice as large as that for X_3 in the opposite direction.

The second possibility was that the transitions arise from a complex, in a similar fashion to that described earlier in the chapter, except that the shift is quite substantial. It is possible that these transitions could originate on the D_2^0 or D_2^+ complexes that give lines seen at lower energy than that of the 1s-2p transition at zero field in GaAs, though this is speculative.

The third possibility is that other impurity transitions are responsible. However transitions out of the 1s ground state can be discarded immediately since all the hydrogenic transitions in this energy region have already been assigned. It is also unlikely that the sharp peaks are due to transitions to states associated with high

field quantum numbers since these are typically rather broad (eg $1s \rightarrow 1\bar{1}0$). However in addition to transitions out of the 1s ground state transitions can also take place between excited states. These are discussed in detail in Chapter 6. For example, a group of four transitions, A_1 to A_4, involving transitions from n=2 to 3 and n=3 to 4 ought to appear between 5.37 and 5.78 T for λ=118.8μm, and between 9.37 and 9.92 T for λ=70.5μm. There will also be a great number of transitions between other excited states, perhaps involving n=2 to 4 transitions, that would occur at higher energy than the A lines, and thus at lower fields in the spectra. One problem with this interpretation concerns the expected intensities of these inter-excited state transitions, which ought to be much lower than the intensities of transitions originating on the 1s ground state. Certainly the A lines cannot be seen, and these are the strongest (and only) group seen at fields below the cyclotron resonance in the spectra showing inter-excited state transitions appearing in Chapters 6 and 7. Thus it seems unlikely that the intensities of any of the other inter-excited state transitions would be sufficiently great to be observed next to the $1s-2p_{+1}$ transition.

Clearly further experimental studies are required in order to establish the origin of these transitions.

Chapter 5.

Central Cell Structure on the $1s-2p_{+1}$ Transition in InP.

In the previous chapter the central cell structure on the $1s-2p_{\pm1}$ transition of neutral shallow hydrogenic donors in n-type GaAs was studied. By using the combination of FIR laser spectroscopy and high magnetic fields, where $\gamma=\hbar\omega/2R^{*}\sim1$, significant improvements in resolution and linewidth were obtained over Fourier Transform Spectrometer studies, particularly on the $1s-2p_{-1}$ transition. At such high magnetic fields the linewidth should be sufficiently small for perturbations to the central cell structure due to complexing effects to be observable.

In this chapter attention will be concentrated on the $1s-2p_{+1}$ transition of neutral shallow donors in n-type indium phosphide. As noted in chapter 2 indium phosphide and gallium arsenide are very similar, both having a direct energy gap with a single nearly parabolic conduction band minimum at the Γ point. The effective masses and dielectric constants are of similar magnitudes. Consequently the general behaviour of the shallow donor energy levels in a magnetic field in InP is very similar to that in GaAs, and the effective mass approximation is still accurate. A comparison of some of the significant properties relating to magneto - optics is given in Table 5.1.

Table 5.1.

	GaAs	InP
Energy Gap E_G (eV)	1.5177	1.4236
m_e^*	0.0665	0.0803
ϵ_s	12.53	12.61
g_e^*	-0.44	1.26
R^* (cm^{-1})	46.1	59
Fröhlich α	0.068	0.113

The most important parameters are the electron effective mass m_e^* and the macroscopic static dielectric constant ε_o since these determine both the value of the effective Rydberg R^* for the shallow donors and the effective magnetic field γ. The effective Rydberg R^* in InP is 28% greater than that in GaAs while the electron effective mass is 21% greater. Consequently at a given magnetic field γ is lower in InP than in GaAs. For example, at 10 Tesla γ=1.52 for GaAs but only 0.99 for InP. Since the central cell splitting is a function of γ, the percentage change in splitting in InP at any particular magnetic field will be smaller than that in GaAs. However this effect is partially compensated by the increased zero field central cell splitting in InP since it was noted in the previous chapter that ΔE_{cc} at B=0 is proportional to m^*.

The larger value of the Fröhlich coupling constant α for InP indicates that it is a more polar material than GaAs and so perturbations from the effective mass approximation due to polarons, such as those seen in GaAs by Sigg, Bluyssen and Wyder (1983) and in InSb by Kaplan and Wallis (1968), would be expected to be larger. These effects occur when the $1s\text{-}2p_{+1}$ transition energy is near to resonance with the LO phonon energy. In GaAs E_{LO} is 296 cm^{-1} which is equivalent to $6.4R^*$ and in a simple parabolic band the theoretical $1s\text{-}2p_{+1}$ transition energy would cross this at ~18 Tesla. In InP E_{LO} is at a higher energy, 349 cm^{-1} but this is equivalent to $5.9R^*$, lower than in GaAs. However as the effect of magnetic field on the energy levels in InP is smaller the theoretical $1s\text{-}2p_{+1}$ energy does not cross the LO phonon energy until ~25 Tesla. In fact the fields at which these level crossings occur are even higher as the calculations take no account of non-parabolicity and use the band edge effective mass. Consequently the perturbations

to the energy levels due to polaron interactions in the magnetic field region from zero to ~10 Tesla should be as negligible as they were in GaAs.

As the band gap of InP is smaller than in GaAs one would expect non- parabolicity to be greater since non-parabolicity is influenced by the proximity of additional bands. However the most obvious consequence of non-parabolicity in GaAs is spin splitting of the $1s-2p_{+1}$ and cyclotron resonance transitions, and this is not observed in our spectra of InP. Thus with λ=70.5μm radiation the $1s-2p_{+1}$ transition in InP falls at ~8.6T or γ=0.84 but shows no spin splitting, whereas in GaAs at λ= 96.5μm the $1s-2p_{+1}$ transition at γ=0.76 shows a small but clearly resolved spin splitting. One possible explanation for this difference involves the effective g-factor g_e^*. In InP it is three times as large and of the opposite sign to its value in GaAs. Consequently the separation in energy between the two ladders of spin states will be three times larger in InP compared to GaAs, and thus the higher excited ladder may be significantly less populated in InP. As a result spin splitting may not be observed in InP simply because the amplitude of the second component of the split peak is too low.

However a more likely explanation for the absence of spin splitting is that to argue that a smaller band gap leads to greater non-parabolicity is not correct for materials with a large band gap such as InP and GaAs, and account must be taken of other bands. In fact Zawadzki et al (1985) have shown that a simple three band $\underline{k}.\underline{p}$ theory is unable to account for the magnitude of the spin splitting in GaAs, whereas a five band approach describes the observed splittings very well up to magnetic fields of ~20 Tesla.

Apart from this last major difference, GaAs and InP are

qualitatively very similar, and all the discussions of magneto-optical effects (for example line broadening mechanisms) in the previous chapter apply equally well to InP.

In practice the major difference between the two materials has been that the best InP available is still considerably less pure than the best GaAs. While high purity LPE and VPE GaAs has been grown since the early seventies, with 77K mobilities up to 200,000 $cm^2V^{-1}s^{-1}$ and N_D-N_A of the order of 10^{13} cm^{-3}, it is only in the last few years, ie the early eighties, that InP has been grown with 77K mobilities greater than 100,000 $cm^2V^{-1}s^{-1}$ and $N_d-N_a<10^{14}$ cm^{-3} (Fairhurst et al 1981, Taylor and Anderson 1983). Consequently the linewidths of the shallow donor transitions in InP are greater than in GaAs and the resolution of the central cell splitting is significantly worse.

As a result of the absence of high quality material the number of studies of the central cell structure of InP is small when compared to studies of GaAs. An interesting feature of the studies described here, and observed in other work not covered in this thesis (Armistead et al 1984), is that while the linewidths of the impurity transitions in GaAs can decrease by almost an order of magnitude as the 77K sample mobility increases from 50,000 to 100,000 $cm^2V^{-1}s^{-1}$, the quality of InP spectra does not appear to change significantly over the same mobility range. Only in samples with $\mu_{77}>100,000$ $cm^2V^{-1}s^{-1}$ is there any noticeable improvement.

The first magneto-optical studies of shallow donors in InP were reported by Chamberlain et al (1971) using Fourier Transform Spectroscopy and photoconductive detection. The behaviour of the transition energies with magnetic field indicated an electron effective mass of 0.0810 ±0.0005 m_o, in good agreement with masses

obtained from earlier observations of cyclotron resonance (Chamberlain et al 1970), magneto-phonon structure (Eaves et al 1970) and Shubnikov-de-Haas oscillations (Askenazy et al 1971). However the linewidth of the impurity transitions was too great for any central cell structure to be observed.

Observations of central cell structure on shallow donor transitions were first reported by Stradling et al (1972) using both Fourier Transform and FIR Laser spectroscopy. Since then a number of authors have reported central cell structure in VPE InP (Kirkman 1975 and Davidson et al 1980) and in VPE, MOCVD and bulk material (Armistead et al 1982, 1984). The structure observed by Kirkman using Fourier Transform spectroscopy was rather poorly resolved whereas the samples studied by Davidson et al using laser spectroscopy showed a large number of sharp well resolved central cell components.

Near Band Gap Photoluminescence Studies of High Purity InP.

It was noted in the previous chapter that the direct observation of the transitions of shallow donors or acceptors in the FIR is not the only method that can be used to study shallow impurities, and that the luminescence from a photo-excited semiconductor at low temperatures (~4K) at energies below the band gap is particularly rich in impurity related features.

As Dean and co-workers at RSRE have performed detailed studies of the near gap photoluminescence in high purity InP and are able to observe central cell split transitions (Dean, Skolnick and Taylor 1984) this section examines their technique in more detail.

In near band gap photoluminescence measurements (NGPL) samples of the semiconductor at a temperature of ~4K are illuminated with radiation at an energy near the band gap (λ~870nm for InP). This

radiation is usually generated with an argon or krypton ion laser or a tuneable dye laser.

If the laser energy is greater than the band gap free electrons and holes are created and if the excitation energy is well above the band gap high electron temperatures (~100K) can be achieved. These hot electrons and holes relax rapidly to the bottom of the band by acoustic and LO phonon emission. Electron-hole recombination may then occur through various radiative and non-radiative mechanisms. The principle radiative mechanisms are

i. formation of free electron-hole pairs - ie free excitons - followed by radiative recombination of the free excitons.

ii. formation of excitons bound to impurities in various charge states, followed by radiative recombination of these 'impurity bound excitons' - (D^0,X), (D^+,X), (A^0,X) and (A^-,X) are excitons bound at neutral and positively charged donors and neutral and negatively charged acceptors respectively.

iii. capture of electrons or holes at shallow impurity sites followed by direct donor-acceptor pair recombination

$$D^0 + A^0 \rightarrow D^+ + A^- + \hbar\omega$$

iv. band-acceptor and band-donor recombination

$$\text{free } e^- + A^0 \rightarrow A^- + \hbar\omega \qquad (A^0,e)$$

$$\text{free } h^+ + D^0 \rightarrow D^+ + \hbar\omega \qquad (D^0,h)$$

Figure 5.1, reproduced from Dean and Skolnick (1983), shows the photoluminescence spectrum for a high purity VPE InP sample (KV468 'etched') under 'moderately weak dyelaser excitation near E_G', with the peaks labelled according to the recombination mechanism involved. The donor-acceptor and (A^0,e) recombination bands are at lower energy and are not shown. The multiple peaks of the donor bound exciton $(D^0,X_n;\ n=1...6)$ are not due to central cell structure but

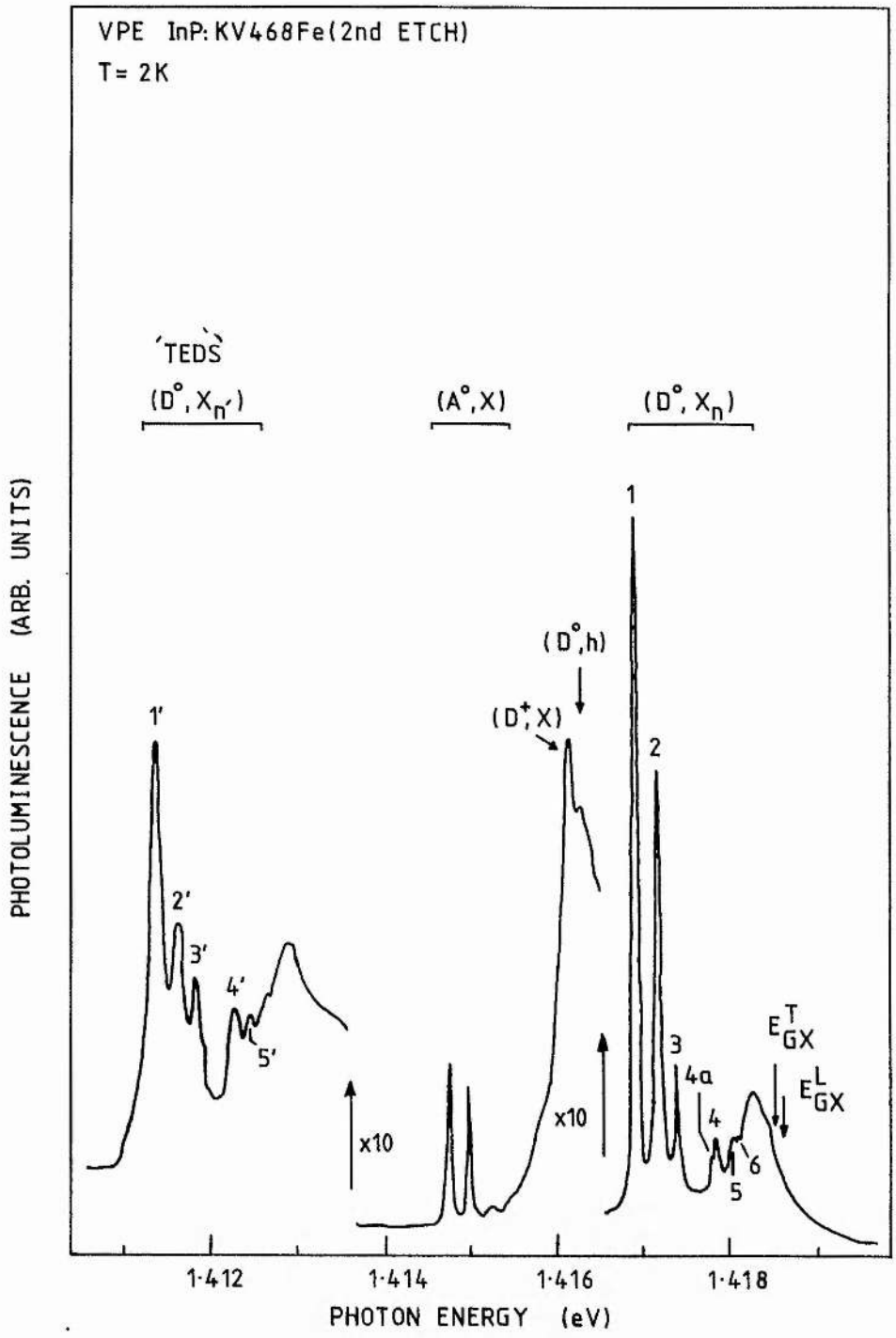

Figure 5.1: Near band gap photoluminescence spectrum of the high purity InP sample KV468 at a temperature of 2K (from Dean and Skolnick 1983). The various different types of transition due to different recombination routes are indicated. The transitions marked 'TEDS' are the 'two electron donor satellites' of the D^0, X_n transitions. E_{GX}^T and E_{GX}^L are the transverse and longitudinal free exciton energies.

arise as a result of the different angular momenta possible for a j=3/2 hole in the Γ_8 valence band maximum. This set of peaks is replicated at lower energy and corresponds to when, after recombination of the exciton, the neutral donor is left in the 2p or 2s excited state rather than the 1s ground state. Each peak in this second set, known as the 'two electron donor satellite' or 'TEDS' set (after Dean et al (1967a)) is separated from the equivalent (D^0,X_n) peak by the 1s-2p,2s transition energy, and thus TEDS peaks should show central cell shifts and splittings. In InP at zero magnetic field the linewidths of the TEDS transitions are too great for any central cell splitting to be resolved, but VPE GaAs (Almassy et al 1981), ZnTe (Dean and Herbert 1979) and ZnSe (Dean, Herbert and Lahee 1980) have all shown central cell split peaks.

Various techniques have been employed by Dean and co-workers which have enabled them to resolve central cell splitting in InP using NGPL. As in FIR spectroscopy the application of a high magnetic field reduces the spatial extent of wavefunctions and narrows transitions significantly. This also has the effect of splitting the TEDS peaks into groups with final states $2p_{\pm1,0}$ and 2s.

A further technique that reduces the linewidth is referred to as 'selective excitation' or 'resonant enhancement'. With this method a dyelaser is tuned to resonance with one of the (D^0,X_n) components at an energy below the band gap. Neutral donor bound excitons are then created at neutral donor sites. In high quality samples where there are no lattice strains in the crystal the major contribution to the linewidths of the exciton transitions is from inhomogeneous broadening due to the random electric fields of ionized impurities within the crystal. As the shift of the transition energy depends on the electric field at the exciton site, which in turn depends on the distance from

the nearest ionized impurity site, each excitation energy within the overall linewidth will correspond to excitons bound at sites with specific nearest-neighbour distances. Then provided that the laser excitation has a linewidth much less than the overall linewidth of the (D^0,X_n) transition, neutral donor bound excitons will be selectively excited at only those sites with a specific nearest neighbour distance. If these resonantly excited neutral donor bound excitons recombine leaving the electron in the 2p,2s state (ie giving a TEDS line) then the photoluminescence lines should have the same linewidth as the laser excitation - much less than the natural linewidth of the TEDS transition. The factor limiting the practical reduction in linewidth that can be achieved depends on how the electric field broadening compares with other broadening mechanisms (eg strain) and on whether the radiative recombination of the exciton occurs before the exciton migrates to a neighbouring D^0 site. If the inter-donor migration rate is too fast recombination does not occur at the site at which the exciton was created but at a site which experiences a different random electric field and thus the photon energy is shifted and no line narrowing can occur. As the inter-donor migration rate is proportional to the impurity concentration it is only in very high purity material that line narrowing can be achieved using selective excitation techniques.

In the initial studies of InP using selective excitation with a large number of VPE grown samples no linewidth reductions were observed and no central cell structure could be resolved (Dean and Skolnick 1983). Subsequent experiments using higher magnetic fields and higher purity samples from a different growth reactor have shown line narrowings under selective excitation and central cell splitting due to residual donors (Dean, Skolnick and Taylor 1984). The specific

results of this work and its relation to the residual donors seen with FIR laser spectroscopy are discussed in later sections of this chapter.

Choice of Transition Line and Laser Wavelength for FIR Studies of Central Cell Structure in InP.

All the studies of central cell structure in InP and GaAs have concentrated on either the $1s-2p_{+1}$ or $1s-2p_{-1}$ transitions since these are the strongest lines. Fourier Transform studies are usually made of the $1s-2p_{-1}$ transition, since it is narrower than the $1s-2p_{+1}$, and its energy changes only slowly with magnetic field. Although a low value of $\partial E/\partial B$ is useful in FIR laser spectroscopy in that it spreads the transition out over a large field range, it is also a disadvantage since it implies that a laser line must be found within a narrow wavelength range. Consequently most FIR laser studies concentrate on the $1s-2p_{+1}$ transition which is accessible over a large range of laser wavelengths since its energy increases rapidly with magnetic field, and so the transition can be studied at various magnetic fields.

As the advantages of being able to study the $1s-2p_{-1}$ transition are significant a number of different gases were tried in the laser to see if a line lasing in the correct wavelength region could be obtained. Figure 5.2 shows the theoretical variation of the $1s-2p_{-1}$ energy in a parabolic band (solid line) (Makado 1982) over the field range $0<B<12.7T$ available at St. Andrews. The dotted line represents the theoretical transition energy for a donor with $2cm^{-1}$ central cell splitting at zero magnetic field (using the figures of Cabib et al (1972) for $|\Psi(r=0)|^2$ in a magnetic field to calculate the variation of central cell splitting with field). If all the donors have central cell shifts within the range 0 to 2 cm^{-1} then in order for them all to appear within the 12.7 Tesla maximum field of the

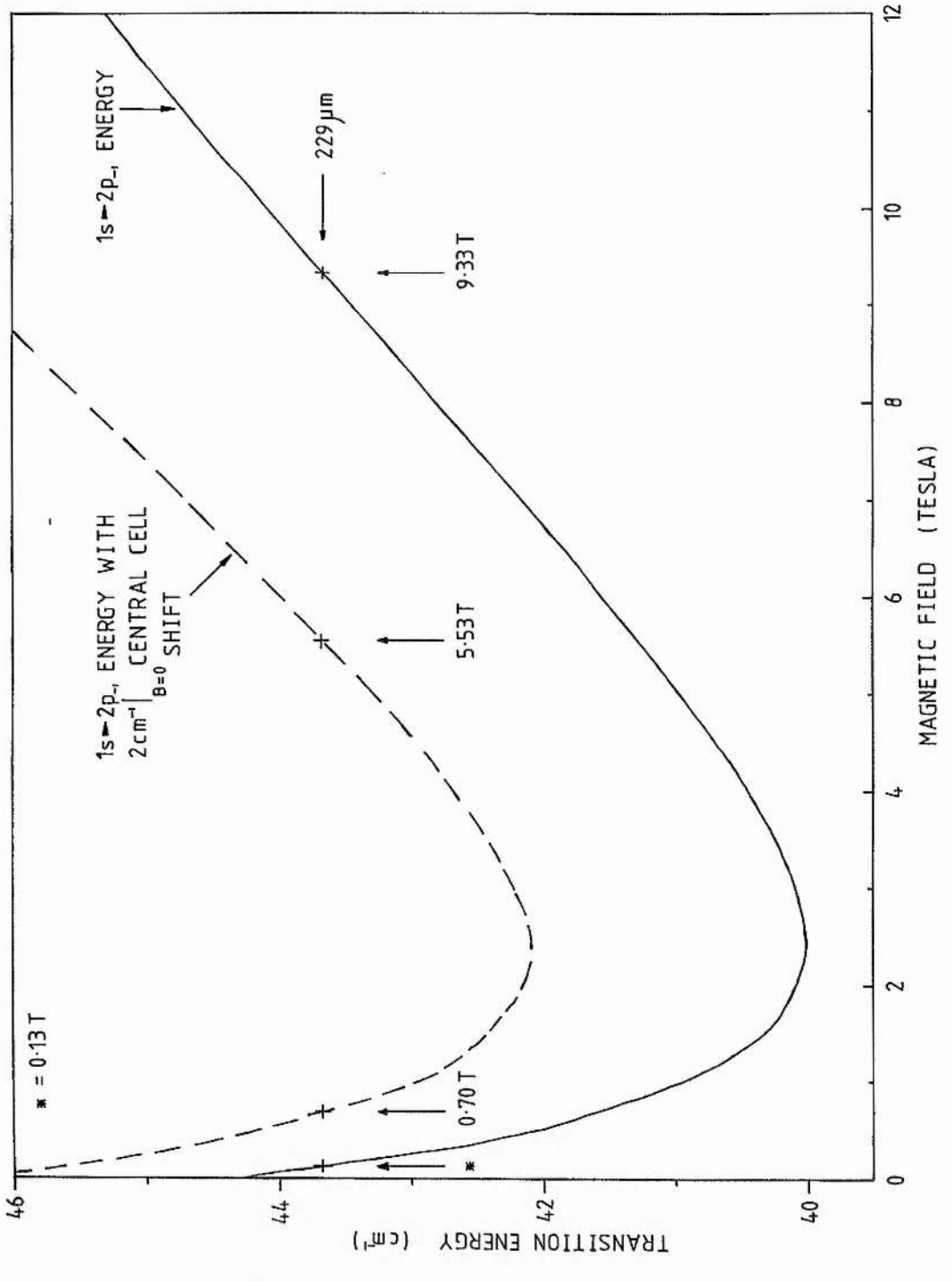

Figure 5.2: The solid curve shows the $1s-2p_{-1}$ transition energy in a parabolic band plotted against magnetic field and scaled for InP assuming $R^* = 59cm^{-1}$ and $m^* = 0.0803m_0$. The dotted curve shows the transition energy of a donor with a central cell shift of 2 cm^{-1} at B=0. The magnetic fields at which the transitions would appear are shown for a laser wavelength of 229μm (from CH_3OD).

magnet the laser energy must lie in the range 42.1 to 45.7 cm^{-1} corresponding to wavelengths in the range 219 to 238 μm, a range of only 19 μm.

None of the gases available would lase within this region. These gases (see chapter 3 for a list) included CH_3OD which is supposed to lase at 229μm, and which would be ideal, placing the $2\rightarrow0 cm^{-1}$ range of central cell splittings between 5.54 and 9.67 Tesla. In chapter 4 the spectrum of the $1s-2p_{-1}$ transition in Figure 4.17 was taken using this line with the laser system at the Max-Planck Institute in Grenoble. Considering the ease with which the Grenoble system lased at 229 μm, it is not fully understood why the St. Andrews laser would not do the same. It is possible that contamination of the CH_3OD used when the experiment was performed, or the possibility that the deuterium may migrate to other sites, resulted in increased FIR thresholds. The Grenoble laser system has the advantage of running with a continuous flow of gas, whereas the St. Andrews system runs in a sealed mode. A supply of flowing gas ensures that clean uncontaminated gas is always present in the FIR cavity. Furthermore the gas pressure is more easily controlled in a flowing gas system, simply by adjusting a needle valve, and since variations in gas pressure sometimes critically affect the FIR power output it is useful to have this control. Alternatively poor alignment of the CO_2 pump laser with the FIR cavity at the time of the experiment (which was early in the author's experience with the system) could have led to a much higher lasing threshold, preventing correct operation.

As the author's visit to Grenoble took place at the end of the program of experimental work there was insufficient time for a new set of experiments to be tried with CH_3OD or even for the gas to be tried again in the laser, based on the experience gained during the visit.

Experimental Results.

Sample Characteristics

A total of twelve different undoped InP samples were studied with three different growth techniques being represented. All of these were grown at the Royal Signals and Radar Establishment, Malvern.

Six of the twelve were grown by Dr.D.Robertson and co-workers using chloride transport vapour phase epitaxy ($In/PCl_3/H_2$). Growth of this material, the best InP available at the time, has been discussed in detail by Fairhurst et al (1981). More recently RSRE has produced InP with higher mobilities using the same technique but a different reactor (known as the NAG reactor as opposed to the earlier KV reactor) (Taylor and Anderson 1983).

The electrical characteristics of these samples are given in Table 5.2 and were determined from 300 and 77K Hall effect measurements. (Data supplied by RSRE).

Studies were also made of a section of one of the VPE wafers, KV468, which had had part of its epitaxial layer etched away. The etching, performed at RSRE, used a standard bromine-methanol solution to remove approximately half of the epitaxial layer. The part of this wafer used in our experiments is referred to as KV468(etched) to distinguish it from the as-grown sample KV468(unetched) (the two samples are physically different).

Of the remaining six samples, five were grown using 'metal organic chemical vapour deposition' (MOCVD or sometimes MOVPE, and occasionally known as the 'alkyl' process) by Dr. S.Bass (Bass, Pickering and Young 1983). In the process used by Bass et al the indium is transported to the substrate as an alkyl gas (tri-methyl indium or TMI) while phosphine is used to transport the phosphorous.

Table 5.2.

Electrical Characteristics of Indium Phosphide Samples.

Sample	Thickness μm	Concentration $x10^{14}$ cm^{-3} 300K	77K	Mobility $cm^2V^{-1}s^{-1}$ 300K	77K	Substrate Doping
VPE Grown	Source: Dr. D.A.Roberston (RSRE Malvern)					
KV288	8.4	1.0	0.78	5419	110000	Cr
KV308	8.0	1.3	0.73	4906	80864	Not known
KV309	8.4	4.0	2.6	5334	89556	Cr
KV348	8.6	7.8	6.5	5000	103000	Cr
KV454	12.6	1.8	1.7	5100	99000	Cr
KV468	9.0	1.5	1.6	5323	92494	Fe
KV469	8.5	4	4	5300	83000	Fe
MOCVD Grown	Source: Dr. S.J.Bass (RSRE Malvern)					
792	7	15	15	3841	51000	Fe
800A	5	25	22	4300	26600	Fe
805A	No information available					
806A	4.5	18	18	4702	55300	Fe
807A	4	20	20	4430	49300	Fe
Bulk Grown	Source: Dr. B.Cockayne (RSRE Malvern)					
L816	N/A	35	34	5200	39400	Undoped

i. All samples are undoped.

ii. Epitaxial samples were grown on <100> semi-insulating substrates cut from bulk LEC boules.

The remaining sample studied was cut from a bulk crystal grown by the liquid encapsulated Czochralski (LEC) technique by Dr. B.Cockayne.

All of the epitaxial samples were grown on <100> semi-insulating Cr or Fe doped substrates cut from single crystal LEC boules.

Experiments were performed at a temperature of 4.2 or 1.8K with λ=118.8 or 70.5μm radiation obtained using methanol gas in the FIR laser system. The maximum sample bias voltage was 400mV at zero magnetic field which, assuming a minimum contact separation of 2mm, corresponds to a maximum bias field of ~2V/cm, well below breakdown.

Residual Contamination in VPE Grown InP Samples:

A Discussion of Central Cell Structure on the $1s-2p_{+1}$ Transition.

Figure 5.3 shows the $1s-2p_{+1}$ shallow donor transition at ~3.6T using a laser wavelength of 118.83 μm for the six samples grown by the chloride transport VPE process. The spectrum of the etched sample of KV468 is also shown. The spectra were recorded under the conditions of temperature and band gap optical excitation which gave the best resolved central cell structure and have been normalized to the same maximum amplitude. The actual conditions for each sample are given in the figure caption.

The most striking feature of the central cell structure in all of these undoped samples is the presence of the strong component #5 at 3.660T. The donor responsible for this peak is apparently the major contaminant in samples KV288, KV309 and KV348, and is also a major contaminant in KV468(unetched), KV468(etched) and KV469. In KV288, KV309 and KV348 a second donor is present at lower amplitude and appears to be at the position of line #3 (3.699T). In KV348 there is a sharp spike on the high field side of donor #3 which was reproduced in other experimental runs. In KV468(unetched), KV468(etched) and KV469

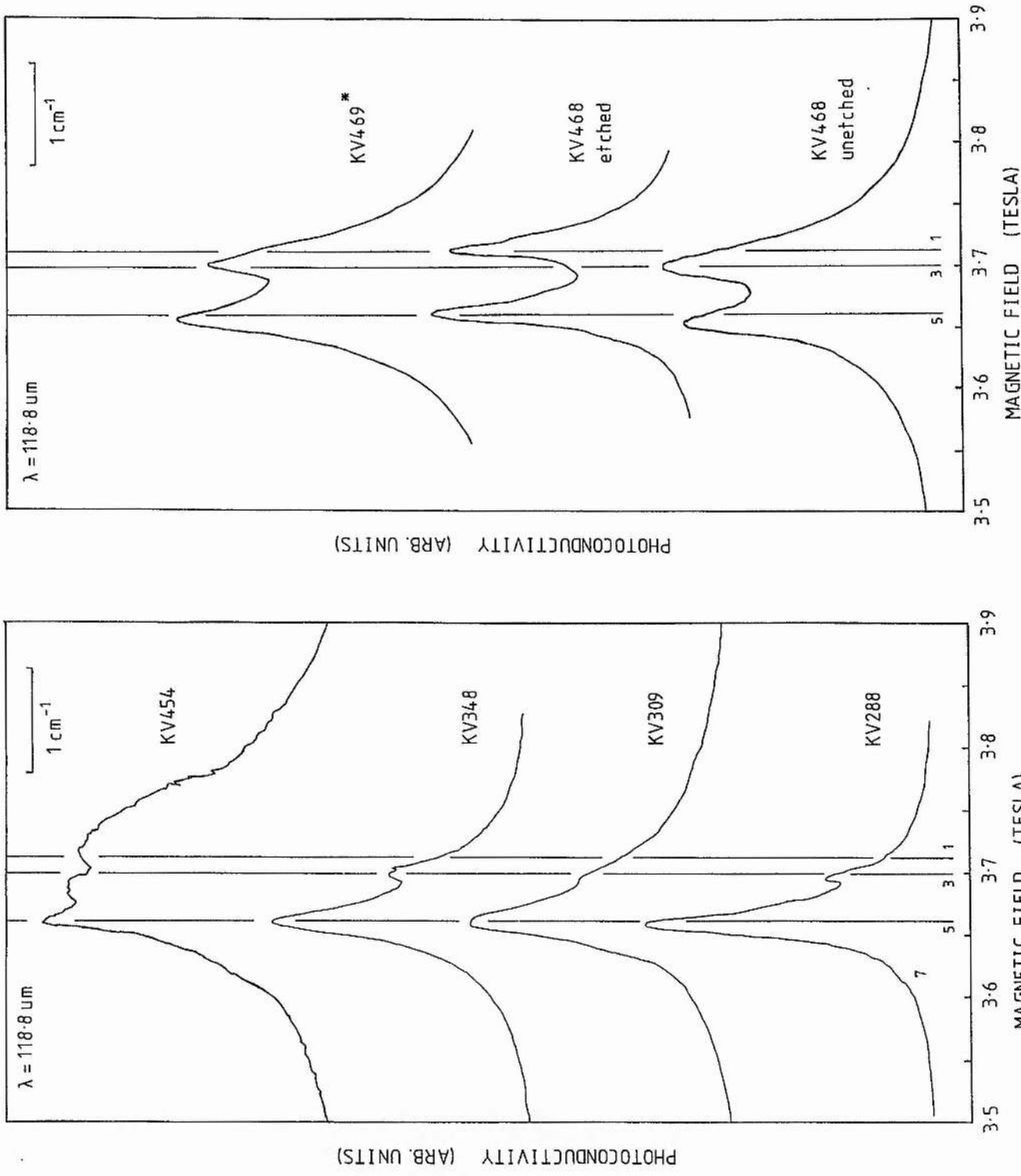

Figure 5.3: Spectra showing the central cell structure on the $1s-2p_{+1}$ transition for the high purity VPE InP samples using λ=118.8μm radiation. The sample temperature was 4.2K except for KV288, KV348 and KV468(unetched) which were at 1.8K. Optical excitation was used for all samples except KV468(unetched) and KV469. The recording of KV469 was taken using the 6.7T magnet and is shifted slightly to low field by ~0.01T.

the situation is slightly different as the second component is at approximately the same amplitude as donor #5. In KV468(unetched) and KV469 it appears to be at the position of line #3, whereas in KV468(etched) it appears at the slightly higher field of line #1 (3.710T). In KV469 there is a slight shoulder present on the high field side of donor #3 suggesting that donor #1 may also be present at lower amplitude. KV288 also shows a very small shoulder at the position of donor #1. In addition some spectra of KV288 showed a shoulder at the position indicated by the label #7.

Up until now no mention has been made of KV454. Although in common with the other samples the dominant peak appears to be that of donor #5, two peaks appear at higher field with a longer and unusually shaped tail to high fields compared to the other samples. Neither of these two peaks are in good agreement with the two donors #3 and #1 seen in the other five samples. However it is significant that the minimum between the two high field peaks lies near the positions of donors #3 and #1. This suggests that the 'peak inversion' or 'notch' effect may be present. Although peak inversion on strong components has been noted in GaAs it has not been reported in InP. If a notch is present in the spectrum of KV454 then the high field donor must be present at much higher concentration than donor 5 and this could go some way towards explaining the unusual high field tail. It is interesting to note that KV454 is unusual amongst the VPE samples in having a particularly thick epitaxial layer - 12.6μm compared to the 8 to 9 μm thicknesses of the other five samples. In view of the recent work of Stillman et al (1985) on the dependence of the notch effect on epitaxial layer thickness the 50% difference in layer thickness could be significant.

A sample from the same reactor (KV308) has been studied by other

workers under similar conditions (Davidson et al 1981). Figure 5.4 (top) shows a spectrum of KV308 taken at the same time as the one published by Davidson et al but under slightly different conditions of optical excitation and bias voltage (Knowles and Sessions, unpublished). The electrical characteristics of KV308 are included in Table 5.2 for comparison. An H_2O gas discharge laser (λ=118.591μm) was used and the sample temperature was ~1.6K (the small difference in wavelength compared to the 118.8μm methanol line shifts the $1s-2p_{+1}$ transition energy 0.019T to higher field). When the spectra of KV308 (Fig 5.4 top) and KV309 (Fig 5.3) are compared it is clear that the spectrum of KV308 has a much lower linewidth and far more structure is visible. Although the spectrum shown of KV309 was taken at a temperature of 4.2K rather than the 1.6K used for KV308, spectra of KV309 at 1.8K showed no significant changes. At first sight this is surprising as KV308 has a lower 77K mobility than KV309 and might be expected to be less well resolved. However since KV308 also has a particularly low impurity concentration, $7x10^{13}$ cm^{-3}, it is probably highly compensated. Thus the impurity transitions may well show a significant reduction in linewidth as the temperature is reduced due to the correlation effect (discussed in chapter 4) where in compensated material as the temperature is reduced the distribution of ionized impurities tends towards a collection of ionized donor-acceptor pairs rather than a random collection of isolated ions. As an ionized donor-acceptor pair has a dipolar charge distribution it has a shorter range electric potential than an isolated impurity and thus the contribution to the linewidths of the impurity transitions due to electric field broadening is reduced. As KV309 is less compensated it does not show as great a reduction in linewidth on reducing the temperature from 4.2 to 1.8K.

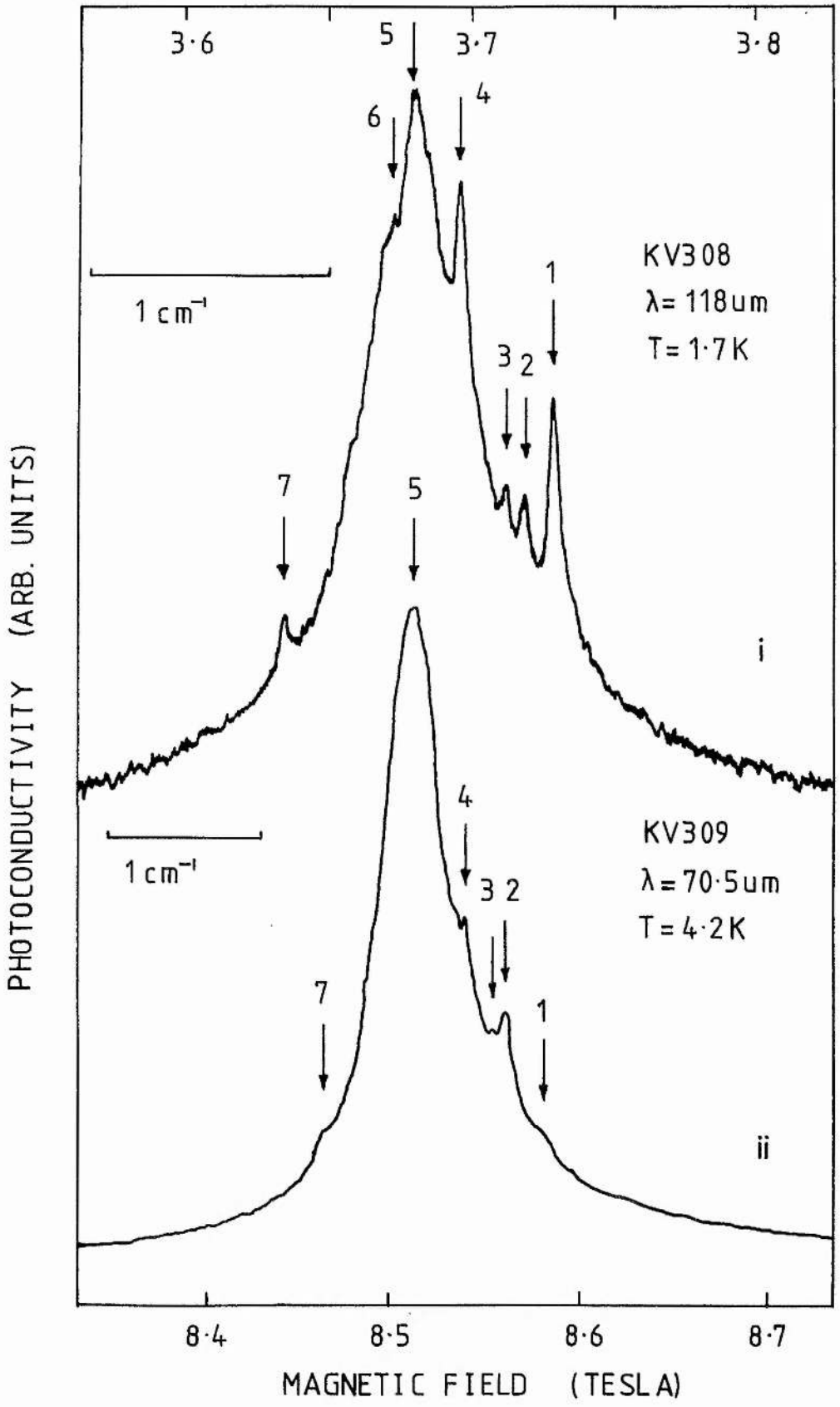

Figure 5.4: The upper recording shows the central cell structure of KV308 at T=1.8K and with optical illumination using 118μm radiation from an H_2O gas discharge laser (obtained by Knowles and Sessions (unpublished). The lower trace shows the spectrum of KV309 at T=4.2K with optical illumination, but obtained at St. Andrews at higher magnetic field using 70.5μm radiation from the optically pumped FIR laser system.

In order to achieve an improvement in the linewidths the spectra were also studied at higher magnetic fields using the 70.5μm laser line. The lower portion of Figure 5.4 shows the spectrum of KV309 at 4.2K with this line. It is clear that a considerable reduction in linewidth has been achieved and six of the seven components seen in KV308 in Fig 5.4(top) have now been resolved in KV309. (All the features indicated on KV309 were reproduced in other spectra). However the central cell structure is still not as well resolved as that of KV308 at 3.6T and 1.6K. Unfortunately it was not possible to obtain a spectrum of KV309 at λ=70.5μm and 1.8K.

Comparing the upper and lower portions of Figure 5.4 it is clear that no spin splitting can be resolved on λ=70.5μm spectra, whereas at this field in GaAs the $1s-2p_{+1}$ transition showed strong splittings which made interpretation of spectra difficult if there were any number of central cell components present. Various explanations for the absence of spin splitting in InP were discussed earlier in the chapter.

Figure 5.5 shows all the spectra for the KV series samples with the exception of KV454 which was very noisy at high fields. KV309 is shown again for convenience. Sample 807A is an MOCVD sample and is discussed later. All the recordings have been normalized to the same maximum amplitude. The lines 1→7 (excluding 6 which was not resolved in these samples) have been drawn to coincide with the components in KV309. No allowance has been made for any shifts in the positions of the low amplitude peaks in KV309 which may have occurred due to the proximity of the dominant peak #5 (a peak pulling effect). The magnetic field positions of the lines (and thus of the peaks in KV309) are given in Table 5.3 together with the central cell splitting from the dominant donor #5 measured in cm^{-1} and meV (calculated assuming

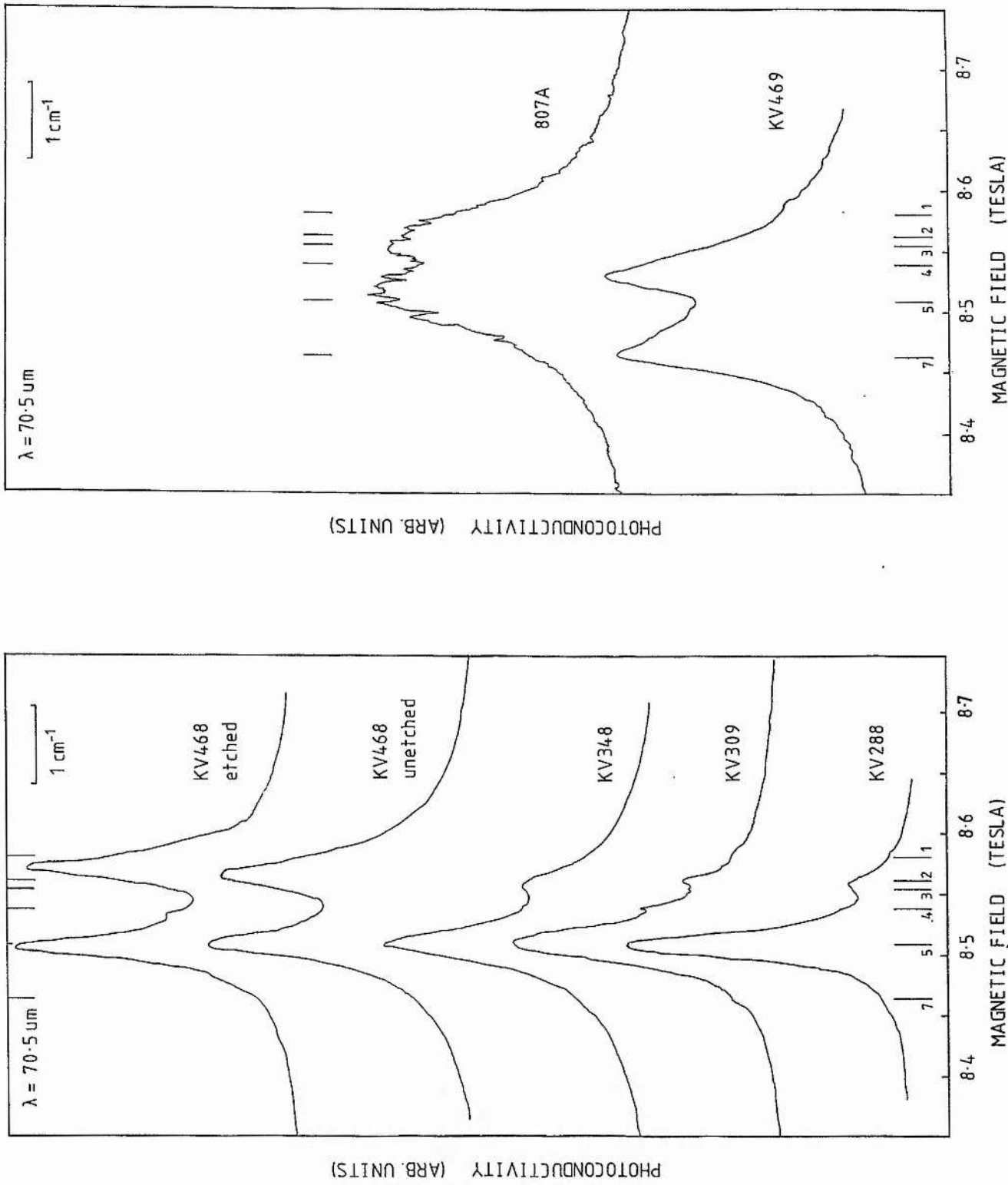

Figure 5.5: Spectra showing the $1s-2p_{+1}$ central cell structure for the VPE InP samples and an MOCVD sample (807A) using λ=70.5μm radiation. The sample temperature was 4.2K except for KV288 which was at 1.8K. The spectra of samples KV288, KV309, KV468(etched) and KV468 (unetched) were taken using optical excitation. The recording of KV469 is shifted to low field by instrumental effects.

Table 5.3.

Peak	Magnetic Field	Central Cell Splitting	
	Tesla	Relative to donor #5	
		(cm^{-1})	(meV)
1	8.583	-0.91	-0.113
2	8.561	-0.64	-0.079
3	8.555	-0.57	-0.070
4	8.538	-0.36	-0.044
5	8.509	0	0
6	Not observed	-	-
7	8.464	+0.55	0.069

$\partial E/\partial B$ = 12.3 cm^{-1}/T for the $1s-2p_{+1}$ transition in InP at 8.5T.

The λ=70.5μm spectra clearly confirm the features seen in the lower field λ=118.8μm spectra. Donor #5 is present in all of the samples. However as noted in the λ=118.8μm results the position of the high field components varies from sample to sample. Both KV288 and KV348 show either donors 2 or 3 (or perhaps even both). However the linewidths of the two samples, together with possible peak shifting effects would make any attempt at pinning the identification to either possibility pointless.

Identifying the high field component in KV468(unetched), KV468 (etched) and KV469 presents even more of a problem. The spectrum of KV469 in Figure 5.5 has been shifted by instrumental effects to the low field side of its true position (a combination of too fast a magnetic field sweep rate with too long a time constant on the PSD). Other spectra of KV469 at 70.5μm confirm that the low field peak is donor #5. There does not appear to be any strong correlation between the peak positions of the high field donor in the three samples and the three donors #1, #2 and #3. Furthermore, when the spectra of KV468(unetched) and KV468(etched) are compared it is apparent that the etched sample has a narrower linewidth. This would suggest that the etching process has removed material which had a higher impurity concentration than the material closer to the substrate. These points are discussed in more detail in the following section. However, the reduced linewidth of the etched sample has resolved a third donor at approximately the position of donor 4.

The structure observed in these KV samples is consistent with that seen in high quality samples from the NAG reactor at RSRE. These NAG samples consistently show the same two dominant central cell components as KV468 and KV469 with similar amplitudes, and the highest

purity NAG samples also show a number of weak central cell components which correlate well with the weaker peaks in KV308 and KV309 (Armistead et al 1982, 1984, Najda 1985).

Tentative assignments of some of the central cell components seen using Far infrared photoconductivity techniques (FIRPC) have been made using back doped samples (Kirkman 1975, Davidson et al 1980, Armistead et al 1982, 1984 and Najda 1985). FIRPC studies show that the dominant donor #5 present in all samples appears to be associated with sulphur while weak doping with silicon produces a stronger peak in the region of the high field donors, (#1, #2 and #3). However it is not clear which, if any, of these sharp components in KV308 and KV309 is due to silicon.

The conclusions of NGPL studies of back doped NAG samples are in agreement with these silicon and sulphur assignments (Dean, Skolnick and Taylor 1984). In FIRPC studies the splitting between the two dominant donors in KV468(unetched) at 8.5 Tesla is 0.056 Tesla. As the gradient of the $1s\text{-}2p_{+1}$ transition at this field is ~12.3 cm^{-1}/T this corresponds to a splitting of 0.69 cm^{-1}. This is in good agreement with the splitting between the sulphur and silicon donors in the NGPL experiments which was 0.088meV or 0.71 cm^{-1} at a field of ~9 Tesla.

Further NGPL and FIRPC studies of Ge and Sn doped samples agree that Ge donors produce a broad peak in the region of the deep donor #7 and Sn donors produce a broad peak slightly to low magnetic field of the sulphur donor #5, and so may be associated with donor #6 in KV308 (Skolnick et al 1984).

Thus the relative ordering of the central cell components in InP is (Ge : Sn : S : Si) which is different to that in GaAs where the order is (Ge : S : Sn : Si). At one time it was thought that Sn donors

gave a peak with a particularly shallow central cell shift, ie on the high magnetic field side of the spectra in the region of donor #1, on the basis of spectra of a neutron transmutation doped sample (indium transmutes into tin on irradiation with neutrons). However re-examination of the sample five years later showed that the 'tin' peak had disappeared and was almost certainly due to some form of radiation damage which gradually annealed out (Stradling, unpublished). Neutron transmutation doped InSb has shown similar effects - after irradiation a sample showed one principle central cell component and two satellites, but after deliberate annealing the two satellites had disappeared leaving the main peak which was attributed to introduced Sn donors. The satellites were tentatively attributed to complexes due to radiation induced damage (Kuchar et al 1984). There is also tentative evidence for changes in the spectra of KV series samples over a period of time - when KV469 was re-examined one year after the spectra shown in Figures 5.3 and 5.5 were taken the intensity of the Si peak had reduced to approximately a half that shown in the figures.

Studies of the Central Cell Structure of Etched Samples.

As noted earlier, spectra have been obtained from a sample of KV468 which had had approximately half its layer removed by chemical etching, as well as from an as-grown sample from the same wafer. The ideal situation would have been to study the same sample both before and after etching, but this was not possible. In the following discussion it is assumed that there were no variations in the impurity concentration across the epitaxial wafer.

Figure 5.6 shows the spectra of the two samples under various conditions of temperature and optical excitation. The left hand column

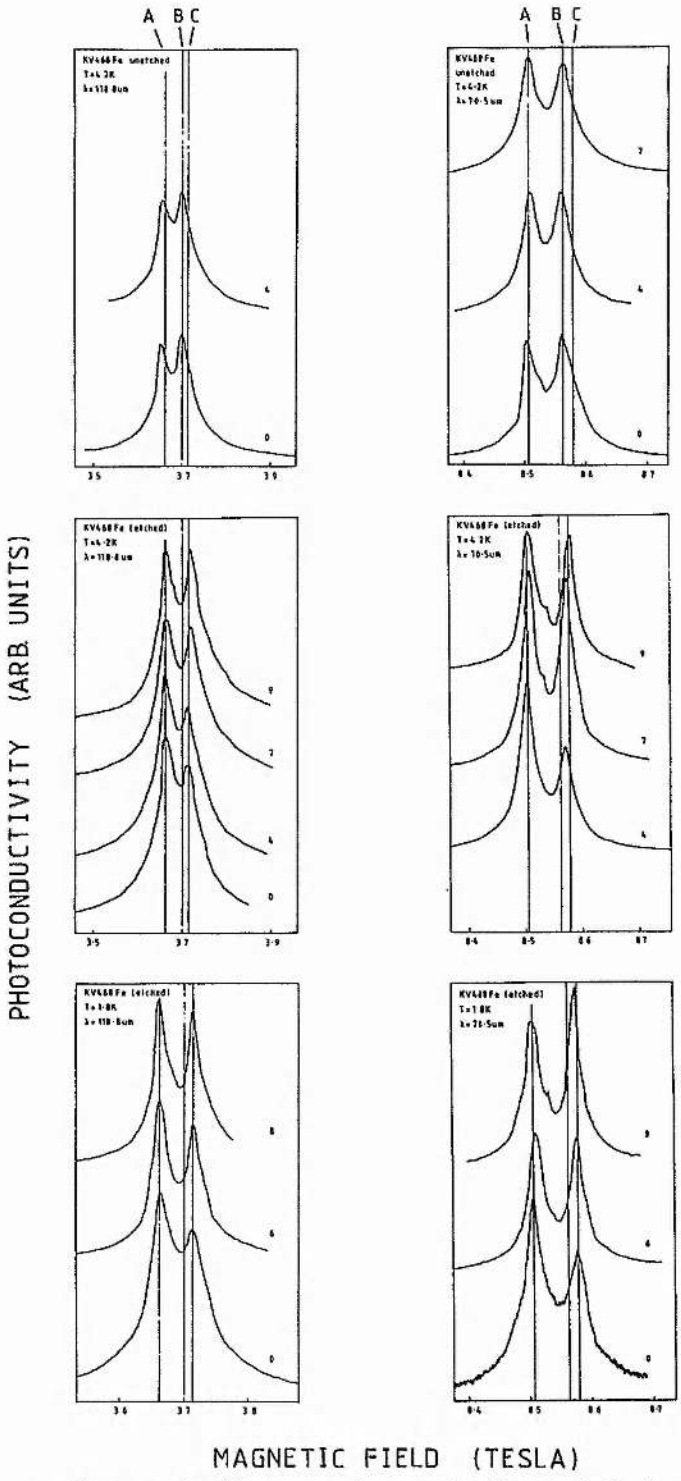

Figure 5.6: Comparison of the spectra of the etched and unetched samples of KV468. Spectra in the left hand column are at 3.6 Tesla with λ=118.8μm radiation while those in the right hand column are at 8.5 Tesla with λ= 70.5μm. The top row shows the unetched sample at 4.2K; the middle and bottom rows show the etched sample at 4.2K and 1.8K respectively. Each figure shows the spectrum under various conditions of optical excitation (indicated by 0, 4, 6, 7 and 9). Note how the high magnetic field donor appears at B in the unetched sample but at C in the etched sample.

shows the spectra obtained at λ=118.8μm with B~3.5T while the right hand column shows spectra obtained at λ=70.5μm and B~8.5T. The top row shows KV468(unetched) at 4.2K while the bottom and middle rows show KV468(etched) at 4.2K and 1.8K respectively. Each of the diagrams shows the spectra at different levels of optical excitation, though the level indicated is only a general guide: 0 is 'no light', 4 is 'medium', 8 and 9 are 'strong'. The spectra confirm the points noted earlier that

a. the linewidths of the central cell components in KV468(etched) are significantly narrower than those in KV468(unetched).

b. irrespective of magnetic field, temperature or level of optical excitation the position of the highest field donor peak in KV468(etched) is at a significantly higher magnetic field (ie at position 'C') than in KV468(unetched) where it is at position 'B'. The lines on the diagrams are at the following magnetic fields:

Line	λ=118.8μm	λ=70.5μm
A (#5)	3.662	8.506
B	3.700	8.562
C	3.714	8.579

The separation B-C at 118.8μm is 0.014T equivalent to 0.17 cm^{-1} (0.021meV) while at 70.5μm it is 0.017T or 0.21 cm^{-1} (0.026meV).

c. the ratio of the peak amplitudes of the two dominant central cell components in KV468(unetched) are relatively unaffected by the level of optical excitation and are close to 1:1. In KV468(etched) the high field peak without optical excitation is at lower amplitude relative to donor #5 than in the unetched sample, but consistently increases in amplitude relative to donor #5 as the optical excitation is increased.

It is possible that the 'notch effect' investigated by Stillman et al (1985), and observed in spectra of GaAs samples in chapter 4 and possibly present in spectra of KV454, could produce the differences in linewidths observed in these spectra. This would appear as a reduction in linewidth as samples are etched, as Stillman et al showed that notching is greatest for samples with thick layers. However these samples are already very thin compared with the thicknesses that Stillman was refering to, and no clear evidence exists for notches in the spectra of KV468. However one cannot rule out the possibility that some precursor of the notch effect is distorting the lineshape of transitions in the unetched sample and giving the impression of a misleadingly broad transition.

A further mechanism by which a reduction in linewidth might occur would be if the surface was subject to significant strain, which was removed on etching. However strain is much more important in photoluminescence experiments where the spectral features are significantly broader if strain is present and the as-grown wafers all showed narrow features. In fact Dean, Skolnick and Taylor (1984) often observed that etching samples for NGPL studies resulted in a decrease in spectral quality, which they attributed to deformation of the sample during the etching process, with a consequent increase in strain. If significant strain was present in the as-grown layers then one would expect to see much wider variations in the quality of the central cell structure from sample to sample than actually occurs.

The most attractive explanation for the reduction in linewidth when part of the surface is removed is that the impurity concentration was higher at the surface than within the epitaxial layer, and when the high concentration region was removed layers of lower concentration and hence lower linewidth were exposed. It has been

noted by Dean and Skolnick (1983) that several of the KV series samples had non-uniform impurity concentrations with depth when measured with a C-V plotter and often showed an increase in N_D-N_A at the surface of the layers. Occasionally the profiles were U-shaped with an increase in concentration at the interface with the substrate in addition to the surface. Unfortunately no profile data is available specifically for KV468.

An alternative explanation to a variation of donor concentration with depth would be a variation of acceptor concentration with depth. The total number of ionized sites and thus the overall linewidth would then change with depth. However this explanation is unlikely to be the case for KV468, since if the compensation was high one would expect to see some indication of a change in linewidth as the temperature is reduced, due to the increasingly dipolar nature of the electric fields characteristic of the correlated ionized donor-acceptor distribution that forms as the temperature is reduced (see chapter 4 for a more detailed discussion).

The general impression gained from the spectra without band gap illumination shown in Figure 5.6 is that the etched sample of KV468 has a lower proportion of the high field component C present than component B in the unetched sample, where the concentrations are approximately equal. This suggests that the higher impurity concentration at the surface is due to the donor responsible for the high field peak, whereas donor #5 was incorporated more uniformly throughout the sample. The dependence of the ratio of the high field donor to donor #5, ie [C]/[A], with optical excitation in KV468(etched) supports this observation, since an increase in the intensity of the high field component with excitation suggests that the donor is present mainly in the region of material influenced by band gap radiation, ie the surface of the epitaxial layer.

Having established that the donor responsible for peak B in KV468(unetched) is predominantly at the surface of the epi-layer, the question remains as to why its central cell shift is reduced by etching.

The effect of peak pulling (ie a shift in the apparent position of a peak as a result of its proximity to another strong peak) cannot be responsible for the change in the position of the high field component (B or C) on etching. This is clear from the observation that in Fig 5.6 changes in the peak ratio and linewidth caused by variations in the level of optical excitation have no significant effect on the peak positions.

The possibility that the change in peak position is due to a change in the relative amplitudes of two chemically different isolated donors, sufficiently close together to be under-resolved is also unlikely since KV468(unetched) clearly shows very little signal at the position of peak C seen in KV468(etched) and vice versa for peak B.

The two possible peak positions must then be due to the same donor, whose central cell shift has been changed with etching. One effect which may change the central cell shift is that of lattice strain. Theoretical work by Fedders (1983) has shown that random variations in strain can cause additional broadening and the magnitude of this broadening may vary according to the donor species. It is possible that a uniform strain could produce an overall shift of the central cell components. However one would expect to see at least some indication of strain induced shift on the other donor species, and yet the position of donor #5 has clearly not been affected by the etching process. Furthermore, the variations in strain from sample to sample will usually be much larger than the variations within an epitaxial layer, and yet there are no significant differences in the magnetic

fields of the other central cell components from sample to sample.

A further possibility is that some feature associated with the silicon donors responsible for the component B|C, but which is predominantly present in the surface layer, is responsible for the change in central cell shift. The type of feature envisaged is that of a complex involving a shallow donor with a deep impurity or a lattice defect such as a lattice vacancy. As the variation in central cell structure would depend on the interaction between the shallow donor and the defect, ie the distance between them, discrete shifts in central cell correction could occur. The mechanism noted above by which lattice strain shifts transitions could also be responsible. For example, it can easily be imagined that a shallow donor in close proximity to a vacancy site would experience a local strain and appear at a given central cell shift, while if the vacancy was twice as far away it would experience a different local strain and appear at a different central cell shift. It is also easy to imagine that the relative separation between shallow donors and defect sites could vary systematically through the epitaxial layer. Clearly some form of complexing must be taking place in these InP samples since far more discrete central cell components have been seen than there are contaminants to attribute them to (Armistead et al 1984). Further evidence for complexes giving rise to additional central cell components is provided by the observation that a component in the central cell structure of a neutron transmutation doped sample disappeared over a five year period, presumably as some form of radiation induced damage gradually annealed out (Stradling, unpublished).

Recent work on deep level complexes has shown that some of the many deep traps observed in GaAs and InP may also have relatively

shallow levels associated with them. For example Lagowski et al (1982) and Walukiewicz (1983) have associated the EL2 level in GaAs with an As_{Ga}-V_{As} defect and found electrical activation from a shallow level 25meV below the conduction band. Although this level is five times deeper than the 5.7 meV binding energy of shallow hydrogenic donors in GaAs it shows that shallow levels can exist at normally deep impurity complexes.

Comparison of Results from FIRPC and NGPL.

At this stage it is important to compare the results obtained from the FIRPC studies with those from the NGPL studies of Dean and Skolnick (1983) and Dean, Skolnick and Taylor (1984). Differences between the results from the two techniques have usually been attributed to the fact that FIRPC and NGPL techniques differ in one major respect: FIRPC spectra are representative of the whole of the epitaxial layer while NGPL spectra are representative of only the first few microns of the epitaxial layer, since the exciting radiation is strongly absorbed within this region, and the photoluminescence signal can only escape from this region. Thus differences between the FIRPC and NGPL results can occur if non-uniform impurity profiles are present. However, when examined in more detail the situation seems more complicated than this.

Dean and Skolnick (1983) observed only a single central cell component on each TEDS line for the KV series samples including KV468 and KV469, even though the linewidth was sufficiently low for the two donors seen in the FIRPC experiments to be resolved. They tentatively associated this single component with the high magnetic field component (B|C) in KV468 and 469 which has been attributed to silicon, and suggested that the strong sulphur component observed in

the FIRPC spectra was due to a substantial accumulation of sulphur donors at the epilayer-substrate interface. However this observation of silicon as the dominant donor in NGPL studies of KV series samples is difficult to reconcile with the results of FIRPC studies of KV samples reported earlier in the chapter which show sulphur to be the dominant contaminant in all samples. With the exception of KV468 and 469 FIRPC spectra show that silicon is only present at very low levels.

Further problems arise when FIRPC and NGPL results on undoped NAG series samples are compared. As noted earlier FIRPC spectra of undoped NAG samples appear very similar to those of KV468 and 469 with two strong sulphur and silicon components at approximately equal intensities. However NGPL studies of these samples show strong sulphur components but low levels of silicon, in complete contrast to the NGPL results on the KV samples. Dean, Skolnick and Taylor (1984) suggested that the strong silicon component seen in the FIRPC study was all concentrated close to the epilayer-substrate interface. However they found no evidence for sharp increases in the Si/S ratio at the interface when they profiled one of the NAG samples in question by studying NGPL spectra from successively etched layers.

A further problem is that neither of these NGPL studies can be reconciled with the FIRPC results from the study of etched and unetched samples of KV468, which were interpreted as an increase in silicon concentration at the surface.

In view of these conflicting results it is unfortunately not possible to come to any satisfactory conclusion with regard to the differences between the FIRPC and NGPL observations and on the distribution of sulphur and silicon in the NAG and KV layers.

A further complication arises since the peak attributed to silicon in FIRPC studies of KV468(unetched) has clearly moved to

higher magnetic field after etching, suggesting that a simple Si_{In} donor cannot be responsible for the peak and that some form of silicon related complex must be involved. Some form of complexing is also suggested by the large number of peaks present in InP and by the three discrete peaks seen close to the silicon position in KV308/309, and by changes in the spectra of a neutron irradiated sample with time.

Though there is little evidence to support this claim it is possible that the variable intensity of the silicon peak observed in NGPL studies when compared to FIRPC spectra of the same samples could be a consequence of a complex rather than a simple donor being involved. As NGPL relies on observing central cell structure via a process involving bound excitons it is possibly more likely to be affected by the subtleties of exciton formation at a complex dispersed over more than one lattice site, or alternatively at a site with significant lattice strain, resulting in differences in the PL signal compared to the sulphur line.

To conclude this section on VPE residual contaminants, it can be said that all the work and the discussions in this chapter highlight the necessity for continued high resolution spectroscopy of InP central cell structure using both FIRPC and NGPL techniques. The most simple way of extending the work is to study the $1s-2p_{-1}$ transition using the 229μm CH_3OD laser line since this will show reduced linewidths and lower sensitivity to magnetic field variations and magnet homogeneity.

Central Cell Structure in MOCVD InP.

Figure 5.7 shows the central cell structure on the $1s-2p_{+1}$ transition for the five MOCVD samples. The spectra were taken using the λ=118.8μm methanol laser line and at a temperature of 4.2K. All of the recordings have been normalized to the same maximum amplitude. The asterisk superscript on the spectra of samples 792A - 806A indicates that these were taken in the 6.7T superconducting magnet, whereas the spectrum of 807A was taken in the 12.7T superconducting magnet. Inaccuracies in the 6.7T magnet calibration are responsible for the ~0.01T shift to low magnetic field of all the spectra when compared to that of 807A.

Sample 792A shows a very broad absorption centred on the $1s-2p_{+1}$ transition energy. This large linewidth is somewhat unexpected since the electrical characteristics are similar to those of the other samples and which have lower linewidths. It is possible that this sample was affected by non-uniform doping profiles giving it a much higher impurity concentration at the surface or alternatively that it was more compensated than the others.

The remaining four samples 800A, 805A, 806A, and 807A all show very similar spectra with two equally strong components only minor differences in linewidth. The central cell structure of these MOCVD samples is almost identical to that of VPE samples KV468 and KV469, but with significantly poorer resolution. Thus it is apparent that the low field donor at ~3.66 T in 807A (and at ~3.65T in 800A, 805A and 806A) is the same as the most common residual contaminant in VPE material, ie donor #5, which has been associated with sulphur. It is also apparent that the high field donor in these MOCVD samples lies at the field of donor #3 in the VPE material, which is probably associated with silicon, though in view of the large linewidths of

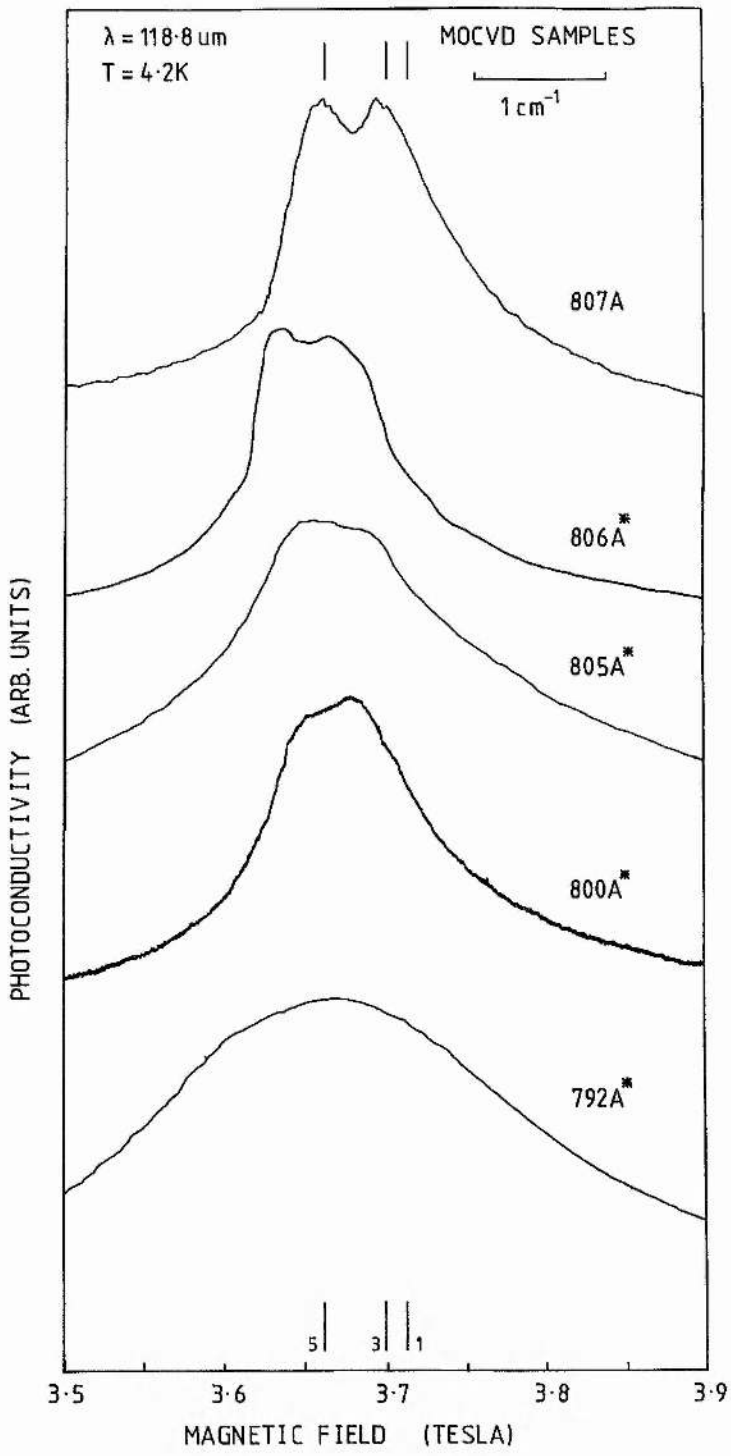

Figure 5.7: Spectra showing the central cell structure of the $1s-2p_{+1}$ transition for the MOCVD InP samples at T=4.2K using λ=118.8μm radiation. Optical excitation was used for samples 792A and 800A but not for 805A, 806A and 807A. All spectra except for 807A were taken in the 6.7T magnet and are shifted slightly to low field.

these samples and possible peak pulling effects, together with the multitude of components known to exist in VPE samples in this region, the actual assignment must be tentative.

Only one sample was studied at higher magnetic field: that of 807A at λ=70.5μm. This spectrum was shown in Figure 5.5 along with the KV series VPE samples. Note that the spectrum of KV469 was displaced to low magnetic field by instrumental effects. Comparison of 807A with the other samples in Fig 5.5 confirms the comments made in the previous paragraph: the low field donor is the same as donor #5 (sulphur) while the high field donor is close to that attributed to silicon in KV468/469. The Si/S ratio appears to be approximately 1:1 for all the samples with the exception of 792A.

None of these samples have been studied by NGPL techniques. A much later wafer (981A) was examined by Dean, Skolnick and Taylor, who note a large linewidth, but apparently centred on the silicon peak. NGPL results on undoped MOCVD material from Thomson-CSF showed principally silicon contamination. FIRPC studies of a Thomson-CSF sample showed very similar results to the RSRE samples, but with the silicon peak being dominant (Armistead et al 1984).

To summarize this section, with the exception of 792A which had too great a linewidth for any structure to be resolved, the MOCVD samples showed two residual contaminants with approximately equal concentrations and at the same positions as the two dominant residual contaminants present in VPE samples KV468 and KV469 which have been associated with silicon and sulphur. This is a quite different result from that seen when comparing GaAs grown by the LPE, VPE and MOCVD techniques where each of the three growth techniques shows a unique set of residual contaminants (Cooke et al 1978).

Central Cell Structure in Bulk Grown InP.

In general material grown by the bulk growth technique is considerably inferior to that grown by the various epitaxial techniques and usually the $1s-2p_{+1}$ transition is too broad for any central cell structure to be resolved. However a single sample L816 grown at RSRE by the 'liquid encapsulated Czochralski' technique (LEC) was available which had good electrical properties: a 77K mobility of 39,400 $cm^2V^{-1}s^{-1}$ and N_D-N_A of 3.4×10^{15} cm^{-3}.

The spectrum of this sample was taken at 4.2K using the λ=118.8μm laser line and is shown in Figure 5.8. No band gap excitation was used. All spectra of this sample showed a high background level which increased with magnetic field, probably due to photovoltaic effects and consequently the position of the spectrum relative to the baseline is arbitrary.

Two shoulders are resolved at 3.651 and 3.688 Tesla and are indicated by arrows on the figure. The three lines 1, 3 and 5 are the same as those used for the λ=118.8μm spectra in Figs 5.3 and 5.8 and represent the components seen in the VPE samples. As the spectrum of L816 was taken in the 6.7T magnet, which was not well calibrated, the spectrum is shifted by ~0.01 Tesla to low field. If this shift is allowed for the two low field shoulders in L816 agree well with the two residual contaminants present in VPE samples KV468 and KV469 and also the MOCVD samples. These are the features which have been associated with sulphur (~3.662T) and silicon (~3.70 T).

However the dominant features in L816 are the two peaks appearing at magnetic fields above the sulphur and silicon positions and corresponding to donors with very shallow central cell shifts (X_0 and X_1). The shallowest of these two donors (X_0) probably has a negative central cell shift. No trace of these components was seen in

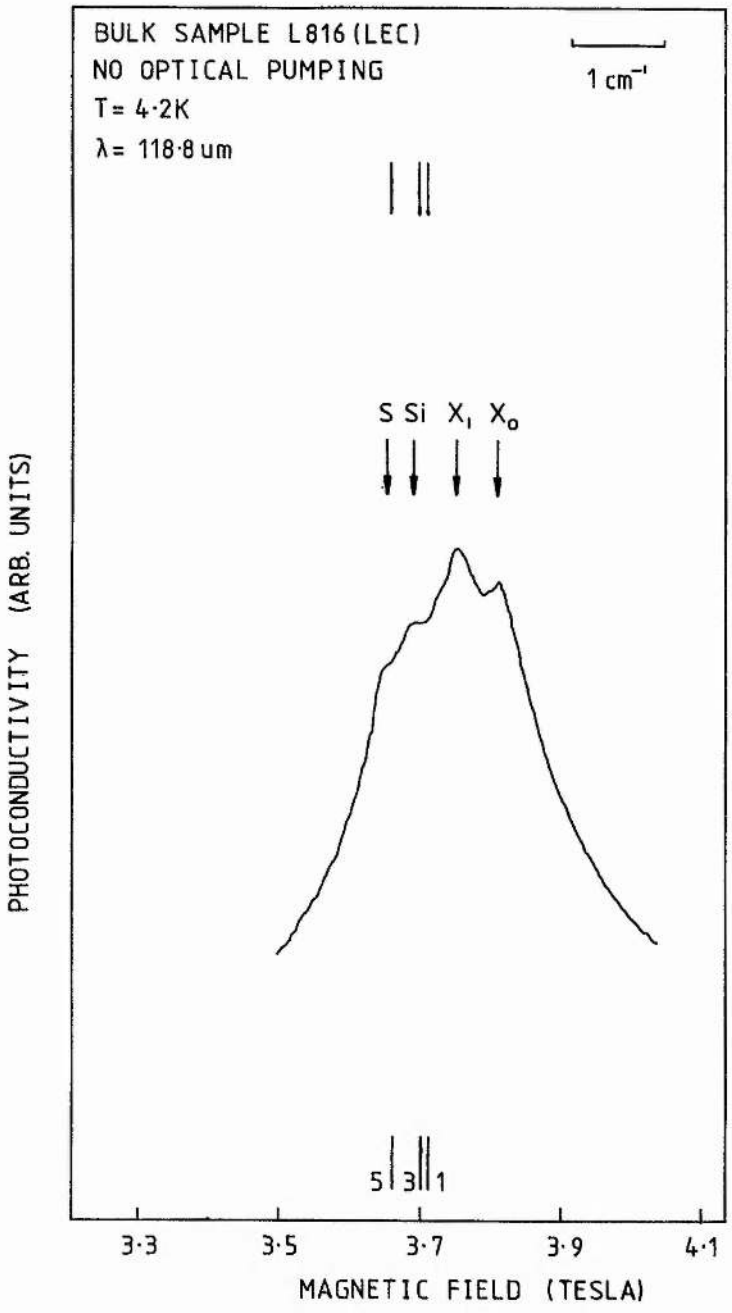

Figure 5.8: Spectrum showing the central cell structure of the $1s-2p_{+1}$ transition for the bulk InP sample L816 at T=4.2K and with λ=118.8μm radiation. No optical excitation was used. The lines labelled 1, 3 and 5 refer to the positions of the lines in Figure 5.3 representing the positions of the common residual contaminants in VPE material.

any of the VPE or MOCVD samples studied in this work, though they are present in other bulk samples (Armistead et al 1984 and Najda 1985). Very similar structure has also been observed in this sample using NGPL techniques, with two strong components with much shallower central cell shifts than sulphur and silicon (Dean, Skolnick, Cockayne et al 1984). Structure has been reported at higher fields in KV series VPE samples by Davidson et al (1980) and Armistead et al (1984), while Dean, Skolnick and Taylor reported two components much shallower than the silicon line in NGPL studies of NAG series VPE samples. It has already been noted that studies of a neutron transmutation doped sample using laser spectroscopy also showed a peak in this region after irradiation which was attributed to Sn (since In transmutes into Sn when it absorbs neutrons), but this peak had disappeared when the sample was re-examined some years later (Stradling unpublished).

Studies of bulk InP grown by the SSD technique (synthesis, solute -diffusion), which yielded very high quality (μ_{77}~100,000) material has shown two strong contaminants which were attributed to the same two donors present in VPE material, ie S and Si (Kubota et al 1986). These workers also studied LEC material grown using SSD material as the starting material and found two extra components in addition to S and Si, though they did not specify where they lay with respect to S and Si.

In conclusion, of all the samples studied, the bulk grown sample was the only one with a radically different set of residual donors, showing two donors with a smaller central cell shift than those commonly seen in VPE and MOCVD material (S and Si).

Chapter 6

Inter-Excited State Transitions in n-GaAs

In the previous chapters on the identification of the different species of residual shallow donors in GaAs and InP the discussion centred on the group of transitions originating on the 1s ground state of neutral donors. These transitions are analogous to the Lyman series lines in atomic hydrogen, which also originate on the 1s ground state. Atomic hydrogen also shows the Balmer and Paschen series of lines involving the n=2 and n=3 excited states respectively as the lower state. By analogy, hydrogenic shallow donors in semiconductors are also expected to show similar sets of transitions between excited states.

Magneto-optical studies of a variety of elemental and III-V semiconductors, using radiation sources generally in the millimetre and sub-millimetre region of the spectrum, have revealed a multiplicity of spectral lines which can be assigned to transitions between the excited states of shallow neutral donors (Chamberlain et al 1972a,b; Gershenzon et al 1973, 1974, 1977; Simmonds et al 1974; Skolnick et al 1977; Davidson et al 1980, Makado 1982).

A variety of reasons exist for the interest in inter-excited state transitions. One of the most important is that states not usually accessible from the ground state in optical studies, due to their being of the same parity, can now be studied. A prime example is that of the 2s state. The 1s-2s transition is only weakly allowed as a result of the 2s state mixing with the $2p_{\pm1}$ states when electric fields from ionized donors cause a quadratic Stark effect. However the inter-excited state transitions $2p_{-1}$-2s and 2s-$2p_{+1}$ are not forbidden and appear as strong lines in the spectra, and so the behaviour of the 2s state can be studied in detail.

A further reason for the interest in inter-excited state transitions is that the magnitudes of perturbations to the effective

mass theory of donors in a material with a parabolic band are much lower than those on the ground state. As the excited states have lower binding energies and more extended wavefunctions compared to the ground state (and hence are more localized in wavevector space) non-parabolicity and central cell effects contribute to a much lower extent to shifts away from the transition energies expected for impurity states under an isotropic and parabolic band at zero magnetic field. However, in a magnetic field excited states associated with higher Landau levels (where N>0) may be significantly perturbed by non-parabolicity.

Recent studies of negatively charged donors (or positively charged acceptors), known as D^- (A^+) states, have provided a spur to studies of inter-excited state transitions. D^- states are discussed extensively in Chapter 7, but briefly, they are formed when a neutral donor captures an electron: it is the semiconductor analogue of a free space H^- ion where two electrons are bound to a single proton. Since the neutral donor state has no long-range coulomb field associated with it, the second electron binds to the short range dipolar field presented by the first electron and the D^+ state. The binding energy of the second electron is much lower than that of the electron on a neutral donor: 0.0555 R* for the isolated D^- state in zero magnetic field (Pekeris 1958). This is the same order of magnitude as the binding energies of electrons in the excited states of neutral donors, and so transitions involving the D^- state or its excited states occur in the same energy region as the inter-excited state transitions. It is thus essential to be able to positively identify all the inter-excited state transitions in a spectrum before associating spectral features with transitions involving D^- states.

Some of the more important aspects of the inter-excited state transitions will now be discussed in more detail.

Magnetic Field Positions of the Inter-excited State Transitions

All the theoretical work in this chapter on the positions of the various transitions uses data published by Makado (1982), unless otherwise stated. The data in that work was obtained from a variational calculation using basis functions suggested by Aldrich and Greene (1979) to provide the energies of all the hydrogenic states up to the n=4 level (a total of 30 states), based on the assumption of a single parabolic isotropic conduction band. The energy levels were calculated over a closely spaced set of magnetic fields from γ=0 to 10 and used a larger basis set than Aldrich and Greene to improve on the accuracy of the calculation. Figure 2.4 showed the behaviour of the energies of the hydrogenic states with magnetic field in dimensionless units in the range γ=0 to 2.0, together with the positions of the first three Landau levels. The computer program used by Makado to interpolate his results to any value of γ has been refined to provide either the expected transition energy at any magnetic field or the expected magnetic field position for any energy of incident radiation. Alternatively, given a magnetic field the program will print out all transitions whose theoretical energies lie within say 10% of an experimental transition energy. These energies were also used to plot the theoretical curves of transition energy against magnetic field and to calculate the rate of change of transition energy with field ($\partial E/\partial B$) for any transition (see for example Figures 4.1 and 4.2).

Central Cell Effects on the Excited States

The central cell or chemical shift on the 1s ground state was discussed in detail in chapter 4, where it was noted that the magnitude of the perturbation is proportional to the square of the wavefunction amplitude at the impurity centre, ie

$$\Delta E_{cc} \propto |\psi(0)|^2$$

Consequently the ratio of the chemical shifts on the excited states will be of much lower amplitude than those on the ground state, since they are more extended and thus spend more time away from the central cell region. The largest shift will be on the 2s level and at zero magnetic field the ratio of the shifts on the 2s and 1s levels will be

$$\frac{\Delta E_{cc}(2s)}{\Delta E_{cc}(1s)} = \frac{1}{8}$$

However, as noted in chapter 4, polaron effects can increase this ratio. Shifts on the remaining even parity states will be considerably smaller than this, while the shift is negligible for the odd parity states (although it has been observed on the 2p state in silicon, Ramdas and Rodriguez 1981). While a number of calculations on the magnetic field behaviour of the central cell shift on the 1s state have been published (see eg Cabib et al 1972, Larsen 1974), similar calculations on the behaviour of the 2s state are less common. (Unfortunately the variational calculations of Makado (1982) were not extended to give values for the oscillator strength $|\psi(0)|^2$ for the states). However, Cabib et al (1972) also calculated the ratio of the 2s central cell splitting to the zero magnetic field 1s splitting over the range γ=0.1 to 2.0. These values, along with their values for the 1s state splitting, have been plotted in Figure 6.1. It can be seen from this figure that the theoretical central cell splitting of

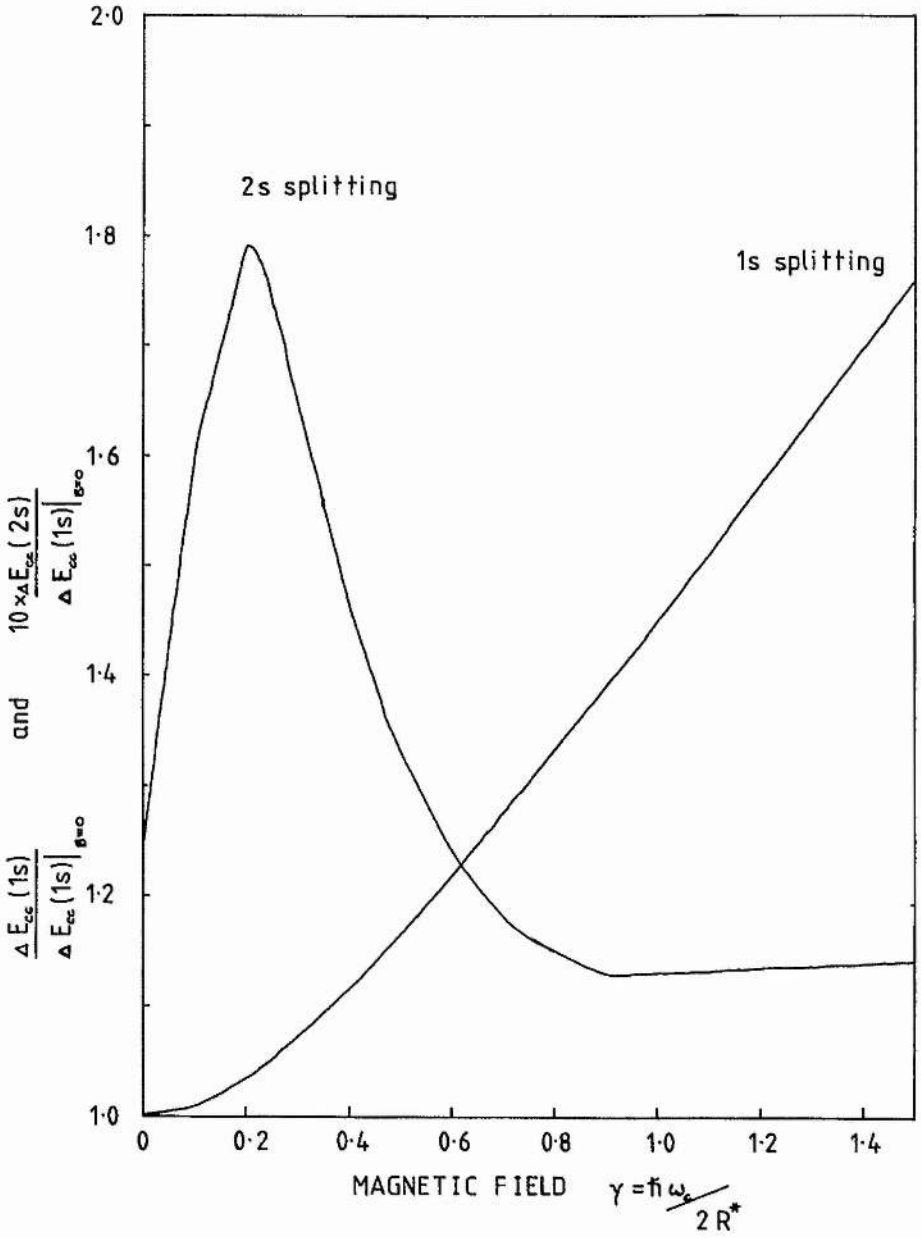

Figure 6.1: This graph shows the theoretical variation of the central cell splitting on the 1s and 2s states of a shallow hydrogenic donor in a parabolic band in a dimensionless magnetic field (from Cabib, Fabri and Fiorio 1972). The variation is shown by plotting the ratio of the splitting on the state to the splitting on the 1s state at zero magnetic field.

the 2s state is quite different to that on the 1s state and increases sharply with magnetic field to approximately 0.18 of the zero field splitting on the 1s ground state at a field of approximately γ=0.3 before decreasing to approximately 0.11 $\Delta E_{1s}(B=0)$. Thus in GaAs the largest central cell splitting on transitions involving the 2s state will be at approximately 2 Tesla.

Perturbations Other Than From Central Cell Effects

One of the principle perturbations from a parabolic band theory of hydrogenic donors in GaAs is due to non-parabolicity. As pointed out earlier, the excited states are considerably more extended than the ground state, with an effective Bohr radius for the nth excited state given by

$$a_n^* = a_o^* n^2$$

at zero magnetic field, where a_o^* is the effective Bohr radius of the ground state. Consequently, since the spread of the state in wavevector space is given by $k \propto 1/a^*$ (see chapter 2) the spread of the states in wavevector space will vary as the inverse square of n, i.e.

$$k \propto n^{-2}$$

The effect of non-parabolicity will thus diminish rapidly for the higher excited states which are bound below the N=0 Landau level, since it is directly related to this spread in k-space. However inter-excited state transitions involving states in higher Landau levels where N>0 (e.g. A_3: $2p_{+1}$-$3d_{+2}$) where the second state can be at high energy may well show effects due to non-parabolicity. In practice such states increase rapidly with magnetic field and are only observed at low fields below the cyclotron resonance transition, up to ~2 Tesla, where non-parabolicity is not as significant.

A consequence of non-parabolicity noted in the discussion of the $1s-2p_{+1}$ transition was the spin-splitting of the individual central cell split peaks. No spin-splitting was observed on the $1s-2p_0$ or $1s-2p_{-1}$ peaks since these lie below the same Landau level (N=0) whereas the $1s-2p_{+1}$ peak represents a transition between the N=0 and N=1 Landau levels. Thus a spin-splitting effect might theoretically be expected on any inter-excited state transitions between states associated with different Landau levels, at high fields where the $1s-2p_{+1}$ or $1s-3p_{+1}$ transitions appeared split (i.e. fields greater than 5 Tesla).

A further perturbation can be caused by polaron effects. These effects are most easily observed in the more polar semiconductors such as CdTe where the coupling between the electrons and LO phonons, measured in terms of the Fröhlich coupling constant α, is large. The effective mass can be significantly perturbed from the band edge mass and the transition energies may be pinned to the LO phonon energy (Simmonds 1974; Skolnick et al 1977). In semiconductors with a low effective mass, such as InSb, where the transition energies attain magnitudes comparable to the LO phonon energy at easily attainable magnetic fields, level crossing effects may be observed (Kaplan and Wallis 1968).

In GaAs polaron effects are small as a result of the low coupling between the electrons and the lattice (α=0.068) and are only significant for excited states associated with Landau levels where N>0. Simmonds et al (1974) estimated that the energies of the A_1 and A_2 inter-excited state transitions ($2s-3p_{+1}$ and $2p_0-3d_{+1}$) would be decreased by ~5% in CdTe and ~0.5% in GaAs. Consequently no allowance has been made in the calculations for polaron effects and the accepted band edge effective mass of 0.0665 m_o and effective

Rydberg of 46.1 cm^{-1} (Stillman et al 1971) have been used in the calculations concerning GaAs.

In spite of the previous statements it is still possible to observe strong polaron induced shifts in certain types of experiments with GaAs. Lindemann et al (1983) conducted FIR absorption and emission studies of the cyclotron resonance line at very high electric fields. The high electric fields created electron temperatures up to 180 K, at which stage the upper Landau levels are significantly populated. Under these conditions the cyclotron resonance at ~6 Tesla was observed to split into up to four components which were attributed to transitions between the N = 0 - 1, 1 - 2, 2 - 3, and 3 - 4 Landau levels, all at slightly different energies. (The splittings observed were up to an order of magnitude greater than the spin splittings seen on the cyclotron resonance in Figure 4.8). These splittings are believed to be due to the Landau levels becoming pinned to the LO phonon energy (296 cm^{-1}) though there will also be a significant contribution from non-parabolicity.

A further perturbation which may occur is the result of the Stark broadening mechanism, as discussed in the following section and previously in Chapter 4. The shift in the peak positions that occurs is generally a fraction of a linewidth and will be negligible compared to the effects mentioned above.

Lineshapes and Linewidths of Inter-excited State Transitions

An extensive discussion of linewidths and lineshapes of transitions involving the 1s ground state and principally the $2p_0$ and $2p_{\pm1}$ states was presented in chapter 4, and those mechanisms are equally valid for transitions between excited states. Briefly, although the electron-phonon interaction and other mechanisms such as

ionization into the conduction band (for states above the N=0 Landau level) contribute to the lifetime of the states, the dominant broadening mechanism is due to random electric fields from distant ionized impurities interacting with the wavefunctions of the neutral donors and causing Stark shifts of the energy levels. Larsen's theory of line-broadening, based on this mechanism must be restricted even further to the very dilute regime of impurity concentration since it relies on the impurities being isolated and the electric field being constant over the extent of the neutral donor wavefunction, which is more extended for the excited states. The linewidth of inter-excited state transitions should be larger than the linewidth of transitions originating on the ground state as a result of this increased delocalization. However, Simmonds et al (1974) commented that in general there was no significant difference in the observed linewidths for inter-excited state transitions compared to those originating on the ground state. Part of the reason for this could be that many of the observed transitions originating on the 1s level could have unresolved central cell splittings which would contribute to the observed linewidth and lead to an overestimate of the actual linewidth of the transitions. Furthermore, it will be seen that the bulk of the observed inter-excited state transitions are between states associated with the N=0 Landau level, whereas the most easily observed transitions from the ground state are to states associated with a different Landau level. Since these states are then degenerate with the conduction band the possibility of electric field ionization can lead to additional broadening.

Coincidental cancellation of the quadrupole moments may be responsible for the very low linewidths observed on certain inter-excited state transitions, eg $2p_{-1}$-$3d_{-2}$ (I_1) (Simmonds et

al 1974; Skolnick et al 1977). If this occurs, then the second order quadratic Stark effect becomes the principle broadening mechanism.

Figure 4.3 of chapter 4, reproduced from Larsen (1973), shows the quadrupole moments of a number of the excited states. It can be seen that the quadrupole moment of the 2s state rises rapidly at low values of γ, so that the $2s-2p_{\pm1}$ transition should broaden rapidly at low magnetic fields. Notice though that it crosses the $2p_0$ level at $\gamma \sim 0.2$ and so the $2p_0-2s$ linewidth should be a minimum at ~1.3T for GaAs. This would thus be the field best suited to observing central cell structure on the $2p_0-2s$ transition.

Effect of Intrinsic Illumination on the Inter-excited State Transitions

As in the previous work on the $1s-2p_{\pm1,0}$ transitions, optical excitation from a quartz halogen lamp at an energy close to that of the bandgap was extensively used, and resulted in dramatic reductions in the linewidths of many inter-excited state lines in compensated samples. It is significant that the narrowing obtained in the uncompensated sample was not as great as that obtained in the more compensated sample.

The application of bandgap excitation also modifies the normal thermal distribution of carriers among the excited states of the impurities, resulting in many more transitions being observed. Reducing the temperature of the sample to <2 K from 4.2K may also reduce the linewidths of transitions in compensated samples. This was also noted on the transitions involving the ground states and appears to be a consequence of the preferential formation of ionized donor-acceptor pairs at low temperatures (discussed in chapter 4) (Golka et al 1977).

Once the concentration increases out of the regime where Larsen

type broadening is qualitatively applicable, interaction between adjacent donors may cause additional broadening. In uncompensated samples with low impurity concentrations this 'van der Waals' type broadening may be as significant as the broadening from ionized impurities. If the donor concentration is $N_d = 2.0 \times 10^{14} cm^{-3}$ then the average donor-donor separation is:

$$\langle d \rangle = \left(\frac{3}{4\pi N_d} \right)^{1/3}$$

which equals ~1060Å, equivalent to 10.7 a_o^*, where a_o^* = 99Å is the ground state effective Bohr radius for neutral donors in GaAs. However, the separation of adjacent donors when measured in units of the effective Bohr radius of the excited states will be proportional to n^{-2} where n is the principle quantum number of the state concerned. Thus, for example, the separation is only 1.19 a_3^* and only 0.67 a_4^* and so at zero magnetic field the n=3 and n=4 states of donors separated by the average distance <d> overlap. However, as the magnetic field is increased the donor electron orbits are substantially compressed and generally donor-donor effects do not appear to be substantial in samples of this purity.

Experimental Results

The samples used in the series of experiments on inter-excited state transitions in n-GaAs were the two VPE samples RR98B and S1. Their characteristics were given previously in Table 4.1. The inter-excited state transitions in sample R137 had already been studied extensively by Makado (1982) using millimetre wave Impatt oscillators, while the MBE grown samples were of insufficient purity to observe narrow inter-excited state lines. The samples were mounted as described in chapter 3 and immersed in liquid helium at 4.2K or 1.8K, in Faraday Geometry, in the 12.7 T magnet (unless otherwise noted). The Optically Pumped FIR Laser System was used with a variety of gases to provide extrinsic radiation at wavelengths between 394 μm and 1.224 mm, as detailed in Chapter 3. A quartz halogen bulb was used as a source of intrinsic radiation.

Identification of Inter-Excited State Transitions.

As noted previously a number of papers have been published on inter-excited state transitions in III-V and II-VI semiconductors and most of the transitions observed in this study have already been positively identified. These transitions are listed in Table 6.1 along with the nomenclature used by Skolnick et al (1977) and Makado (1982). Table 6.1 also lists three transitions reported previously which were not observed in this study.

Figure 6.2 illustrates the photoconductivity spectra obtained using sample S1 at wavelengths of 458.5 and 570.6 μm. The sample was at a temperature of 4.2K and was illuminated with band gap radiation. Note that the peaks labelled D^- are $D^- \rightarrow N=1, 2, ..$ transitions and are discussed in detail in the following chapter. The arrows indicate the theoretical magnetic fields for the transitions obtained

Table 6.1.

Transitions Corresponding To Lines Observed Between 1500 and 300μm.

Only those lines which have been positively assigned to transitions in the referenced works have been included in this list.

A_1	$2s-3p_{+1}$	iii,iv,vii
A_2	$2p_0-3d_{+1}$	iii,iv,v,vi,vii
A_3	$2p_{+1}-3d_{+2}$	vi,vii
A_3'	$2p_{-1}-3s$	iv
B_1	$2p_{-1}-3d_{-1}$	iii,iv,v,vi,vii
B_2	$2p_{-1}-2s$	i,ii,iii,v,vi,vii
B_3	$2s-2p_{+1}$	i,ii,iii,v,vi,vii
I_1	$2p_{-1}-3d_{-2}$	iii,v(in CdTe only),vi,vii
I_2	$3d_{-2}-4f_{-2}$	vi,vii
I_3	$2p_{-1}-2p_0$	i,ii,iii,v,vii
D	$2p_{-1}-3d_0$	iv,v (CdTe only),vii
G	$3d_{-2}-3p_{-1}$	iv,v
	$2p_0-2p_{+1}$	iii

A number of transitions which have been reported by other authors but which were not observed in the current work are listed below:

E	$2p_0-3s$	iv,v
H	$3d_{-1}-4d_{-1}$	v,vii
M	$2p_0-2s$	iii,v,vi,vii

References: i. Gershenzon et al (1973) ii. Gershenzon et al (1974)
iii. Gershenzon et al (1977) iv. Simmonds et al (1974)
v. Skolnick et al (1977) vi. Davidson et al (1980)
vii. Makado (1982)

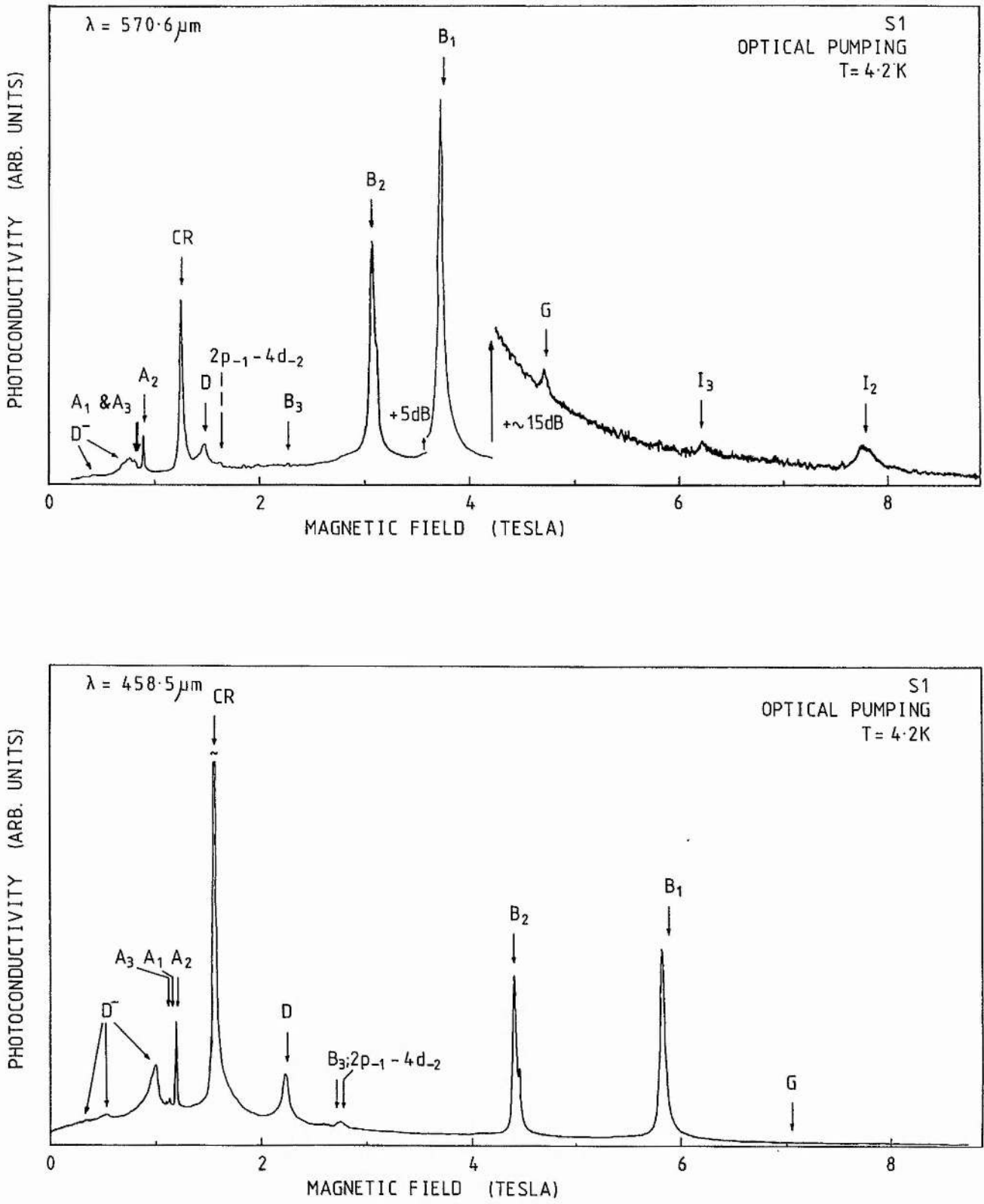

Figure 6.2: Spectra showing the inter-excited state transitions in high purity n-GaAs (sample S1) at T=4.2K with optical excitation using laser wavelengths of 570.6 and 458.5μm. Transitions labelled D^- are discussed in the following chapter.

from the data of Makado (1982) using $m^*=0.0665m_0$ and R^* = 46.1 cm^{-1}. It is immediately apparent that the theoretical field positions are in very good agreement with the experimentally observed field positions. The agreement could probably be improved further if the theory was fitted to the experimental positions using the effective mass and effective Rydberg as adjustable parameters. The principle strong lines can be followed over a wide range of magnetic fields and laser energies: further experimental recordings showing this variation may be found in Figure 7.6 of the next chapter.

Figure 6.3 illustrates the spectrum obtained at the longest wavelength available from the laser: 1.224 mm. At this energy one of the principle lines, B_1: $2p_{-1}$-$3d_{-1}$ appears very close to the cyclotron resonance: in the upper trace of RR98B at T=4.2K this cannot be seen. The lower trace shows S1 at T=1.8K and here the B_1 line appears as a shoulder on the low field side of the cyclotron resonance. The structure appearing in the region of B_2 and B_3 is due to central cell structure and is discussed in detail later.

In Figure 6.4 all the data from the various experiments showing inter-excited state transitions has been collated and a graph plotted of the transition energy in units of $\hbar\omega_c/R^*$ against the dimensionless magnetic field γ for both the theoretical calculations of Makado (solid curves) and the experimental points (crosses). The crosses represent limits greater than a reasonable estimate of the error values. Figure 6.5 shows the diagram for the low field region where $0<\gamma<0.2$.

New Assignments of Lines.

Except for one set of points connected by the dotted line 'Z' all the observed peaks are in excellent agreement with one of the

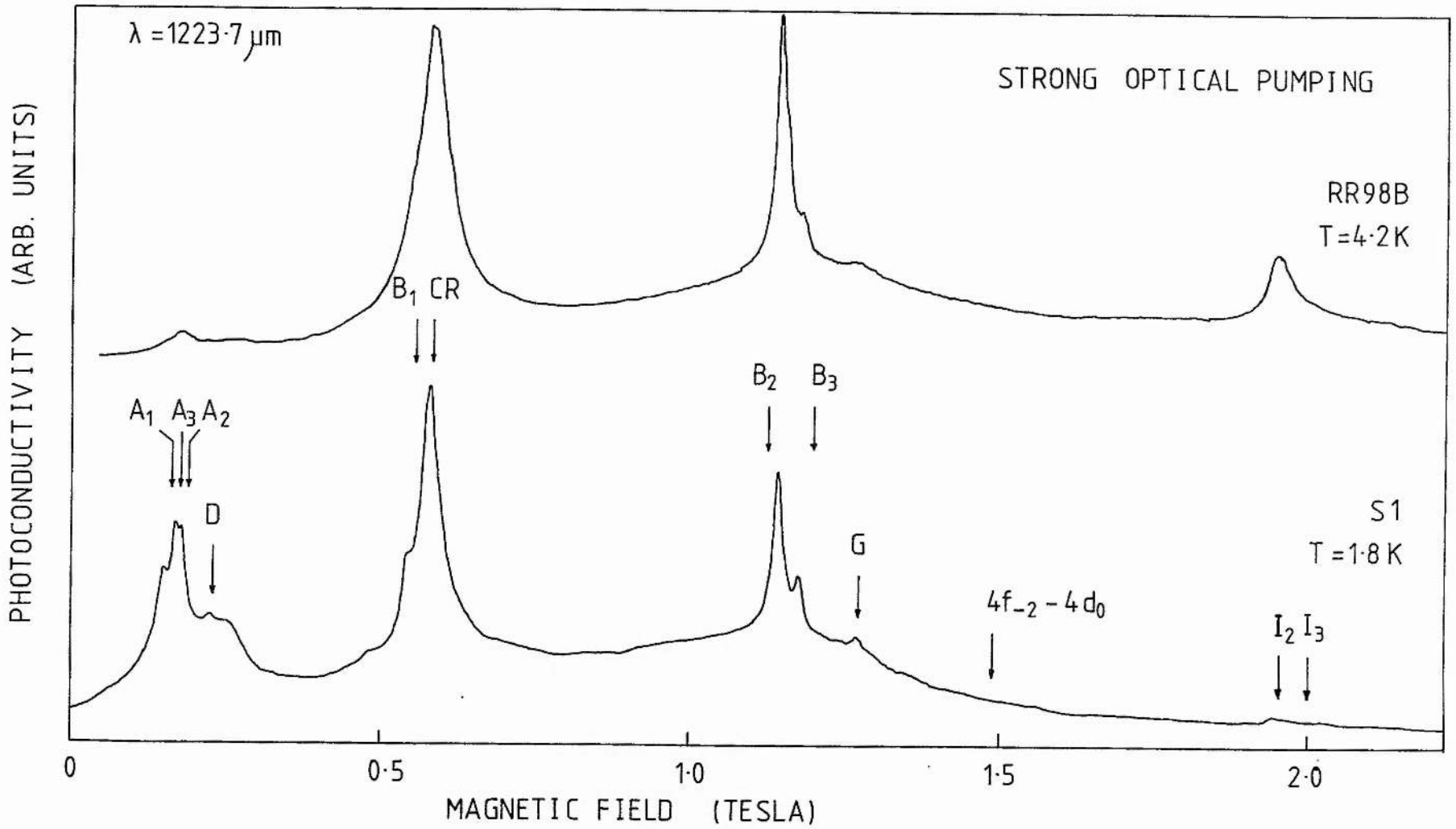

Figure 6.3: Spectra showing the inter-excited state transitions in S1 at T=1.8K and RR98B at T=4.2K with optical excitation using a laser line of wavelength 1.2mm.

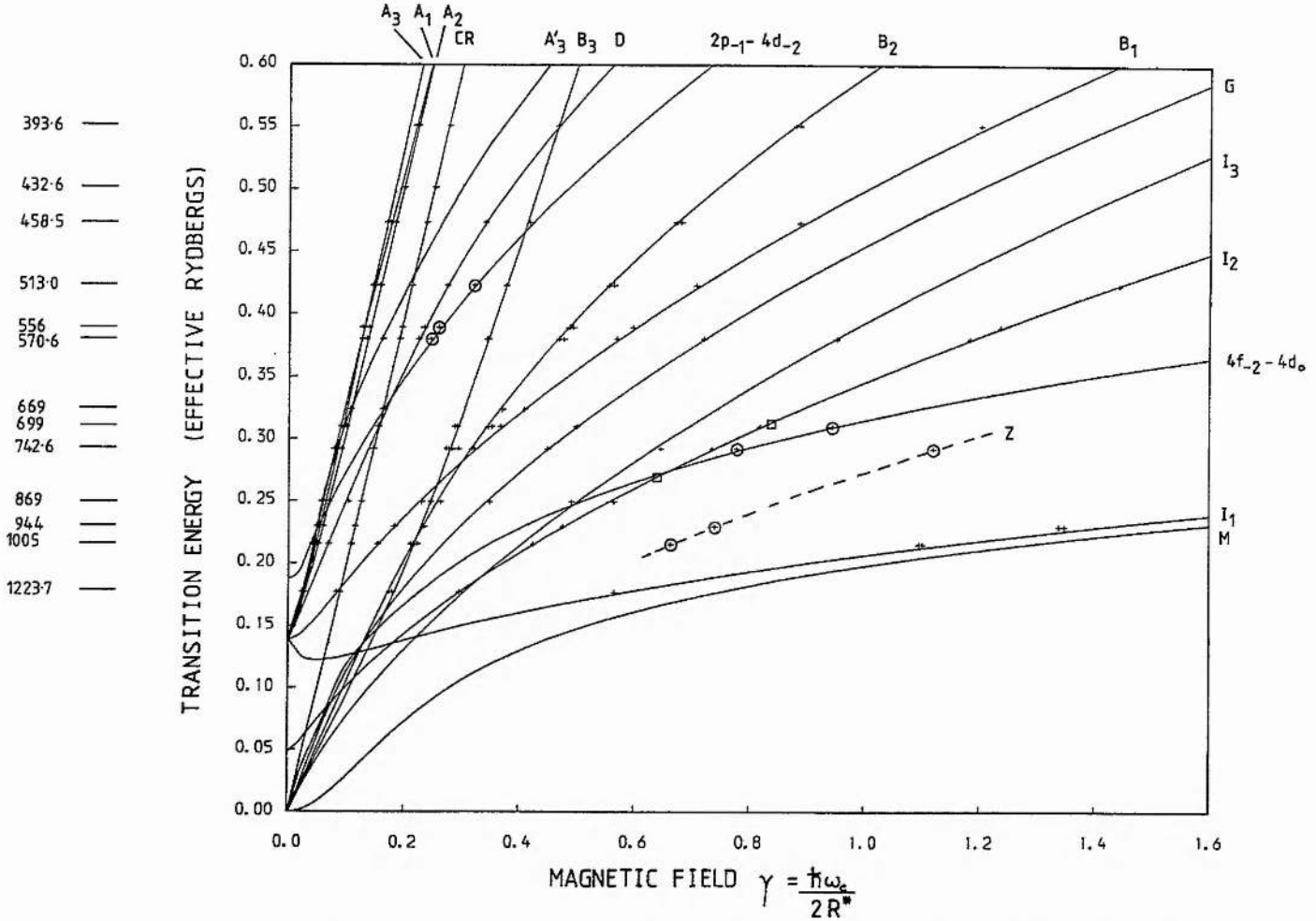

Figure 6.4: Diagram in dimensionless units showing the magnetic field dependance of the inter-excited state transition energies observed in the GaAs samples RR98B and S1. The experimental points marked by crosses have been converted to dimensionless units assuming $m^{*}=0.0665m_{0}$ and $R^{*}=46.1cm^{-1}$. The solid curves show the theoretical transition energies for a shallow donor in a parabolic band and were obtained from the data of Makado (1982). The

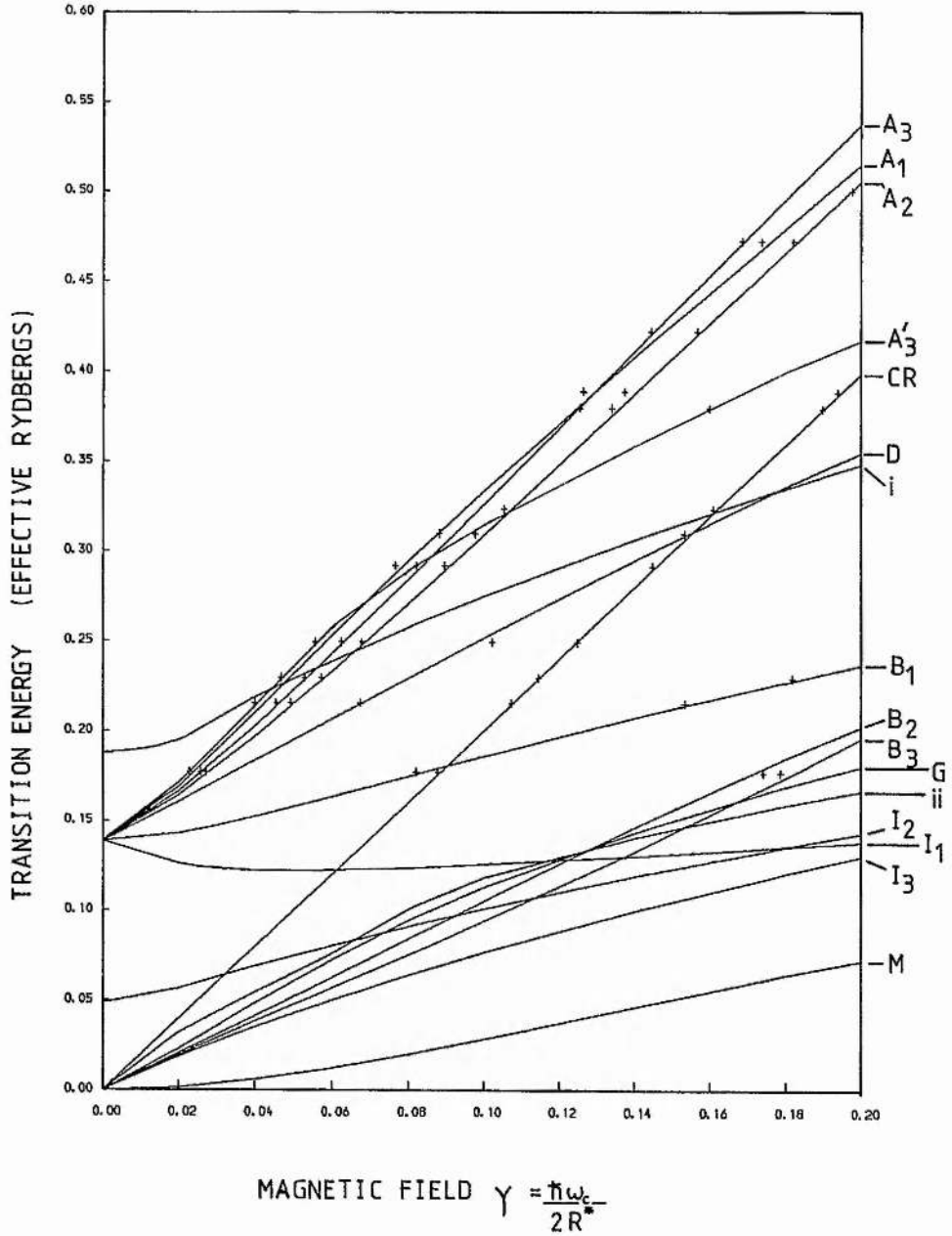

Figure 6.5: This diagram is the same as Figure 6.4, but concentrates on the low magnetic field region up to $\gamma=0.2$. The transition labelled 'i' is $2p_{-1}-4d_{-2}$ while that labelled 'ii' is $4f_{-2}-4d_{0}$.

theoretical curves. Only two new identifications were required to obtain this excellent agreement: $4f_{-2}$-$4d_0$ and $2p_{-1}$-$4d_{-2}$. The experimental points concerned are indicated by the symbol ⊕.

$\underline{4f_{-2}-4d_0}$:-

This new assignment was made to fit a line observed at slightly higher magnetic fields than I_2 in spectra at 699 and 742μm. It was of much lower amplitude than I_2 though it increased in amplitude considerably at high levels of electric field bias, as illustrated in the sequence of recordings in Figures 7.15 and 7.16, which principally show the electric field dependence of the $D^- \rightarrow N=0$ transition in sample S1. The $3d_{-1}$-$4f_{-1}$ (H) transition assignment made by Makado (1982), which should appear in this field region does not appear to provide a satisfactory explanation: the error in energy at the observed field for the two peaks, ie

$$\text{error} = \left(\frac{\text{laser energy} - \text{theoretical energy}}{\text{laser energy}}\right) \times 100 \quad (\%)$$

is >2% for both laser energies (see the comments in the following paragraphs with regard to H and transition $3d_{-1}$-$4f_{-1}$). The new transition agrees to better than 0.7% with the experimental energy at the two energies at which it was clearly observed.

Table 6.2 compares the error in the theoretical energy and experimental energies at the magnetic fields where the peaks are observed. For completeness all the observed transitions have been listed, but note that a number of peaks appear twice when it is not clear which transition they belong to.

$\underline{2p_{-1}-4d_{-2}}$:-

This new assignment was made to fit a line observed between the D ($2p_{-1}$-$3d_0$) and B_3 ($2s$-$2p_{+1}$) transitions in spectra at λ =

Table 6.2.

The table on the following pages lists the laser wavelength and magnetic field for each inter-excited state transition observed in the experiments. The theoretical energy at the observed magnetic field is also listed together with the error between the theoretical energy and the laser energy. Experimental magnetic fields and laser energies have been converted to dimensionless units assuming $m^* = 0.0665m_o$ and $R^* = 46.1\ cm^{-1}$. Where more than one hydrogenic transition agrees well with an observed line the wavelength and magnetic field are listed under each possible assignment, given a label and noted at the foot of the page. For example, the transition appearing at 0.826 Tesla in spectra with $\lambda = 570.6\mu m$ radiation could be either A_1 with an error of -0.50%, or A_3 with an error of -0.14%, so the line is listed under both the A_1 and A_3 assignments with the label --(1).

Experimental Observations			Theoretical Energies			
Laser Wavelength (μm)	Field Tesla	Gamma	Energy R^*	Energy cm^{-1}	Error %	
$2s-3p_{+1}$ (A_1)						
742.6	0.504	0.077	0.28781	13.27	1.48	
699.4	0.580	0.088	0.31101	14.34	-0.28	
570.6	0.826	0.126	0.38208	17.61	-0.50	(1)
556.9	0.831	0.127	0.38348	17.68	1.55	
513.0	0.951	0.145	0.41667	19.21	1.46	(2)
458.5	1.141	0.174	0.46854	21.60	0.96	
393.6	1.426	0.217	0.54720	25.23	0.70	
				average error	0.77%	
$2p_0-3d_{+1}$ (A_2)						
1223.7	0.178	0.027	0.17525	8.08	1.14	
1005.3	0.324	0.049	0.21342	9.84	1.09	
944.0	0.376	0.057	0.22784	10.50	0.85	
869	0.446	0.068	0.24766	11.42	0.78	
742.6	0.589	0.090	0.28915	13.33	1.02	
699.4	0.642	0.098	0.30476	14.05	1.74	
669.5	0.693	0.106	0.31986	14.75	1.27	(3)
570.6	0.881	0.134	0.37601	17.33	1.10	
556.9	0.904	0.138	0.38292	17.65	1.70	
513.0	1.030	0.157	0.42088	19.40	0.46	
458.5	1.196	0.182	0.47109	21.72	0.42	
432.1	1.297	0.198	0.50170	23.13	-0.06	
393.6	1.456	0.222	0.54998	25.35	0.20	
				average error	0.90%	
$2p_{+1}-3d_{+2}$ (A_3)						
1223.7	0.169	0.026	0.17607	8.12	0.68	
1005.3	0.299	0.046	0.21354	9.84	1.03	
944.0	0.348	0.053	0.22853	10.54	0.55	
869	0.411	0.063	0.24811	11.44	0.61	
742.6	0.540	0.082	0.28876	13.31	1.15	(4)
570.6	0.826	0.126	0.38071	17.55	-0.14	(1)
513.0	0.951	0.145	0.4210	19.41	0.41	(2)
458.5	1.192	0.182	0.49917	23.01	0.44	
				average error	0.59%	
$2p_{-1}-3s$ (A_3')						
1223.7	0.150	0.023	0.17635	8.13	0.52	
1005.3	0.263	0.040	0.21482	9.90	0.44	
944.0	0.309	0.047	0.23052	10.63	-0.32	
869	0.366	0.056	0.24882	11.47	0.32	
742.6	0.540	0.082	0.29229	13.47	-0.06	(4)
699.4	0.693	0.106	0.32119	14.81	0.86	(3)
570.6	1.051	0.160	0.38004	17.52	0.04	
				average error	0.26%	

(1)— A_1 or A_3
(2)— A_1 or A_3
(3)— A_2 or A_3
(4)— A_3 or A_3'

Experimental Observations			Theoretical Energies		
Laser Wavelength (μm)	Field Tesla	Gamma	Energy R^*	Energy cm^{-1}	Error %
$2p_{-1}$-$3d_{-1}$ (B_1)					
1223.7	0.539	0.082	0.17600	8.11	0.72
1005.3	1.008	0.153	0.21461	9.89	0.54
944.0	1.193	0.182	0.22867	10.54	0.48
869	1.507	0.229	0.25118	11.58	-0.62
699.4	2.411	0.367	0.30844	14.22	0.55
669.5	2.678	0.408	0.32371	14.92	0.08
570.6	3.725	0.567	0.37841	17.44	0.47
556.9	3.911	0.596	0.38741	17.86	0.54
513.0	4.623	0.704	0.42027	19.37	0.61
458.5	5.818	0.886	0.47073	21.70	0.50
393.6	7.871	1.199	0.54743	25.24	0.66
				average error	0.41%
$2p_{-1}$-2s (B_2)					
1223.7	1.142	0.174	0.17994	8.30	-1.51
1005.3	1.426	0.217	0.21798	10.05	-1.03
944.0	1.538	0.234	0.23216	10.70	-1.03
869	1.723	0.262	0.25424	11.72	-1.85 —⑤
742.6	2.082	0.317	0.29317	13.52	-0.36
699.4	2.270	0.346	0.31180	14.37	-0.53
669.5	2.426	0.369	0.32647	15.05	-0.77 X_1
570.6	3.072	0.468	0.38118	17.57	-0.26
556.9	3.187	0.485	0.39008	17.98	-0.14
513.0	3.689	0.562	0.42665	19.67	-0.90
458.5	4.398	0.670	0.47323	21.82	-0.03
393.6	5.760	0.877	0.55117	25.41	-0.02
				average error	-0.70%
1223.7	1.173	0.179	0.18429	8.50	-3.96
1005.3	1.460	0.222	0.22236	10.25	-3.05
869	1.723	0.262	0.25424	11.72	-1.85 —⑤
742.6	2.111	0.321	0.29612	13.65	-1.37
699.4	2.306	0.351	0.31524	14.53	-1.64
570.6	3.123	0.476	0.38515	17.76	-1.31 X_3
556.9	3.226	0.491	0.39305	18.12	-0.90
513.0	3.689	0.562	0.42665	19.67	-0.90
458.5	4.451	0.678	0.47652	21.97	-0.73
393.6	5.813	0.885	0.55397	25.54	-0.53
				average error	-1.62%

As the B_2 and B_3 transitions show central cell structure separate entries have been made for both the X_1 and X_3 central cell components.

⑤— No central cell structure was resolved on B_2 in the λ=869μm spectra.

Experimental Observations			Theoretical Energies		
Laser Wavelength (μm)	Field Tesla	Gamma	Energy R^*	Energy cm^{-1}	Error %
$2s-2p_{+1}$ (B_3)					
1005.3	1.411	0.215	0.21370	9.85	0.96
869	1.609	0.245	0.24921	11.49	0.17
742.6	1.817	0.277	0.28847	13.30	1.25
699.4	1.907	0.290	0.30600	14.11	1.34
570.6	2.270	0.346	0.37955	17.50	0.17
513.0	2.465	0.375	0.42070	19.39	0.51
458.5	2.733	0.416	0.47879	22.07	-1.21
393.6	3.053	0.465	0.55013	25.36	0.17
				average error	0.42%
1005.3	1.384	0.211	0.20901	9.64	3.13
742.6	1.786	0.272	0.28251	13.02	3.29
699.4	1.886	0.287	0.30188	13.92	2.66
570.6	2.252	0.343	0.37580	17.32	1.15
				average error	2.56%
$2p_{-1}-3d_0$ (D)					
1005.3	0.443	0.067	0.21535	9.93	0.19
869	0.672	0.102	0.25448	11.73	-1.95
699.4	1.008	0.153	0.30966	14.28	0.16
570.6	1.466	0.223	0.37803	17.43	0.57
556.9	1.528	0.233	0.38669	17.83	0.73
513.0	1.796	0.273	0.42185	19.45	0.24
458.5	2.232	0.340	0.47214	21.77	0.20
393.6	3.053	0.465	0.55001	25.36	0.19
				average error	0.04%
$3d_{-2}-3p_{-1}$ (G)					
869	2.287	0.348	0.25201	11.62	-0.96
742.6	2.948	0.449	0.29165	13.45	0.16
699.4	3.271	0.498	0.30939	14.26	0.24
570.6	4.714	0.718	0.37959	17.50	0.16
				average error	-0.10%
$2p_{-1}-3d_{-2}$ (I_1)					
1223.7	3.712	0.565	0.17582	8.11	0.82
1005.3	7.189	1.095	0.21273	9.81	1.41
	7.220	1.099	0.21301	9.82	1.28
944.0	8.784	1.338	0.22619	10.43	1.57
	8.847	1.347	0.22669	10.45	1.35
				average error	1.29%

X_1

X_3

⑥— B_3 or $2p_{-1}-4d_{-2}$

The I_1 transition at λ=1005.3 and 944μm was split, probably due to peak inversion effects such as those seen on the $1s-2p_{\pm1}$ transitions. The magnetic field for each of the split peaks is shown.

Experimental Observations			Theoretical Energies		
Laser Wavelength (μm)	Field Tesla	Gamma	Energy R^*	Energy cm^{-1}	Error %
$3d_{-2}$-$4f_{-2}$ (I_2)					
1223.7	1.946	0.296	0.17709	8.16	0.10
1005.3	2.786	0.424	0.21536	9.93	0.19
944.0	3.126	0.476	0.22945	10.58	0.15
869	3.703	0.564	0.25194	11.61	-0.93
742.6	4.816	0.733	0.29145	13.44	0.23
699.4	5.363	0.817	0.30937	14.26	0.25
570.6	7.759	1.182	0.37968	17.50	0.13
556.9	8.102	1.234	0.38887	17.93	0.17
513.0	9.463	1.441	0.42373	19.53	-0.21
				average error	0.01%
$2p_{-1}$-$2p_0$ (I_3)					
869	3.217	0.490	0.24620	11.35	1.37 —(7)
742.6	4.228	0.644	0.29565	13.63	-1.21
570.6	6.237	0.950	0.38081	17.56	-0.16
				average error	0.00%
$4f_{-2}$-$4d_0$					
869	3.217	0.490	0.24686	11.38	1.11 —(7)
742.6	5.095	0.776	0.29025	13.38	0.64
699.4	6.190	0.943	0.30956	14.27	0.19
				average error	0.65%
$2p_{-1}$-$4d_{-2}$					
570.6	1.607	0.245	0.37780	17.42	0.63
556.9	1.696	0.258	0.38596	17.79	0.92
513.0	2.104	0.320	0.42121	19.42	0.39
458.5	2.733	0.416	0.46995	21.66	0.66 —(6)
				average error	0.65%
Z - Unidentified					
1005.3	4.346	0.662			
944.0	4.849	0.738			
742.6	7.351	1.119			

(6)— B_3 or $2p_{-1}$-$4d_{-2}$
(7)— I_3 or $4f_{-2}$-$4d_0$

570, 556 and 513 μm. The theoretical fields for the transition are in good agreement with the observed position, with an average error in the theoretical transition energy of 0.6%.

Lines Absent From the Spectra.

No peaks were observed at the magnetic fields where the $3d_{-1}$-$4f_{-1}$ (H) transition should appear, and the assignment of $3d_{-1}$-$4f_{-1}$ to transition H causes considerable confusion here. Skolnick et al (1977) originally observed a transition at 4 magnetic fields which they called H, without attributing it to a transition. Two of the points were observations of a transition in CdTe at $\gamma \sim 0.2$, while the remaining two were observations of a transition in GaAs at $\gamma = 0.639$ and 0.840. On the basis of the two CdTe points and the $\gamma=0.639$ GaAs point Makado (1982) assigned the transition to $3d_{-1}$-$4f_{-1}$, even though the errors were rather large: 2% for the CdTe points and 3% for GaAs.

The two GaAs points observed by Skolnick et al ($\gamma=0.639$ and 0.840) have been plotted on Fig 6.4 with the symbol □: they are undoubtedly due to I_2 (which is a strong and narrow transition in spectra at similar magnetic fields, see eg Figure 7.4), with errors at $\gamma=0.639$ and 0.840 of 0.00 and 0.08% respectively. Having correctly identified these points it is now clear that no transition has been observed which can be assigned to the $3d_{-1}$-$4f_{-1}$ transition in either this or previously reported work on GaAs.

In CdTe the situation is less clear. The two points observed by Skolnick et al cannot be misidentified as I_2, which is at substantially lower energy than the two experimental points. Confusion could occur with the $4f_{-2}$-$4d_0$ transition which crosses the expected $3d_{-1}$-$4f_{-1}$ transition energy slightly above $\gamma=0.2$.

However the errors are still large, ~2-3%. Furthermore the large polaron induced shifts in CdTe noted earlier considerably confuse the situation. Consequently no further attempt has been made to pin down the origin of the transition in CdTe reported by Skolnick et al (1977).

The absence of the $3d_{-1}$-$4f_{-1}$ transition in this region is somewhat surprising in view of the amplitude of the $3d_{-2}$-$4f_{-2}$ (I_2) transition and the presence of the new transition $4f_{-2}$-$4d_0$ which ought to be forbidden by the selection rules. This could in part be due to the experiment being conducted in near Faraday Geometry, since in pure Faraday Geometry the $\Delta m=0$ transitions are forbidden, although in spite of the geometry the $2p_{-1}$-$3d_{-1}$ (B_1) transition is a $\Delta m=0$ transition and is usually the strongest in the spectrum.

The population distribution within the excited states may be significant in explaining the absence of certain transitions. Figure 2.4 showed the behaviour of the hydrogenic energy levels over the range $0<\gamma<2$. It can be seen that for fields where $\gamma>1$ the four lowest states are, in sequence, 1s, $2p_{-1}$, $3d_{-2}$ and $4f_{-3}$. Although the population distribution will be modified by the optical excitation and electric fields, one would still expect the most heavily populated states to be the lower states. This would explain qualitatively why the $2p_{-1}$-2s (B_2) and $2p_{-1}$-$3d_{-1}$ (B_1) transitions are usually the strongest, often followed by I_2 ($3d_{-2}$-$4f_{-2}$). On this basis one would expect a relatively low amplitude $3d_{-1}$-$4d_{-1}$ (H) transition since the $3d_{-1}$ state is at substantially higher energy than the $3d_{-2}$ state.

A further point when considering the amplitudes of transitions is that the selection rules (eg $\Delta l = \pm 1, 0$) only hold rigourously at zero magnetic field and they become less valid as the field increases since the magnetic perturbation is no longer small compared to the

coulomb energy and the states specified by the hydrogenic quantum numbers (n, l, m) no longer represent true eigenstates of the impurities. At very high fields where $\gamma \gg 1$ the electrons can be considered to be in cyclotron orbits and are only weakly perturbed by the impurity potentials and so quantum numbers (N, m, υ) are appropriate. However in the intermediate field regime where $\gamma \sim 1$ neither of the two sets of quantum numbers is particularly valid.

To further complicate matters the quadratic Stark effect caused by the electric fields from ionized donors mixes states of opposite parity. The amplitudes of transitions which are weakly allowed as a result of this mixing are likely to reduce when intrinsic radiation is applied, since this reduces the average electric fields causing the quadratic Stark effect.

The points detailed above may be responsible for the fact that certain lines seen by Gershenzon et al (1974, 1977) and Skolnick et al (1977) have not been observed. In addition to the $2p_{-1}$-$2p_0$ (I_3) transition both Gershenzon and Skolnick claim to have observed the $2p_0$-2s (M) transition while Gershenzon claims to have observed the $2p_0$-$2p_{+1}$ transition. While I_3 is observed consistently in the spectra shown in this thesis the other two transitions are usually absent.

A broad line at the position expected for $2p_0$-$2p_{+1}$ is occasionally observed when no optical excitation is present but disappears when the excitation is applied. This can be seen in Figure 7.5 which principally shows the dependence of the $D^- \rightarrow N=0$ transition under different band gap excitation conditions. However Gershenzon et al commented that it was of low amplitude and often merged with the cyclotron resonance. As no other lines in this region were assigned at that time it is possible that the transition was

confused with one of the other transitions which appear on the high field side of the cyclotron resonance, eg D ($2p_{-1}$-$3d_0$).

The near Faraday Geometry of the experiment may be responsible for the absence of the $2p_0$-2s (M) transition. It ought to appear at magnetic fields just above the I_1 ($2p_{-1}$-$3d_{-2}$) transition which is the strongest transition in spectra at λ= 1224, 1005 and 944 μm. However it was present in spectra taken with the Impatt devices at $\lambda\sim$ 3 mm. Gershenzon et al (1977) reported that its amplitude was strongly dependent on the polarization of the radiation and that it was strongest in Voigt Geometry, as expected for a $\Delta m=0$ transition, when others such as I_1 ($2p_{-1}$-$3d_{-2}$) were suppressed.

Five identifications made by Makado (1982) have not been observed in this work and there is a straightforward explanation for this. These were

A_4	$3d_0$-$4p_{+1}$
15	$3d_0$-$3p_{+1}$
17	unidentified
19	$2p_0$-$3d_0$
20	$3d_0$-$2p_{+1}$

and were made on the basis of a single recording of a sample of n-GaAs (R137) at a wavelength of 742μm. While the principle A and B groups of lines in this recording were reproduced in spectra of samples RR98B and S1 at λ=742μm, the extra strong peaks, which were given the identifications listed above, were not observed. Examples of recordings at 742μm can be found in Figures 7.4 and 7.5. Further analysis of Makado's recording shows that the positions of the five extra lines A_4, 15, 17, 19 and 20 agree to within a few percent with those expected for the A_2, cyclotron resonance, D, B_1 and B_2 transitions respectively for a laser wavelength of 669μm. Apparently

this would appear to be a classic case of lasing occurring in the FIR laser at two wavelengths: the gas used was formic acid (HCOOH) and the 9R40 CO_2 line pumps the 742μm FIR line while the 9R30 line pumps the 669μm FIR line. Apparently a rather unusual set of circumstances allowed both lines to lase at once with almost equal intensity. As noted in Chapter 3 lasing at more than one wavelength is not unusual, but for this to occur when the pump lines are so widely separated is most unusual. Considerable care was taken in the analysis of the recordings in this work to ensure that the peaks observed were not due to the presence of laser wavelengths other than that expected.

Unidentified Transitions Observed Experimentally.

Only one set of data points, labelled 'Z' in Figure 6.4, cannot be identified. A spectrum showing 'Z' is shown in Figure 7.4 of the following chapter. Although the three points linked by the line 'Z' appeared to be associated with the same transition, no transition involving any of the thirty states with principle quantum numbers 1 to 4 would fit all three points satisfactorily. Since the agreement obtained for other transitions is generally of the order of 1% this suggests that the transition must involve other excited states. Two alternatives exist for possible candidates:

i. states with principle quantum number n>4 are involved, or

ii. states not associated with any particular zero field level may be involved. An example would be the $(1\bar{1}0)$ state which has no low field equivalent and so does not appear in Makado's variational calculation of the energy levels.

However as the transition is relatively broad and of low amplitude no further attempts have been made to identify it. Recent calculations by Rosner et al (1984) of hydrogenic energy levels in a

magnetic field include n=5 and n=6 states and would be of considerable use when trying to identify inter-excited state transitions involving these states.

Central Cell Structure on the 2s Excited State.

Central cell structure has previously been reported on transitions involving the 2s state in CdTe on the $2p_{-1}$-2s and $2s-2p_{+1}$ transition: (Simmonds et al 1974) and in GaAs on the $2p_0$-2s transition (Davidson et al 1980). The experiment involving GaAs was performed at low magnetic fields with millimetre wave Impatt oscillators operating at $\lambda \sim 3$mm. The $2p_0$-2s transition appeared at 1.47 Tesla or $\gamma \sim 0.22$. Referring back to Figure 6.1 showing the variation of the central cell splitting of the 2s state with field it is apparent that this is where the central cell splitting should be greatest. Furthermore the graph of the quadrupole moments (Figure 4.3) shows that the moments of the 2s and $2p_0$ states cross near $\gamma \sim 0.2$, leading to a negligible contribution to the linewidth from quadrupole broadening. However as the quadrupole moment of the 2s state increases above this field the linewidth of the transition will also increase. Consequently if the $2p_0$-2s transition could be observed in the field region above ~3 Tesla it is unlikely that any splitting due to central cell effects would be observed.

The remaining strong transitions involving the 2s state are the $2s-2p_{+1}$ (B_3) and the $2p_{-1}$-2s (B_2) lines. The most likely sample in which to observe central cell splitting would be one with very high purity but with two widely separated central cell components of near equal amplitude: sample S1 has both X_1 and X_3 present in almost equal quantities (see Figure 4.6) and is well suited.

In practice S1 shows central cell structure on the $2p_{-1}$-2s (B_2) line between magnetic fields of ~1T (at λ=1.224mm) and ~6T (λ=393μm). The $2s-2p_{+1}$ (B_3) line also showed similar structure, though not as consistently due to its lower amplitude. The central cell structure is apparent on B_2 in the λ=458μm recording shown in Figure 6.2, while it is barely resolved in the λ=570.6μm recording.

Figure 6.6 shows an expanded portion of the 570.6μm spectrum in Figure 6.2 taken at a lower magnetic field sweep rate. The arrows show the theoretical positions of the transitions. The sample was at T=4.2K and illuminated with intrinsic light. The central cell splitting of the B_2 and B_3 lines is clearly resolved and unambiguously confirms the identification of these lines.

In Figure 6.7 the B_2/B_3 region of the spectrum is shown using wavelengths of 1005μm (i) and 1224μm (ii and iii). At 1005μm the theoretical magnetic field positions for the B_2 and B_3 lines are almost coincident. Consequently, as the central cell structure is pushed to high field (ie low energy) for B_2 and to low field for B_3, both sets of central cell components can be seen. Traces (ii) and (iii) of Figure 6.7 show the 1224μm spectra for S1 (at T=1.8K) and RR98B (T=4.2K) respectively. At this lower energy B_2 ought to appear at lower field than B_3, but since the central cell shift pushes B_2 upwards and B_3 downwards in field the transitions overlap. It is apparent in trace (i) at 1005μm that the intensity ratio B_3:B_2 is approximately 1:3, and since the fields of B_2 and B_3 in the 1005 and 1224μm recordings are reasonably close the ratio can be assumed to be the same for traces (ii) and (iii) also.

On this basis one could argue that the observed structure is due entirely to B_2, with B_3 only contributing to the linewidth of the

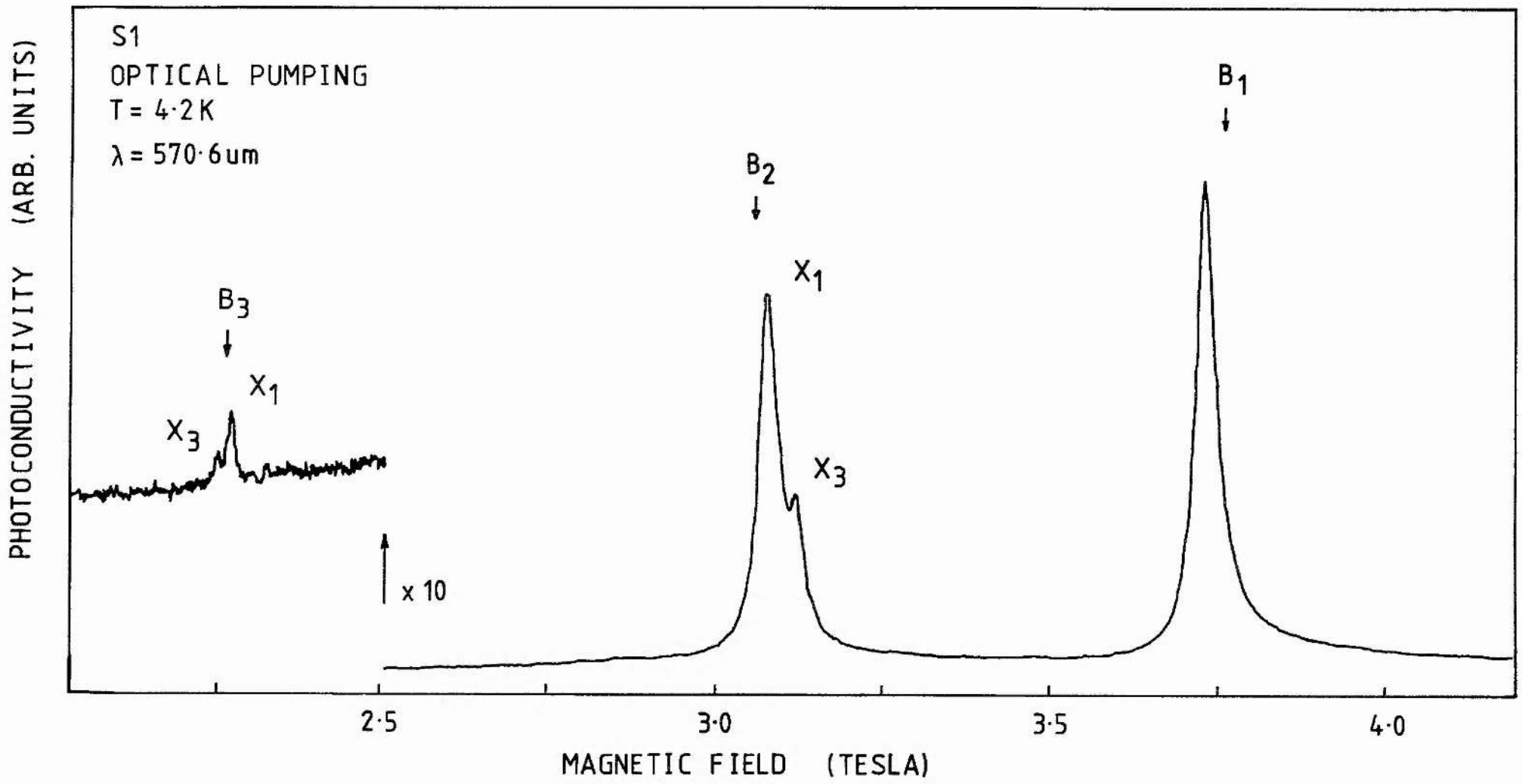

Figure 6.6: Spectrum showing central cell splitting of the B_2 ($2p_{-1}$-2s) and B_3 (2s-$2p_{+1}$) transitions in S1 at T=4.2K using λ=570.6μm radiation and optical excitation. B_1 ($2p_{-1}$-$3d_{-1}$) does not show central cell splitting. The X_2 central cell component is not

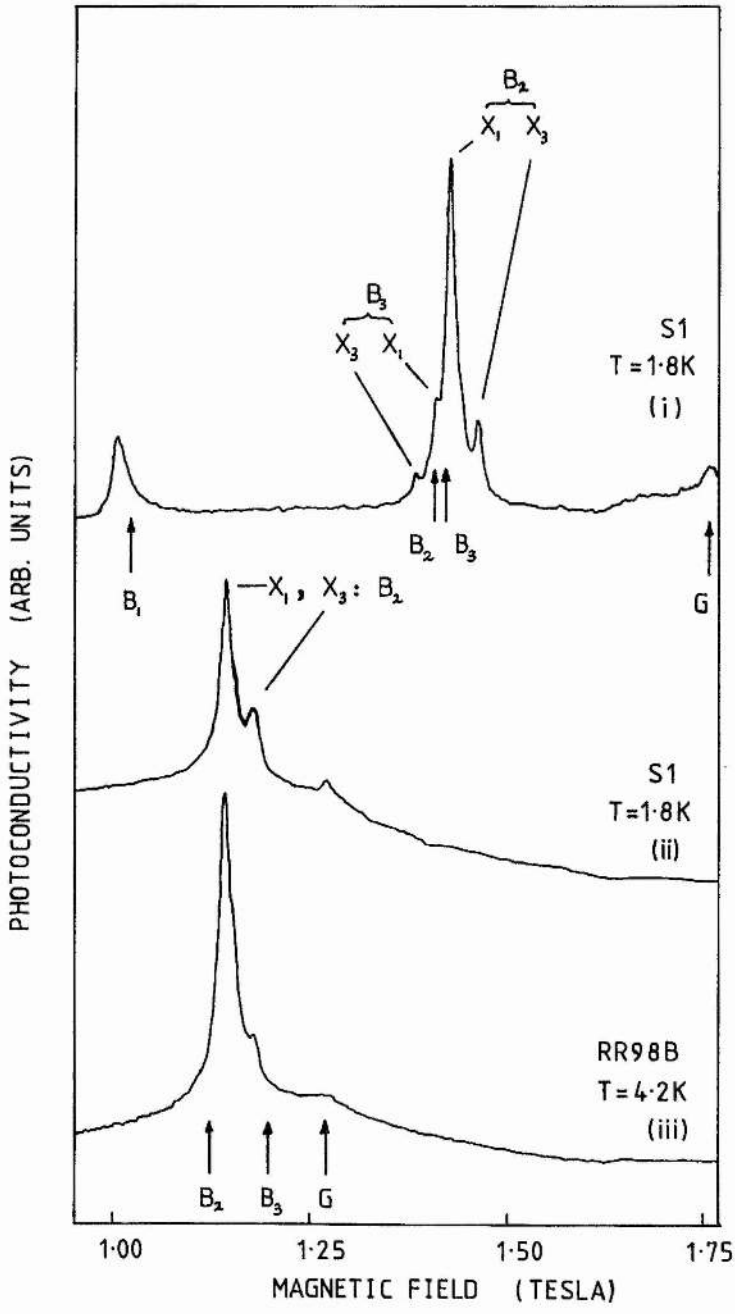

Figure 6.7: Spectrum showing central cell splitting of the B_2 ($2p_{-1}$-2s) and B_3 (2s-$2p_{+1}$) transitions in S1 and RR98B with optical excitation. Trace i is with λ=1.005mm radiation while ii and iii are at 1.224mm. Theoretical magnetic fields are marked by arrows.

observed transition, and that this is consistent with the actual structure observed at 1224μm: the central cell structure on B_2 in (i) and (ii), both showing S1, is almost identical, whereas trace (iii) of RR98B, which is known to have only a small proportion of donor X_3, only has a shoulder in the X_3 position.

However one could also argue that the shoulder on B_2 in RR98B at 1.2mm is in fact due to B_3 and is not due to central cell structure at all, and consequently the peak labelled as X_3 in trace ii is also due to B_3, but better resolved due to the better quality sample S1.

Unfortunately there is no definitive solution to this argument. In the following we have assumed that the splitting on B_2 in the λ = 1.2mm spectra is due to central cell splitting alone.

If a figure for the slope of these transitions with magnetic field is obtained from the data of Makado (1982), the energy difference between the two central cell components can be calculated, and the variation in central cell shift with field can be studied. Table 6.3 shows these values. An estimate of the linewidths can also be made. Those given in the table are for the X_1 donor only: these will be larger than the true linewidth as a result of the unresolved donor present on X_1 (ie X_2). The amplitude of the X_3 component is too small for a meaningful figure for the linewidth to be obtained.

In order to calculate the ratio

$$\frac{\Delta E_{cc}\ 2s\ (B)}{\Delta E_{cc}\ 1s\ (B=0)}$$

the zero magnetic field splitting between the X_1 and X_3 components of the 1s state is required. As Fourier Transform spectra of S1 at zero magnetic field were not sufficiently well resolved to give an accurate value for the splitting, a better approach is to use the splitting measured on the $1s\text{-}2p_{+1}$ transition at 3.6 Tesla and

Table 6.3.

	Field (T)	Splitting (T)	Gradient cm^{-1}/T	avge	Splitting cm^{-1}	FWHH (T)	FWHH cm^{-1}
B_2 X_1	3.078	0.045±8%	3.607	3.590	0.162±8%	0.041	0.15
B_2 X_3	3.123		3.572				
B_3 X_1	2.272	0.020±17%	9.608	9.595	0.192±17%	0.016	0.16
B_3 X_3	2.252		9.581				
B_2 X_1	1.427	0.036±10%	5.970	5.914	0.213±10%		
B_2 X_3	1.463		5.858				
B_3 X_1	1.411	0.027±13%	8.042	8.021	0.217±13%		
B_3 X_3	1.384		7.999				
B_2 X_1	1.141	0.033±10%	6.563	6.512	0.215±10%		
B_2 X_3	1.173		6.460				

correct this to the zero field splitting. The spectra of S1 at 3.6 Tesla using λ=118.8μm laser radiation were shown in Figure 4.6. The magnetic fields for X_1 and X_3, measured on the recording taken without optical excitation, are

$$\left.\begin{array}{ll} X_1 & 3.667\pm0.001T \\ X_3 & 3.577\pm0.001T \end{array}\right] \quad (X_1 - X_3) = 0.090\pm0.002T\ (\pm2.2\%)$$

The slope of the $1s\text{-}2p_{+1}$ energy with respect to field, calculated using the data from the theoretical calculation of Makado (1982), is 14.7 cm^{-1}/T at 3.63T. This implies that the ground state energy splitting at 3.6 T of the X_1 and X_3 central cell components is

$$E_{1s}\ (X_1\text{-}X_3) = 1.32\ cm^{-1} \pm 2.2\%$$

In order to obtain the zero magnetic field splitting the calculation of Cabib et al (1972) for the ratio

$$\Delta E_{1s}(B)/\Delta E_{1s}(0)$$

is used. This ratio, along with the equivalent ratio for the 2s state, was plotted against γ in Figure 6.1. At a field of 3.62T then γ=0.551 and $\Delta E_{1s}\ (3.62T)/\Delta E_{1s}\ (0) = 1.20$.

Thus the $X_1\text{-}X_3$ splitting at zero magnetic field is 1.10 cm^{-1} ±2.2%. The error here only represents the error in taking the peak positions and no account has been taken of the error involved in

i the overall calibration of the magnet (this was performed using NMR techniques and should be of high accuracy although no error figures are available)

ii estimating $\partial E/\partial B$ from the theoretical calculations

iii correcting the ground state splittings to zero field.

With regard to ii, this is difficult to assess. Makado's calculation, from which $\partial E/\partial B$ was obtained, describes to within 1%

the positions of the inter-excited state transitions and ought to provide a good basis for calculating $\partial E/\partial B$. The ground state splitting calculated by Cabib et al has also been shown to be in excellent agreement with experiment (Larsen 1974).

In Figure 6.8 the ratio of the 2s state central cell splitting obtained in Table 6.3 to the zero field ground state splitting of $1.10\ cm^{-1} \pm 2.2\%$ obtained above has been plotted against γ and compared to Cabib's calculation. The error bars represent the sum of the errors on the 2s splitting and the ~2% error in the 1s(B=0) splitting. The error in the 2s splitting (like that for the 1s splitting) takes no account of points (i) or (ii) noted above. However errors due to (i) (ii) and (iii) above only shift the points on the graph up or down by the same amount for each point and do not contribute to any increase in the size of the error bars.

Although the data is limited in terms of the magnetic field range covered and the error bars are large it is clear that the agreement with Cabib's calculation is good.

Experimental Linewidths of Inter-Excited State Transitions.

It has already been noted that the width of transitions measured in magnetic field terms depends on the gradient of the energy versus field curve and that transitions that are in fact quite narrow in energy can appear to be spread over a large magnetic field range if this gradient is small. In the earlier section on linewidths it was noted that Skolnick et al (1977) observed a number of inter-excited state transitions that were as narrow as transitions originating on the ground states. Measurement of the linewidths of some selected transitions are presented below to emphasize this point.

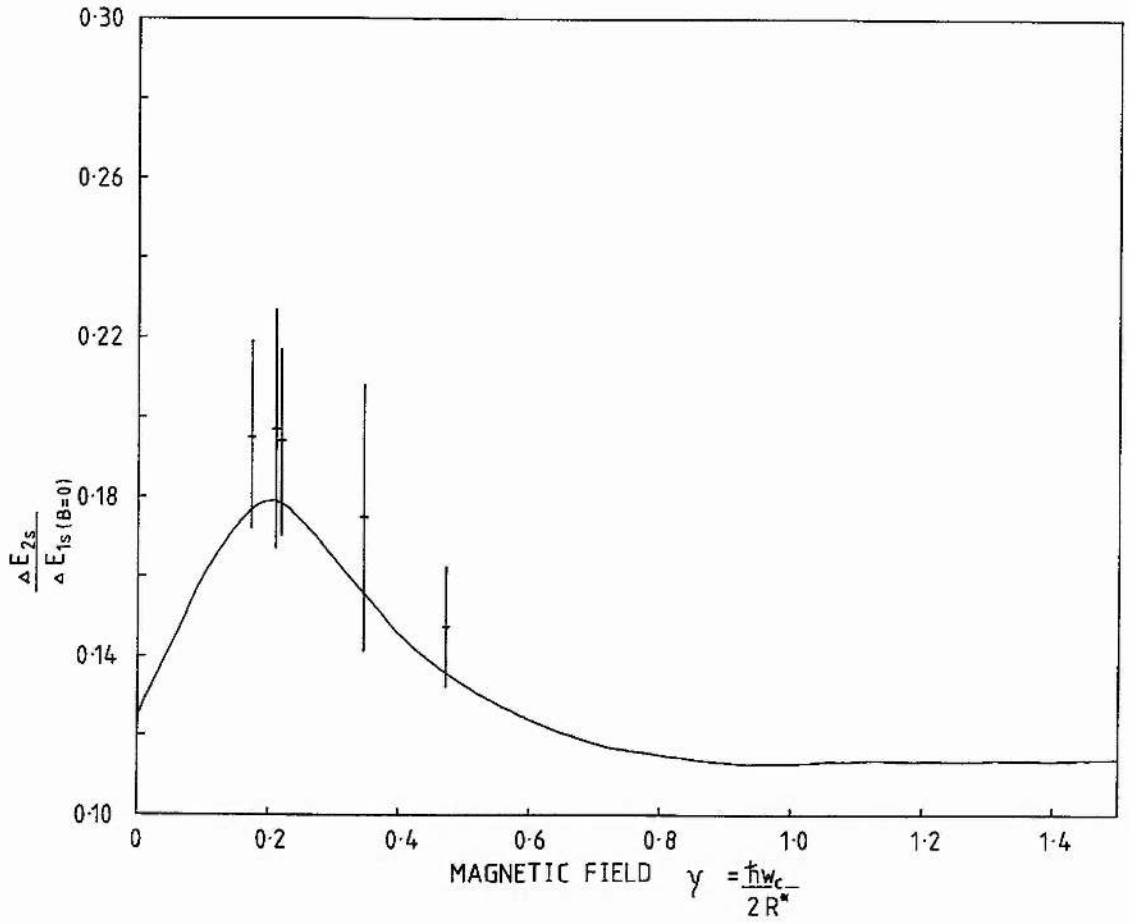

Figure 6.8: The central cell splitting of the 2s excited state in sample S1 plotted against magnetic field. The actual value plotted is the ratio of the splitting on the $2p_{-1}$-2s or 2s-$2p_{+1}$ transitions to that on the 1s state at B=0. The experimental points and error bars are those given in Table 6.3. The solid curve shows the theoretical calculation of Cabib et al (1972).

Figure 6.6 shows the three lines in the 'B' group with a laser wavelength of 570.6μm. In addition to providing figures for the central cell splitting in the previous section the linewidths (FWHH) were also calculated in Table 6.3: for B_2 and B_3 the X_1 width is 0.15 and 0.16 cm^{-1} respectively at T=4.2K. Note that this width is increased due to the presence of the unresolved donor X_2 on the X_1 component. The linewidth of the B_1 peak is 0.057T, but the lower slope of B_1 with field, 2.25 cm^{-1}/T at 3.73T, leads to a very small linewidth in energy of 0.084 cm^{-1} (FWHH and at T=4.2K). This is in fact much less than the linewidths obtained on some of the $1s-2p_{+1}$ transitions: the X_2 donor of R137 had a linewidth of 0.12 cm^{-1}. In the 302μm $1s-2p_{-1}$ spectra of S1 (Figure 4.10) X_1 and X_2 had linewidths of 0.08 and 0.10 cm^{-1} (FWHH) respectively, very similar to the B_1 linewidth, but note that the comparison is not quite fair as the $1s-2p_{-1}$ linewidths were measured on the spectrum without band gap illumination since the spectra taken with band gap illumination were distorted by peak inversion effects.

The two transitions I_1 $(2p_{-1}-3d_{-2})$ and I_2 $(3d_{-2}-4f_{-2})$ also appear to be quite narrow. Table 6.4 shows the linewidth (FWHH) at various fields at a temperature of 4.2K. As peak inversion appeared to be occurring on I_1 at both 1005 and 944μm (as shown in Figure 6.9) the linewidths are an upper limit. Reducing the temperature of the samples from 4.2 to 1.8K should normally reduce the linewidths to a certain extent as a result of the formation of ionized donor-acceptor complexes (see earlier discussion), particularly if the material is compensated. At low magnetic fields this certainly does seem to occur: Figure 6.10 shows the 'A' group of lines and the cyclotron resonance at λ=1005μm at the two temperatures 4.2 and 1.8K, under nearly identical bias and optical pumping conditions. It is clear that the linewidths of the 'A' lines have reduced with

Table 6.4.

Linewidths (FWHH) of the I_1 and I_2 transitions at T=4.2K and with band gap illumination.

Line	Laser Wavelength μm	Field T	Gradient cm^{-1}/T	Linewidth T	Linewidth cm^{-1}
I_1	1223.7	3.700	0.593	0.09	0.06
	1005.3	7.203	0.411	<0.11	<0.04
	944	8.802	0.366	<0.14	<0.05
I_2	699.4	5.361	1.475	0.08	0.12

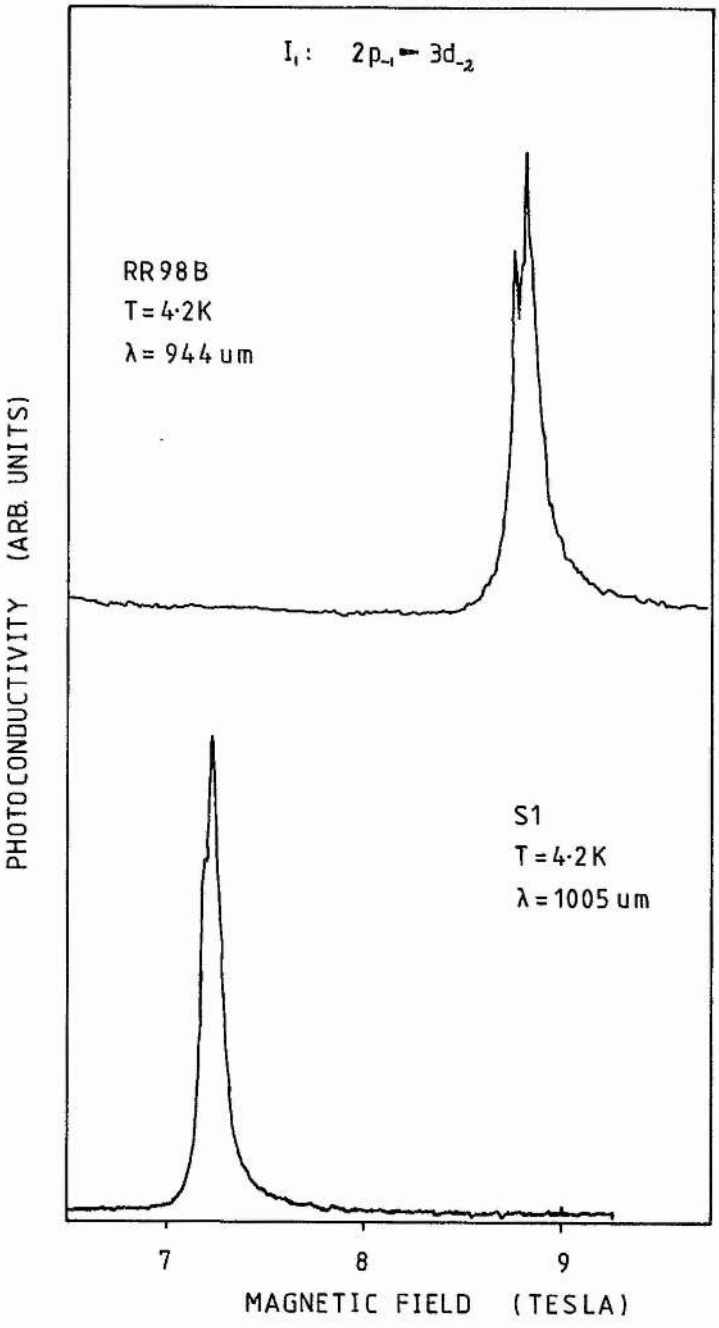

Figure 6.9: Spectra of the I_1 ($2p_{-1}$-$3d_{-2}$) transition at high magnetic fields. The distortion and splitting of the transition is probably due to peak inversion. The upper trace shows sample RR98B using λ=944μm radiation, while the lower trace shows sample S1 using λ=1005μm radiation. Both traces were obtained at T=4.2K and with band gap illumination.

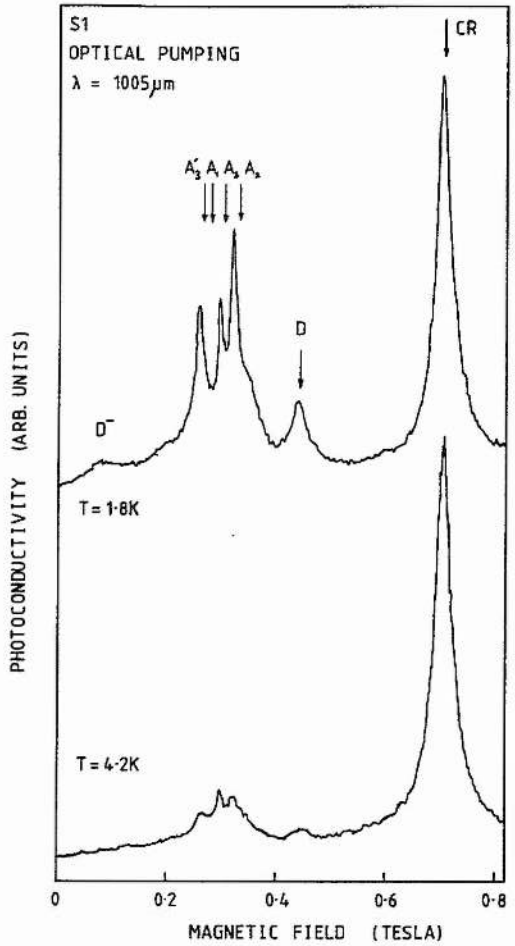

Figure 6.10: Spectra of S1 at T=1.8 and 4.2K using λ=1.0mm radiation and optical excitation showing the A series and D inter-excited state transitions and the cyclotron resonance.

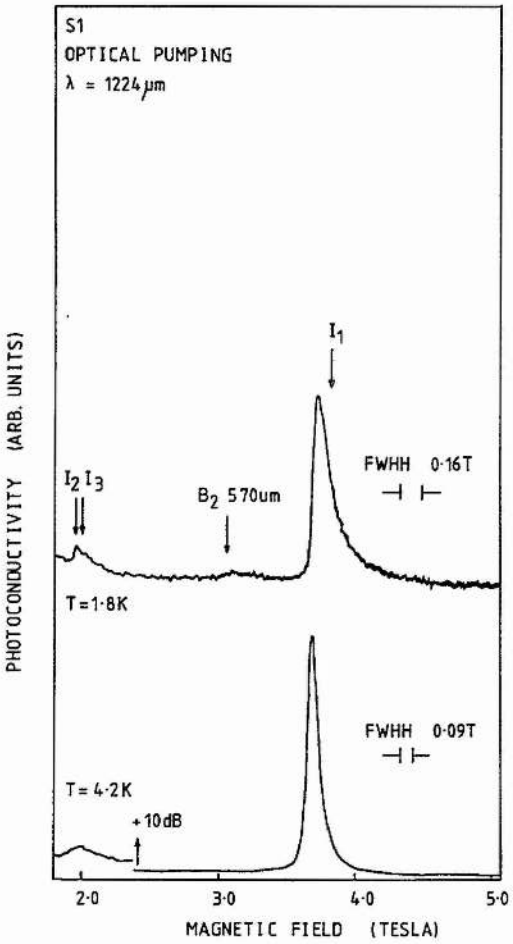

Figure 6.11: Spectra of S1 at T=1.8 and 4.2K using λ=1.2mm radiation and optical excitation showing the I series inter-excited state transitions.

temperature, although the linewidth of the cyclotron resonance does not appear to have changed significantly (an $\omega\tau$ of 36 at 4.2K compared to 40 at 1.8K). However Figure 6.11 shows the 'I' group of transitions at a wavelength of 1224μm under similar conditions. Here I_1 is clearly broader at 1.8K than at 4.2K: 0.16T (~0.09 cm^{-1}) compared to 0.09T (~0.06 cm^{-1}). This is quite unexpected. A possible explanation exists in that, as noted earlier, at shorter wavelengths and much higher magnetic fields (8 & 10 Tesla) I_1 showed a double peaked structure which was probably due to peak inversion. Examples of these spectra are shown in Figure 6.9. Thus if I_1 at 3.5 Tesla was being distorted by peak inversion this could increase the apparent linewidth. A more interesting explanation for the increased broadening could be that, for whatever reason, there is either a more monopole charge distribution or that there are many more ionized sites. It is possible that the D^- states already mentioned briefly (and discussed extensively in the following chapter) are responsible for this additional broadening.

Briefly the D^- state is only significantly populated at high magnetic fields and low temperatures when the binding energy has increased sufficiently that thermal depopulation is not as significant. Thus the number of D^- sites is far greater at 1.8K than 4.2K, and also far greater at the magnetic fields where the 'I' group lines appear than at the fields where the 'A' group lines appear. Consequently the 'A' lines are relatively unaffected by the low population of D^- states and show the expected reduction in linewidth with temperature, whereas I_1, and other transitions above ~3 Tesla, are broadened at the lower temperature by the far greater population of ionized impurities, except that the ionized impurity is a negatively charged donor rather than the more normal (for compensated material) positively charged donor.

Chapter 7.

Negatively Charged Shallow Donors in n-GaAs.

In the previous three chapters the energy levels of neutral shallow donors in high purity n-type GaAs and InP have been studied in detail. Positively charged donors do not have any identifiable shallow energy levels and in our spectra their presence simply results in a broadening of the neutral donor transitions as a result of field gradient and quadratic Stark shifts. Consequently high purity samples with low compensation and hence a low ionized impurity concentration are observed to have narrower neutral donor transitions.

However in addition to these two charge states of a shallow donor a further state can exist. This is the negatively charged donor, or D^- state, where a second electron is bound at a neutral donor site, ie

$$D^0 + e^- \rightleftharpoons D^- + \hbar\omega$$

This state is the solid state analogue of the negatively charged hydrogen ion, H^-, where two electrons are bound to a single proton.

Extensive calculations of the binding energy and wavefunctions of the H^- ion have been made since it is of great interest to atomic and astro-physicists, being one of the simplest forms of three body system, a form of helium-like atom and since it is thought to play a significant role in the physics of stellar atmospheres (Chandrasekar 1944). These calculations, confirmed by experimental data, show that in the absence of a magnetic field the H^- ion has only one bound state, a singlet ^1S state with a one electron binding energy of 0.754 eV or 0.0555 Rydberg. That is

$$H^- + 0.754 \text{ eV} \rightarrow H^0 + e^-$$

(see eg Bethe and Salpeter: 'Quantum Mechanics of One and Two Electron Systems'). The application of a magnetic field allows triplet and other excited states to bind. At zero magnetic field the H^- ion can be represented as a proton with two distinguishable electrons, one electron having a characteristic radius of $\sim 0.9a_o$ (a_o being the

Bohr radius of a neutral hydrogen atom) and the second electron with a much larger radius of $\sim 2.1a_0$.

The first suggestion that a similar state to the H^- ion might exist in a semiconductor, where an electron is bound at a neutral donor, was made by Ansel'm (1953). Such bound states were incorporated into a theory of neutral impurity scattering by Sclar (1956). The binding energy of a D^- state in a semiconductor with a spherical, parabolic and non-degenerate band at zero magnetic field was given by Lampert (1958) as 0.0555 R* (where R* is the effective Rydberg in the semiconductor).

Although the D^- ground state is much shallower than the D^0 ground state it is metastable, ie it cannot decay into a D^0 state and free electron - energy must be supplied to ionize it first. Consequently, under suitable conditions (discussed later), substantial populations of D^- states can accumulate in semiconductors.

Experimental evidence for D^- states in semiconductors was first seen by Dean et al (1967b) who used them to explain features in the low temperature photoluminescence of silicon and germanium. More direct evidence for D^- states was seen by Gershenzon et al (1971) who observed broad low energy features in FIR photoconductivity spectra of Si:P corresponding to transitions from loosely bound states which they attributed to the photoionization of D^- states. Thornton and Honig (1973) also observed a loosely bound state in experiments on spin-polarized electrons in Si:P. However in these initial experiments a large variation in binding energy was observed, from 0.8 to 4 meV. This was not explained until later work on the concentration dependence of the spectrum of D^- states in silicon showed that as the D^- state population increases interaction between D^- and D^0 states leads to the formation of D_2^- complexes which are more

deeply bound than isolated D^- states (Taniguchi et al 1975, Norton 1976 and Taniguchi and Narita 1976).

In parallel with the work on D^- states in silicon there was additional work on the positively charged acceptor state, A^+. Indirect evidence for such states has been seen in measurements of the carrier lifetime in the temperature region were neutral impurity capture is important (Godik et al 1971; Gershenzon et al 1971 and Ohyama et al 1973). No direct spectrosopic evidence for photoionization of A^+ states has been reported to date.

Returning to the D^- state, since 1976 there have been many papers on various aspects of the D^- state, principally in n-type silicon and germanium. This may be partly due to the suggestion by Norton (1976) that D^- states could be used as the basis for highly sensitive low noise detectors of FIR radiation, though no devices have yet been made.

Work on D^- states that specifically relates to the studies described in this thesis concerns theoretical calculations of the D^- state binding energy in intermediate magnetic fields ($\gamma \sim 1$): Natori and Kamimura (1978), Larsen (1979a,b and 1980), or experimental studies of D^- states in magnetic fields: Taniguchi and Narita (1979), or studies of the effects of interactions between D^- states and either D^0, D^+ or D^- states: Taniguchi et al (1978) and Thomas et al (1981).

Work on D^- states in material other than silicon and germanium is very limited. GaAs was studied at St. Andrews prior to this author but no evidence for D^- states was seen (Davidson et al 1980 and Makado 1982). Larsen (1979a) claimed to identify D^- states in CdS with the aid of experimental work by Cohn et al (1971) while Ichiguchi and Drew (1983) used D^- states to explain features in the FIR

spectrum of the semi-magnetic compound CdMnSe. However it is unlikely that D^- states were responsible for the features seen in both of these papers since, although the work on silicon and germanium is sufficiently extensive to support the existence of D^- states, no authors have taken into account the possibility that the spectral features they observe could be due to transitions between excited states of a neutral donor, or been able to simultaneously observe inter-excited state transitions and transitions due to the photoionization of D^- states. The importance of inter-excited state transitions can be seen when one considers that the n=4 D^0 state has a binding energy of 0.0625 R* at zero magnetic field, which is only marginally deeper than the D^- binding energy. In addition, the n=3 to n=4 inter-excited state transition of a neutral donor at zero magnetic field occurs at 0.049 R* which is very close to the energy required to photoionize a D^- state, 0.0555 R*. Thus it is clear that in addition to expecting both inter-excited state D^0 transitions and the D^- state photoionization transition in the same spectral region the conditions under which D^- states and D^0 excited states become populated will be very similar and confusion over the origin of spectral features can occur.

Application of a magnetic field may cause additional identification problems as the inter-excited state transitions Zeeman split into a multitude of peaks. In less pure samples than the two used for the studies described in this chapter these transitions will be broader and certain of the groups of peaks, for example the A-series lines at higher energy than the cyclotron resonance, can merge to produce one anomalously broad feature. This was precisely the situation for the A and B lines as originally reported by Chamberlain et al (1972) in GaAs, CdTe, CdS and InP. One particularly useful

feature of working with GaAs is that within the range of fields up to 12 Tesla the inter-excited state spectrum is now very well characterized and any new peaks which cannot be attributed to inter-excited state transitions of neutral donors are easily identified.

D^- Bands.

Although the binding energy of D^- states in semiconductors is very small and of the same order of magnitude as the binding energies of the excited states of neutral donors it is believed that they play an important role in the low temperature conductivity of highly doped semiconductors. Initially, at very low doping levels the D^0 and D^- states can be regarded as isolated and non-interacting and have discrete energy levels. As the impurity concentration increases interaction between neighbouring states occurs and broadens the energy levels (Townsend 1978, Thomas et al 1981). Since the D^- state is more extended than the D^0 ground state it is the first to broaden and forms a band of states known as the Upper Hubbard Band. At still higher concentrations the ground state of neutral donors broadens and forms the Lower Hubbard Band. Electron transport can occur in the Upper Hubbard Band as electrons tunnel from charged donor to neutral donor. As electrons must first be excited into the Upper Hubbard Band from the Lower Hubbard Band this type of conduction is characterized by a thermal activation energy ε_2 which is less than the ionization energy of donors in the Lower Hubbard Band (ε_1). ε_2 can be regarded as the difference between the Fermi level in the Lower Hubbard Band and the bottom of the Upper Hubbard Band. Conduction characterized by the ε_2 activation energy is only observed in uncompensated material over a limited range of temperature, as at

higher temperatures thermal ionization of the donors, characterized by ε_1 which may only be slightly higher than ε_2, is dominant. At lower temperatures hopping conduction in the Lower Hubbard Band with activation energy ε_3 may take over as the dominant conduction mechanism if compensation is present.

As the donor concentration continues to increase the D^0 and D^- bands broaden, manifested by a reduction in ε_2 until ε_2 reaches zero, at which point the D^0 and D^- bands overlap. At this point metallic conduction (with a weak temperature dependence and no activation energy) takes over and a metal-insulator transition is said to have occurred. This type of transition is usually referred to as a Mott or Mott-Hubbard transition. Considerable work has been carried out on the role of D^- states in conduction on the insulating side of the metal - insulator transition. See eg: Kobayashi et al 1982.

Review of Theoretical Calculations of D^- State Binding Energy in a Magnetic Field.

Various calculations have been made of the binding energy of an isolated H^- state at zero magnetic field. Until recently the most accurate calculation, using a variational method with 24 parameters, gave a binding energy of 0.05545 Ry (Hyleraas and Mitdal 1956), but calculations using over 200 parameters and giving ground state energies accurate to more than 8 significant figures have been reported (Freund et al 1984). By analogy with the H^- state, the D^- state in the effective mass approximation will have a binding energy of 0.05545 R*.

When a magnetic field is applied to a D^- state the wavefunction will be compressed in the plane perpendicular to the magnetic field direction. In the direction parallel to the magnetic field direction

compression will also occur but to a lesser extent. The compression can be incorporated within the framework of the model used by Yafet, Keyes and Adams (1956) to describe a neutral hydrogenic donor in a magnetic field. The YKA approach, where each electron is characterized by an effective Bohr radius parallel and perpendicular to the magnetic field direction ($a_{\perp}$ and $a_{/\!/}$ respectively) has been applied to the D^- state by Natori and Kamimura (1978). For the D^- state four parameters, two for each electron, $a_{\perp}$, $a_{/\!/}$, $a'_{\perp}$ and $a'_{/\!/}$ are used. The individual electron wavefunction they use is

$$\psi(r) = [(2\pi)^{3/2} a_{\perp}^2 \; a_{/\!/}]^{1/2} \exp\left\{\frac{(x^2+y^2)}{4a^2} + \frac{z^2}{4a^2}\right\}$$

The total D^- state wavefunction is then written

$$\Psi(\underline{r}_1,\underline{r}_2) = 2^{-1/2}[\psi(\underline{r}_1)\psi'(\underline{r}_2) \pm \psi'(\underline{r}_1)\psi(\underline{r}_2)]$$

where the function using the positive sign corresponds to the symmetric singlet ground state and the function using the negative sign is the antisymmetric triplet state. The ground state energy of a D^- state can then be evaluated analytically in terms of the four 'a' parameters, and then the parameters are varied to obtain the minimum ground state energy at any given value of the dimensionless magnetic field γ. The ground state energy of a neutral donor is calculated in the same way and the binding energy of the D^- state in a magnetic field (defined as the energy required to excite one electron from a D^- state to the lowest Landau level leaving a neutral donor in its ground state) is given by

$$\varepsilon_{D^-} = \gamma + E_{D^0}(\gamma) - E_{D^-}(\gamma)$$

Natori and Kamimura (1978) gave the explicit analytic expressions necessary to calculate $E_{D^-}(\gamma)$ and $E_{D^0}(\gamma)$, and the D^- binding energy shown in Figure 7.1 has been recalculated using these. The binding energy curve attributed to Larsen will be discussed in due

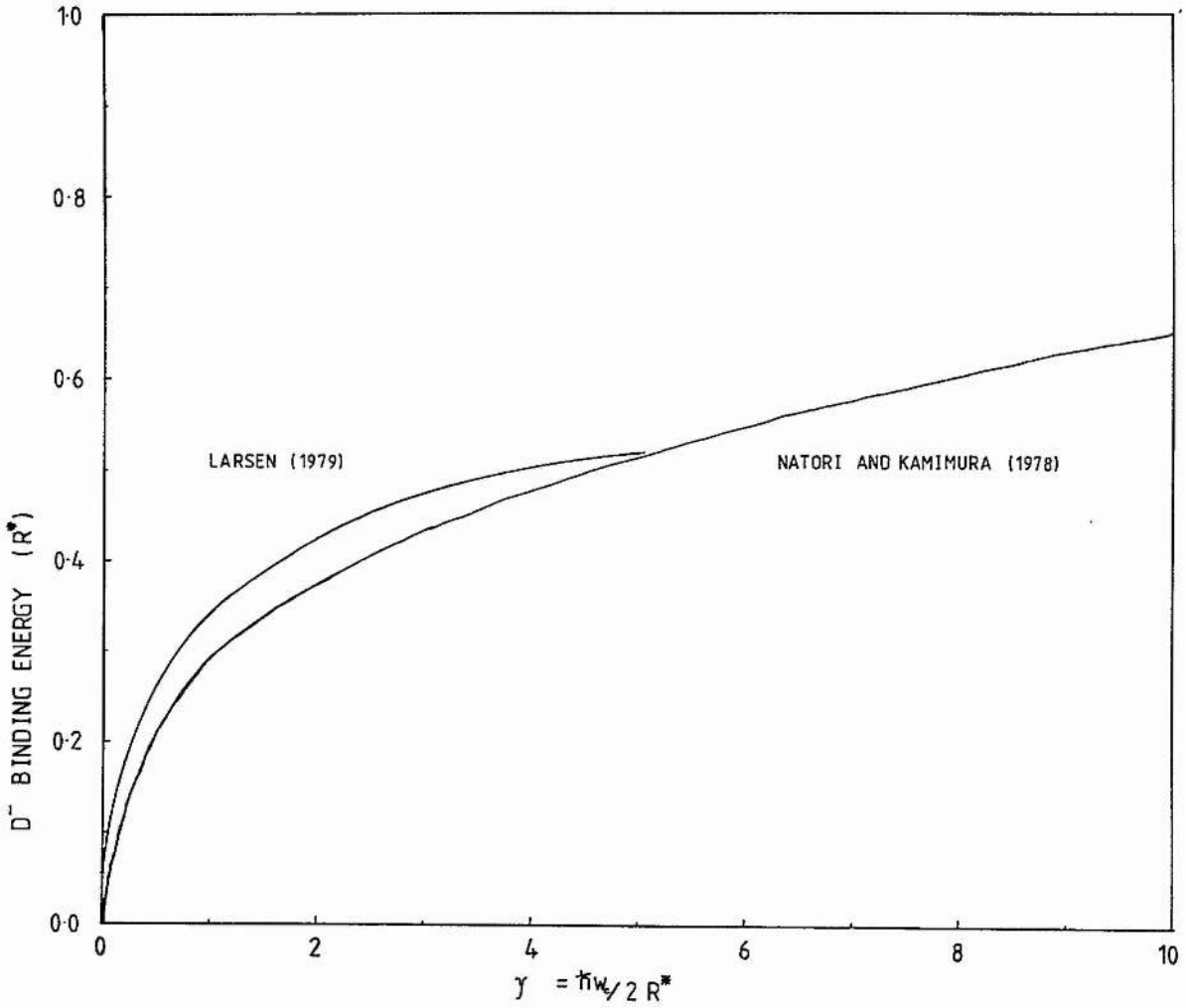

Figure 7.1: The magnetic field dependance of the D^- state binding energy in dimensionless units obtained from variational calculations by Natori and Kamimura (1978) and Larsen (1979).

course. Figure 7.2 shows the behaviour of the four variational parameters ($a_\perp$ $a_{/\!/}$ $a'_\perp$ $a'_{/\!/}$) which minimize the ground state energy at each magnetic field, as well as the parameters D^0 $a_\perp$ and D^0 $a_{/\!/}$ which minimize the neutral donor binding energy, and the behaviour of the cyclotron radius (equal to $\gamma^{-1/2}$). All radii are expressed in terms of the neutral donor Bohr radius a_B^* at zero magnetic field.

It can be seen from the graph of binding energy against γ that Natori and Kamimura's calculation is not particularly accurate at low values of γ. This can be seen from the fact that:

i. it gives a negative binding energy at $\gamma=0$, with the outer electron parameters $a'_\perp$ and $a'_{/\!/}$ tending to infinity (ie the state is not bound).

ii Larsen's calculation for $\gamma<5$ gives a better result (as the 'better' variational calculation is the one giving the greatest binding energy).

This inadequacy in the YKA approach is a consequence of the simplicity of the trial wavefunction. The decoupling of the electron motion into components perpendicular and parallel to the field is only strictly valid at infinite magnetic field, and is only a good approximation for $\gamma>>1$, hence the unsatisfactory behaviour at $\gamma<1$. Furthermore the behaviour of the wavefunction as $r\to\infty$ is proportional to $\exp(-r^2)$ which is not a good approximation to the zero field wavefunction which is proportional to $\exp(-r)$. However even at $\gamma>>1$ the results are unlikely to be particularly accurate as the YKA method is known to seriously underestimate the neutral donor binding energy, even at fields where $\gamma\sim100$ (Larsen 1968).

In spite of these limitations Natori and Kamimura's calculation is useful since it demonstrates the effect of a magnetic field on the wavefunctions of a D^- state and sets a lower limit to the binding

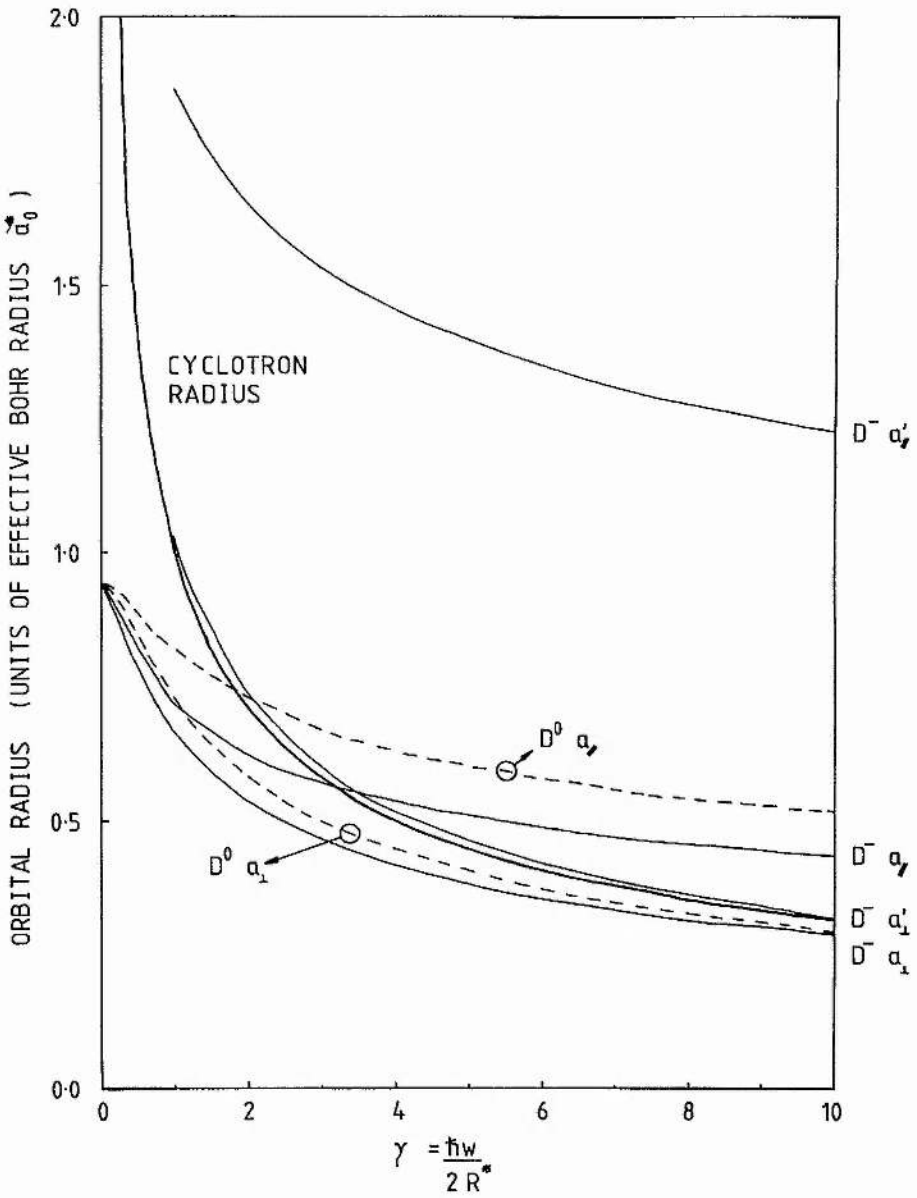

Figure 7.2: The magnetic field dependance of the orbital radius of the two electrons (a and a') in a D^- state in dimensionless units from the variational calculation by Natori and Kamimura (1978). The radii in the direction parallel to and in the plane perpendicular to the magnetic field are shown. The neutral donor radii and the cyclotron radius are also shown.

energy. Above γ=0 the binding energy increases rapidly to ~0.3 R* at γ~1 while the four radii parameters show that the two electrons remain distinguishable: one looks much like the electron bound at a neutral donor though slightly more compressed (the inner electron), while the second electron (the outer electron) is much more resistant to compression along the field direction but is strongly compressed in the perpendicular plane and has a radius similar to that of the cyclotron orbit. As the magnetic field increases beyond γ~1 the binding energy continues to increase but less rapidly, so that by γ~10 the binding energy is only approximately twice that at γ~1.

Consider now the results of Larsen's calculation. The wavefunction used was significantly more complex than that of Natori and Kamimura and was much better suited to the low field regime, giving a zero magnetic field binding energy of 0.0518 R*, which should be compared with the exact value of 0.0555 R*. Consequently Larsen's binding energy is clearly better than Natori and Kamimura's up to γ~5. However one possible source of inaccuracy in Larsen's calculation was his use of an 'extrapolation' technique to go from a limited number of terms in his wavefunction to many terms in order to obtain a figure for the binding energy. In addition he appears to have performed the somewhat dubious process of adding 0.0037 R* to all his results, this being the difference between the 0.0518 R* zero field binding energy in his calculation and the widely accepted value of 0.0555 R*. Thus while a proper variational procedure gives a true lower bound to the binding energy the extrapolated values might not be true lower bounds. These problems are most significant for γ>1 where Larsen's energies for 1, 2 and 3 parameter wavefunctions diverge rapidly. However for 0<γ<1 the binding energy should be reasonably accurate. Within this region the binding energy increases very rapidly

with field, then more slowly, passing through 0.26 R* at γ=0.5. This is more than four times the zero field binding energy and is greater than the binding energy of a neutral donor 2p level at zero magnetic field.

Larsen's calculation can be used to give an indication of which part of the spectrum to examine for transitions involving D^- states. In GaAs at zero magnetic field the photo-ionizing $D^- \rightarrow$ conduction band transition occurs at 0.0555 R* equivalent to 77 GHz (λ=3.9 mm). At 3.3 Tesla (γ = 0.5) the energy of the $D^- \rightarrow N=0$ Landau level transition is at 0.262 R* or 362 GHz ($\lambda \sim 830\mu m$), which is well within the range accessible to FIR laser systems.

Earlier searches for D^- states in GaAs concentrated on the low magnetic field regime $\gamma<0.1$ using Impatt diode sources operating at 80 → 100 GHz (Davidson et al 1980 and Makado 1982), and observed a peak below the cyclotron resonance which can now be identified as the $D^- \rightarrow N=0$ transition but at that time could equally well have been identified as one of the many $n=3 \rightarrow 4$ inter-excited state transitions which should occur in the same region. This is discussed in more detail later in the section on the studies with Impatt diode sources.

Factors Affecting D^- State Populations.

It was noted earlier that the D^- state is metastable and will not spontaneously decay into a neutral donor and free electron, thus allowing substantial populations of D^- states to accumulate. The principal experimental conditions which affect the rate of D^- state formation are summarized below and then discussed in more detail.

1. The relation of temperature to the binding energy of D^- states in a magnetic field.
2. The compensation ratio.

3. The intensity of background extrinsic excitation where $\hbar\omega > E_o$ (the neutral donor binding energy) and of excitation at above the D^- binding energy.

4. The intensity of intrinsic excitation $\hbar\omega > E_g$.

5. The applied electric bias field.

1. Thermal Conditions Necessary for D^- State Formation.

Consider the situation of shallow neutral donors in GaAs. Although the binding energy at zero magnetic field is approximately 46 cm^{-1} corresponding to a temperature of 67K, significant depopulation of the neutral donors by thermal ionization occurs at temperatures above ~10K (see eg Stillman, Wolfe and Korn 1973 and Miyao and Narita 1977). By comparison the D^- states with a binding energy of 0.0555 R* (equivalent to 3.7K) would be expected to begin to depopulate at temperatures above approximately 0.5K. Thus at the temperature normally used for photo- conductive studies in GaAs, ie 4.2K, any D^- states formed will rapidly dissociate through thermal ionization. However, as noted earlier, the D^- state binding energy increases significantly in a magnetic field, so that at γ=0.5, equivalent to 3.3 Tesla in GaAs, the binding energy is 0.26 R*, which is four times the zero magnetic field binding energy. Since the probability of thermal ionization of the D^- state is proportional to exp(-E/kT), the effect of going from γ=0 to 0.5 is to reduce the thermal depopulation rate by a factor of 25 at 4.2K. Although reducing the thermal depopulation rate by a large factor will not necessarily result in the D^- state population rising by the same factor it is clear that there will be a much greater possibility of building up a substantial population of D^- states in high magnetic fields.

In silicon and germanium the larger value of the effective

Rydberg moves the temperature limit upwards, making it possible to build up a substantial population of D^- states at 4.2K even at zero magnetic field. An additional factor which is at least as important in silicon and germanium is that both have indirect energy gaps and consequently one of the principal recombination mechanisms for photoexcited electrons and holes, D-A recombination, is slow compared to GaAs. Thus the carrier lifetime of photoexcited electrons is much longer and the probability that an electron will collide with a neutral donor and be captured forming a D^- state is much greater.

2.The Role of Compensation in D^- State Formation.

It has been noted by previous workers that significant populations of D^- states are found only in samples with low compensation (eg Schiff 1982). In addition the ε_2 activation energy which is attributed to the existence of a band of D^- states is only observed in samples with low compensation. In silicon and germanium this is not a great problem as a high degree of control can be achieved over the compensation ratio during crystal growth. This is not the case with GaAs and InP where compensation ratios have not been controllable and are usually greater than ~0.4.

The significance of the compensation ratio in the formation of D^- states can be seen from the following simple argument. If n-type material is considered, any compensating acceptors present will be negatively charged resulting in an equal number of ionized donors. If the compensation ratio is high then the population of D^+ states will be much greater than the population of D^0 states, so that when electrons are excited into the conduction band, either by ionization of neutral donors or by photoexcitation across the band gap, there will only be a small probability of a D^0 state capturing an electron

and forming a D^- state. In addition an electron is far more likely to be trappped at a D^+ site as a result of the attractive Coulomb force than at a D^0 site. In contrast, if the compensation ratio is low then D^0 states will outnumber D^+ states, and electron capture at the D^0 state is much more likely and greater populations of D^- states can form. A further point is that in compensated material, if the donor concentration is sufficiently high the D^- state wavefunction may overlap with an adjacent D^0 state wavefunction and the extra electron may hop towards a D^+ site. Eventually the D^+ and D^- states will lie on adjacent lattice donor sites and direct neutralization can occur.

3. Background Extrinsic Excitation.

The requirement for background excitation where $\hbar\omega > E_o$ (where E_o is the neutral donor binding energy) can be seen when one considers that a population of conduction electrons must exist in order that neutral donors can trap additional electrons to form D^- states. However in GaAs background excitation alone will be insufficient to form significant populations of D^- states (intrinsic excitation and electric field bias being required), since the conduction electron population that can be achieved is rather small, due to the very fast D-A recombination path. This can be seen from the effect of intrinsic excitation on neutral donor linewidths - only in the purest samples where D-A recombination rates are slower does bandgap excitation reduce the D^+ and A^- ionized impurity concentrations and lead to a reduction in linewidths. A disadvantage of background excitation is that it will cause photo-ionization of D^- states, and at very low temperatures where $kT \ll E_{D^-}$ and thermal depopulation is not as significant the background excitation may limit

the D^- population.

Background extrinsic excitation is almost always present in the experiments as any parts of the light pipe system (used for directing the laser radiation to the sample) which are at room temperature will be emitting black body radiation at the appropriate energy. Elimination of this room temperature radiation would involve the use of cooled filters close to the sample. However it would then be difficult to observe photoionization of D^- states spectroscopically as the cooled filters would absorb the laser radiation.

4. Intrinsic excitation.

Intrinsic excitation where $\hbar\omega > E_g$ has two effects. Firstly it increases the free electron concentration and hence the rate of formation of D^- states. Secondly it effectively reduces the compensation ratio as many of the D^+ and A^- states formed as a result of compensation are neutralized by the extra electrons and holes in the conduction and valence bands respectively, as part of the recombination process. Both effects will result in an increase in the population of D^- states.

5. Applied Electric Field Bias.

At first sight one would expect D^- states to be more susceptible to electric fields compared to neutral donors, since as a result of their low binding energy they could be impact ionized more easily. However it will become clear in the experimental section that this is definitely not the case, and that as the electric bias field is increased the amplitude of the $D^- \rightarrow$conduction band transition increases relative to the amplitudes of the inter-excited state transitions. Furthermore at low values of electric bias the D^- state

transition is not visible in the spectra. The explanation for this behaviour is discussed later in the section on the experimental results.

Experimental Work.

Equipment.

The arrangement of the equipment used for the work on D^- states was identical to that used for the photoconductivity measurements on the central cell structure and inter-excited state transitions in GaAs and was discussed in detail in Chapter 3.

Experiments were also performed at and with the support of the Max Planck Institut für Festkörperforschung Hochfeld-Magnetlabor in Grenoble where magnetic fields up to 23 Tesla could be generated in a Polyhelix electromagnet. The experiments were carried out with the help of Dr. J.C.Maan. An optically pumped laser system similar to that at St. Andrews was permanently mounted above the magnet and was operated at wavelengths of 393, 417, 433 and 469 μm for the D^- work.

Samples.

All the experimental work discussed in this chapter was performed using the two very high purity VPE n-GaAs samples RR98B and S1. The electrical properties of these samples were given in Chapter 4 and their central cell spectra were also discussed.

Results.

When RR98B first became available and studies of the inter-excited state transitions were started the initial spectra taken at a temperature of 4.2K in the 6.7 Tesla magnet with a laser line at λ=869μm showed an anomalous broad peak in the photoconductivity amongst the inter-excited state transitions at a magnetic field of ~4 Tesla, which was close to the ~4.5 Tesla field limit of the

magnet at the time. A spectrum taken at λ=742μm was noisy, distorted by laser drift and confused by the presence of a second laser line at λ=669μm and did not conclusively show any anomalous peak similar to that at λ=869μm. However the significance of the broad peak in the λ=869μm spectra was not appreciated at the time. When sample S1 became available spectra were taken with the 12.7T magnet using laser wavelengths of λ=118.8 and 70.5μm in order to study the central cell structure of the $1s\text{-}2p_{+1}$ transition. In the course of taking λ=70.5μm spectra an unusual spectrum shown in Figure 7.3 was obtained. The spectrum is unusual on two counts:

i. as noted in the discussion in Chapter 3 on optically pumped lasers, more than one laser wavelength may be produced from one pump line, and in this case two lines with widely differing wavelengths are lasing: 70.5 and 699μm. The recording thus shows a combination of inter-excited state transitions seen with the low energy 699μm line and high energy $1s\text{-}2p_{+1}$, $3p_{+1}$, $3d_{+2}$ peaks seen with the 70.5μm line.

ii. an anomalous transition (which is attributed to the $D^- \rightarrow N=0$ Landau level transition, though this is not justified until later) can be seen amongst the inter-excited state transitions at high field, and resembles an absorption edge with a cut-off on the high magnetic field (low energy) side.

Further spectra taken of samples RR98B and S1 showed the feature more clearly. As RR98B was known to be unusual in that it had particularly low compensation, manifested by the appearance of a second peak in the mobility versus temperature graph at ~10K (Figure 4.4) due to the reduction in ionized impurity scattering which occurs as electrons freeze out onto the donor sites, it was suspected that D^- states might be present and so a more systematic study of the transition was made.

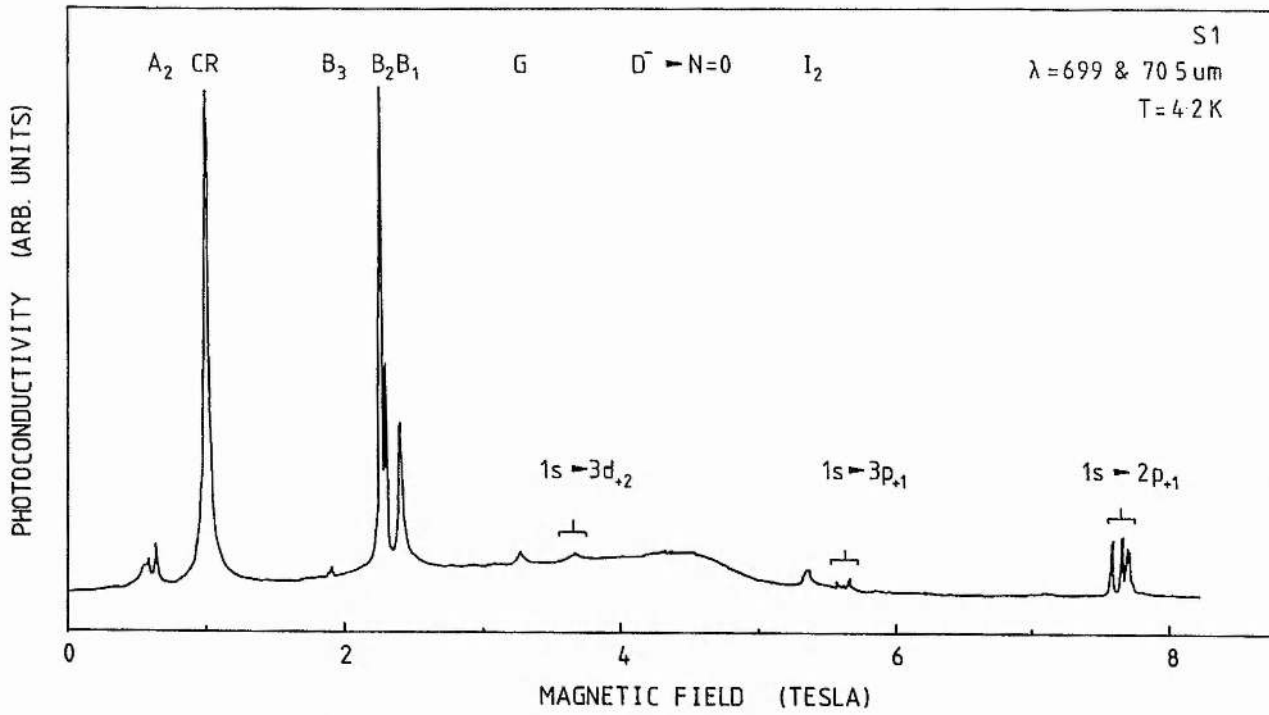

Figure 7.3: Spectrum of S1 at T=4.2K with optical excitation. The FIR laser is lasing at two well separated wavelengths, 70.5μm and 699μm, resulting in transitions from the 1s ground state and between excited states respectively. Amongst the inter-excited state transitions there is an anomalous broad peak/absorption edge which is attributed to photoionization of D^- states.

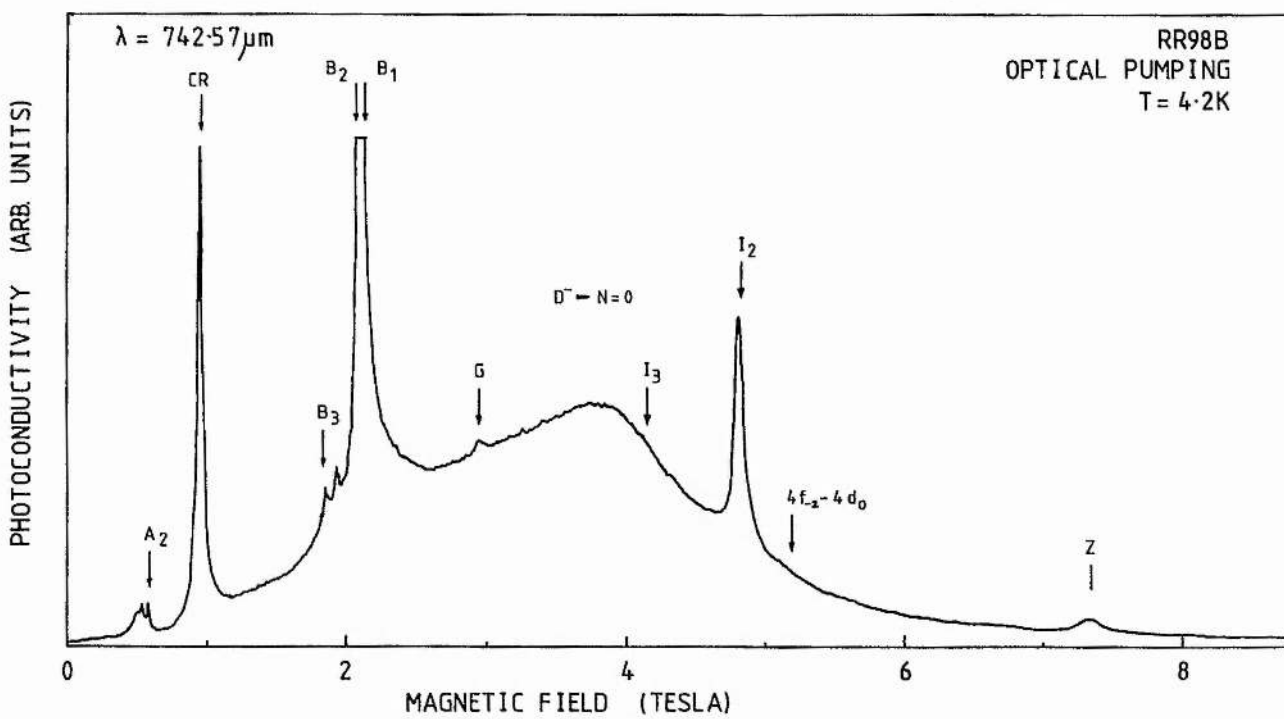

Figure 7.4: Spectrum showing the inter-excited state transitions of RR98B at T=4.2K using λ=742.57μm radiation and optical excitation. The theoretical magnetic fields of the major inter-excited state transitions are shown. Transition 'Z' has not been identified. The anomalous broad peak at 4 Tesla is attributed to the photoionization of D^- states (the $D^- \rightarrow N=0$ Landau level transition).

Figure 7.4 shows the photoconductivity spectrum of RR98B at λ=742μm, at T=4.2K and with intrinsic illumination. The theoretical positions of known inter-excited state transitions of neutral donors have been indicated on the figure using the results of the theoretical work by Makado (1982). The peak labelled 'Z' is believed to be an inter-excited state transition but has not been identified. The anomalous feature is again labelled $D^- \rightarrow N=0$, and clearly does not coincide with any of the more common inter-excited state transitions. It is significantly broader (measured in magnetic field units) than any of the inter-excited state transitions by almost an order of magnitude and is noticeably asymmetric, with a sharp cut off on the high magnetic field side and a long tail to low magnetic fields.

Although the inter-excited state transition I_3 is indicated on the figure close to the anomalous peak it is not responsible for the anomalous peak, and under different conditions I_3 appears clearly as a separate peak. This can be seen in Figure 7.5 which shows how the spectrum of S1 at λ=742μm varies with the intensity of intrinsic illumination. Without any intrinsic illumination no anomalous peak is present, but I_3, I_2 and $4f_{-2}$-$4d_0$ are clearly visible between 4 and 5.5 T. At moderate levels of intrinsic illumination a well defined edge in the photoconductivity can be seen at ~4T, already masking I_3 completely. At higher levels of illumination the edge develops into a peak just below 4T, while a substantial contribution to the photoconductivity is present at fields down to the B_1 and B_2 inter-excited state transitions at 3T (which are coincident at this wavelength).

In order to establish how the transition energy varies with magnetic field, spectra were taken of RR98B and S1 at a variety of

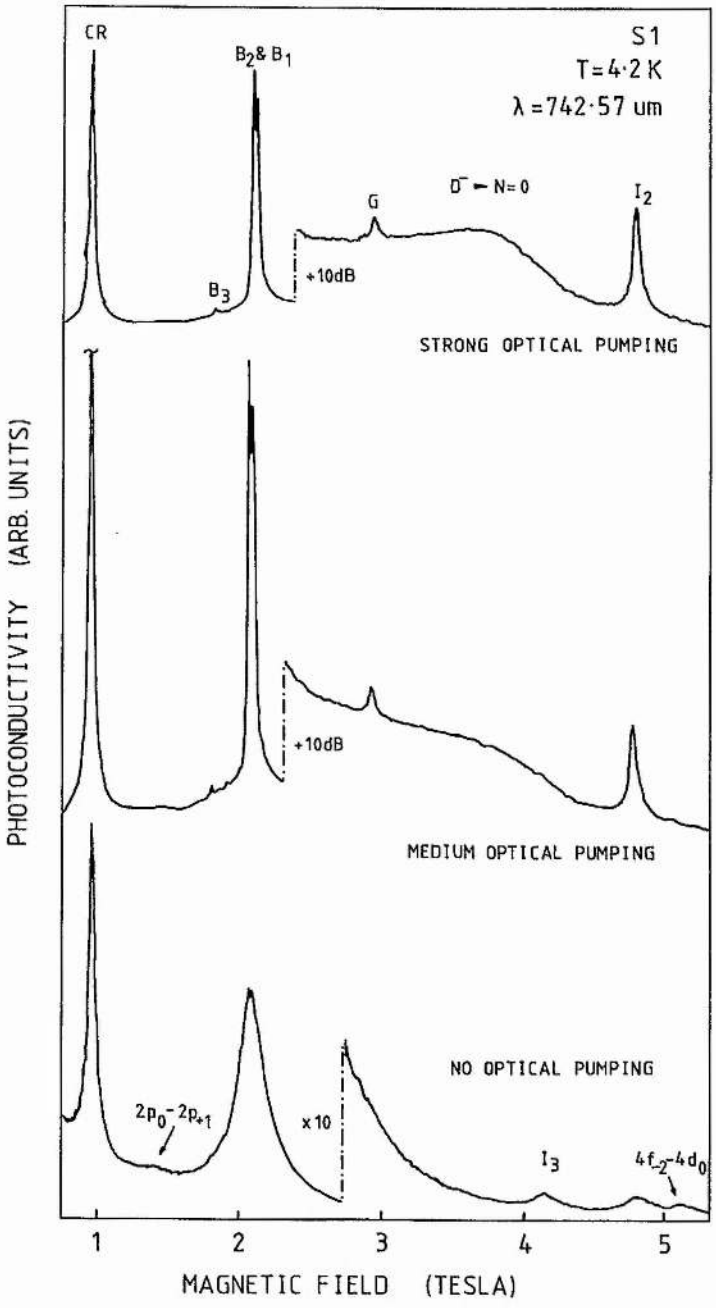

Figure 7.5: Spectra showing the increase in the intensity of the $D^- \rightarrow N=0$ transition as the level of optical excitation is increased in S1 at T=4.2K with λ=742μm radiation. At this wavelength B_1 and B_2 appear at almost coincident magnetic fields.

wavelengths between ~400μm and 1.2mm, all at a temperature of 4.2K and under a variety of conditions of intrinsic illumination. These spectra are shown in Figure 7.6, although some of the spectra have been omitted to improve the clarity of the figure. Note that the laser power generated may vary strongly from one wavelength to another and so the photoconductivity scale is quite arbitrary. A number of points are immediately apparent from Figure 7.6:

i. The anomalous transition (labelled $D^- \rightarrow N=0$) is far stronger in RR98B than it is in S1, whereas the inter-excited state transitions in both samples are of similar magnitudes (minor variations occur due to differences in the electric field bias, intrinsic illumination, laser power etc.

ii. The anomalous transition is clearly much broader than the inter-excited state transitions under all the conditions shown.

iii. Under certain conditions the anomalous transition can attain a substantial amplitude relative to the inter-excited state transitions, eg in RR98B at 571μm it is of the same order as B_1 and B_2 and the cyclotron resonance, and its integrated intensity is many times that of these features, whereas in S1 at the same wavelength it is barely visible above the noise. However care must be taken when comparing the integrated intensity of transitions when working at fixed wavelengths, particularly if the transition is spread over a wide range of magnetic field, as the transition energy may not vary linearly with field. A further complication is introduced when working with photoconductivity since if the electric bias field varies with magnetic field the amplitude of the photoconductive signal can vary.

iv. The magnetic field of the peak of the anomalous transition is increasing as the laser energy increases at a slightly faster

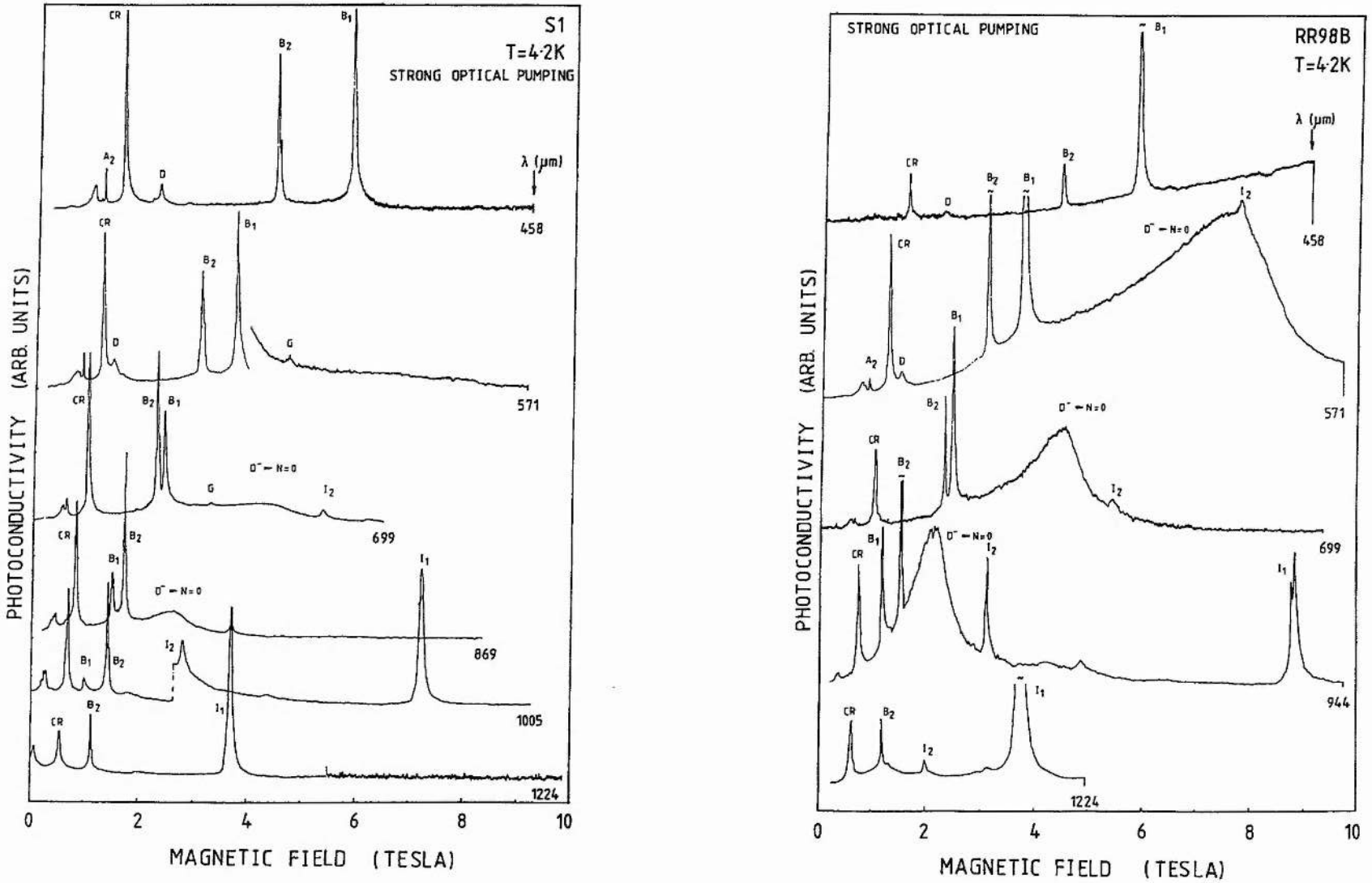

Figure 7.6: Spectra showing the $D^- \rightarrow N=0$ transition using various FIR laser wavelengths in RR98B

rate than I_2, but at a similar order of magnitude.

From iv. it is clear that the width in energy terms of the anomalous peak is significantly greater than that of the inter-excited state transitions in general, and I_2 in particular, and its apparently large width in the spectra when compared to the width of I_2 is not simply a manifestation of the difference in $\partial E/\partial B$ between the two transitions. This observation, taken together with the facts that the anomalous peak

i. has an amplitude which varies strongly in relation to the inter-excited state features with optical excitation,

ii. has an amplitude which depends on which sample is used and is stronger in the uncompensated (but less pure) sample RR98B,

iii. cannot be fitted to an inter-excited state transition using any of the likely n=2, 3 and 4 initial and final states, and

iv. has been conspicuously absent in previous studies which have looked at this field region with sub-millimetre sources (eg Skolnick et al 1977)

suggests that the peak cannot be due to an inter-excited state transition. Any inter-excited state transition of this strength would surely have been seen in previous studies, would have similar width and variation with optical excitation as other inter-excited state transitions and would probably be fitted by one of the n=2, 3, 4 transitions, though transitions involving n=5 states obviously cannot be ruled out as a possible explanation. Furthermore, compensation should have little effect on the strength of the inter-excited state transitions and if a new transition was to be found the higher purity sample S1 ought to be the one most likely to show it.

Alternative Explanations for the Anomalous Transition.

Having ruled out the possibility that an inter-excited state transition is responsible for the anomalous transition only two other plausible explanations exist for it:

i. an excited state transition in a complex

ii. a transition involving D^- states.

Transitions between excited states of a complex are difficult to rule out with any certainty. If a complex was responsible for the anomalous transition then its amplitude ought to show a dependence on the impurity doping level, with an increase in amplitude as the doping increases since more complexes at likely to form. However there is insufficient data to determine whether such a trend exists. No calculations of the transition energies between excited states of complexes exist to make comparisons with. Qualitatively they have effects which may vary from minor perturbations to the central cell structure as discussed in chapters 4 and 5 to the appearance of new lines in the zero field spectrum due to neutral and ionized donor pairs (D_2^0 and D_2^+) eg Bajaj et al (1975) and Golka et al (1977). However as RR98B and S1 do not show any significant departures from effective mass like behaviour at shorter wavelengths and no perturbations to the central cell structure have been observed it is unlikely that a complex can be responsible for an additional strong line within the inter-excited state transitions similar to that seen in the experiments.

The remaining explanation for the anomalous transition seen in the experimental recordings is that it is due to photo-ionization of D^- states where a D^- state absorbs a photon, ionizing the D^- state and exciting the extra electron into the lowest Landau level (N=0) leaving the neutral donor in its ground state. This transition

is henceforth referred to as the D^-→N=0 transition.

Justification for this argument exists in that all the features which D^- states should exhibit theoretically (as discussed in the introductory sections to this chapter) are seen in the experimental recordings, ie

i. the peak is much stronger in the low compensation sample RR98B.

ii. it increases substantially on illumination with band gap radiation.

iii. it has a very different appearance and behaviour with optical pumping, dc electric field bias, temperature etc compared to the inter-excited state transitions.

In addition to these three points, perhaps the most compelling evidence in favour of the D^-→N=0 assignment is the comparison between the experimental observations and the binding energy of D^- states calculated by Larsen (1973). Figure 7.7 shows the experimental relationship between the D^-→N=0 transition energy and the magnetic fields of the peak and the high field edge (defined as being at half the height of the peak on the high magnetic field side) of the transition, and compares it with the theoretical energies for the D^- binding energy calculated by Larsen. This diagram includes data obtained at very high magnetic fields above 12 Tesla in a series of experiments at the Max-Planck Institut in Grenoble. These experiments are discussed in more detail later in the chapter. It is clear that the agreement over the range of magnetic fields available is very good. At the highest magnetic fields at which the peak and edge could be observed in St. Andrews, ie just above 10T, there is an indication that experiment and theory are beginning to diverge, with the experimental energies being higher than theory. This is confirmed by the Grenoble experiments with λ= 469, 432, 417, 393 μm. The

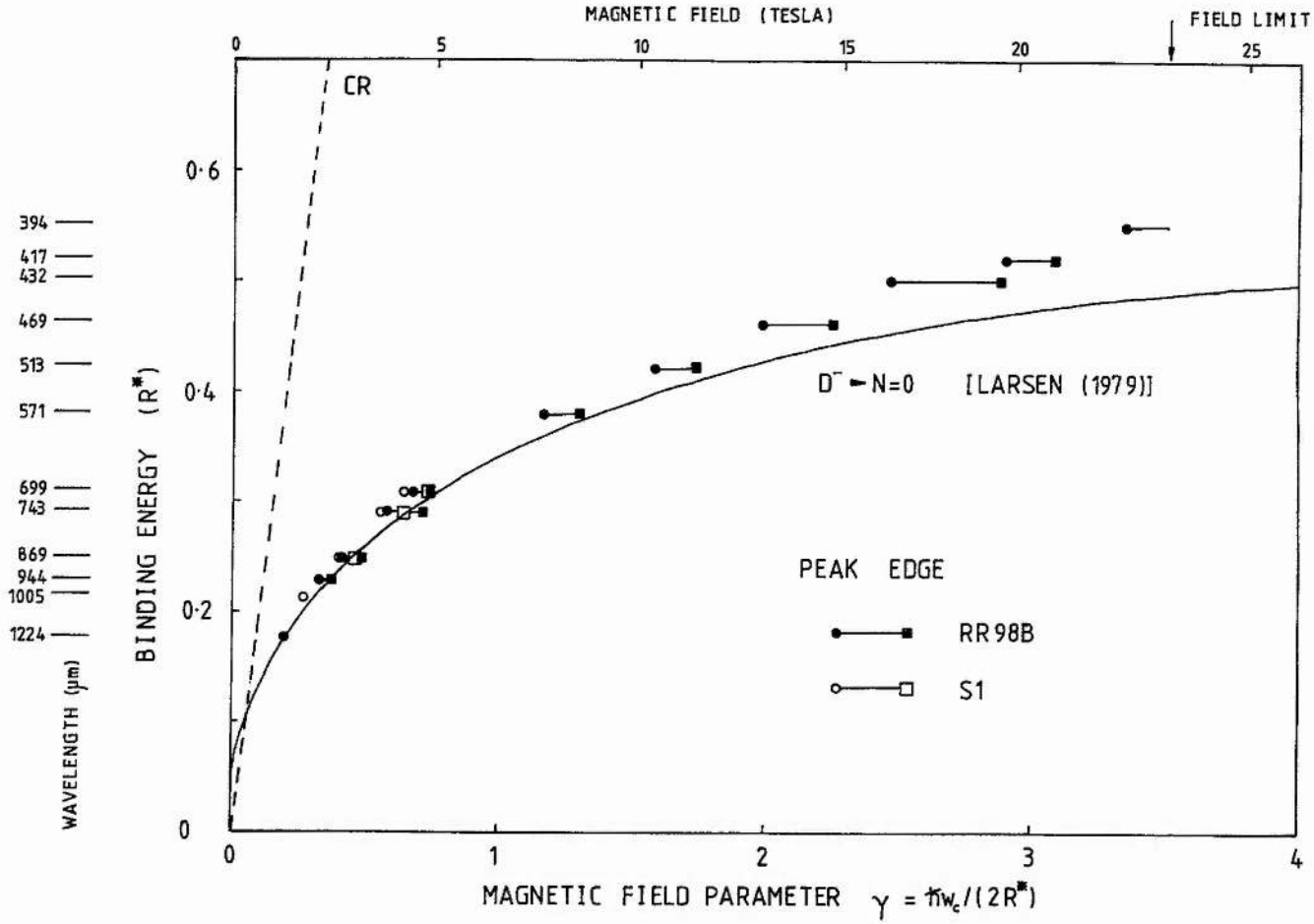

Figure 7.7: Graph showing the magnetic field dependance of the $D^- \rightarrow N=0$ transition energy up to very high magnetic fields. Both the magnetic field of the peak in the photoconductivity and the magnetic field at the point on the high field edge where the signal has fallen to half the peak intensity are shown. The solid curve shows the results of the variational calculation of the D^- binding energy by Larsen (1979). The laser wavelengths used in the experiments are also shown.

divergence is more pronounced if the peak of the photoconductive transition is taken as opposed to the high field edge.

Although this point concerning the significance of the peak and edge positions of the $D^-\rightarrow N=0$ transition leads directly into a discussion of the broadening mechanisms, this discussion is deferred while further experimental results providing additional justification for the $D^-\rightarrow N=0$ assignment and relating to the broadening issue are introduced.

Transitions to Excited Landau Levels where N>0.

Studies of the D^- state in silicon and germanium at low magnetic fields, where $\gamma\sim0.1$, by Taniguchi et al (1979) showed that the D^- to conduction band transition splits into transitions to the N= 1, 2, 3 ... Landau levels in addition to the basic $D^-\rightarrow N=0$ transition with each peak in a spectrum at constant magnetic field being separated from its neighbour by the cyclotron energy $\hbar\omega_c$. If the $D^-\rightarrow N=0$ transition has been correctly identified then duplicated structure should be seen at magnetic fields below the cyclotron resonance. This is indeed the case, and a typical spectrum of the magnetic field region up to the cyclotron resonance is shown in Figure 7.8 (sample S1 at λ=458μm). At T=4.2K the spectrum shows a strong cyclotron resonance and two of the inter-excited state transitions usually seen in this region, A_1 ($2s-3p_{+1}$) and A_2 ($2p_0-3d_{+1}$). At magnetic fields below A_1 and A_2 three peaks have been resolved, all much broader than the inter-excited state transitions and the cyclotron resonance. When the temperature is reduced to 1.8K (Figure 7.8ii)

i. more features are resolved extending to lower magnetic fields in an approximate B^{-1} series.

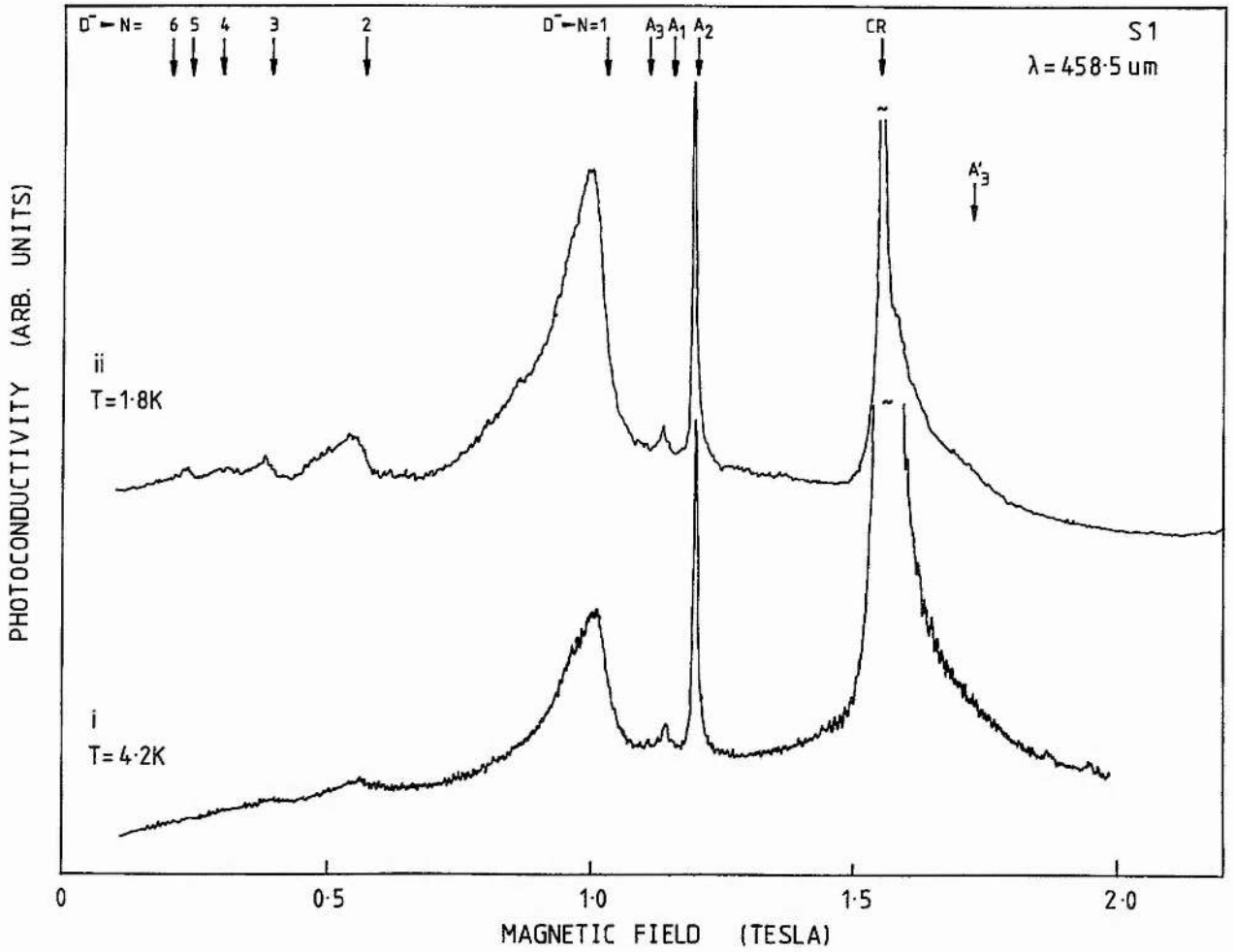

Figure 7.8: Spectra of sample S1 at T=4.2 and 1.8K using λ=458.5μm radiation and optical excitation showing transitions where an electron is excited from the D^- state to an excited Landau level. The theoretical positions of the $D^- \rightarrow$ N=1, 2, 3... transitions are shown together with the A series inter-excited state transitions and the cyclotron resonance.

ii. the features at ~0.5 and 1.0T have become significantly stronger. At 4.2K the peak at ~1.0T is approximately half the amplitude of the A_2 transition whereas at 1.8K the peak is almost equal to A_2 which in turn is larger with respect to the cyclotron resonance.

These features can be identified as transitions from the D^- ground state to excited Landau levels with N>0 and their positions are in very good agreement with the theoretically predicted positions of the D^-→N=1, 2, ... transitions. The theoretical positions shown on Figure 7.8 were obtained by adding multiples of $\hbar\omega_c$ to the results of Larsen's calculation (1979) for the D^-→N=0 binding energy and then interpolating between the data points for the specific laser wavelength.

Further experiments at different wavelengths established the magnetic field dependence of these peaks. Figure 7.9 shows some of the spectra obtained of RR98B at 1.8K. Note how strong the series of lines has become in this low compensation sample. The lines now have an amplitude many times that of A_2 and are of the same order of magnitude as the cyclotron resonance, so clearly a substantial population of D^- states is able to form relative to the population of neutral donors in excited states. At λ=393 and 432μm five peaks can be counted and the original recordings possibly showed a sixth corresponding to excitation into the N=6 Landau level.

Figure 7.10 shows the magnetic field positions of the D^-→N=0, 1, 2.. peaks plotted against energy, together with the theoretical transition energies for excitation out of a D^- state into the upper Landau levels. These theoretical energies were obtained by adding multiples of $\hbar\omega_c$ to Larsen's variational D^- binding energies. The theoretical energies of the cyclotron resonance and the A_2

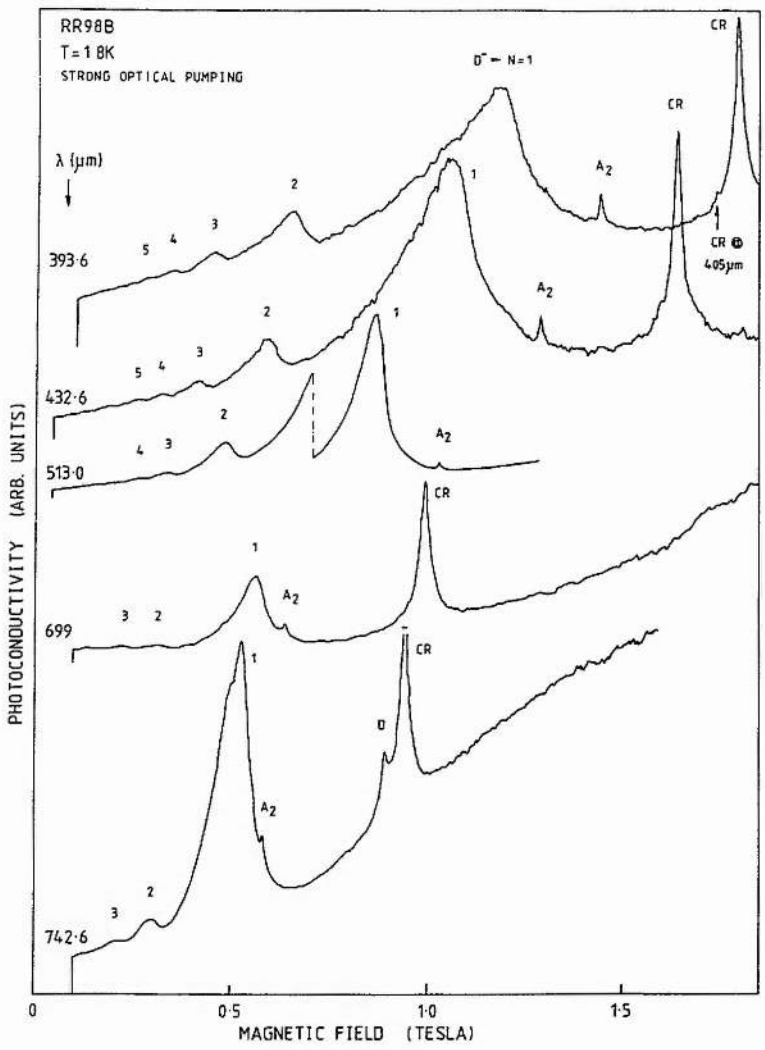

Figure 7.9: Spectra showing the $D^- \rightarrow N=1, 2, 3 \ldots$ transitions at various laser wavelengths in sample RR98B at a temperature of 1.8K and using optical excitation. The A_2 inter-excited state transition and the cyclotron resonance are also present.

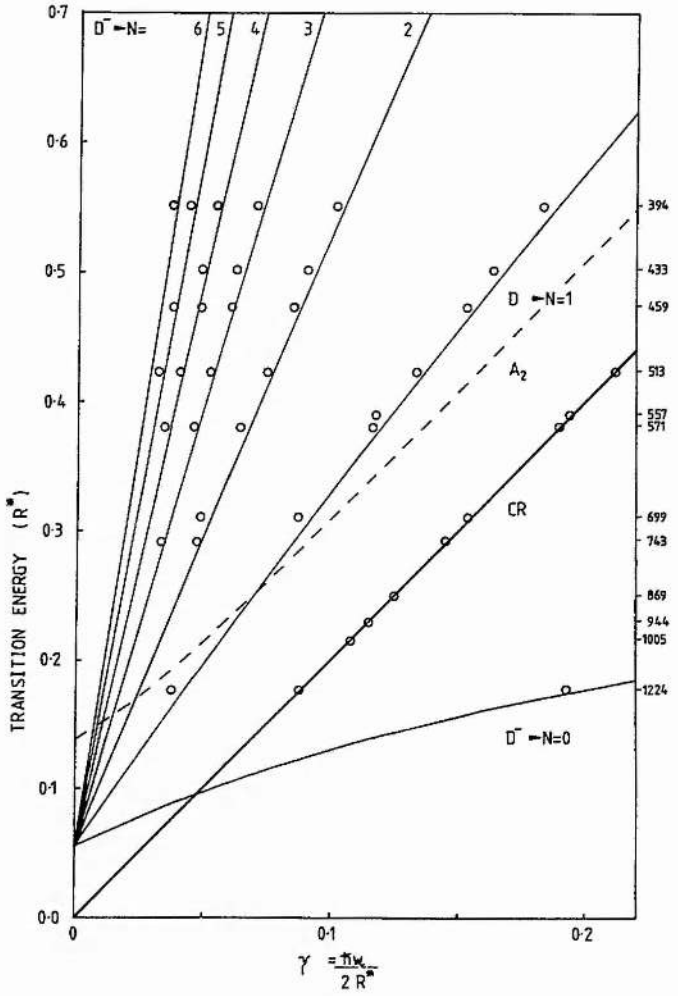

Figure 7.10: Graph showing the magnetic fields of the peaks of the $D^- \rightarrow N=1, 2, 3 \ldots$ transitions at different laser energies in dimensionless units. The solid curves show the theoretical energies obtained by adding multiples of $\hbar\omega_c$ to the theoretical $D^- \rightarrow N=0$ transition energy calculated by Larsen (1979). The laser wavelengths (in μm) for GaAs are shown on the right hand axis. The cyclotron resonance transition and the

inter-excited state transition are also shown. It is apparent that very good agreement exists between theory and experiment and confirms that a transition originating on a D^- state is responsible for the peaks.

It is interesting to note that at low magnetic fields the electrons are being excited a number of steps up the Landau ladders, to N=5 and 6 Landau levels, and it is possible that cyclotron emission could be observed as the electrons relax down the ladder. For example, if the 393.6μm wavelength is used and the magnetic field adjusted to the maximum of the D^-→N=3 Landau level transition at ~0.46 Tesla as shown in Figure 7.9 then emission at the cyclotron energy corresponding to a wavelength of ~1.5mm or a frequency of ~200 GHz might occur as the electrons relax from the N=3 through the N=2 and N=1 levels to the N=0 Landau level. Alternatively choosing a field of ~0.65T with λ=393.6μm excites the D^-→N=2 transition and emission might occur at a wavelength of ~1.1mm or ~270 GHz. Similarly using λ=742μm pump radiation at ~0.3T also excites the D^-→N=2 transition but with the possibility of emission at a wavelength of ~2.4mm or 120 GHz. Thus if emission with reasonable power levels could be achieved in this way it could provide very useful coverage of the millimetre wave region. As each D^-→N=1, 2, ... transition is relatively broad a useful degree of tuneability might be available by adjusting the magnetic field.

A further point which Figure 7.10 shows is that there appears to be a magnetic field below which no D^- peaks are seen, irrespective of how far up the Landau ladder the electrons are excited. Thus the lowest magnetic field at which a peak is seen is at 0.2T or γ=0.03 for the D^-→N=5 transition at λ=513μm. This field limit is probably set by the ratio of temperature and binding energy in a

magnetic field. Below the critical field for a given temperature thermal depopulation is too large for an observable population of D^- states to accumulate.

This has a particular bearing on studies of D^- states at low energies and low magnetic fields with Impatt or Gunn diode microwave sources. The limit of $\gamma \sim 0.03$ at a temperature of 1.8K corresponds to a $D^- \rightarrow N=0$ transition energy of ~110GHz. This is in fact the highest frequency of Impatt device available and since the $D^- \rightarrow N=5$ transition was observed at this field it suggests that the $D^- \rightarrow N=0$ transition ought to be observable using the Impatt device. Experiments with the Impatt and Gunn devices are discussed later in the chapter.

That the population of D^- states is substantial relative to the population of D^0 states can be seen from Figure 7.11. This shows a spectrum of RR98B at $\lambda=255\mu m$. The principal peaks are due to the $1s-2p_{+1}$, $1s-2s$ and $1s-2p_0$ transitions which all exhibit central cell splitting. The theoretical positions of these transitions (obtained in the usual way) are shown, together with the theoretical positions of the A_2 and A_3 inter-excited state transitions and the cyclotron resonance. In addition to these sharp features there appears to be a broad background peak in the photoconductivity centred at approximately 2 Tesla. This background is attributed to the $D^- \rightarrow N=1$ transition which ought to appear at ~2.1 Tesla at this wavelength. Although the mechanisms for changing the conductivity differ for $D^- \rightarrow$ N= 0, 1, 2... transitions (direct ionization to the Landau levels) and transitions within a neutral donor (the photothermal mechanism), and thus the relative amplitudes of the $D^- \rightarrow$ N= 0, 1, 2 ... peaks cannot be compared directly with the amplitudes of the $1s-2p_{\pm1,0}$ etc peaks, it is clear that a substantial population of D^- states must be accumulating to cause such a significant

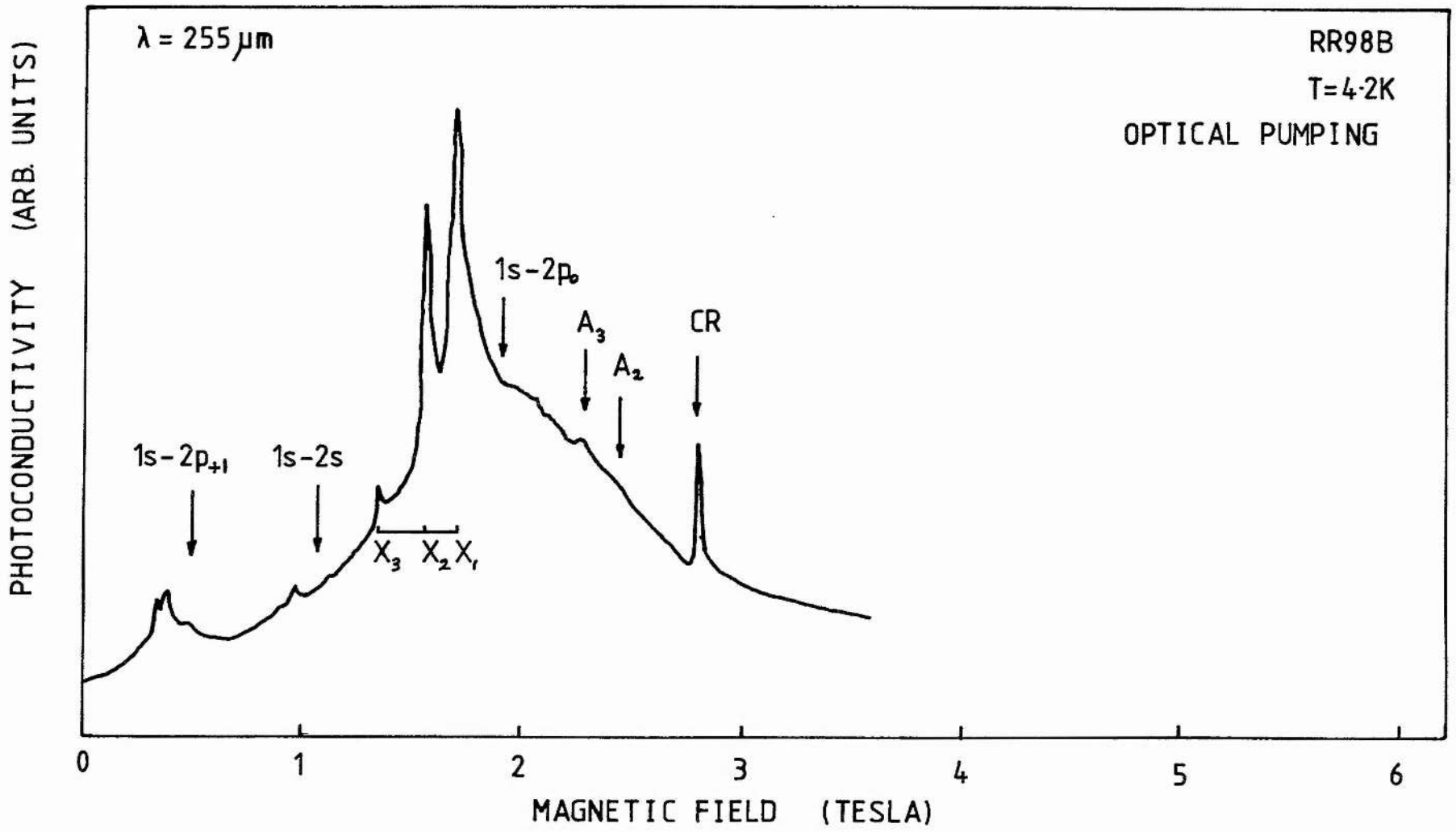

Figure 7.11: Spectrum of RR98B using λ=255μm radiation showing central cell splitting on the $1s-2p_{+1}$, 1s-2s and $1s-2p_0$ transitions. The cyclotron resonance is also present together with an inter-excited state transition. The theoretical magnetic fields for transitions are shown by arrows. The broad background signal under the $1s-2p_0$ transition is believed to be due to

D^-→N=1 peak compared to the 1s-$2p_0$ peak.

Note that there does not appear to be any structure in Figure 7.11 due to D^-→N= 2, 3 .. transitions. Theoretical studies of the lineshapes of D^- to Landau level transitions in the high field limit ($\gamma \gg 1$) show that only the D^-→N= 0 and 1 transitions should be allowed for unpolarized radiation in Faraday Geometry (Natori and Kamimura 1979). Thus the absence of D^-→N= 2, 3 transitions in the λ=255μm spectra might be due to the influence of selection rules, even though the magnetic fields where the transitions ought to occur (~1 Tesla) are well below those were 'high field approximations' are valid. As noted earlier it is rather difficult to interpret intensities when working at fixed wavelength and photoconductivity, but it does appear that the D^-→N=1 transition in Figures 7.8 and 7.9 is significantly stronger than a simple monotonic increase in strengths of the N = ... 4, 3, 2, 1 transitions would predict.

Broadening Mechanisms on D^- → Landau Level Transitions.

Returning to the graph of energy versus magnetic field for the D^-→N=1, 2, 3 ... transitions (Fig 7.10) it can be seen that although the general agreement with theory is good the observed peak positions are all at slightly lower magnetic fields than predicted by theory. As with the D^-→N=0 transition, all the transitions to the upper Landau levels show a very marked asymmetric broadening. Examining Figure 7.9 again, the following features can be noted:

i. reducing the temperature from 4.2K to 1.8K does not appear to have had any significant effect on the linewidth of either the D^-→ N=1, 2 ... transitions or the A_2 inter-excited state transition.

ii. both the A_2 and the $D^- \rightarrow N=1$ transitions can be assumed to be moving in energy at very nearly the same rate as the cyclotron resonance, ie at ~14 cm^{-1}/Tesla. The FWHH of the $D^- \rightarrow N=1$ is then ~0.10T or ~1.4 cm^{-1}. By comparison the FWHH of A_2 is <0.13 cm^{-1} which is a full order of magnitude less than the $D^- \rightarrow N=1$ width.

The broadening mechanisms for the D^- → Landau level transition can be divided into two classes:

i. broadening due to the dispersion of the D^- energy levels themselves, perhaps as a result of mechanisms similar to those responsible for neutral donor broadening, eg inhomogeneous broadening due to the effects of electric fields from compensating D^+ states (or perhaps also D^- states) which result in field gradient and quadratic Stark broadening. It is well established that in neutral donors field gradient broadening is characterized by symmetrically broadened transitions whereas quadratic Stark broadening results in a strongly asymmetric lineshape with its peak energy shifted away from the unperturbed transition energy. Qualitatively one might expect the D^- ground state, consisting of an electron loosely bound in the dipolar field of a neutral donor, to be significantly affected by the random electric fields present within a sample, which could result in the D^- state being broader than the neutral donor states.

Alternatively, interactions between neighbouring neutral donors and the D^- state may broaden the D^- energy levels, or result in the formation of D_2^- states (Norton 1976). Both Norton and Taniguchi et al (1978, 1979) have attributed

additional peaks on the high energy side of the $D^- \rightarrow N=0$ peak to complex formation. Theoretical calculations at zero magnetic field indicate that the D_2^- state has a greater binding energy than the isolated D^- state for most $D^- - D^0$ inter-donor separations (Norton 1976). The formation of complexes represents the first stage in the trend towards the formation of the Upper Hubbard Band seen in material with two orders of magnitude greater impurity concentration than the samples being studied here.

ii. The large linewidth of the $D^- \rightarrow N= 0, 1, 2 \ldots$ transitions may be due to the photoionization mechanism itself which intrinsically gives rise to an asymmetrical lineshape. Photoionization mechanisms will show a threshold energy, when excitation to the bottom of the band at $\underline{k}=0$ can occur, and a long tail to high energy (ie low magnetic fields) as transitions occur away from k=0. The intensity of the tail is governed by the matrix element between the two states and the density of states in the Landau level. In the early work of both Norton and Taniguchi et al the asymmetric broadening observed was attributed to this source and Norton's lineshape was in very good qualitative agreement with the lineshape observed in H^- photoionization experiments at zero magnetic field. As noted earlier Natori and Kamimura (1979) studied theoretically the D^- transitions in high magnetic fields. In the absence of broadening on the D^- state itself they found that the $D^- \rightarrow N=0, 1, 2, \ldots$ lineshapes reflect the Landau level density of states. As the spectra of the two samples studied all show narrow cyclotron resonance transitions it is likely that the density of states width of the Landau levels is small and the broadening seen on

the $D^- \rightarrow N= 0, 1, 2, \ldots$ transitions is mostly due to broadening of the D^- states.

Undoubtedly both types of mechanism will contribute to the observed $D^- \rightarrow$Landau level lineshapes. If the dominant broadening is due to the photoionization mechanism, or alternatively some other form of asymmetric broadening which moves the peak of the transition away from the unperturbed energy then the magnetic field to compare with theory would be an energy away from the peak. Clearly the half height peak positions shown in Figure 7.7 correspond better with theory than the peak positions. On Figure 7.8 the positions where the $D^- \rightarrow N=1,2$ transitions would be expected to lie, according to Larsen's figures, are indicated, and it can be seen that the theoretical position corresponds well with the threshold magnetic field.

However if the broadening of the D^- state is due mostly to a dispersion of the ground state energies as a result of interactions with neighbouring D^0 states the correct position to compare with theory is the magnetic field at the peak of the transition. In these circumstances there is clearly a discrepancy between the experimental energies and Larsen's calculation, particularly at magnetic fields where $\gamma>1$.

No mention has yet been made of the $D^- \rightarrow N=0$ transition at the lowest temperature available: 1.8K. Figure 7.12 shows how the spectrum of RR98B at 4.2K and $\lambda=570\mu m$ varies with optical excitation. This figure should be compared with Figure 7.13 which shows the sample under the same conditions but at 1.8K. Reducing the temperature has dramatically changed the shape of the $D^- \rightarrow N=0$ transition and at 1.8K it has double peaked structure with the high field peak remaining in approximately the same position as it was at the higher temperature but with the new peak appearing at significantly lower magnetic fields

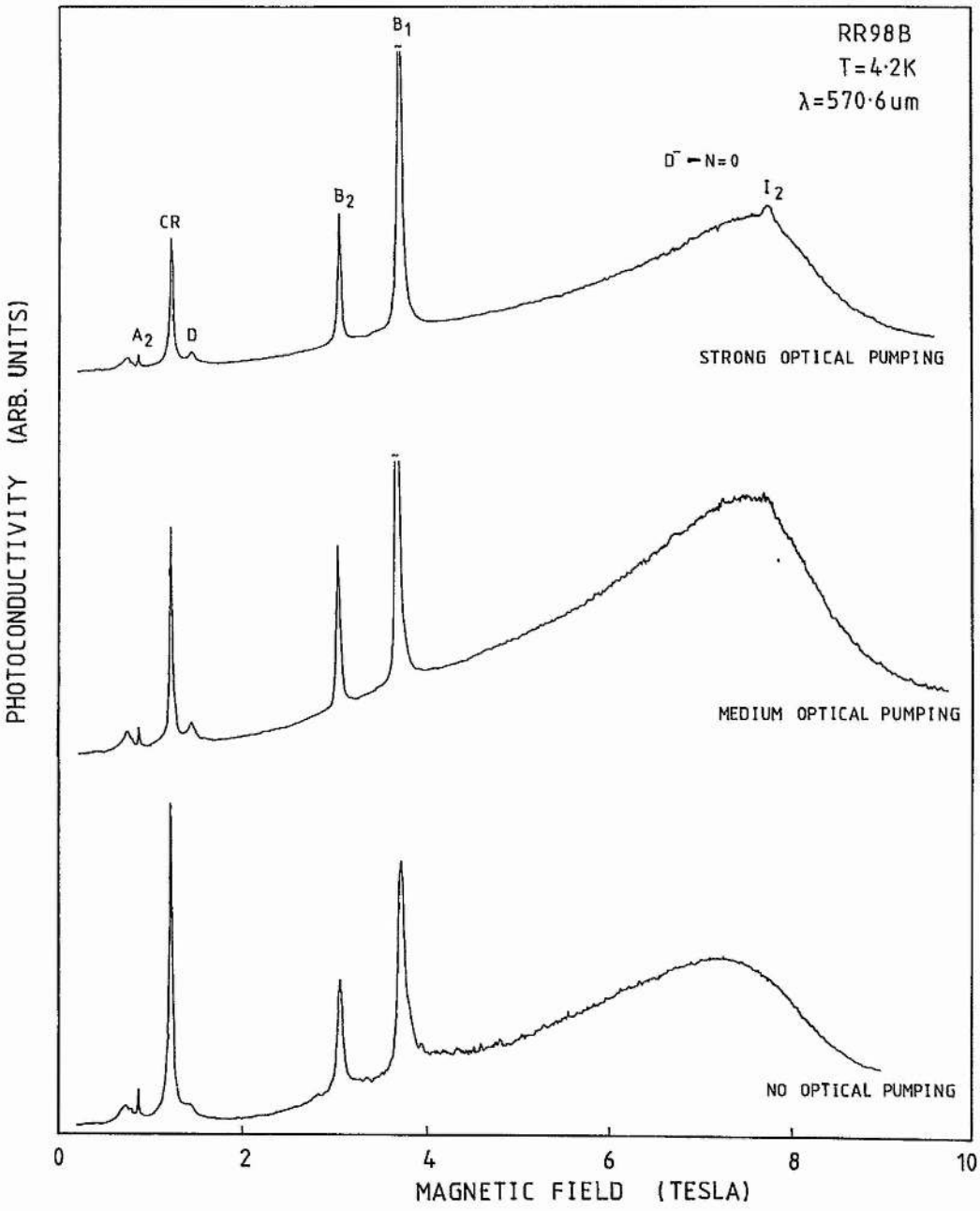

Figure 7.12: Spectra showing the $D^- \rightarrow N=0$ transition with three levels of optical excitation in RR98B at T=4.2K and using λ=570.6μm radiation.

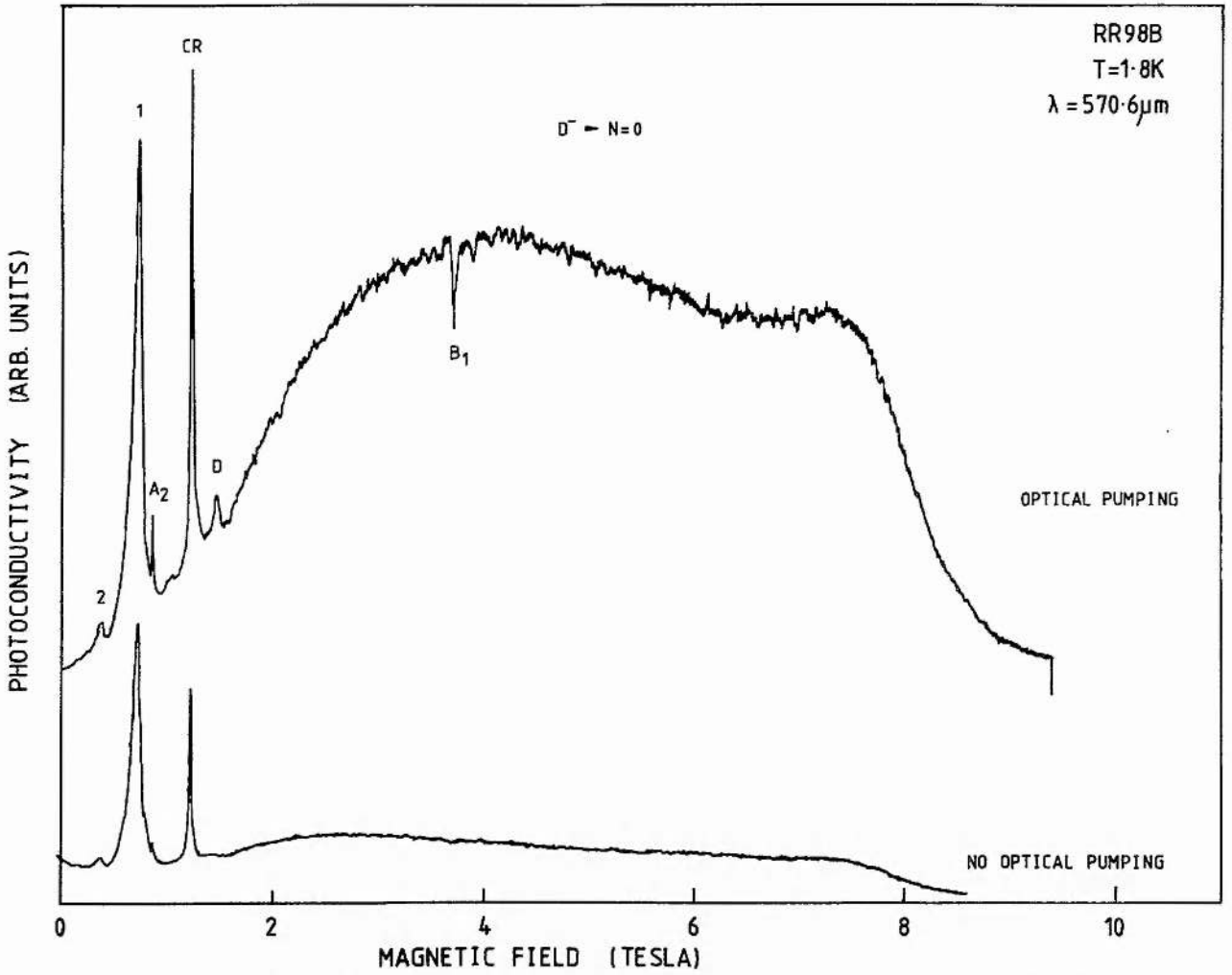

Figure 7.13: Spectra showing the $D^- \rightarrow N=0$ transition without and with optical excitation in RR98B at T=1.8K and using λ=570.6μm radiation. Compare this spectra with Figure 7.12 showing the same sample but at T=4.2K. Note how at this lower temperature the $D^- \rightarrow N=0$ transition has become very strong and broad and the B_1 inter-excited state transition appears as a negative going signal. This double peaked structure is attributed to the formation of some form of complex. Also note how strong the $D^- \rightarrow N=1$ and 2 transitions (labelled '1' and '2') have become.

(ie higher energy). The double peaked structure is apparent even without optical excitation, but no similar structure can be seen on the peaks involving transitions to higher Landau levels in the lower magnetic field regions of either spectrum. A further interesting feature apparent in Figure 7.13 is that the B_1 inter-excited state transition appears as a negative going signal in the photo-conductivity. Peak inversion such as this often occurs when there is competition between processes.

Measurements at a variety of wavelengths at 1.8K with RR98B are shown in Figure 7.14 and show that the double-peaked structure is only seen in spectra at $\lambda \sim 699\mu m$ and shorter wavelengths equivalent to magnetic fields greater than ~3 Tesla. Measurements on sample S1 at 1.8K showed similar double peaked structure, though at lower amplitude.

The double peaked structure is very similar to that observed by Norton (1976) and Taniguchi et al (1978) in experiments at zero magnetic field and attributed to the formation of D_2^- states, and the appearance of the second peak at lower magnetic fields (higher binding energies) is consistent with theoretical calculations of the binding energy of D_2^- states, which are more strongly bound than isolated D^- states over a wide range of impurity separations. However while the structure observed by Norton and Taniguchi et al is consistent with the expected behaviour of D_2^- states it is at odds with the behaviour of the structure seen in RR98B and S1. Notably, Norton and Taniguchi et al observed a double peak in Si:P at 1.8K which evolved into a single peak centred on the more deeply bound D_2^- state as the temperature was raised to 4.2K. In contrast, as the temperature is raised to 4.2K in RR98B and S1 the double peak evolves into a single peak centred on the isolated D^- state.

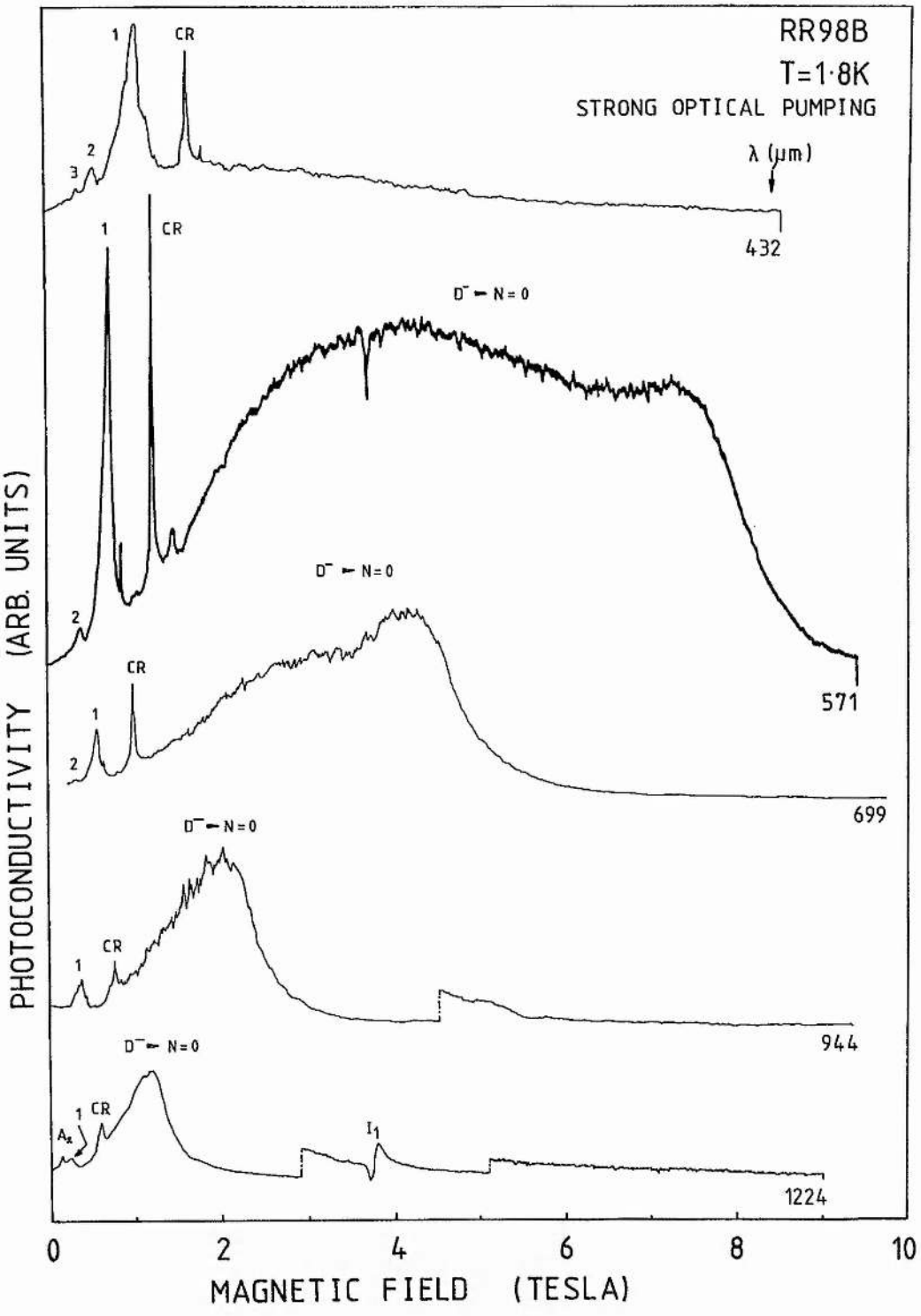

Figure 7.14: Spectra showing the $D^- \rightarrow N=0$ transition in RR98B at T=1.8K at various laser wavelengths and with optical excitation. The $D^- \rightarrow N=1$, 2 .. transitions are labelled '1', '2' etc. Note the strength of the $D^- \rightarrow N=0$ transition, and that the double-peaked shape is only present at wavelengths shorter than 800μm. No double peaked structure can be seen on the $D^- \rightarrow$ N=1, 2 .. transitions (these are shown in more detail in Figure 7.9).

If a D_2^- state is responsible for the deeper state seen in RR98B and S1 then it would be populated preferentially at 4.2K, simply from thermal considerations, as seen by Norton and Taniguchi et al. The disappearance of the peak cannot be attributed to a reduction in the D_2^- population relative to the D^- population as changes in temperature will not alter the number of sites at which D_2^- states should form.

The implication here is that the state responsible for the higher energy transition can only form at low temperatures when the D^- population is large. One can speculate that the state is due to some interaction between adjacent D^- states, eg two D^- states in close proximity forming a D_2^{2-} state. At low D^- concentrations such states would not form due to coulomb repulsion between the two extra electrons, but as the temperature is reduced and the D^- concentration rises then the probability of having two D^- states close enough together to interact increases.

Whatever the actual explanation for the low magnetic field peak seen at 1.8K turns out to be, it will almost certainly involve the interaction of D^- states with neighbouring donor states, suggesting that much of the asymmetry seen on the T=4.2K recordings of the $D^-\rightarrow N=0$, 1, 2, ... transitions may be due to the same effect. Clearly there is considerable scope for further experimental studies on this point.

Central Cell Effects on D^- States.

The central cell effect for neutral donors has been discussed extensively in the previous three chapters and the question arises as to whether the energy of a D^- state will be perturbed by central cell effects.

The simplest model of a D^- state is that of an electron bound in the dipole field of a neutral donor. The electron is very loosely bound and in a fairly large orbit and so spends very little time near the core of the neutral donor. Hence as the central cell potential is a short range potential which only perturbs the energies of states where the wavefunction penetrates the donor core (ie $\Delta E_{cc} \propto |\Psi(0)|^2$) one would expect the central cell shifts to be much smaller than those for neutral donor states.

Fairly substantial differences in D^- binding energy are seen in silicon and germanium for different impurity species, but this is attributed to the multi-valley nature of the conduction bands in these materials. When high uniaxial stress is applied to Si and Ge, removing the valley degeneracy, the chemical shifts are significantly reduced (Taniguchi and Narita 1977). However this situation applies to zero magnetic field. Natori and Kamimura's calculation shows that magnetic fields of the order of $\gamma \sim 1$ result in significant compression of the electron orbits in the plane perpendicular to the magnetic field and thus central cell shifts could become much more significant than at zero fields.

However the results reported in this thesis that have been obtained for GaAs do not appear to show any signs of splitting due to central cell effects, though unresolved central cell splittings could be contributing to the linewidths in the spectra. Even small central cell shifts could become significant since the low rate of change of the D^- binding energy with magnetic field would spread the changes out over a large range of magnetic field. More recent experimental work on D^- states in a number of n-GaAs samples does show shifts in the peak position and changes in the lineshape which can be correlated with the residual impurities which appear as central cell structure on the neutral donor $1s-2p_{\pm 1}$ transitions (Najda 1985).

Electric Field Dependence of D^- State Spectra.

Figure 7.15 shows a series of spectra obtained at various values of electric field bias for sample S1 at 4.2K with a laser line at λ=742μm. It should be noted that the experimental arrangement does not hold the bias field constant as the dc magnetoresistance changes with magnetic field. However even if the bias voltage across the sample was fixed the bias conditions within the sample would change since as the magnetic field increases the donor binding energy increases and the sample is effectively 'cooled'. The bias fields quoted in the figure captions are those measured at zero magnetic field and were calculated from the bias voltage assuming a contact separation of ~2mm.

At very low electric fields as in trace A the $D^-\rightarrow N=0$ transition cannot be identified, though it is probably contributing to the slow fall in photoconductivity above ~3 Tesla. At slightly higher levels of electric field as in trace B a noticeable edge has developed in the photoconductivity while at much higher electric fields as in trace C the $D^-\rightarrow N=0$ transition is well developed and is of almost equal amplitude to the I_2 inter-excited state transition of neutral donors. Thus it is clear that for the same level of band gap illumination the electric bias field across the sample can significantly affect the strength of the $D^-\rightarrow N=0$ transition relative to the inter-excited state transitions of neutral donors.

It is interesting to note the appearance of a new inter-excited state transition at high electric fields at a magnetic field above I_2. This was identified as $4f_{-2}$-$4d_0$ in the previous chapter. Clearly the relative strengths of inter-excited state transitions can also be significantly affected by electric field bias.

Figure 7.16 shows in more detail the bias dependence of the

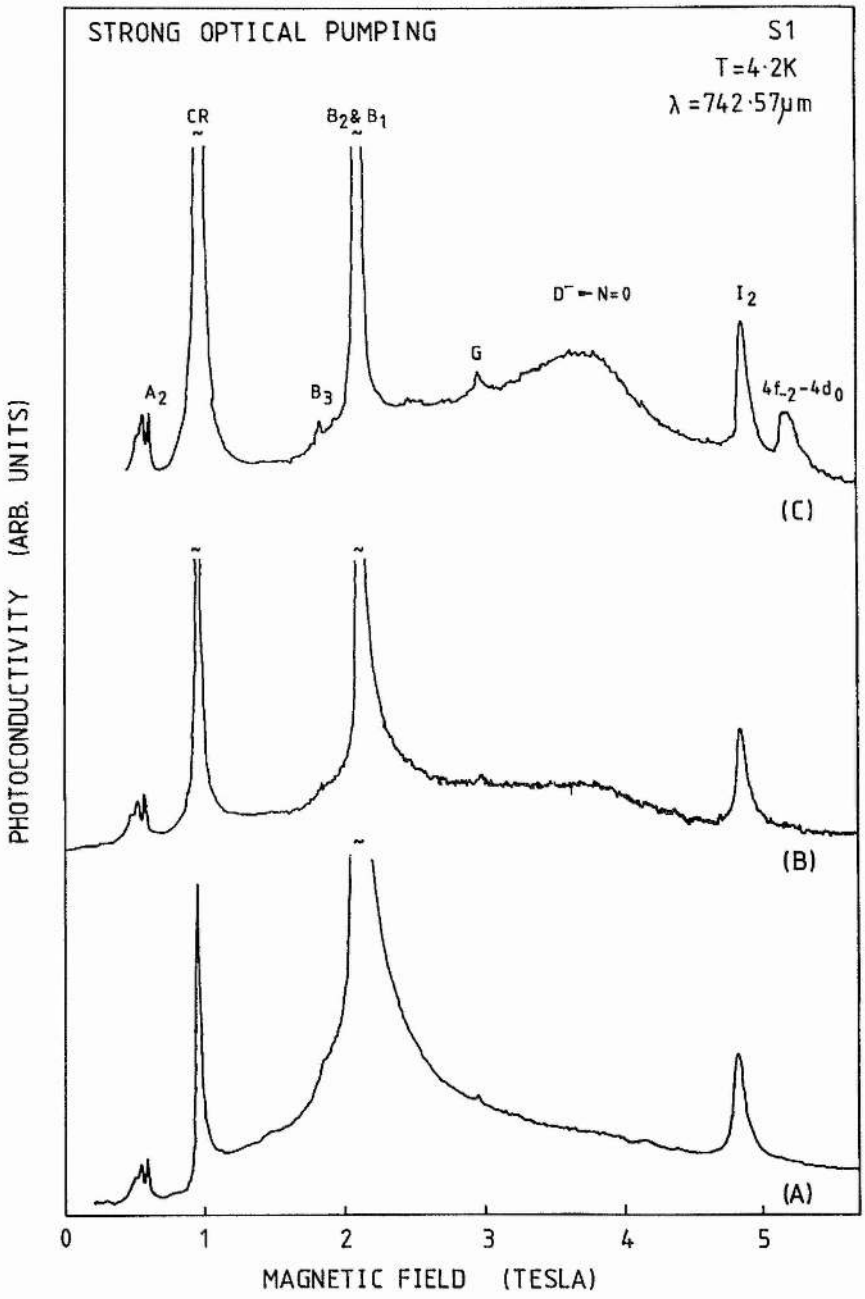

Figure 7.15: Spectra showing the electric bias field dependance of the $D^- \rightarrow N=0$ transition in sample S1 at T=4.2K using λ=742.57μm radiation and optical excitation. The electric field bias at zero magnetic field was approximately - A: <0.01 V/cm, B: ~0.03 V/cm and C: 0.35 V/cm (assuming ~2mm contact separation). However note that the bias increases with magnetic field. Note the appearance of the $4f_{-2}$-$4d_0$ inter-excited state transition at high bias fields.

$D^-\rightarrow N=0$ transition in sample S1 at two levels of amplification and at a different laser wavelength (λ=699μm). At the higher level of amplification the development of the asymmetric shape of the $D^-\rightarrow N=0$ transition can be followed from low to high electric fields. The appearance of the $4f_{-2}$-$4d_0$ transition at high electric fields seen in the λ=742μm spectra in Figure 7.15 is also confirmed. At the lower level of amplification in Figure 7.16 it can be seen that at the lowest electric field the $D^-\rightarrow N=0$ transition is small compared to the cyclotron resonance and B_1 and B_2 peaks, and increases relative to these peaks as the field increases.

At first sight the increase in the intensity of the $D^-\rightarrow N=0$ transition relative to the inter-excited state transitions is the opposite of what one might expect, which is that the weakly bound D^- state would be ionized more easily in high electric fields, whereas the neutral donors, being bound in a central coulomb field would be relatively unaffected by electric fields.

However the observed effect can be understood in terms of the influence of the electric field on the relative rates of formation of D^- and D^0 states.

Formation of the D^- state requires that a neutral donor captures a free electron, which will be relatively unaffected by electric fields in contrast to the formation of D^0 states where a D^+ state must capture a free electron which will have a significantly reduced cross section at high electron velocities. An additional effect here is that D^- states are formed by electron capture direct to the ground state, whereas the D^0 state is formed by electron capture to a loosely bound excited state followed by a cascade fall through the excited states, and impact ionization may occur again from one of the shallow excited states.

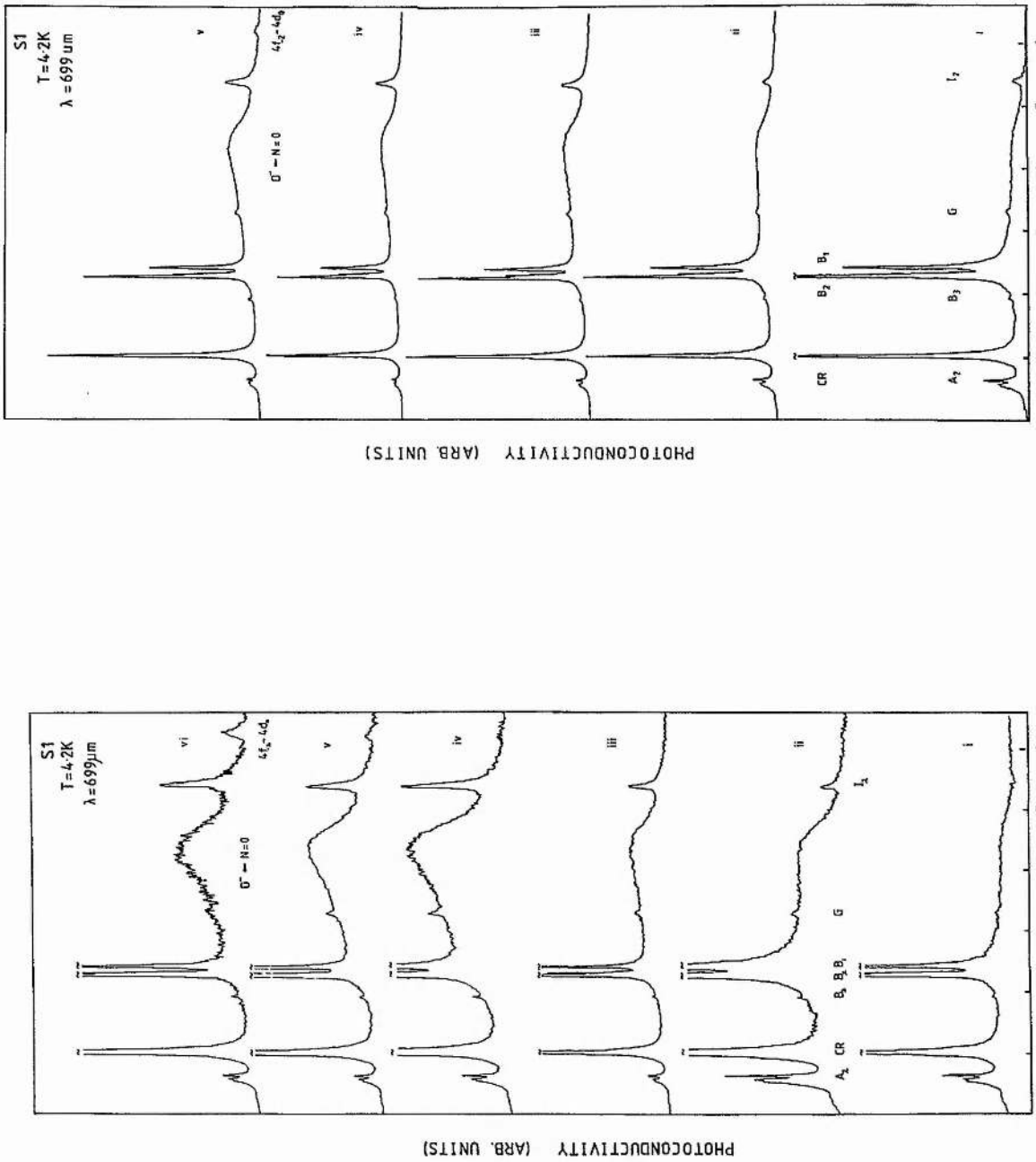

Figure 7.16: Spectra showing the electric bias field dependance of the $D^- \rightarrow N=0$ transition in sample S1 at T=4.2K using λ=699μm radiation and optical excitation. The left hand diagram shows the spectra with high gain while the right hand diagram shows the spectra with lower gain. The electric field bias at zero magnetic field was approximately - i: 0.05, ii: 0.1, iii, 0.17, iv: 0.25, v 0.37, vi: 0.5 V/cm (assuming ~2mm contact separation). However note that the bias increases with magnetic field. Again note the appearance of the $4f_{-2}$-$4d_0$ inter-excited state transition at high bias fields.

Thus the effect of electric field on the formation of D^- and D^0 states is that the D^- population will be favoured relative to the D^0 population as the electric field increases.

The part of the argument above relating to neutral donors is the same as that used by Norton (1976) to explain the temperature dependence of the free electron lifetime in Si:P. At low bias fields he observed that the electron lifetime was dramatically reduced on reducing the temperature from ~20K to ~9K, whereas at high bias fields this change in temperature produced only a small reduction in lifetime. From this Norton inferred that

i. at low electric fields as the temperature was reduced to 9K capture of electrons at D^+ states could occur by cascade capture through the upper excited states, leading to a reduction in the free electron lifetime.

whereas

ii. at high electric fields the excited states are much less efficient at capturing free electrons and so reducing the temperature to 9K has little effect on the free electron lifetime.

D^- States in Very High Magnetic Fields.

In the work discussed so far the maximum field at which a peak in the photoconductivity due to $D^-\rightarrow N=0$ transitions in GaAs could be seen was 10.4 Tesla using a wavelength of 513μm. This field was limited by the maximum field available from the superconducting magnet - 12.7 Tesla. Within this field range there appeared to be an increasing discrepancy between the peak/edge positions of the $D^-\rightarrow N=0$ transition and the theoretical binding energy calculated by Larsen (1979).

In order to extend the experimental results to higher magnetic

fields, arrangements were made to use the facilities at the Max Planck Institute für Festkörperforschung Hochfeld-Magnetlabor in Grenoble. The experimental equipment available was described in Chapter 3. As the background noise level in the electronics was high the lock-in detection system was used on a very narrow bandwidth which led to some distortion and overshoot on the sharp inter-excited state transitions (eg the sharp B_1 transition was split by this instrumental effect in spectra at λ=393 and 433μm).

Spectra of both RR98B and S1 were obtained at four wavelengths, 469, 433, 417 and 394 μm. Interpolation of Larsen's figures for the D^- binding energy indicates that the $D^-\rightarrow N=0$ transition should appear at 17, 27, 32 and 47 Tesla respectively, with the latter three being well above the maximum available field.

The actual spectra obtained using sample RR98B at 4.2K are shown in Figure 7.17, all with intrinsic illumination provided with a GaAs LED mounted close to the sample. The point most immediately apparent is that the $D^-\rightarrow N=0$ peak position is well within the field limit at all four wavelengths. The broadness and asymmetry of the $D^-\rightarrow N=0$ transition compared to the inter-excited state transitions (B_1 and B_2) is also dramatically illustrated.

The magnetic fields of the peak and edge of the $D^-\rightarrow N=0$ transition (defined in the same way as before) have been plotted in Figure 7.7, along with the data obtained at St.Andrews, and compared with Larsen's calculation. Clearly the discrepancy between the theoretical and experimental results first seen in experiments at lower fields (where $\gamma>1$) becomes more significant as the magnetic field increases, to the extent that at 22 Tesla ($\gamma\sim3.5$) the theory underestimates the $D^-\rightarrow N=0$ peak position by nearly 12%. An underestimate of the binding energy is expected from variational theories

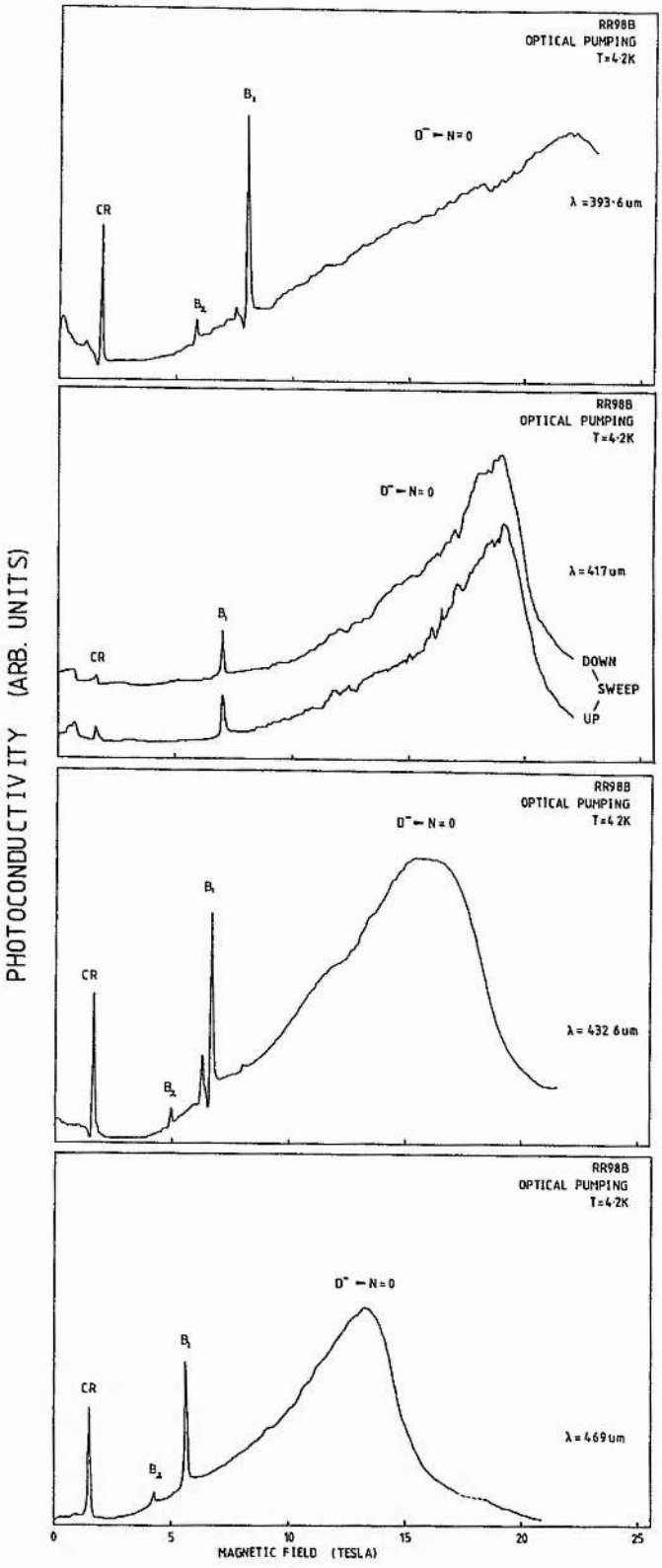

Figure 7.17: Spectra of the $D^- \rightarrow N=0$ transition in RR98B at very high magnetic fields obtained using an electromagnet at the Max-Planck Institute in Grenoble. The sample temperature was 4.2K and optical excitation was used. The splitting on the B_1 peak in the 394 and 433μm spectra is not real and is of instrumental origin.

and suggests that the trial wavefunction used by Larsen is not a good approximation to the actual D^- wavefunction in the region $\gamma>1.5$ (though it is still much better than the four parameter wavefunction of Natori and Kamimura which is 18% low). Alternatively greater central cell shifts at high fields could be responsible for the increased binding energy. However it is possible that the discrepancy is not due to a poor choice of wavefunction or central cell effects but due to the extrapolation method that Larsen used to obtain the binding energies.

Larsen (1980) commented on various ways in which the trial wavefunction used for his 1979 calculation could be improved. These principally involve the 'correlation factor' which expresses the effect of Coulomb repulsion between the two electrons. In the wavefunction used to produce the energies with which all the experimental results have been compared the correlation factor was spherically symmetric: $1+ C (\underline{r}_1 - \underline{r}_2)$ where C is one of the variational constants. Clearly the correlation factor at intermediate magnetic fields will not be spherically symmetric and the function along the direction parallel to the magnetic field will be different to that in the plane perpendicular to the magnetic field. Larsen (1980) also investigated a more complex wavefunction with linear correlation along the magnetic field direction. This would be valid at very high magnetic fields but over the range $0<\gamma<5$ it gave a significantly worse binding energy than the 'intermediate field' wavefunction that has been referred to.

To conclude this section, spectra taken at a temperature of 1.8K at wavelengths of 432 and 417μm are shown in Figure 7.18. The double peaked structure seen in experiments at 1.8K with RR98B and attributed to transitions involving complexes is clearly observed at these high

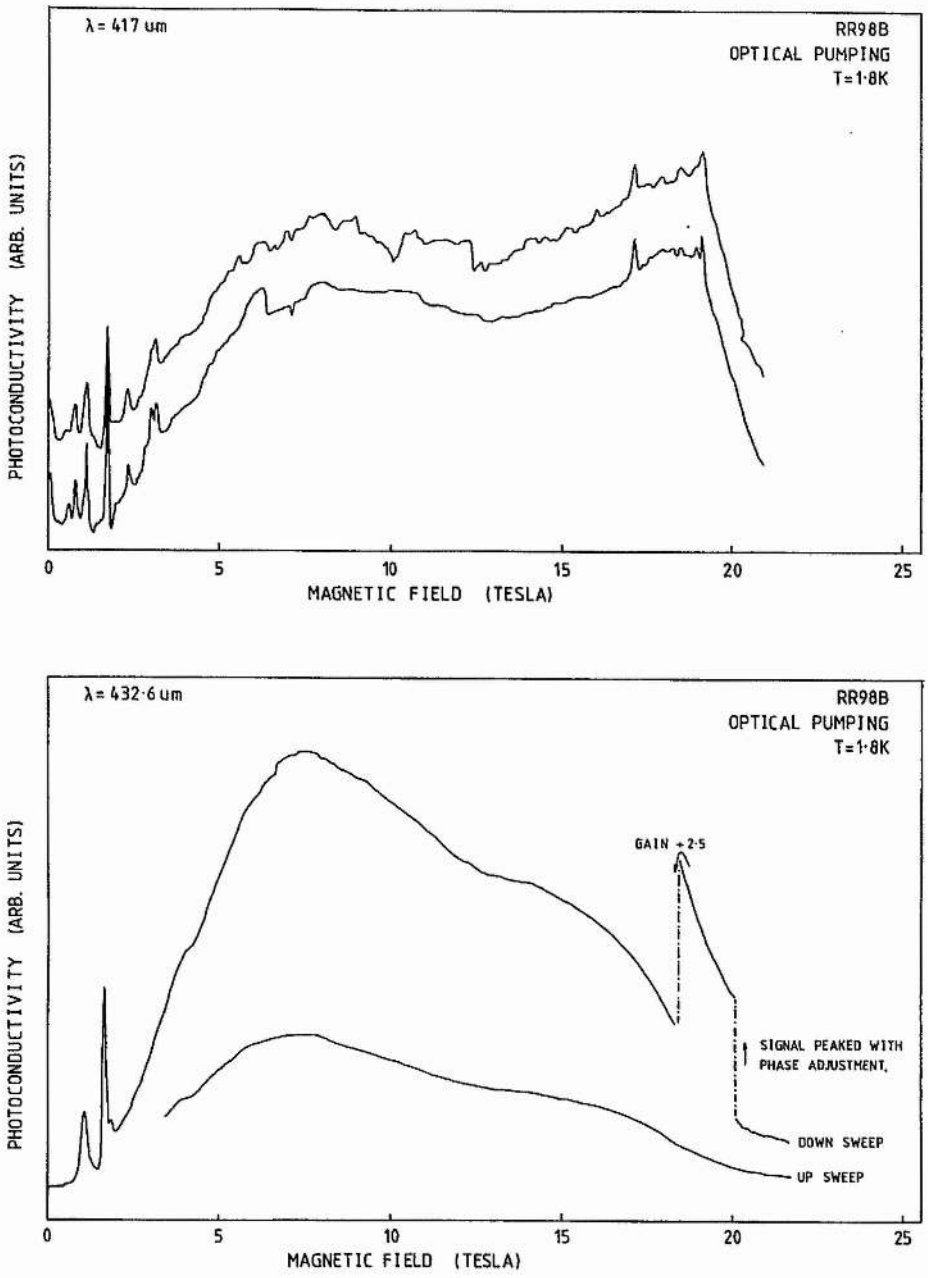

Figure 7.18: Spectra of the D^-→N=0 transition in RR98B at very high magnetic fields obtained at the Max-Planck Institute in Grenoble. The sample temperature was 1.8K and optical excitation was used. As the spectra were rather noisy both the up and down sweeps of the magnet are shown. Note the double peaked shape of the D^-→N=0 transition that was previously observed at lower magnetic fields at this temperature.

magnetic fields. At 432μm the absorption reaches a peak at ~7 Tesla, well below the energy for isolated D^-→N=0 transitions. This figure can be compared with the peak position of the high energy complex at 570μm of ~4 Tesla (Figure 7.13). Thus it appears that while the D^-→N=0 transition energy moves slowly with field the energy of the complex transition moves much more rapidly with field.

D^- States in n-GaAs at Low Magnetic Fields.

In addition to the studies of n-GaAs using the submillimetre laser system, experiments were also carried out using millimetre wave Impatt and Gunn diode sources between 80 and 110 GHz (λ=3.8 to 2.7 mm).

One advantage of using sources at this frequency is that the n=2→3 neutral donor transitions are no longer excited (at zero field n=2→3 transitions occur at 192 GHz), thus simplifying the spectra considerably since many of the strongest inter-excited state transitions of neutral donors are absent: eg all of the A group (A_1, A_2, A_3 and A_3'), B_1 and I_1. However B_2 and B_3 are n=2→2 transitions and are still present, together with other 2→2, 3→3, 4→4 and 3→4 transitions. Most of these transitions have been identified by Davidson et al (1980) and Makado (1982). Davidson et al (1980) noted that in a sample of high purity n-GaAs at a temperature of 1.5K a spectrum taken with a 110GHz Impatt diode showed two shoulders on the low magnetic field side of the cyclotron resonance, one of which was identified as the inter-excited state transition A_4 ($3d_0$-$4p_{+1}$), while the other (labelled 'X') was unidentified. According to Larsen's theoretical calculations (1979) the D^-→N=0 transition energy should cross the cyclotron resonance energy at γ~0.048 which in n-GaAs corresponds to 0.32 Tesla and 133

GHz, so at the Impatt frequencies the $D^- \rightarrow N=0$ transition ought to appear on the low field side of the cyclotron resonance. However though the unidentified peak seen by Davidson et al was in the correct place there was insufficient evidence to attribute it to the $D^- \rightarrow N=0$ transition and it was thought to be another inter-excited state transition.

Studies have been made of samples RR98B and S1 at temperatures of 4.2 and 1.8K using millimetre wave sources. Figure 7.19 shows a series of spectra taken with the 88.2 and 95.5 GHz Impatts at 1.8K under various conditions of electric field bias and band gap excitation. The principal peak seen is the cyclotron resonance at ~0.2 T while the inter-excited state transitions G and B_2/B_3 can be seen at higher fields. At 110 GHz B_2 and B_3 were resolved as separate peaks but at 88 and 95 GHz the transitions merge into one peak. In all four spectra at 88 GHz there is substantial photoconductivity at zero magnetic field. As the $n=3 \rightarrow 4$ transition at zero magnetic field occurs at 67.2 GHz, only just below the Impatt frequency (by 0.7 cm^{-1}), and as the linewidth at zero magnetic field will be much larger than the 0.1 cm^{-1} typical of inter-excited state transitions in a magnetic field, it is likely that much of the zero magnetic field photoconductivity is due to this transition. Alternatively photoionization of the n=4 excited state occurs at 86.4 GHz, which is within 0.06 cm^{-1} of the 88.2 GHz Impatt frequency. For both high and low electric field bias conditions optical excitation reduces the cyclotron resonance linewidth and sharpens the inter-excited state transitions B_2/B_3. This sharpening of the inter-excited state transitions with optical excitation is probably also responsible for the reduction in zero field photoconductivity that occurs with excitation. This is particularly noticeable when comparing the lower

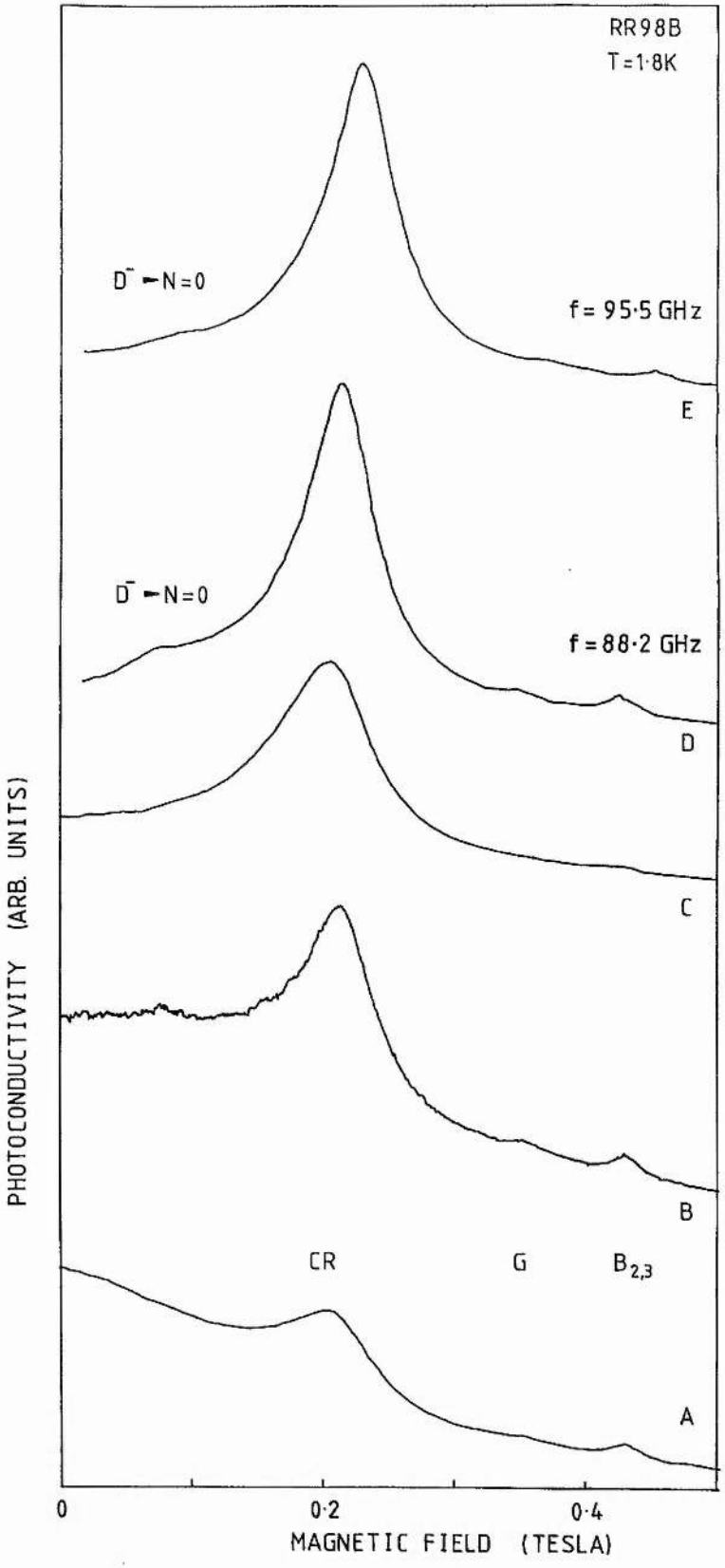

Figure 7.19: Spectra of RR98B at T=1.8K using millimetre wave radiation at 88.2 (traces A, B, C and D) and 95.5 GHz (trace E). Traces A and C are without optical excitation, but B, D and E are with optical excitation. A and B were taken with a low electric field bias (~0.4 and ~0.25 V/cm respectively) but C, D and E were taken with a high electric field bias (~2, ~1.2 and ~1.2 V/cm). A contact separation of ~2mm was assumed when calculating the bias fields. The dominant peak is due to the cyclotron resonance and the transition below it is attributed to $D^- \rightarrow N=0$ transitions.

two traces 'a' and 'b'. The increase in strength of the cyclotron resonance is probably due to the increased conduction electron population present when the optical excitation is present. A further important comparison to make is the relative amplitude of the zero field photoconductivity between the high and low bias conditions. Clearly comparing traces 'a' and 'c', both without optical excitation, the low bias trace 'a' has much greater zero field photoconductivity. The most likely explanation here is that at high bias fields impact ionization is depopulating the loosely bound D^0 states. Such effects are noted much less when the magnetic field is applied as the excited states become more localized and tightly bound as the field is increased, resulting in a lower cross section for impact ionization.

The final point about this diagram concerns the identity of the peak in photoconductivity below the cyclotron resonance at a field of ~0.1T. S1 at 1.8K also showed a similar peak to that seen in RR98B, but no peak was seen in similar spectra of RR98B or S1 at 4.2K. The peak is only observed when band gap excitation is present and is better resolved in the trace at high electric field bias. Unfortunately no spectra could be obtained at 1.8K using the 110GHz Impatt due to failure of the device. The inter-excited state transition A_4 observed by Davidson et al can be ruled out as a possible explanation for the peak as it ought to appear very close to zero magnetic field at both 88 and 95 GHz. Although it is difficult to rule out the possibility that other inter-excited state transitions might be responsible for the peak it is most likely that the $D^- \rightarrow N=0$ transition is responsible. It is already clear from spectra taken at high energy (eg λ=458μm), showing low amplitude peaks attributed to $D^- \rightarrow N=1, 2, 3...$ transitions, that D^- states can exist at fields of ~0.2 Tesla. This, together with the dependence

of the peak on temperature, band gap excitation and electric bias, suggests that it is due to $D^- \rightarrow N=0$ transitions. It is also likely that the peak seen by Davidson et al and labelled X was a $D^- \rightarrow N=0$ transition. Although RR98B shows significant populations of D^- states at higher magnetic fields and energies, the peak shown in Figure 7.19 is only barely resolved and apparently of lower amplitude than that seen by Davidson et al. This can be explained in terms of the sensitivity of the D^- state population to magnetic field and temperature. It is at the very low fields used in these experiments that the D^- binding energy changes most rapidly, and as the binding energy is small compared to kT the small change in temperature from 1.8K in this work to the 1.5K in the work of Davidson et al, together with the larger binding energy will significantly favour the formation of D^- states in their sample by reducing the thermal depopulation rate at 110GHz and 1.5K by a factor of 3.2 compared to that at 88GHz and 1.8K.

Figure 7.20 shows the energy of the transition plotted against the magnetic field of the photoconductivity peak for both this work and the one observation of Davidson et al and compares this with the theoretical work of Larsen. Note that the theoretical curve was obtained by interpolating between three very widely spaced theoretical energies given by Larsen for $\gamma=0$, 0.1 (0.7 Tesla) and 0.2 (1.3 Tesla) and so is only approximate. Only the most important inter-excited state transitions within the field range of the diagram are shown.

It is interesting to note that if these experiments with the Impatt devices could be repeated using the He^3 cooling system designed for use with the superconducting magnet the temperature could be reduced to 0.38K and the thermal depopulation rate, which is the

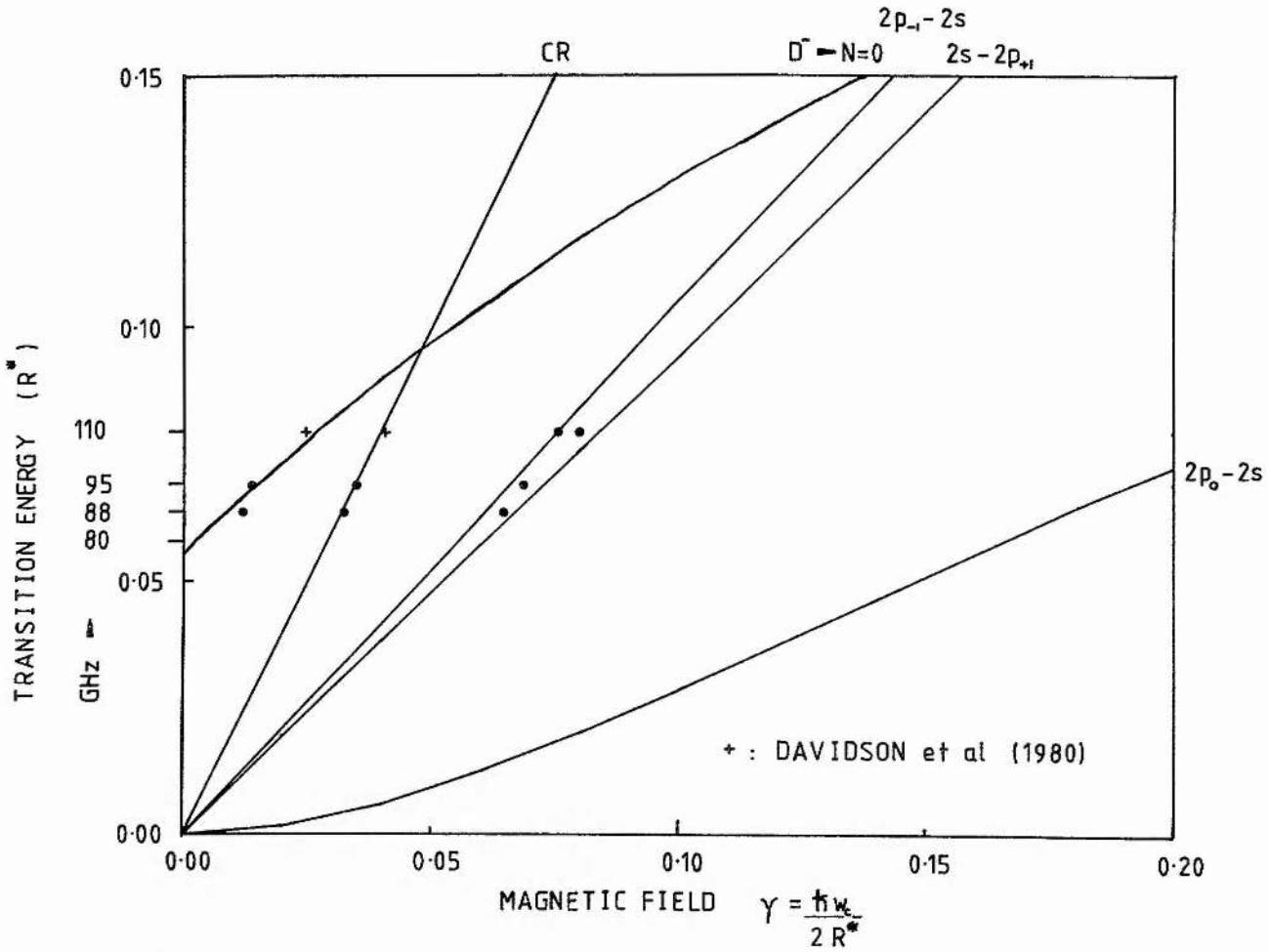

Figure 7.20: The points on the diagram show the magnetic fields of the $D^- \rightarrow N=0$, inter-excited state and cyclotron resonance transitions in dimensionless units observed at low magnetic fields in samples RR98B and S1 using millimetre wave sources. The solid curves show the theoretical energies for the $D^- \rightarrow N=0$ (Larsen 1979) and inter-excited state transitions (Makado 1982). The unidentified transition and cyclotron resonance observed by Davidson et al (1980) using a 110 GHz

dominant factor determining the D^- state population in both RR98B and S1 in these millimetre wave experiments, would be reduced by a factor of almost 6,500 at 88GHz and observation of D^- states at low magnetic fields would be much easier. Unfortunately the He^3 system suffered from vacuum leaks and was not available.

D^- Triplet States in n-GaAs.

The experimental results discussed in this chapter conclusively show that a substantial population of D^- states can form in low compensation n-GaAs at low temperatures and in high magnetic fields and that photo-conductivity due to photoionization of D^- singlet ground states by FIR radiation can be observed. It was noted earlier that although the $m_L=0$ singlet is the only bound state at zero magnetic field additional excited states may be bound in the presence of a magnetic field.

Of the excited states of the D^- ion studied theoretically to date, the most tightly bound is the $m_L=-1$ triplet state. The theoretical studies suggest that the binding energies of the excited states decrease monotonically with increasing $|m_L|$ at intermediate magnetic fields (Larsen 1979 and Avron et al 1977). For a given m_L ($\neq 0$) the anti-symmetric triplet state will always be more tightly bound than the singlet state as electron-electron repulsion (which depends on the overlap between the two wavefunctions) will be lower for the triplet state. As $|m_L|$ increases, and binding becomes weaker the spatial extent of the outer electron orbit increases. Associated with this increase will be a reduction in the overlap between the inner and outer orbitals since the inner orbital remains hydrogen-like. Hence the energy difference between the singlet and triplet states is expected to decrease as $|m_L|$ increases.

Larsen's results for m_L = -1, -2 and -3 show this trend.

Natori and Kamimura used the YKA approach (described earlier for the ground state) and found that the triplet state becomes bound at low fields where $\gamma \sim 0.1$ but that the increase in binding energy with magnetic field is of smaller magnitude than for the singlet states. However their theory will be even less applicable for triplet states in the low field region than for singlet states, which were not well described.

Calculations in the low field region have been made by Henry et al (1974) for H^-, which showed that the m_L=-1 triplet became bound at $\gamma \sim 0.15$. This calculation gives the curve E_{SO} in Figure 7.21, where SO refers to the Slater Orbital expansion used (the actual data used to plot the curve were obtained from Larsen (1979)).

Larsen has attempted to describe the intermediate field regime $0<\gamma<3$ and his results are also shown in Figure 7.21. $E_T^{(0)}$ and $E_T^{(1)}$ were obtained variationally using a series expansion for the triplet wavefunction with zero and first order coefficients respectively and are true variational lower bounds to the binding energy. E_T^{Ex} represents the triplet binding energy obtained by extrapolating $E_T^{(0)}$ and $E_T^{(1)}$ to an infinite number of terms. It is not clear from Larsen's paper how this extrapolation is performed. Up to $\gamma \sim 1$ E_T^{Ex} and $E_T^{(1)}$ are in good agreement and E_T^{Ex} can be considered a true variational lower bound to the triplet D^- binding energy. However above $\gamma \sim 1$ the large discrepancy between $E_T^{(0)}$, $E_T^{(1)}$ and E_T^{Ex} suggests that the extrapolation procedure may be dubious and E_T^{Ex} no longer represents a true lower bound to the binding energy.

Three possible source energies of FIR/millimetre wave radiation for GaAs are shown on the Figure. Thus in GaAs λ=1224μm radiation

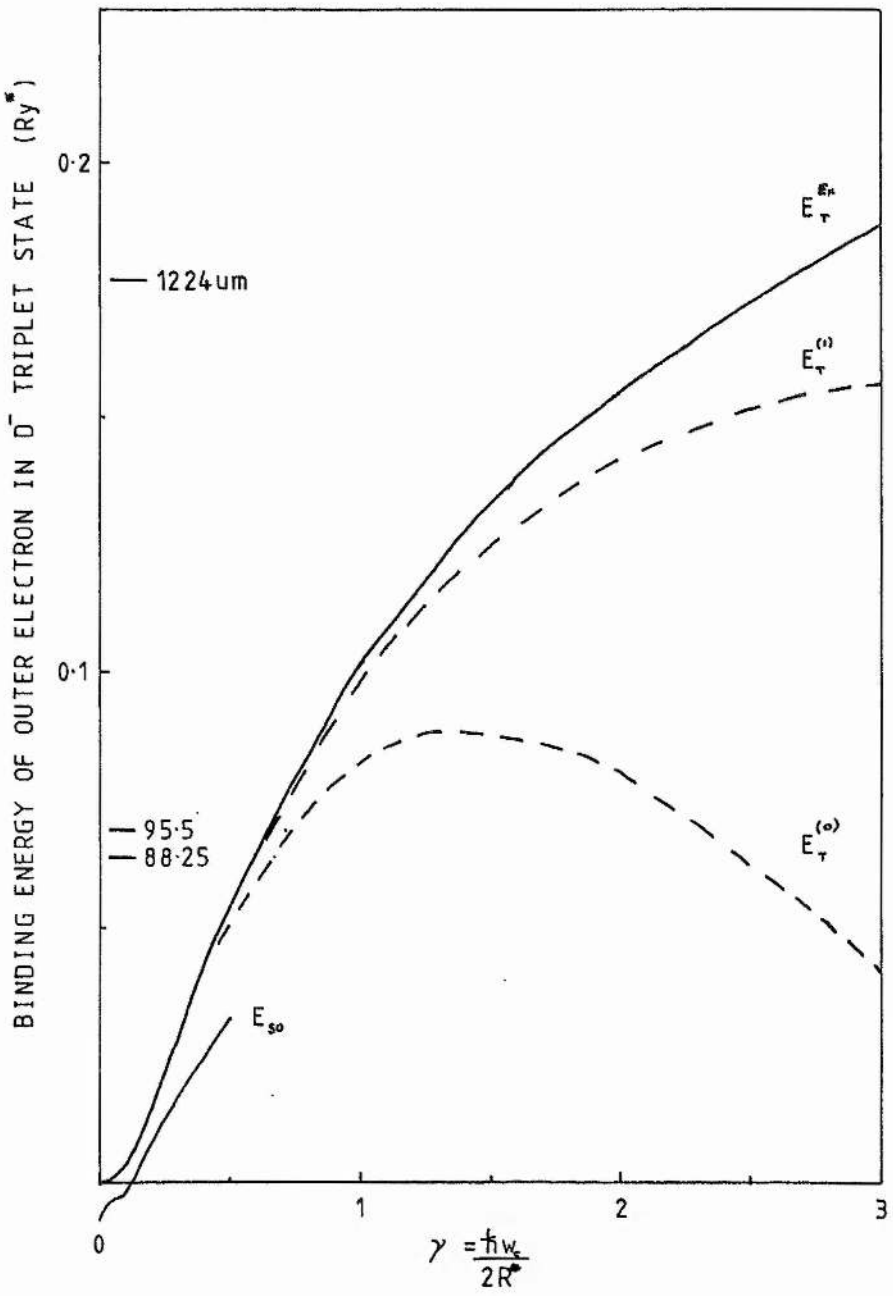

Figure 7.21: Graph showing the theoretical binding energy of the m_L=-1 triplet state of a negatively charged donor. The solid curve marked E_{so} is the result of a calculation using Slater Orbitals (Henry et al 1974). The curves marked $E_T^{(0)}$, $E_T^{(1)}$ and E_T^{Ex} are from a variational calculation by Larsen (1979) and are discussed in the text. The equivalent energies for GaAs of the 1.2mm FIR laser line and the 88 and 95 GHz Impatt diodes are shown.

would place the triplet state photoionization peak at $\gamma \sim 2.7$ or 18 Tesla according to the extrapolated energy curve, well outside the capability of the 12.7 T magnet. However with the millimetre wave devices the theoretical photo-ionization peak occurs at $\gamma \sim 0.7$ or ~4 Tesla.

Spectra were taken of RR98B and S1 using the various Impatt and Gunn devices at magnetic fields up to 10 Tesla and are shown in Figure 7.22.

Spectra of RR98B at 1.8K using the 88 and 95 GHz Impatts (traces A and B) show the usual structure seen at low fields (0 - 2 T: see eg Davidson et al 1980 and Makado 1982), together with a single weak broad peak at ~4 Tesla superimposed on a decaying background photoconductivity.

As the magnetic field of this broad peak is very close to the expected position of the D^- triplet state → conduction band transition it was initially thought that a triplet transition had been found. However a spectrum of S1 at 4.2K with the 80GHz Gunn diode (trace D in Figure 7.22) also showed a transition at ~4 Tesla together with other transitions at 2.1 and 3.6 Tesla. At 95GHz S1 did not show the broad peak but showed another transition at ~6.7 Tesla. These peaks seen in S1 can all be attributed to excited state transitions. It is extremely unlikely that the triplet state would be seen in S1 at 4.2K at these millimetre wave frequencies as kT (4.2K) is equivalent to 87GHz and so the triplet state population will be strongly influenced by thermal ionization. It has already been noted that even at 1.8K the D^- ground state →N=0 is only just observable at these frequencies.

As no studies of the inter-excited state transitions at millimetre waves energies for magnetic fields above 4 Tesla have been

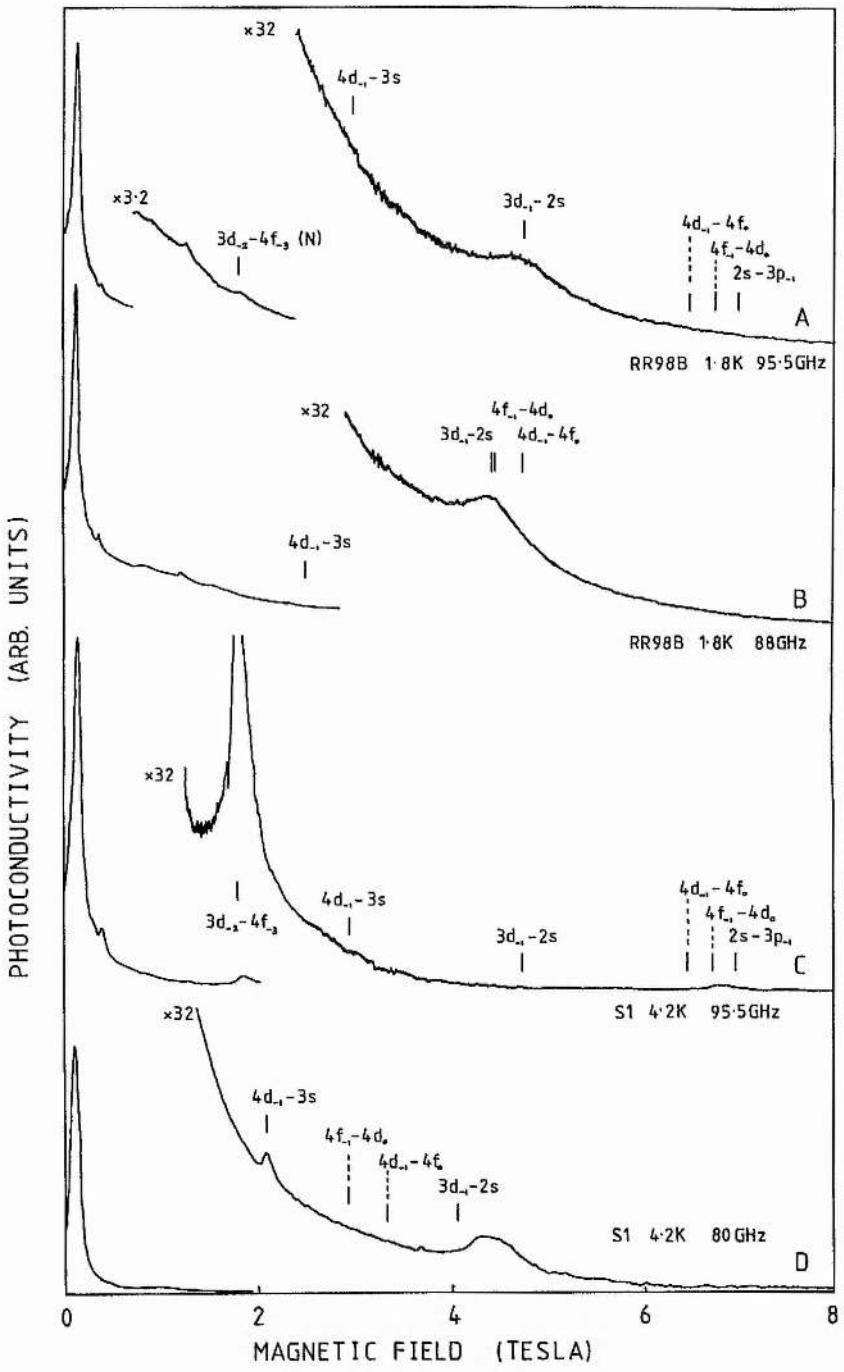

Figure 7.22: Spectra showing inter-excited state transitions in RR98B and S1 at intermediate magnetic fields using millimetre wave sources and with optical excitation. The theoretical energies for various transitions are shown (from the data of Makado 1982). The strong peak just above zero field is the cyclotron resonance. Figure 7.21 suggests that the D^- triplet state to N=0 Landau level transition ought to appear near 4 Tesla.

made the results of Makado's theoretical calculations were again used to predict where the different inter-excited state transitions would appear. On Figure 7.22 the theoretical magnetic fields of various possible inter-excited state transitions are shown while Figure 7.23 shows where the observed peaks fall compared with some possible inter-excited state transitions. Only one transition can be positively identified: the broad peak seen in both samples at ~4 Tesla is assigned to $3d_{-1}$-2s. This transition is unusual in that its energy passes through zero at a finite magnetic field - ie at low fields where $\gamma<0.35$ the transition is $2s \rightarrow 3d_{-1}$ with the 2s state being lower but increasing in energy faster than the $3d_{-1}$ state until it crosses the $3d_{-1}$ energy and the transition becomes $3d_{-1} \rightarrow 2s$. As the 2s state is involved the transition will be subject to central cell shifts. At ~4 Tesla the central cell shift will deepen the 2s state, thus reducing the $3d_{-1} \rightarrow 2s$ transition energy which will push the magnetic field position at a given Impatt frequency higher. In RR98B the transition appears smooth with no indication of structure, whereas S1 at 80 GHz shows a peak with a long high field tail. However it must be noted that there is some doubt as to the exact shape of the transition in S1 at 80 GHz as a second spectrum under identical conditions showed a sharper peak with no high field tail. A long high field tail would be consistent with the central cell structure of S1 seen on the $1s-2p_{\pm 1,0}$ transitions and the $2p_{-1}$-2s transitions. S1 has a strong X_3 (Ge) component, which, being deeper than X_1 and X_2, will appear on the high field side of the $3d_{-1}$-2s transition and could give rise to a high field tail. RR98B has only a small X_3 component and so will not show a high field tail, and the smooth shape is simply due to the unresolved X_1 and X_2 components.

The transition at 2.1 Tesla in S1 (80GHz) in Figure 7.22 is in

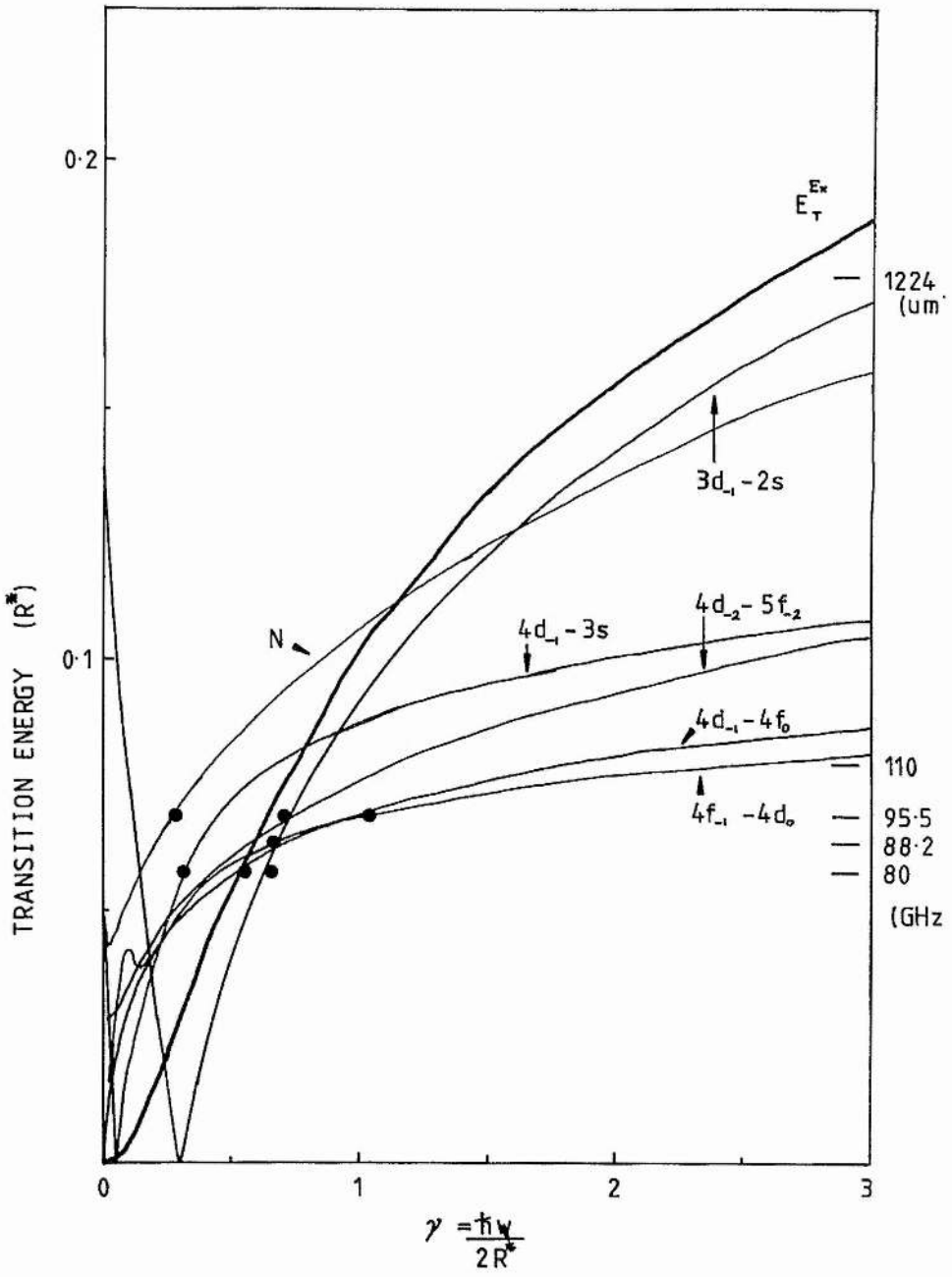

Figure 7.23: Diagram showing the experimental magnetic fields and energies of the inter-excited state transitions observed at intermediate magnetic fields in RR98B and S1 at millimetre wave energies. The D^- triplet state binding energy is shown as the heavy curve marked E_T^{Ex}. Theoretical transition energies are shown as solid curves calculated from the data of Makado (1982) with the exception of the $4d_{-2}$-$5f_{-2}$ transition which was obtained from the data of Rosner et al (1984).

good agreement with the theoretical position of the $4d_{-1}$-3s transition. However as the peak is only seen at this one wavelength it is not possible to make a positive identification. Similarly the peak at 7 Tesla in trace 'C', S1 at 95GHz, could be either $4d_{-1}$-$4f_0$ or $4f_{-1}$-$4d_0$, or even 2s-$3p_{-1}$ (which is an unusual transition in that it decreases consistently in energy over the whole range $0<\gamma<10$).

Thus all the transitions seen in the millimetre wave spectra at magnetic fields above that of the cyclotron resonance can be associated with inter-excited state transitions (even if positive identifications cannot be made) and no transitions originating on D^- triplet states can be identified. Even though the D^- singlet state population appears to be substantial in RR98B for magnetic fields above a few Tesla there will be far fewer triplet states able to form as thermal depopulation will still be dominant when the triplet binding energy is an order of magnitude lower than the singlet ground state binding energy. Future searches for D^- triplet states in n-GaAs will need to go to temperatures significantly below 1.8K (eg 0.38K in a He^3 system) or to magnetic fields up to 20 Tesla in order to use the longest FIR laser wavelengths.

Irrespective of which course is taken considerable care will be needed to avoid mistaking inter-excited state transitions of neutral donors for transitions involving D^- triplet states since it is clear from Figure 7.23 that the two different types of transition can appear at similar magnetic fields. In addition to the n=2, 3 and 4 states of neutral donors which have been the main concern so far account must be taken of n=5 and n=6 states. Recent calculations of the energy levels of neutral hydrogen over a very wide magnetic field range included n=5 and n=6 states (Rosner et al 1984 and Forster et al 1984). A typical

transition $4d_{-2}-5f_{-2}$ (cf $3d_{-2}-4f_{-2}$ (I_2) and $2p_{-1}-3d_{-1}$ (B_1) which are both strong transitions) has been plotted on Figure 7.23 using this data to show that the transition falls at similar energies to that of the D^- triplet states.

Clearly there is enormous scope for experimentation in the search for further bound states of negatively charged donors, using very high magnetic fields, very low temperatures, and a combination of 'state of the art' FIR and microwave technologies at frequencies around 150GHz. Furthermore the dependence of the D^- state population on experimental parameters such as optical excitation and electric field bias that has been shown in this work can be exploited to distinguish features in the spectra associated with either D^- or D^0 states.

References.

Afsar M.N., Button K.J. and McCoy G.L.: Proc. Conf. on 'GaAs and Related Compounds', Vienna, p547 1980

Aldrich C. and Greene R.L.: Phys. Stat. Sol., 93B p343 (1979)

Almassy R.J., Reynolds D.C., Litton C.W., Bajaj K.K. and McCoy G.L.: Solid State Comms., 38 p1053 (1981)

Ansel'm A.I.: Zh. Eksp. Teor. Fiz., 24 p83 (1953)

Armistead C.J., Davidson A.M., Knowles P., Najda S.P., Stradling R.A., Nicholas R.J. and Sessions S.J.: Proc. Conf. on 'Applications of High Magnetic Fields in Semiconductor Physics', Grenoble, p289 (1982)

Armistead C.J., Najda S.P., Makado P.C., Stradling R.A., Colter P.C. and Stillman G.E.: Solid State Comms., 48 p51 (1983)

Armistead C.J., Knowles P., Najda S. and Stradling R.A.: J. Phys. C: Solid State Phys., 17 p6415 (1984)

Askenazy S., Barbaste R., Leotin J., Portal J.C., Ulmet J.P., Chamberlain J.M. and Stradling R.A.: Solid State Comms., 9 p729 (1971)

Avron J., Herbst I. and Simon B.: Phys. Rev. Lett., 39 p1068 (1977)

Bajaj K.K., Birch J.R., Eaves L., Hoult R.A., Kirkman R.F., Simmonds P.E. and Stradling R.A.: J. Phys. C: Solid State Phys., 8 p530 (1975)

Bass S.J., Pickering C. and Young M.L.: Proc. 2nd NATO Workshop on 'Materials Aspects of InP', Lancaster (1983)

Bassani F., Iadonisi G. and Preziosi B.: Rep. Prog. Phys., 37 p1099 (1974)

Bethe H.A. and Salpeter E.E.: 'Quantum Mechanics of One and Two-Electron Atoms', (Springer, Berlin) (1957)

Blakemore J.S.: J. Appl. Phys., 53 R123 (1982)

Bluyssen H.J.A., Maan J.C., van Ruyven L.J., Williams F. and Wyder P.: Solid State Comms., 25 p895 (1978)

Bluyssen H.J.A., Maan J.C., Tan T.B. and Wyder P.: Phys. Rev. B, 22 p749 (1980)

Cabib D., Fabri E. and Fiorio G.: Il. Nuovo Cimento, 10B p185 (1972)

Carter A.C., Carver G.P., Nicholas R.J., Portal J.C. and Stradling R.A.: Solid State Comms., 24 p55 (1977)

Chamberlain J.M., Simmonds P.E., Stradling R.A. and Bradley C.C.: J. Phys C: Solid State Phys., L38 (1970)

Chamberlain J.M., Ergun H.B., Gehring K.A. and Stradling R.A.: Solid State Comms., 9 p1563 (1971)

Chamberlain J.M., Simmonds P.E., Stradling R.A. and Bradley C.C.: Solid State Comms., 11 p463 (1972 a)

Chamberlain J.M., Simmonds P.E., Stradling R.A. and Bradley C.C.: Proc. 11th Int. Conf. on Phys. of Semicon., Warsaw, p143 (1972 b)

Chandrasekar S.: Rev. Mod. Phys., 16 p301 (1944)

Clark C.W. and Taylor K.T.: J. Phys. B: Atom. Molec. Phys., 13 L737 (1980)

Cohn D.R., Lax B., Button K.J. and Dreybrodt W.: Solid State Comms., 9 p441 (1971)

Colter P.C., Look D.C. and Reynolds D.C.: Appl. Phys. Letts., 43 p282 (1983)

Connerade J.-P., Gay J.-C. and Liberman S.: Comments At. Mol. Phys., 13 p189 (1983)

Cooke R.A., Hoult R.A., Kirkman R.F. and Stradling R.A.: J. Phys. D.: Appl. Phys., 11 p945 (1978)

Cowan D.A.: PhD Thesis, University of St. Andrews (1985)

Davidson A.M., Knowles P., Makado P., Stradling R.A., Porowski S. and Wasilewski Z.: Proc. Conf. on 'Applications of High Magnetic Fields in Semiconductor Physics', Hakone, p84 (1980)

De Temple T.A. and Danielewicz E.J.: in 'Infrared and Millimetre Waves', Volume 7, Ed. Button K.J., Acad. Press (1983)

Dean P.J., Cuthbert J.D., Thomas D.G. and Lynch R.T.: Phys. Rev. Letts., 18 p122 (1967 a)

Dean P.J., Haynes J.R. and Flood W.F.: Phys. Rev., 161 p711 (1967 b)

Dean P.J. and Herbert D.C.: 'Excitons' (Springer, Berlin) p55 (1979)

Dean P.J., Herbert D.C., and Lahee A.M.: J. Phys. C: Solid State Phys., 13 p5071 (1980)

Dean P.J. and Skolnick M.S.: J. Appl. Phys., 54 p346 (1983)

Dean P.J., Skolnick M.S. and Taylor L.L.: J. Appl. Phys., 55 p957 (1984)

Dean P.J., Skolnick M.S., Cockayne B., McEwan W.R. and Iseler G.W.: J. Cryst. Growth, 67 p486 (1984)

Eaves L., Stradling R.A., Askenazy S., Leotin J., Portal J.C. and Ulmet J.P.: J. Phys. C: Solid State Phys., L42 (1970)

Fairhurst K., Lee D., Robertson D.S., Parfitt H.T. and Wilgoss W.H.E.: J. Materials Science, 16 p1013 (1981)

Fedders P.A.: Proc. Conf. on 'GaAs and Related Compounds', Albuquerque, p545 (1982 a)

Fedders P.A.: Phys Rev B., 25 p3846 (1982 b)

Fedders P.A.: Phys Rev. B, 27 p4799 (1983)

Fetterman H.R., Larsen D.M., Stillman G.E., Tannenwald P.E.: Phys. Rev. Letts., 26 975 (1971)

Fetterman H.R., Waldman J., Wolfe C.M., Stillman G.E. and Parker C.D.: Appl. Phys. Letts., 21 p434 (1972)

Forster H., Strupat W., Rösner W., Wunner G., Ruder H. and Herold H.: J. Phys. B.: At. Mol. Phys., 17 p1301 (1984)

Freund D.E., Huxtable B.D. and Morgan J.D. III.: Phys. Rev. A, 23 p980 (1984)

Gershenzon E.M., Gol'tsman G.N. and Melnikov E.P.: JETP Letts., 14 p185 (1971)

Gershenzon E.M., Gol'tsman G.N., Ptitsina N.G.: Sov. Phys. JETP, 37 p299 (1973)

Gershenzon E.M., Gol'tsman G.N. and Ptitsina N.G.: Sov. Phys. Semicon., 7 p1248 (1974)

Gershenzon E.M., Gol'tsman G.N. and Elant'ev A.I.: Sov. Phys. JETP, 45 p555 (1977)

Godik E.E., Kuritsyn Yu.A., Sinis V.P.: JETP Letts., 14 p254 (1971)

Golka J.: Phys. Rev. B, 8 p3895 (1973)

Golka J.: J. Phys. C: Solid State Phys., 7 L407 (1974)

Golka J.: J. Phys. C: Solid State Phys., 8 p1443 (1975)

Golka J., Trylski J., Skolnick M.S., Stradling R.A. and Couder Y.: Solid State Comms., 22 p623 (1977)

Gornik E.: Proc. Conf. on 'Applications of High Magnetic Fields in Semiconductor Physics', Grenoble, p248 (1982)

Henry R.J.W., O'Connell R.F., Smith E.R., Chanmugan G. and Rajagopal A.K.: Phys. Rev. D, 9 p329 (1974)

Hodges D.T.: Proc. SPIE, 'Far Infrared/Submillimetre Waves' 105 p6 (1977)

Hodges D.T.: Infrared Phys. (GB), 18 p375 (1978)

Hönerlage B. and Schröder U.: Phys. Rev. B, 16 p3608 (1977)

Hyleraas E. and Mitdal J.: Phys. Rev., 103 p829 (1956)

Ichiguchi T., Drew H.D. and Furdyna J.K.: Phys. Rev. Letts., 50 p612 (1983)

Kane E.O.: J. Phys. Chem. Solids, 1 p249 (1957)

Kang C.S. and Greene P.E.: Symposium on GaAs and Related Compounds, p18 (1968)

Kaplan R., Bishop S.G. and McCombe B.D.: Proc. 9th Int. Conf. Phys. Semiconductors, Moscow, p317 (1968)

Kaplan R. and Wallis R.F.: Phys. Rev. Letts., 20 p1499 (1968)

Kirkman R.F.: D.Phil. Thesis, University of Oxford (1975)

Kobayashi M., Sawada S. and Narita S.: J. Phys. Soc. Japan, 51 p844 (1982)

Kogan S.M. and Van Lien N.: Sov. Phys. Semicon., 15 p26 (1981)

Kohn W.: Solid State Physics (Eds. Seitz F. and Turnbull D.) 5 p259 Acad. Press, (1957)

Kubota E., Katsui A. and Yamada S.: Electronics Letts., 22 p21 (1986)

Kuchar F., Kaplan R., Wagner R.J., Cooke R.A., Stradling R.A. and Vogl P.: J. Phys. C.: Solid State Phys., 17 p6403 (1984)

Lagowski J., Kaminska M., Parsey J.M., Gatos H.C. and Walukiewicz W.: Proc. Conf. on 'GaAs and Related Compounds', Albuquerque, p41 (1982)

Lampert M.A.: Phys. Rev. Letts., 1 p450 (1958)

Landolt-Börnstein Tables: New Series Group III, 17a (Springer, Berlin) (1982)

Larsen D.M.: J. Phys. Chem. Solids, 29 p271 (1968)

Larsen D.M.: Phys. Rev. B, 8 p535 (1973)

Larsen D.M.: Proc. Int. Conf. on 'Applications of High Magnetic Fields in Semiconductor Physics', Wurzburg, p295 (1974)

Larsen D.M.: Proc. Int. Conf. on 'Applications of High Magnetic Fields in Semiconductor Physics', Oxford, p205 (1978)

Larsen D.M.: Phys. Rev. Letts., 42 p742 (1979 a)

Larsen D.M.: Phys. Rev. B, 20 p5217 (1979 b)

Larsen D.M.: Proc. Conf. on 'Applications of High Magnetic Fields in Semiconductor Physics', Hakone, p120 (1980)

Lindemann G., Gornik E., Schawarz R. and Tsui D.C.: Proc. Conf. on 'GaAs and Related Compounds', Vienna, p631 (1980)

Lindemann G., Lassnig R., Seidenbusch W. and Gornik E.: Phys. Rev. B, 28 p4693 (1983)

Look D.C. and Colter P.C.: Phys. Rev. B, 28 p1151 (1983)

Low T.S., Stillman G.E., Cho A.Y., Morkoc H. and Calawa A.R.: Appl. Phys. Letts., 40 p611 (1982 a)

Low T.S., Stillman G.E., Collins D.M., Wolfe C.M., Twari S. and Eastman L.F.: Appl. Phys. Letts., 40 p1034 (1982 b)

Low T.S., Stillman G.E., Nakanisi T., Udagawa T. and Wolfe C.M.: Appl. Phys. Letts., 41 p183 (1982 c)

Luttinger J.M. and Kohn W.: Phys. Rev., 97 p869 (1955)

Makado P.C.: PhD Thesis, University of St. Andrews, (1982)

Makado P.C. and McGill N.C.: J. Phys. C: Solid State Phys., 19 p873 (1986)

Miyao M. and Narita S.: J. Phys. Soc. Japan, 42 p128 (1977)

Najda S.P.: PhD Thesis, University of St. Andrews (1985)

Narita S. and Miyao M.: Solid State Comms., 9 p2165 (1971)

Natori A. and Kamimura H.: J. Phys. Soc. Japan, 44 p1216 (1978)

Natori A. and Kamimura H.: J. Phys. Soc. Japan, 47 p1550 (1979)

Nicholas R.J., von Klitzing K. and Stradling R.A.: Solid State Comms., 20 p77 (1976)

Nicholas R.J.and Stradling R.A.: J. Phys. C: Solid State Phys., 11 L783 (1978 a)

Nicholas R.J.and Stradling R.A.: Solid State Comms., 20 p77 (1978 b)

Norton P.: J. Appl. Phys., 47 p308 (1976)

Ohyama T., Sanada T. and Otsuka E.: J. Phys. Soc. Japan, 34 p1245 (1973)

Ozeki M., Kitihara K., Nakai K., Shibatomi A., Dazai K., Okawa S. and Ryuzan O.: Jap. Jnl. Appl. Phys., 16 p1617 (1977)

Pantelides S.T.: Rev. Mod. Phys., 50 p797 (1978)

Pekeris C.L.: Phys. Rev., 112 p1649 (1958); 126 p1470 (1962)

Ramdas A.K. and Rodriguez S.: Rep. Prog. Phys., 44 p1297 (1981)

Reeder A.A., Chamberlain J.M., Turner R.J. and Hill G.: Solid State Comms., 57 p355 (1986)

Rösner W., Wunner G., Herold H. and Ruder H.: J. Phys. B: At. Mol. Phys., 17 p29 (1984)

Schiff E.A.: Phil.Mag. B, 45 p69 (1982)

Sclar N.: Phys. Rev., 104 p1559 (1956)

Sigg H., Bluyssen H.J.A. and Wyder P.: Solid State Comms., 48 897 (1983)

Simmonds P.E.: D.Phil. Thesis, University of Oxford (1974)

Simmonds P.E., Chamberlain J.M., Hoult R.A., Stradling R.A. and Bradley C.C.: J. Phys. C: Solid State Phys., 7 p4164 (1974)

Skolnick M.S., Eaves L., Stradling R.A., Portal J.C. and Askenazy S.: Solid State Comms., 15 p1403 (1974)

Skolnick M.S., Carter A.C., Couder Y., and Stradling R.A.: J. Opt. Soc. Am., 67 p947 (1977)

Skolnick M.S. and Dean P.J.: J. Phys. C: Solid State Phys., 15 p5863 (1982)

Skolnick M.S., Dean P.J., Taylor L.L., Anderson D.A., Najda S.P., Armistead C.J. and Stradling R.A.: Appl. Phys. Letts.,44 p881 (1984)

Skromme B.J., Low T.S. and Stillman G.E.: Proc. Conf. on 'GaAs and Related Compounds', Albuquerque, p485 (see also Low et al p515) (1982)

Stillman G.E., Larsen D.M. and Wolfe C.M.: Phys. Rev. Letts., 27 p989 (1971 a)

Stillman G.E., Larsen D.M. and Wolfe C.M.: Solid State Comms., 9 p2245 (1971 b)

Stillman G.E., Wolfe C.M. and Korn D.M.: Proc. 11th Int. Conf. Phys. Semiconductors, Warsaw, p863 (1972)

Stillman G.E., Wolfe C.M. and Korn D.M.: Proc. 13th Int. Conf. Phys. Semiconductors, Rome, p623 (1976)

Stillman G.E., Low T.S. and Lee B.: Solid State Comms., 53 p1041 (1985)

Stradling R.A., Eaves L., Hoult R.A., Miura N., Simmonds P.E. and Bradley C.C.: Proc. 1972 Symp. on GaAs, p65 (1972)

Taniguchi M., Hirano M. and Narita S.: Phys. Rev. Letts., 35 p1095 (1975)

Taniguchi M. and Narita S.: Solid State Comms., 20 p131 (1976)

Taniguchi M. and Narita S.: J. Phys. Soc. Japan, 43 p1262 (1977)

Taniguchi M., Narita S., Hasegawa N. and Kobayashi M.: J. Phys. Soc. Japan, 45 p545 (1978)

Taniguchi M. and Narita S.: J. Phys. Soc. Japan, 47 p1503 (1979)

Taylor L.L. and Anderson D.A.: Proc. 2nd NATO Workshop on 'Materials Aspects of InP', Lancaster (1983)

Thomas G.A., Capizzi M., DeRosa F., Bhatt R.N. and Rice T.M.: Phys. Rev. B, 23 p5472 (1981)

Thornton D.D. and Honig A.: Phys. Rev. Letts., 30 p999 (1973)

Townsend P.: J. Phys. C: Solid State Phys., 11 p1481 (1978)

Trager C.A.: MSc. Thesis, University of St. Andrews, (1985)

Yafet Y., Keyes R.W. and Adams E.N.: J. Phys. Chem. Solids, 1 p137 (1956)

Walukiewicz W., Lagowski J. and Gatos H.C.: Appl. Phys. Letts., 43 p112 (1983)

Weisbuch C. and Hermann C.: Solid State Comms., 16 p659 (1975)

Willardson R.K. and Beer A.C. (Eds.): 'Semiconductors and Semimetals: Physics of III-V Compounds', Vols. 1, 2, 3 and 4 (Acad. Press) (1968)

Zawadki W., Pfeffer P. and Sigg H.: Solid State Comms., 53 p777 (1985)